ANNUAL REPORT 2005

COLUMBIA UNIVERSITY

College of Physicians and Surgeons

Center for Radiological Research – 630 W. 168th St., New York, NY 10032 – http://crr-cu.org

ANNUAL REPORT 2005

Eric J. Hall
Director

Howard B. Lieberman
Editor

Mary T. Coady
Moshe Y. Friedman
Assistant Editors

COLUMBIA UNIVERSITY

College of Physicians and Surgeons

Table of Contents

CONTENTS 1
COLLABORATING DEPARTMENTS AND INSTITUTIONS 3
ACKNOWLEDGEMENT OF SUPPORT 3
RELATED WEB SITES 3
INTRODUCTION 4
STAFF NEWS 5
STAFF LISTING 6
STAFF PHOTO 7
COLUMBIA COLLOQUIUM AND LABORATORY SEMINARS 8
RESEARCH REPORTS

MICROBEAM AND DEVELOPMENT STUDIES

X-Ray Microbeam
Giuseppe Schettino 9

Tuning the Stand-Alone Microbeam at Columbia University
Guy Garty, Gregory J. Ross, Alan W. Bigelow, Giuseppe Schettino, Gerhard Randers-Pehrson and David J. Brenner 10

Under-Dish Detector for the Microbeam at Columbia University
Guy Garty, Gregory J. Ross, Kevin Wu, Gerhard Randers-Pehrson and David J. Brenner 12

Isotopic Source for the Stand-Alone Microbeam
Guy Garty, Gerhard Randers-Pehrson and David J. Brenner 13

Incorporating No-stain Imaging into the Columbia University Microbeam Endstation
Gregory J. Ross, Brian Ponnaiya, Gerhard Randers-Pehrson, Alan W. Bigelow and David J. Brenner 14

Multiphoton Microscope Design for the Columbia University Microbeam II Endstation
Alan W. Bigelow, Gregory J. Ross, Gerhard Randers-Pehrson and David J. Brenner 16

BYSTANDER STUDIES

Further Studies of a Low LET Radiation-Induced Bystander Effect in a 3-Dimensional Cell Cluster Model
Rudranath Persaud, Hongning Zhou, Sarah E. Baker, Tom K. Hei and Eric J. Hall 17

Mechanism of Radiation-Induced Bystander Effect: Role of the Cyclooxygenase-2 Signaling Pathway
Hongning Zhou, Vladimir N. Ivanov, Joseph Gillespie and Tom K. Hei 18

Radiation Induced Genomic Instability in Bystander Cells
Hongning Zhou, Shenbing Gu and Tom K. Hei 21

Disassociation and Re-seeding of 3-D Sliced Tissues
Giuseppe Schettino, Gary W. Johnson and David J. Brenner 22

Where Does the Bystander Effect Start?
Mykyta V. Sokolov, Lubomir B. Smilenov, Eric J. Hall, Igor G. Panyutin, William M. Bonner & Olga A. Sedelnikova 24

Isolation of RNA from Sliced 3-Dimensional Tissues
Sally A. Amundson and Giuseppe Schettino 26

Investigation of Radiation-Induced Bystander Responses in Artificial Skin Tissues
Brian Ponnaiya, Stephen Marino and Charles R. Geard 28

The Role of MAP Kinase Pathways in Radiation-Induced Bystander Responses
Brian Ponnaiya, Stephen Marino and Charles R. Geard 30

MOLECULAR STUDIES

***Rad9* Expression Is Aberrantly High in Human Prostate Cancer Cells**
Howard B. Lieberman and Aiping Zhu 32

Human Rad9 Binds to the *p21* Promoter *in Vivo*
Xiaojian Wang, Kevin M. Hopkins, Koon Siew Lai and Howard B. Lieberman 33

Human Rad9 Regulates Radiation-Induced Expression of *p21* and *Cox-2*
Aiping Zhu, Yuxin Yin, Tom K. Hei and Howard B. Lieberman 34

Histone H2AX is Phosphorylated in Mitotic Cells in the Absence of Exogenous DNA Damage
Adayabalam S. Balajee and Charles R. Geard 36

Expression of Human Drug Metabolism Genes Altered by Organophosphorous Pesticides and Estrogen of Human Breast Epithelial Cells
Gloria M. Calaf, Debasish Roy, Adayabalam Balajee and Tom K. Hei 38

Mutagenicity of Chrysotile Fibers in Primary *gpt* Delta Transgenic Mouse Embryo Fibroblast Cells
An Xu, Lubomir Smilenov, Peng He, Ronald Baker and Tom K. Hei 40

MKP2 Is a Novel Transcription Target of p53 in Singnaling Apoptosis
Wen Hong Shen, Jianli Wang, Victor Zhurkin and Yuxin Yin 41

CELLULAR STUDIES

Deletion of Mouse *Rad9* Leads to High Frequencies of Sister Chromatid Exchange
Kevin M. Hopkins, Adayabalam S. Balajee and Howard B. Lieberman 45

Characterization of *Mrad9B*$^{-/-}$ Mouse ES Cells and Generation of *Mrad9B*$^{-/-}$ Knock-out Mice
Corinne Leloup, Aiping Zhu, Kevin M. Hopkins and Howard B. Lieberman 47

Human Chromosome 11-Encoded Antigens Expressed on A_L Cells: Flow Cytometry Analysis for Detecting Mutations Induced by Arsenic and Asbestos
Michael A. Partridge, SiYuan Yao, An Xu, Hongning Zhou and Tom K. Hei 48

Cellular Responses of Lymphoblasts to 1 GeV ^{56}Fe Particles
Sally A. Amundson and Jaeyong Ahn 51

Regulation of the Susceptibility of Cancer Cells to Apoptosis through the Inhibition of Dynamin-2 Expression
Vladimir N. Ivanov, Sangsoo Kim and Tom K. Hei 53

Combined Treatment with COX-2 Inhibitor and Sodium Arsenite Leads to Induction of Surface Fas Ligand Expression and Fas Ligand-Mediated Apoptosis in Human Cancer Cells
Vladimir N. Ivanov and Tom K. Hei 57

Epigenetic Inactivation of the *Betaig-h3* Gene in Human Cancer Cells
Genze Shao, Tom K. Hei and Yongliang Zhao 62

Loss of Betaig-h3 Protein Is Frequent in Primary Lung Carcinoma and Related to Tumorigenic Phenotype in Lung Cancer Cells
Yongliang Zhao and Tom K. Hei 65

POPULATION-BASED RADIOLOGY OR RADIOTHERAPY ORIENTED STUDIES

IMRT, Protons and the Risk of Second Cancers
Eric J. Hall 68

The Center for High-Throughput Minimally-Invasive Radiation Biodosimetry
David J. Brenner and Sally A. Amundson 69

Estimating Radiation-Induced Cancer Risks at Very Low Doses: Rationale for Using a Linear No-Threshold Approach
David J. Brenner and Rainer K. Sachs 72

THE RADIOLOGICAL RESEARCH ACCELERATOR FACILITY – an NIH-Supported Resource Center

Dir., David J. Brenner, PhD, DSc; Mnger., Stephen A. Marino, MS; Chief Physicist, Gerhard Randers-Pehrson, PhD
Table of Contents / RARAF Professional Staff 75
Research Using RARAF 76
Development of Facilities 78
Van de Graaff Utilization and Operation 81
Training 81
Personnel 81
Recent Publications of Work Performed at RARAF (2004–2005) 82

SPECIAL REPORT: Replacement of the RARAF Accelerator
Stephen A. Marino, Gerhard Randers-Pehrson, Alan Bigelow, Guy Y. Garty, Gregory Ross, Giusseppe Schettino and David J. Brenner 83

THE RADIATION SAFETY OFFICE

Table of Contents 87
Radiation Safety Office Staff 88
Introduction / Overview / Summary of Radiation Safety Office Operations for 2005 89

ACTIVITIES AND PUBLICATIONS

Professional Affiliations & Activities 99
Professional Publications 101

Collaborating Institutions

Individuals from the following alphabetically listed institutions collaborated with the Center's faculty and staff in the research reports included in this year's publication (for individual attributions see specific reports):

Collaborating Institutions:

- Arizona State University, Biodesign Institute, Tempe, AZ
- Brookhaven National Laboratory, Biology Department, Upton, NY
- City of New York Department of Health and Mental Hygiene, New York, NY
- Harvard University School of Public Health, Boston, MA
- Institute of Cell Biology and Genetic Engineering, Department of Radiation Biology and Biophysics, Ukraine
- Mayo Clinic, College of Medicine, Rochester, MN
- Massachusetts General Hospital, Boston, MA
- Okayama University Medical School, Okayama, Japan
- Radiation Effects Research Foundation, Hiroshima, Japan
- Sionex Corporation, Bedford, MA
- Stuyvesant High School, New York, NY (participation in our Small Group Apprenticeship Program)
- Translational Genomics Research Institute, Phoenix, AZ
- University of Bern, Switzerland
- University of California, Berkeley, CA
- University of Pittsburgh Medical Center, Pittsburgh, PA
- University of Tarapaca and Research Center for the Man in the Desert, Arica, Chile
- U.S. Department of Health and Human Services
  - National Institutes of Health, Bethesda, MD
    - Clinical Center, Department of Nuclear Medicine
    - Laboratory of Experimental and Computational Biology
    - National Cancer Institute, Laboratory of Molecular Pharmacology, Center for Cancer Research ■

Acknowledgment of Support

In 2005 the Center for Radiological Research was supported by competitively awarded grants from the following agencies:

Federal:

- Department of Energy
  - Office of International Health Programs
  - Office of Science, Office of Biological and Environmental Research [Low Dose Radiation Research Program]
- Department of Health and Human Services
  - National Institutes of Health:
    - National Cancer Institute [Program Project (PO1) & Individual Research Grants (RO1s)]
    - National Center for Research Resources (S10)
    - National Institute of Biomedical Imaging and Bioengineering (P41)
    - National Institute of Allergy and Infectious Disease
    - National Institute of Environmental Health and Safety (RO1s)
    - National Institute of General Medical Sciences (RO1)
- National Aeronautics and Space Administration

Private:

- Radiological Society of North America ■

Web Sites

- **Center for Radiological Research** ..... **http://crr-cu.org**
- **Radiological Research Accelerator Facility**..... **http://www.raraf.org**
- **Center for High-Throughput Minimally-Invasive Radiation Biodosimetry** ..... **http://www.cmcr.columbia.edu**
- **Web-Rad-Train**..... **http://www.web-rad-train.org**
- **Department of Radiation Oncology** .....**http://cpmcnet.columbia.edu/dept/radoncology**
- **Radiation Safety Office** .....**http://cpmcnet.columbia.edu/dept/radsafety**

- **CRR Annual Reports *(1998–present)*** .....**http://crr-cu.org/reports.htm**

Introduction

The Center for Radiological Research of Columbia University pursues a multidisciplinary approach to understanding the biological effects of a spectrum of ionizing radiations. There are a number of diverse research goals:

- Understanding the mechanisms of the biological effects of radiation at the molecular level.
- Investigating the deleterious effects of low doses of radiation, of interest to the Department of Energy Low Dose Program.
- Investigating the biological effects of high energy heavy ions, of interest to NASA.
- Improving dose-time schedules for clinical radiation therapy and estimating the impact of radiation induced second malignancies.

This report summarizes the principal research initiatives and academic activities during the past year.

In this report there are articles that update research activities utilizing the microbeam facility, which is still one of the most versatile of such facilities in the world. The study of the bystander effect, i.e., the observation of biological effects in cells not traversed by a charged particle, but in close proximity to cells that are, has been extended from in vitro cell cultures to three-dimensional model tissues.

There are a variety of articles at the cellular and molecular level describing events that occur following exposure to low doses of gamma-rays, of particular interest to the Department of Energy, or to high energy Fe ions, of special interest to NASA because they mimic the space environment. The induction of cancer is one of the most important consequences of exposure to ionizing radiations and there are articles that deal with this subject in the context of new modalities for radiation oncology and in the context of radiation protection.

The year 2005 proved to be a highly successful year for the Center in terms of both new funding and new projects. It started with a number of faculty being successful in competing for grant support from DOE and NASA (Drs. David Brenner, Charles Geard, Eric Hall and Adayabalam Balajee).

This was followed by the excellent news that our NIH Program Project Grant, which focuses on investigation of the basic mechanisms of the radiation-induced bystander effect, currently into its 14th year, was successfully funded for another five years, with Dr. Tom Hei taking over from Dr. Hall as principal investigator in the competitive renewal. The other co-investigators of this project are Drs. Sally Amundson, Charles Geard, David Brenner and Howard Lieberman.

In addition, the Center was the recipient of the largest grant it has ever received. This is the new "Center for High-Throughput Minimally Invasive Radiation Biodosimetry" (www.cmcr.columbia.edu), with Dr. David Brenner as principal investigator. This award has a variety of collaborators both within Columbia University and outside. A summary of the work that will be carried out can be found on page 69 of this annual report.

Our facilities at RARAF underwent a major overhaul with the replacement of its 4.2-MV Van de Graaff accelerator, that since 1967 produced charged particle beams at RARAF for neutron irradiations, track segment experiments and the microbeam facilities, with a 5-MV coaxial Singletron from High Voltage Engineering Europa (HVEE). The replacement process and advantages of the new accelerator are described in a special essay on page 83 of this report.

The productivity of the Center continues at a high level, as evidenced by a steady stream of scientific papers in peer-reviewed journals, including several in high profile journals. Given our success during the previous year for obtaining funding for research, we anticipate that the upcoming year will bring many important advances in understanding the biological effects of radiation exposure.

Members of the staff are frequently invited to participate in national and international meetings, and are frequently called upon to serve as consultants, reviewers or site visitors by government and private agencies.

The Center's teaching activities of include teaching radiation biology and radiation physics to undergraduates, medical students and graduate students in the School of Public Health, and to residents in Radiology and Radiation Oncology, and a City-wide course for residents in Radiology. ■

We had much to celebrate at our holiday party (*l–r*): Greg Ross, Alan Bigelow, Ron Baker, Lubomir Smilenov and Margaret Geard.

Staff News

In March, the Center celebrated its 90th year with a very special colloquium presentation. Dr. Hall shared a number of cherished pictures from our photo archives and reminisced about the Center's exceptionally interesting history of prestigious, pioneering work that has been done here. Everyone in attendance was inspired to pursue more future successful discoveries and accomplishments.

Dr. Hall was awarded the Distinguished Scientific Achievement Award for the year 2005 from the Heath Physics Society at their annual meeting in Spokane, Washington (see picture). Dr. Hall was also made an Honorary Fellow of the Society for Radiological Protection at their annual meeting in Cardiff, U.K., in view of "significant contributions to our understanding of radiobiology and to education, and thereby to radiation protection."

Dr. Tom K. Hei continues to serve as an ad hoc member of the NCI cancer etiology study section and as chairman of several special emphasis panels. Dr. Hei's recent study on the role of mitochondrial damage in the genotoxicity of arsenic, published in the April 15 issue of *Cancer Research*, was featured in a piece on Research Highlights from the National Institute of Environmental Health Sciences, as well as in the journal *In Vivo*.

Dr. Howard B. Lieberman served as an ad hoc member of the basic and preclinical Subcommittee C of the NCI Initial Review Group, and as an hoc member of special emphasis grant review panels for NIH. He also served as an ad hoc external advisor for the Joint Center for Radiation Therapy Foundation, Harvard Medical School. He continues to serve on the scientific advisory board for the Israel Cancer Research Foundation.

Dr. Sally Amundson was elected to the National Council on Radiological Protection, joining Drs. Hall and Brenner on the Council. Dr. Amundson also gave invited talks at the Radiation Oncology Gordon Conference in Ventura, CA, in February, and at the American Association for Cancer Research Annual Meeting in Anaheim, CA, in April.

Dr. Corinne Leloup received the Fowler Award at the Annual Radiation Research Society Meeting held in Denver, CO. This award honors a scholar-in-training for submission of an outstanding scientific abstract.

Mr. Siyuan Yao, a third year medical student from the Okayama Medical University, spent three months in Dr. Hei's laboratory studying asbestos-mediated mutagenesis using flow cytometry as part of a physician-scientist training program. Miss Ilana Yurkiewicz, a high school senior from the Lawrence High School in Cedarhurst, NY, under the mentorship of Professor Hei, successfully competed in the Intel Science Talent Search with her project "Epigenetic inactivation of the tumor suppressor gene *Betaig-h3* by promoter hypermethylation." She won a semifinalist title as well as $2,000 in scholarship, and has been accepted into Yale University as a member of the class of 2010.

In the past year a number of staff members have left the Center, either for retirement or to advance their careers in other research institutions:

Dr. Hall receives the "Distinguished Scientific Achievement Award" from Kenneth R. Kase, President of the Health Physics Society, at their annual meeting in Spokane in July 2005.

Dr. Chang Piao, an associate research scientist in the Center, retired in December after 17 years of service as a member of Dr. Tom K. Hei's laboratory. Also retiring is staff associate Su-Xian Liu.

Associate research scientists Catherine and Stephen Mitchell left the Center in order to return to their home base in the U.K. after spending two productive years working with us in New York. We will also miss post-doctorial research scientists, Rajaminickam Baskar, Peng He, Rudranath Persaud and Jianli Wang have left the Center for new positions, and two members of the technical staff, Jessica Berenguer and Joseph Gillespie, who moved on to new positions.

The Center is pleased to have a number of new staff members who have been recruited to pursue research here:

Dr. Peter Grabham has come to the Center from Columbia University's Dept. of Pharmacology and Center for Neurobiology, and will be working as an associate research scientist in Dr. Geard's lab. Dr. Jingjing Wu, will be working in Dr. Yin's lab as a staff associate. A number of new post-doctorial research scientists have also joined the Center, including Drs. Aparajita Dutta (in Dr. Brenner's lab), Burong Hu (in Dr. Geard's lab), Michael Partridge, Gengyun Wen and An Xu (in Dr. Hei's lab), and Guangming Zhou (in Dr. Hall's lab). Ms. Anne Sutthoff has also joined our team as administrator of the new Center for Medical Countermeasures against Radiation under Dr. Brenner's supervision. ■

We note with sorrow the sudden passing of our colleague Dr. Basil Worgul, Professor of Radiation Biology in Ophthalmology and Radiology and Director Eye Radiation and Environmental Research Laboratory, on Jan. 19, 2006. He had collaborated on reports that have appeared in this publication over the years, and he will be very sorely missed.

Faculty and Staff

Faculty:

ERIC J. HALL, D.Phil., D.Sc., F.A.C.R., F.R.C.R.
— ***Director***
Higgins Professor of Radiation Biophysics
Professor of Radiology and Radiation Oncology
Chairman, Joint Radiation Safety Committee

CHARLES R. GEARD, Ph.D.
— ***Associate Director***
Professor of Clinical Radiation Oncology

DAVID J. BRENNER, Ph.D., D.Sc.
— ***RARAF Director***
Professor of Radiation Oncology and Public Health
(Environmental Health Science)

TOM K. HEI, Ph.D.
Professor of Radiation Oncology
Professor of Environmental Health Sciences

HOWARD B. LIEBERMAN, Ph.D.
Professor of Radiation Oncology

SALLY A. AMUNDSON, Sc.D.
Associate Professor of Radiation Oncology

LUBOMIR SMILENOV, Ph.D.
Assistant Professor of Radiation Oncology

YUXIN YIN, M.D., Ph.D.
Assistant Professor of Radiation Oncology

YONG-LIANG ZHAO, Ph.D.
Assistant Professor of Radiation Oncology

Research Staff:

ADAYABALAM BALAJEE, Ph.D.
Research Scientist

GERHARD RANDERS-PEHRSON, Ph.D.
Research Scientist

ALAN BIGELOW, Ph.D.
Associate Research Scientist

GLORIA CALAF, Ph.D.
Adj. Associate Research Scientist

PETER GRABHAM, Ph.D.
Associate Research Scientist

VLADIMIR IVANOV, Ph.D.
Associate Research Scientist

BRIAN PONNAIYA, Ph.D.
Associate Research Scientist

HONGNING ZHOU, M.D.
Associate Research Scientist

KEVIN M. HOPKINS, M.S.
Senior Staff Associate

STEPHEN A. MARINO, M.S.
Senior Staff Associate

CHANG-QING PIAO, M.D.
Senior Staff Associate

JAEYONG AHN, M.S.
Staff Associate

CARL ELLISTON, M.S.
Staff Associate

GUY GARTY, Ph.D.
Staff Associate

JINGJING WU, M.S.
Staff Associate

AIPING ZHU, M.D.
Staff Associate

GREGORY ROSS, M.S.
Programmer Analyst

Post-Doctoral Fellows:

APARAJITA DUTTA, Ph.D.
Post-Doctoral Research Scientist

BURONG HU, Ph.D.
Post-Doctoral Research Scientist

CORINNE LELOUP, Ph.D.
Post-Doctoral Research Scientist

MICHAEL PARTRIDGE, Ph.D.
Post-Doctoral Research Scientist

GIUSEPPE SCHETTINO, Ph.D.
Post-Doctoral Research Scientist

GENZE SHAO, Ph.D.
Post-Doctoral Research Scientist

GENGYUN WEN, Ph.D.
Post-Doctoral Research Scientist

WENHONG SHEN, Ph.D.
Post-Doctoral Research Scientist

AN XU, Ph.D.
Post-Doctoral Research Scientist

GUANGMING ZHOU, Ph.D.
Post-Doctoral Research Scientist

Design & Instrument Shop:

GARY W. JOHNSON, A.A.S.
— ***Design & Instrument Shop Director***
Senior Staff Associate

DAVID CUNIBERTI, B.A.
Instrument Maker

ROBERT ARCHIGIAN
Instrument Maker

Technical Staff:

GLORIA JENKINS-BAKER, B.S.
Research Worker

XIAOJIAN WANG, M.S.
Research Worker

RONALD BAKER, B.S.
Senior Technician

CUI-XIA KUAN
Technical Assistant

Administrative & Secretarial Staff:

MONIQUE REY, B.A.
Center Administrator

ANNE SUTTHOFF, M.A.
Administrator

MARY COADY
Administrative Coordinator

MOSHE FRIEDMAN, B.R.E.
Administrative Assistant

DIANA MORRISON
Administrative Assistant

HEIDY HERNANDEZ
Jr. Accountant

ANGELA LUGO
Clerk Typist

Faculty and Staff

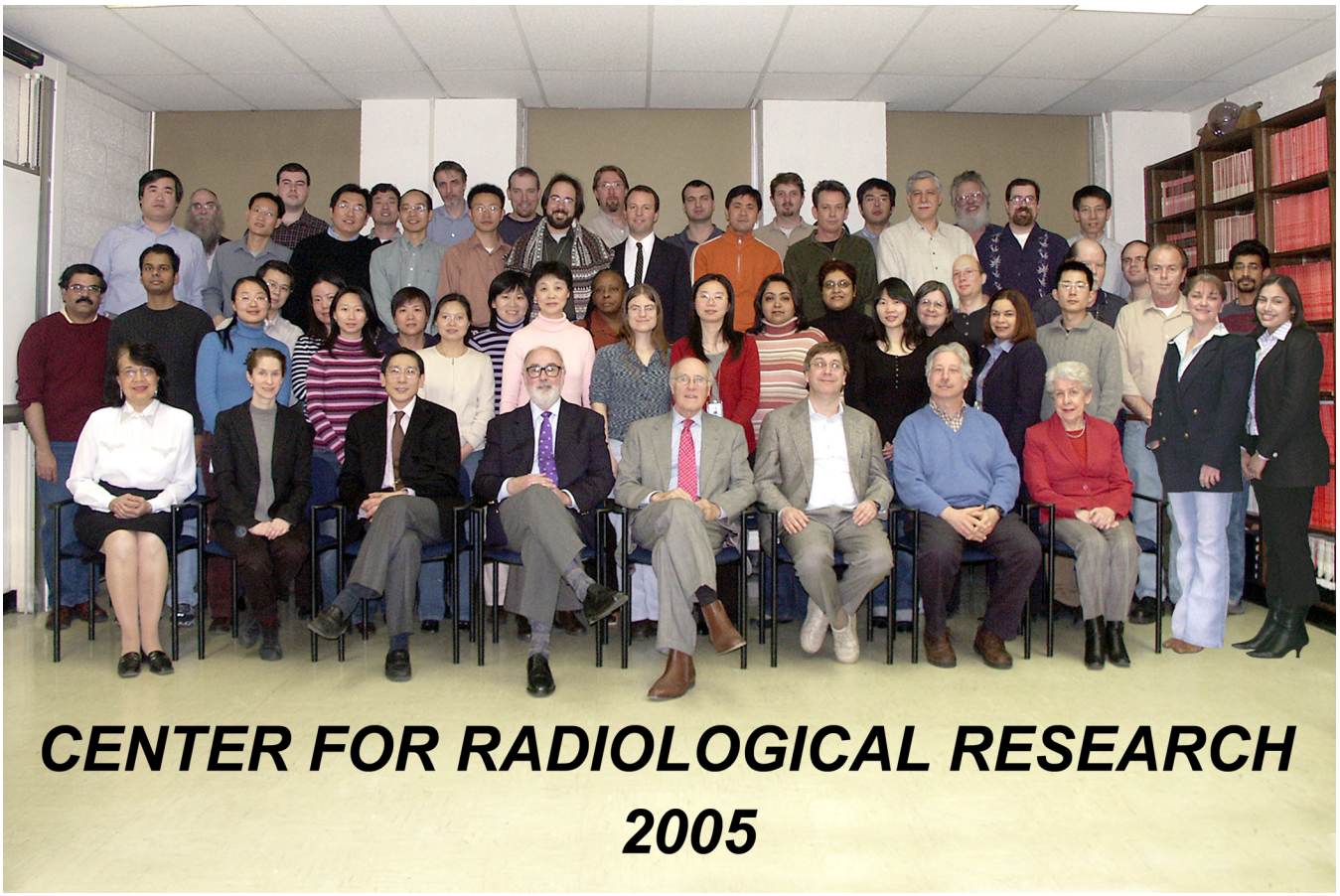

Front row (*l-r*): Ms. Monique Rey, Dr. Sally Amundson, Dr. Tom Hei, Dr. Charles Geard, Dr. Eric Hall, Dr. David Brenner, Dr. Howard Lieberman, Ms. Mary Coady, Ms. Diana Morrison, Ms. Angela Lugo.

2nd row: Dr. Adayabalam Balajee, Dr. Naved Alam, Jingjing Wu, Dr. Gengyun Wen, Dr. Wenhong Shen, Dr. Yu-Chen Lien, Mrs. Cui-Xia Kuan, Dr. Yanrong Su, Ms. Xiaojian Wang, Dr. Aiping Zhu, Ms. Gloria Jenkins-Baker, Dr. Corinne Leloup, Dr. An Xu, Dr. Aparajita Dutta, Dr. Shanaz Ghandhi, Ms. Sarah Huang, Ms. Anne Sutthoff, Mr. David Cuniberti, Ms. Heidy Hernandez, Mr. Yun Fei Chai, Dr. Vladimir Ivanov, Mr. Carl Elliston, Mr. Gary Johnson, Dr. Brian Ponnaiya.

3rd row: Dr. Yuxin Yin, Dr. Genze Shao, Dr. Hongning Zhou, Dr. Shenbing Gu, Dr. Gengyun Wen, Dr. Guy Garty, Dr. Alan Bigelow, Mr. Jaeyong Ahn, Dr. Peter Grabham, Mr. Stephen Marino, Mr. Robert Archigian.

Back row: Mr. Moshe Friedman, Dr. Igor Shuryak, Dr. Burong Hu, Dr. Lubomir Smilenov, Mr. Gregory Ross, Mr. Kevin Hopkins, Dr. Giuseppe Schettino, Dr. Michael Partidge, Dr. Tomoo Funayama, Dr. Gerhard Randers-Pehrson, Dr. Yong-Liang Zhao.

Not pictured: Mr. Ronald Baker, Dr. Gloria Calaf.

Columbia Colloquium and Laboratory Seminars

At approximately monthly intervals during the year the Center for Radiological Research is pleased to welcome accomplished specialists from around the world to present formal seminars and/or spend time discussing ongoing research. The seminars are attended by Center and RARAF professional staff, senior technical staff and graduate students, as well as doctors and scientists from other departments of the College of Physicians & Surgeons interested in collaborative research. Attention has focused on recent findings and future plans, with special emphasis on the interdisciplinary nature of our research effort. The 2005 sessions, included the following guest speakers (listed alphabetically):

- Dr. Alex Almasan, Ph.D., Associate Professor of Molecular Medicine, Depts. of Cancer Biology and Radiation Oncology, The Cleveland Clinic Lerner Research Institute, Cleveland, OH: "Cyclin E at the crossroads of genotoxic stress response."
- Dr. Edouard Azzam, Dept. of Radiology, University of Medicine and Dentistry of New Jersey–New Jersey Medical School, Newark, NJ: "The role of intercellular communication and oxidative metabolism in the propagation of low-level radiation effects."
- Dr. Jaroslaw Dziegielewski, Roswell Park Cancer Institute, Buffalo, NY: "C-1027 – an atypical radiomimetic agent."
- Peter W. Grabham, Ph.D., Dept. of Pharmacology and Center for Neurobiology, College of Physicians & Surgeons, Columbia University: "Cytoskeletal control of axonal growth: Microtubules have their day." Dr. Grabham has since joined our Center.
- Dr. Prakash Hande, National University of Singapore: "Telomere dysfunction and DNA repair deficiency: Markers of susceptibility to mutagens and carcinogens?"
- Dr. Walter Huda, Dept. of Radiology, SUNY Upstate Medical University: "A proposal for a paradigm shift in CT dosimetry."
- Jordan D. Irvin, Ph.D., Department of Biochemistry, Microbiology and Molecular Biology, Penn State University, University Park, PA: "Genome-wide functional analysis of TAF1 and MOT1 regulators of the TATA box binding protein in Saccharomyces cerevisieae."
- Dr. Jarah Meador, NASA, Johnson Space Center, Houston, Texas: "An assessment of DNA damage induced by non-ionizing and ionizing radiation."
- Stephen R. Moore, Ph.D., MRC Career Development Fellow Radiation and Genome Stability Unit Medical Research Council Harwell, Oxfordshire, UK: "Interindividual variation in genomic instability after targeted microbeam irradiation."
- Dr. Otilia Nuta, Sylvius Laboratory, Leiden University Medical Center, Department of Toxicogenetics, Leiden, The Netherlands: "Radiation induced bystander effect."
- Dr. Snirmal Paul, Ph.D., Dept. of Environmental Medicine, NYU School of Medicine, Tuxedo Park, NY: "Processing of pyrimidine dimers with disrupted phosphodiester bonds in E. coli: An elegant but frustrating Russian doll."
- Dr. Guillermo Taccioli, Boston University, School of Medicine, Department of Microbiology: "DNA-PK: breaks apart."
- Robert L. Ullrich, Ph.D., Barbara Cox Anthony University Chair in Oncology, Colorado State University: "Animal models of radiation-induced cancer and their relevance to understanding risks."
- Dr. Fumio Yatagai, head of the Radioisotope Technology Division, RIKEN, Japan: "Detection of the genetic influences by low-dose or low-dose rate ionizing radiation: A challenge using human cultured cell."
- Dr. Guangming Zhou, Biology Dept., Brookhaven Natl. Laboratories, Upton, NY: "Correlation between cell cycle block and cellular radiosensitivity." Dr. Zhou has since joined our Center.

Dr. Tom K. Hei and one of our visiting seminar speakers, Dr. Fumio Yatagai from RIKEN, Japan.

Seminars were also conducted by our own Center staff:

- Dr. David Brenner: "Center for high-throughput minimally-invasive radiation biodosimetry."
- Dr. Guy Garty: "Running a microbeam irradiator without an accelerator."
- Dr. Eric J. Hall: "1915 and all that – A brief history of the Center." This lecture was delivered in honor of the Center's 90th anniversary.
- Dr. Howard Lieberman: "Multiple roles for Rad9 in modulating genomic integrity and the consequences of radiation exposure."
- Mr. Stephen Marino: "The new accelerator at RARAF."
- Dr. Brian Ponnaiya: "Multiple approaches in studying radiation-induced bystander effects."
- Dr. Genze Shao: "Epigenetic inactivation of big-h3 gene in human cancer cell line."
- Dr. Lubomir Smilenov: "Ionizing radiation induces DNA double-stranded breaks in bystander primary human fibroblasts."
- Dr. Yuxin Yin: "An essential role of PTEN in controlling chromosome stability." ■

X-Ray Microbeam

Giuseppe Schettino

Development for the x-ray microbeam started in the early months of 2005. The present proposal is to employ Zone Plate (ZP) lenses to de-magnify to a micron or sub-micron size spot, a small x-ray source (i.e., ~100 μm) produced by bombarding a thin solid target with high-energy protons. ZP technologies are well established and commonly used in applications such as x-ray microscopy where spot size of less than 50 nm can be produced. However, due to the low ZP focusing efficiency (according to the max theoretical first order diffraction efficiency only ~20% of the total incident number of photons can be focused by a ZP) and to the limited brightness of our x-ray source (proton bombardment), the final x-ray spot size has to be compromised in order to obtain a dose rate suitable for biological experiments.

Firstly, we investigated the production of characteristic x-rays (K_α line) as a function of the proton energy for aluminum and titanium (K_α x-rays of respectively 1.45 keV and 4.5 keV). The best cross section for characteristic K_α x-ray production in thick targets is achieved respectively at 2.86 MeV for Al and 9.1 MeV for Ti.[1] The correspondent max penetration range is 75 μm for Al and 370 μm for Ti. For protons of 5 MeV (max energy achievable with the new accelerator), the Ti K_α cross-section drops to 60% of its max value and the max penetration is 135 μm. Based on such calculations, a target thickness of about 100 μm would represent an ideal initial choice. Such a thickness will assure a nearly optimum x-ray production efficiency (i.e., max energy deposited into the target by incident particles and small x-ray self-absorption), although it will result in the x-ray source elongated along the Z-axis. If zone plates are then to be used to produce the final x-ray spot, an extended depth of focus is to be expected as a result of an elongated x-ray source. This effect has been simulated using an x-ray tracing program (SHADOW) and estimated to be approximately ±10 μm with the depth of focus defined as the distance from focal point at which beam size increases by 20%. The relatively thin target will also allow us to use it in transmission mode (i.e., x-rays extracted from the side opposite to the proton bombardment) as this will better suit the present charged particle microbeam configuration (vertical alignment). The final microbeam system will allow a quick switching between charged particles (with ions directly focused into the biological samples) and soft x-rays (with protons focused earlier onto a solid target and x-rays probing the cells). A schematic illustration of the x-ray source–ZP configuration is shown in Figure 1.

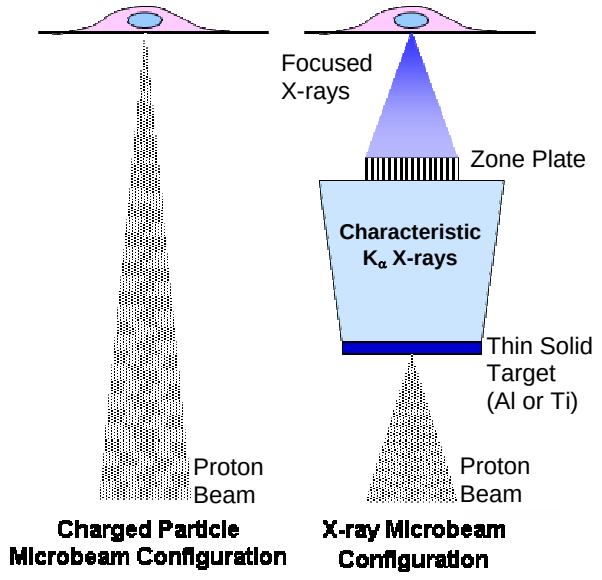

Fig. 1. Schematic illustration of the x-ray source–ZP configuration.

Assuming target thickness of 100 μm, the max power that is possible to dissipate into the target (for an extended period of time) is related to the specific design of the target and the area over which the protons are targeted (i.e., x-ray source size). Extended simulations performed using a finite element analysis (ANSYS), have provided indications of the x-ray source size and the maximum power with which it is possible to bombard the target. The final design consists of 4 thin Ti or Al foils (two foils 15 μm thick and two 30 μm thick) separated by a 5 μm gap through which cooled He is blown. Such a target is able to cope with a substantial amount of power dissipated by the proton beam as shown in Table 1.

Table 1.
Titanium target (15-30-30-15μm thick foils with 5 μm gaps; 1 cm diameter)

Source diameter [μm]	Max Total Power [W]	Current [nA]	K_α X-ray Yield	Dose rate [Gy/s]	X-ray rate [hv/s]	Spot size diameter [μm]
5	0.102	20.4	2×10^{10}	0.045	63	0.8
10	0.36	72	7.6×10^{10}	0.159	220	1.7
25	1.44	288	2.82×10^{11}	0.638	882	4.2
50	3.6	720	7.06×10^{11}	1.59	2206	8.4
100	4.26	852	8.35×10^{11}	1.89	2610	16.8

Dose rates calculated assuming a 300 μm ZP with a 5% first order efficiency placed at a distance of 30 cm from the x-ray source and 1×10^{-12} Kg for a typical cell mass.

References

1. Garcia JD, Fortner RJ, Kavanagh TM. Inner-shell vacancy production in ion-atom collisions. *Review of Modern Physics* **45**:111–75, 1973. ■

Tuning the Stand-Alone Microbeam at Columbia University

Guy Garty, Gregory J. Ross, Alan W. Bigelow, Giuseppe Schettino, Gerhard Randers-Pehrson and David J. Brenner

Introduction

The stand-alone microbeam (SAM), under development at RARAF,[1] presents a novel approach to biological microbeam irradiation studies. Foregoing a conventional accelerator as a source of energetic ions, we propose to use a small, high-specific-activity, α-emitter.[2] In addition to providing a secondary user facility at RARAF, the design is simple and inexpensive enough that the SAM can be reproduced in any large radiation biology laboratory.

SAM layout

The layout of the SAM is shown in Figure 1. At the base of the SAM is a 1 mm diameter isotopic α-particle source (^{210}Po) and a mechanical beam chopper. For tuning purposes, the source was replaced with a foil-covered aperture forming an accelerator-based beam of the same energy spectrum. This allowed the tuning to proceed at a much faster rate.

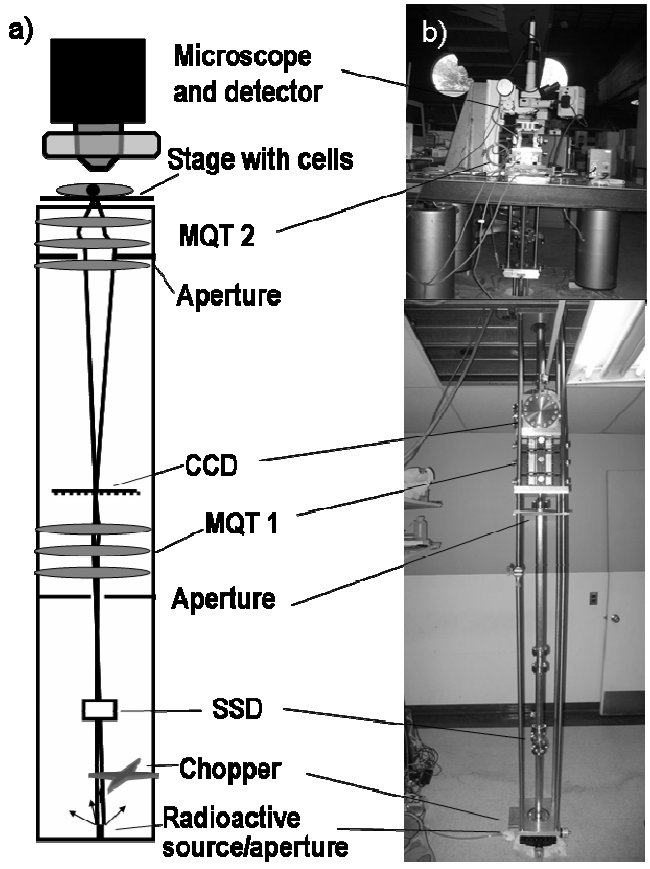

Fig. 1. a) Scheme and **b)** photo of the SAM. See text for details. The two lines in a) are theoretical predictions of the beam profile in the x and y directions.

The compound lens consists of two magnetostatic quadrupole triplets (MQT), the lower placed 2 m above the source and the second lens placed 2 m above the focal plane of the first lens and rotated by 90°. Each triplet consists of 3 sets of 4 permanent magnets on micrometric screws. The magnets can be extended or retracted in a steel yoke, forming an adjustable quadrupole.[3]

Limiting apertures are placed just before the first lens as well as between the first and second elements of the second lens to reject α-particles which have been scattered on the beam line or which possess large aberrations.

The cells to be irradiated are placed at the image plane of the second lens. Details of the microbeam end-station are given elsewhere.[4]

Beam diagnostics is performed via a retractable ion-implanted silicon detector (SSD) and a CCD chip (Kodak model KAF-402E) placed respectively before and after the first triplet. The former enables us to monitor particle energy and tune it to the lens setting. The latter allows us to check the focusing in the first triplet. The final beam size is measured at the image plane using the knife edge technique.[4]

Tuning the magnets

The RARAF accelerator was used to generate a 1 mm collimated beam, mimicking the α-particles generated by an isotopic source. This beam was used to tune the lenses, in two stages. At first we placed a commercial CCD chip at the expected focal plane of the first triplet. α-particles impinging on the CCD chip deposit electrons directly in the CCD well, resulting in a light spot in the obtained image. We have seen that the well depth in the CCD chip used was not sufficiently deep and as a result typically 4–9 pixels were illuminated by each α-particle. Furthermore, at high rates (hundreds of particles/sec) we saw ghosting, i.e., false light spots generated by α-particles hitting the CCD shift register during the readout phase. Both problems were overcome by tuning the beam to a low rate and locating, in each frame, the center of gravity of each light spot. The resulting 2D histogram is shown in Figure 2a. The optimal focusing was found by iteratively adjusting the strength of each quadrupole while monitoring the CCD image.

After the first lens was tuned to its optimal focusing, the CCD was removed. The second lens was brought to the same nominal pole tip strength and the beam spot at the image plane was optimized. During this optimization we maintained Russian symmetry of the lenses.[5] In particular we tried to keep quadrupoles 1, 3, 4 and 6 at the same strength (A) and quadrupoles 2 and 5 at the same strength (B).

Figure 2 also shows theoretical (b) and measured (c) spot

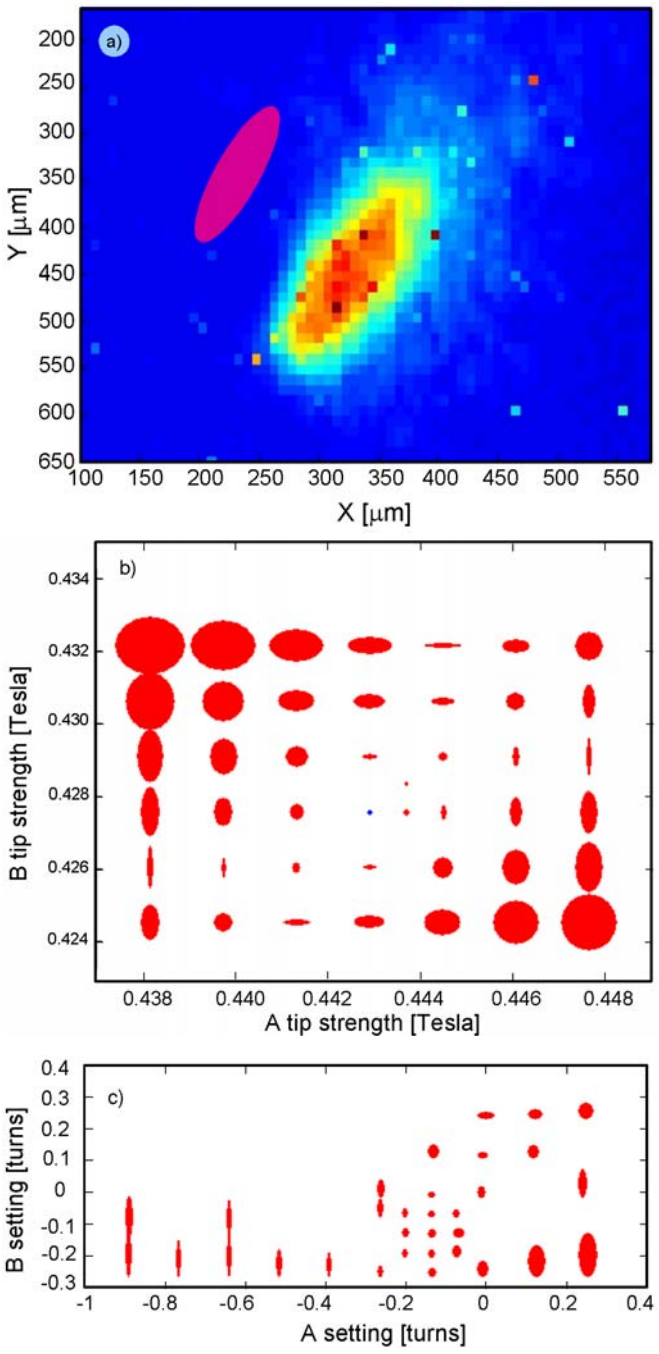

Fig. 2. a) Beam profile at the waist of the beam just above the first magnetic quadtrupole triplet, as measured on the CCD. The elipse represents the theoretical prediction of 50 × 150 μm. The tilt is due to rotation of the CCD with respect to the quadrupoles. **b)** Theoretical and **c)** measured aspect ratio and relative size of the beam at the image plane of the SAM. The axes of **c)** are in turns of the micrometric screw with each turn representing a change in pole tip strength of about 5%.

shapes at various settings in AB space. The theoretical values (Fig. 2b) were obtained by a 5th order matrix calculation using GIOS-2000,[6] and reach an optimal beam spot of 10 μm diameter. Experimentally (Fig. 2c), we have only seen a 20 μm spot reliably although we have seen indications of a 10 μm spot. The apparent discrepancy between the obtained spot size and the theoretically predicted one is probably due to residual high order moments (mostly octapoles) which were not yet completely eliminated from the lenses. Indeed, GIOS calculations show that an addition of 1% octapole moment to the quadrupoles may double the spot size. We have also seen that the spot size is extremely sensitive to the alignment of the lenses with respect to each other. It is possible that this alignment is not yet good enough.

Conclusions

We have built a microbeam irradiator based on a compound magnetostatic lens. The focusing properties agree well with those predicted by an analytical calculation using GIOS-2000. As seen from these calculations the lens is extremely sensitive to its self alignment as well as to high order moments resulting in a factor of 2 degradation of spot size over the theoretically predicted one. We expect to overcome this shortly with better alignment of the magnets and finer tuning of their strength and symmetry.

So far the SAM has only been tested with an accelerator-based beam although it has been designed around operation with a custom-made Po α-emitter. Such a source is currently under development.[2]

Once fully optimized the SAM will provide a useful secondary microbeam facility at RARAF and will enable biology to be performed in parallel with developments on the electrostatic microbeam. Based on our experience, a similar facility can be reproduced in any large radiobiology lab, although the tuning and alignment procedures are faster when an accelerator is available.

References

1. Garty G, Ross GJ, Bigelow A, Randers-Pehrson G and Brenner DJ. A microbeam irradiator without an accelerator. *Nucl Instrum Meth B* **241**:392–6, 2005.
2. Garty G, Randers-Pehrson G and Brenner DJ. Isotopic source for the Stand-Alone Microbeam. Page 13 of this annual report.
3. Gottschalk SC, Dowell DH and Quimby DC. Permanent magnet systems for free-electron lasers. In: Proceedings of the 24th International Free Electron Laser Conference and the 9th Users Workshop. *Nucl Instr Meth A* **507**:181–5, 2003.
4. Bigelow AW, Ross GJ, Randers-Pehrson G and Brenner DJ. The Columbia University Microbeam II endstation for cell imaging and irradiation. *Nucl Instr Meth B* **231**:202–6, 2005.
5. Dymnikov AD, Brenner DJ, Johnson G and Randers-Pehrson G. Theoretical study of short electrostatic lens for the Columbia ion microprobe. *Rev Sci Instr* **71**:1646–50, 2000.
6. Wollnik H, Brezina J, Berz M. Gios-beamtrace – a program package to determine optical-properties of intense ion-beams. *Nucl Instr Meth A* **258**:408–11, 1987. ■

Under-Dish Detector for the Microbeam at Columbia University

Guy Garty, Gregory J. Ross, Kevin Wu,[1] Gerhard Randers-Pehrson and David J. Brenner

Introduction

Currently the RARAF microbeam irradiator[1] delivers a precise number of particles by irradiating the sample and counting the particles traversing it, using a gas-based ionization chamber placed immediately above the cells. This dictates the use of thin samples (i.e. single cells or monolayers covered by little or no medium) and penetrating particles. With the move to thicker sample irradiations and in particular tissue irradiations,[2] it becomes necessary to be able to detect the irradiating particles *before* they enter the sample as they may be fully absorbed in it.

To this end we are currently developing a single particle detector to be placed below the sample to be irradiated. The "Lumped Delay Line Detector" (LD^2) is a non-scattering device based on a capacitive pickup detector, typically used for detection of ion clusters or highly charged ions within ion traps.[3] The LD^2 will enable single particle irradiation of thick samples (tissue for example) by sub-micron beams. It will improve the attainable spot size, since it contains no material within the beam path and therefore does not induce scattering. It will also obviate the current need for removing the medium from cells pre-irradiation.

LD^2 structure

The LD^2 detector, shown in Figure 1, consists of a 1 m long string of (300) cylindrical pickup electrodes. Each projectile particle passing through a pickup electrode induces a mirror charge, identical in magnitude and opposite in polarity to its own on the inside of the pickup electrode. The pickup electrodes are connected to each other by inductors and capacitively coupled to ground forming a lumped delay line. The capacitance of each electrode to ground can be varied by changing the geometry of the ground electrode (see below). Thus the time constant of the delay line can be matched to the velocity of the projectile and the signals from all pickup electrodes will add in phase generating a signal of ~150 electrons, sufficient for detection with current electronics.

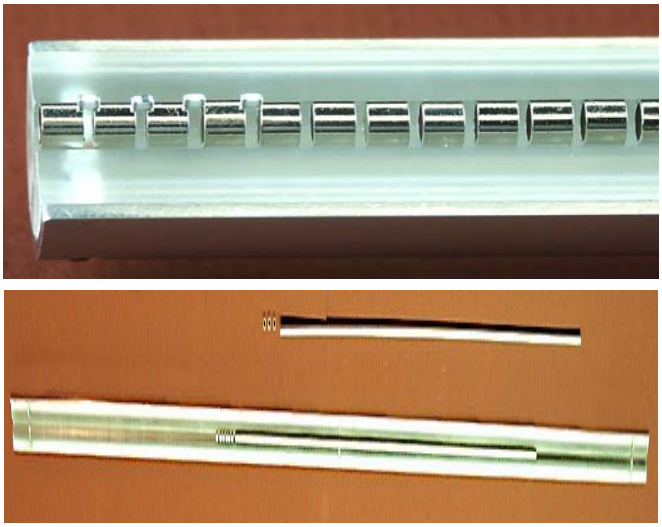

Fig. 1. Top: Close up photo of the LD^2 showing several segments and inductors. **Bottom:** Full length photo.

Tuning mechanism

Tuning of the electrode's capacitance to ground, and hence of the signal propagation velocity, is done by pivoting a grounded electrode around the pickup electrodes as shown in Figure 2. Finite element analysis simulations predict a capacitance variation between 78 and 340 fF/segment, corresponding to a twofold change in particle velocity. By an appropriate choice of inductors this can be made to span most of the available radiation fields at RARAF.

Preliminary tests

A short LD^2 prototype, containing 13 electrodes has been built and is currently undergoing tests. Figure 3 demonstrates the pulse propagation velocity obtained by measuring the time delay between a pulse injected on the

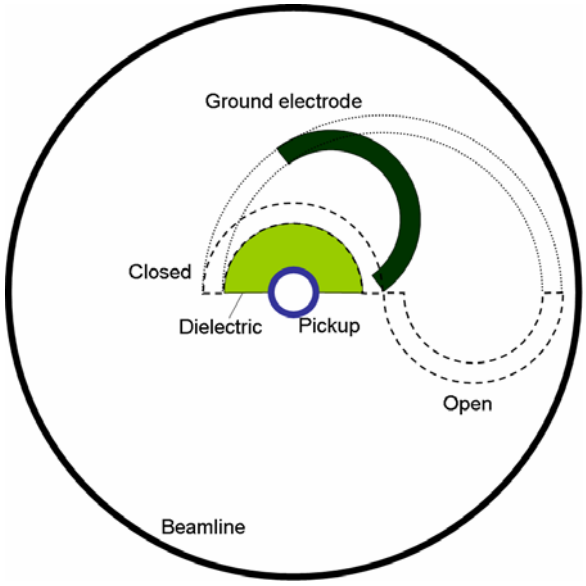

Fig. 2. The tuning mechanism. A grounded electrode is pivoted between the closed position (high capacitance) and the open position (low capacitance).

[1] *Stuyvesant High School student participating in our small group apprenticeship summer program.*

first electrode and measured on subsequent electrodes. There is a good agreement with the predicted velocity (dashed line).

The tuning mechanism is currently under tests.

References

1. Randers-Pehrson G, Geard C, Johnson G, Elliston CD and Brenner DJ. The Columbia University single-ion microbeam. *Rad Res* **156**:210–4, 2001.
2. Amundson SA and Schettino G. Isolation of RNA from Sliced 3-Dimensional Tissues. Page 24 of this annual report.
3. Pederson HB, Strasser D, Amarant B, Heber O, Rappaport ML and Zajfman D. Diffusion and synchronization in an ion-trap resonator. *Phys Rev A* **65**:042704, 2002. ■

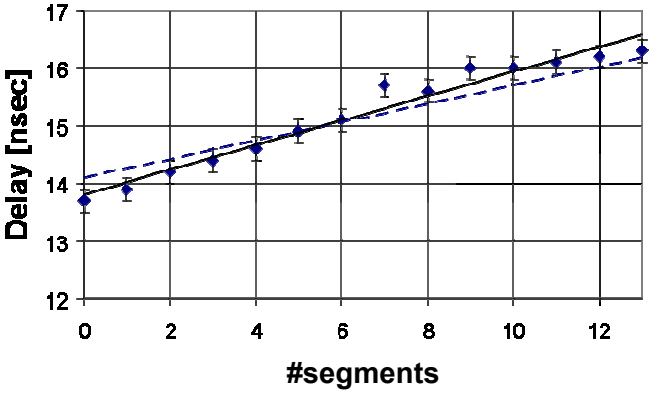

Fig. 3. The measured pulse propagation speed. The solid line is a linear fit (0.21 nsec/segment). The dashed line is the theoretical prediction (0.16 nsec/segment).

Isotopic Source for the Stand-Alone Microbeam

Guy Garty, Gerhard Randers-Pehrson and David J. Brenner

Source specification

The stand-alone microbeam (SAM)[1] necessitates the development of a compact, high intensity, radioactive source. The radioactive source must be a monochromatic α-emitter with a half-life short enough to provide sufficiently high specific activity, yet long enough to allow a few month's of operation between source replacements. The source diameter should be made as small as possible, to minimize spot size for given demagnification, and its thickness should be made as large as possible, to obtain sufficiently high activity. On the other hand, in order to limit the chromatic aberrations, due to the varying degradation of α-particles created within the source, the source must be extremely thin. We have found that ^{210}Po is ideal for this purpose, as it has a half life of 138 days and decays via a single channel (a 5.305 MeV α-particle) into a stable daughter (^{206}Pb). The specific activity of pure ^{210}Po is 4.5×10^3 Ci/g (1.7×10^{14} DPS/g). Based on SRIM as well as beam optics simulations, we have found that the optimal thickness of the source is 200 nm,[1] yielding an energy spread of 40 keV and an activity of 6.5 mCi (2.4×10^8 DPS). Using this source and the SAM layout described in reference 1, beam optics simulations predict beam flux of just over 1 α-particle/sec at the focal plane, which is sufficient for many applications of a single-particle microbeam. At this source thickness the spherical and chromatic aberrations are about the same.

Source fabrication

As such a source is not commercially available, we have designed and built a setup for electroplating ^{210}Po on the tip of a platinum wire (see Fig. 1). As an anode, we use a 1.5 ml Fabmate (graphite) crucible loaded with 1 ml of polonium solution (Isotope Product Laboratories, CA) containing the required activity. Approximately 2 V are placed between the platinum wire and the crucible, using a voltage regulated power supply. The plating setup is placed on an orbital mixer (Thermolyne RotoMix) as mixing the solution assists in preventing depletion of the Polonium from the vicinity of the cathode. The plating processes is done in a vented glove box with an active charcoal filter, as ^{210}Po may become volatile and is extremely toxic.

So far we have made several small sources (0.1 to 100 μCi). We have seen that the rate of plating is proportional to the concentration of polonium in solution. This means that the time required to plate a certain fraction of the polonium present in the solution is independent of the actual amount plated. We therefore expect that a source of any size can be made within 24 hours of plating. A 6.5 mCi source has not yet been produced.

References

1. Garty G, Ross GJ, Bigelow A, Randers-Pehrson G and Brenner DJ. A microbeam irradiator without an accelerator. *Nucl Instr Meth B* **241**:392–6, 2005. ■

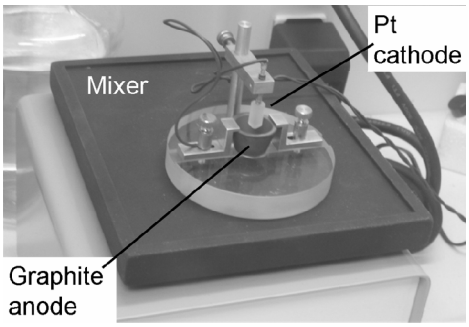

Fig. 1. Setup for electroplating ^{210}Po on the tip of a platinum wire.

Incorporating No-stain Imaging into the Columbia University Microbeam Endstation

Gregory J. Ross, Brian Ponnaiya, Gerhard Randers-Pehrson, Alan W. Bigelow and David J. Brenner

Introduction

Two techniques for rapid location and targeting of cells for microbeam irradiation without use of stain have been fully integrated into the microbeam endstation and have undergone continued testing.[1] They are: 1) Quantitative Phase microscopy and 2) an interim, test-version of a novel immersion-based Mirau interferometry lens. Both approaches accomodate our requirement of using reflected light microscopy due to the location of the incoming ion beam.[2]

Quantitative Phase Microscopy

Software-based Quantitative Phase microscopy (QPm) is now available for use in the Columbia microbeam laboratory as a non-interferometric approach to no-stain imaging. Reflected light-based images are now routinely obtained in focus and with focus set slightly above and below the sample plane. These images are then used to approximately solve the light transport equation using the fourier transform-based software from Iatia.[3,4] The results are used to create a new 2-d map of the sample which is then fed back into the custom microbeam irradiation software. By streamlining the control program, including interleaving the image processing steps with the mechanical motions of the stage, the additional processing time required to convert the raw images into QPm images can be reduced such that it affects throughput by only a factor of about 10%. We are working with Iatia to improve this processing time by taking full advantage of the on-board dual processing, which will cut this factor in half.

In some of the tests, some cells have been missed and also there have been false positives. In general, the quality of the images can be improved by carefully optimizing tuning of the parameters for the approximate solution to the transport equation. However, to optimize for our regular, automated use, there is still work to be done in eliminating false cells and reducing missed cells. Figure 1 shows two different examples. In the first example, there would be no missed cells or false positives in the automatic cell locating routines. In the second example, the imaging routines have trouble locating the cells properly. Several variables have been isolated and eliminated as causes: plating time, cell-type, cell phase, light color, cell growth surface, amount of medium (depth), percent of medium vs. buffer, and use of a cover glass. Continued efforts are aimed at finding a combination of these variables that may affect the images and at exploring other variables that have not yet been considered.

Phase-shifting interferometry

The immersion-based Mirau interferometric (IMI) objective is currently under construction (Fig. 2) and has been designed to function as an immersion lens with standard interferometric techniques using a short coherence length[1] and to otherwise accommodate the endstation requirements for the Columbia University microbeam at RARAF. The preliminary results in-air on 10 μm polystyroid beads[1] were sufficiently encouraging to warrant the efforts to design the new objective. As part of the testing for the design process we modified an off-the-shelf Mirau

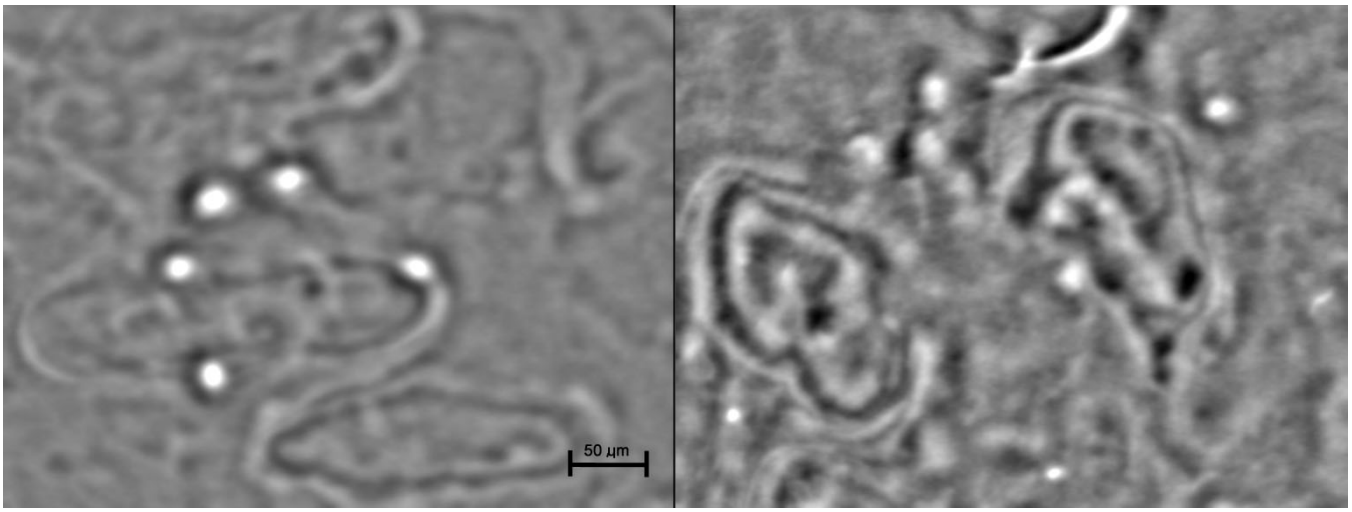

Fig. 1. Left: QPm image taken of normal human dermal fibroblasts under conditions conducive to rapid, automatic cell location. **Right:** QPm image taken under conditions which incur false positives and missing cells when used for rapid, automatic cell location.

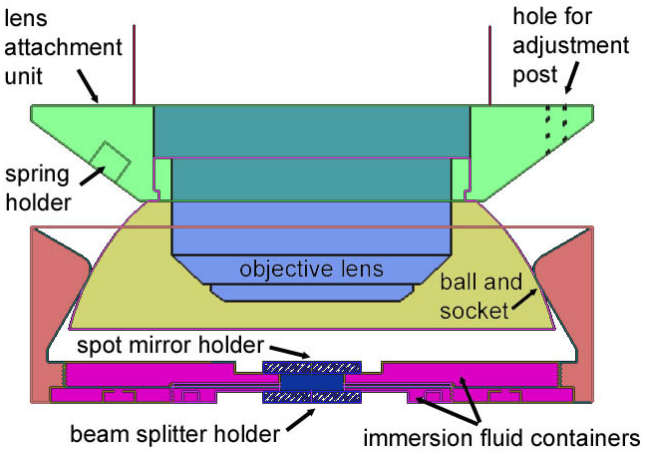

Fig. 2. Drawing of the immersion-Mirau device under construction.

objective such that it became a water immersion lens, and we confirmed that the two equal-arm light pathways will indeed be restored and will then provide interference fringes in the environment with sufficient contrast to perform the biological experiments.

Figure 3 shows preliminary results from the modified objective and confirms that the contrast will be sufficient to merit completing construction of the final objective. The finished objective is expected to support rapidly and automatically locating the cell nuclei under the no-stain scenario. The "banding" in some of the examples shows that further work must be done to eliminate both a slow drift in z-position and some very slight vibrational interference.

Competing solutions

While it is possible that we ultimately will keep both forms of no-stain imaging in the endstation, QPm and IMI are being evaluated in competition with each other. Under consideration are: processing time, reliability, maintenance, and ease of use for the experimenter. IMI is slightly faster in the endstation under regular use than QPm and both are acceptable. QPm is likely to be improved so they will score about the same. Immersion-Mirau interferometry, by judging the preliminary images, is much more reliable than QPm at this stage. QPm is a software solution and does not require introduction of fluids or cleaning, whereas IMI does. QPm does not require any additional equipment and can work in air, while the immersion-Mirau interferometer requires the end-user to use a custom objective and an immersion-based approach. It appears likely that the immersion-Mirau approach will ultimately be favored, but additional work will be done especially on the QPm reliability.

Conclusions

Two techniques for no-stain imaging are under testing. Final construction of the full immersion-Mirau lens will enable a permanent installation for regular use in biological experiments at the endstation without the need for stain. Further development on the QPm approach may yet reveal that it becomes the favored mechanism for no-stain imaging. Either approach will cause the experimenter to incur up to a 10% increase in sample-dish processing time.

References

1. Ross GJ, Bigelow AW, Randers-Pehrson G, Peng CC, and Brenner DJ. Phase-based cell imaging techniques for microbeam irradiations. *Nucl Instrum Meth B* **241**:387–91, 2005.
2. Randers-Pehrson G, Geard CR, Johnson G, Elliston CD and Brenner DJ. The Columbia University single-ion microbeam. *Radiat Res* **156**:210–4, 2001.
3. Barty A, Nugent KA, Paganin D and Roberts A. Quantitative optical phase microscopy *Optics Letters* **23**:817–819, 1998.
4. Barone-Nugent ED, Barty A and Nugent KA. Quantitative phase-amplitude microscopy I: optical microscopy. *J Microsc* **206**:194–203, 2002. ■

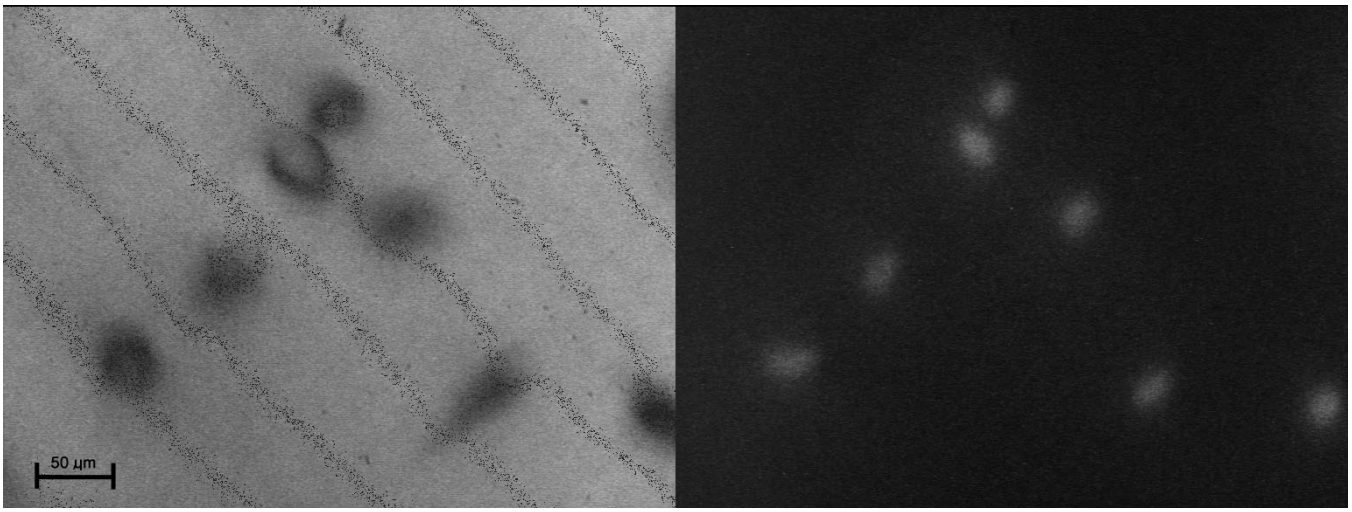

Fig. 3. Left: Left: Preliminary IMI image of normal human dermal fibroblasts taken with the interim immersion-Mirau lens and a neutral density microscope cube. Right: Same sample with a UV cube to reveal the nuclear stain.

Multiphoton Microscope Design for the Columbia University Microbeam II Endstation

Alan W. Bigelow, Gregory J. Ross, Gerhard Randers-Pehrson and David J. Brenner

At the Radiological Research Accelerator Facility (RARAF), we are developing a multiphoton microscope at the endstation of our single-cell single-particle microbeam irradiator for detecting and observing the short-term molecular kinetics of radiation response in living cells. A multiphoton microscope is an infrared laser-based, 3D, minimally damaging imaging tool that, when compared to conventional confocal microscopy, has greater penetration depth and reduced phototoxicity and photobleaching in the sample bulk.[1] The guiding principle of the multiphoton microscope is: when two photons are spatially and temporally coincident within the excitation cross-section of a fluorophore molecule, they can act as one photon with twice the energy to induce an electronic transition.

Our multiphoton microscope design incorporates our current cell-imaging platform, a Nikon Eclipse E600-FN research fluorescence microscope. This Nikon microscope was modified to function over a vertical ion beam; the base was removed from the microscope, which was mounted to a pivot arm for switching between on-line and off-line positions. To improve the kinetic mount for the microscope, a new pivot arm has been designed with a spring-loaded ball and socket connection at the pivot point.

The excitation light source is a Chameleon (Coherent Inc.) tunable titanium sapphire laser that provides 140 fs pulses at a 90 MHz repetition rate. In obtaining our laser an extensive evaluation was made between two similar one-box Titanium Sapphire laser systems: the Chameleon made by Coherent Inc., and the Mai Tai made by Spectra Physics. After comparing the laser specifications and after consulting references from both companies, our conclusion was that either laser would work well for our application. Slight advantages that swayed our decision to purchase the Chameleon were: 1) superior user feedback, 2) a manual control mode in addition to a computer control interface, 3) Coherent's favorable "Advanced Replacement Service Strategy," 4) an internal spectrometer instead of a Look Up Table to monitor the lasing frequency, and 5) a user-friendly diode replacement process.

Along the incident laser beam path shown in Figure 1, a waveplate and polarized beam splitter are placed in the beam path to control the laser beam power. Mirrors direct the laser up through the microscope pivot shaft and into a scan head. A scan lens then focuses the scanned laser beam to a point in an image plane for the microscope (a CCD camera is also placed at such an image plane for fluorescent microscopy). The incident light path continues through the side of the trinocular tube where a retractable mirror directs the laser beam down through the tube lens and the objective lens to a focal point within a specimen. The scanned laser establishes

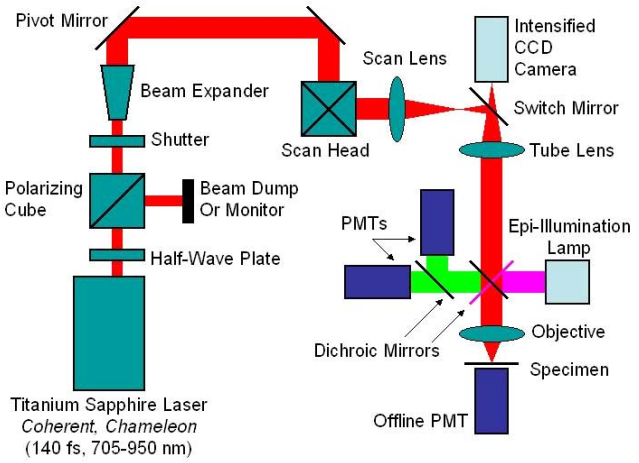

Fig. 1. Diagram of the multiphoton microscope and optics path. See the text for more details.

an optical cross section within the specimen, where multiphoton absorption preferentially occurs. Wavelengths available from our titanium sapphire laser can penetrate to depths of about 100 microns in a biological sample by varying the Z-position of the specimen stage. Returning along the collection pathway, light emitted from the specimen is selectively deflected by a series of dichroic mirrors to an array of photomultiplier tubes (PMTs). An additional PMT for transmitted light collection is available for the microscope in the off-line position. Images are constructed through comparing PMT signal to scan head position.

For control of our multiphoton microscope, we are adopting Karel Svoboda's design from Cold Spring Harbor. Svoboda's control software, ScanImage,[2] runs in the MatLab platform and was obtained through an Internet download. Continuing with these suggestions, we have purchased the recommended multifunction DAQ device (NI-6110, National Instruments) and its break-out box. Tests for scanning voltage waveforms were successful and the microscope assembly process continues.

References

1. Denk W, Strickler JH and Webb WW. Two-photon laser scanning fluorescence microscopy. *Science* **248**:73–6, 1990.
2. Pologruto TA, Sabatini BL and Svoboda K. ScanImage: flexible software for operating laser scanning microscopes. *Biomed Eng Online* **2**:13, 2003. ■

Further Studies of a Low LET Radiation-Induced Bystander Effect in a 3-Dimensional Cell Cluster Model

Rudranath Persaud, Hongning Zhou, Sarah E. Baker, Tom K. Hei and Eric J. Hall

This study involved a three-dimensional cell culture model composed of a mixture of human-hamster hybrid (A_L) and Chinese hamster ovary (CHO) cells. The CHO cells were labeled with tritiated thymidine and mixed with A_L cells before being centrifuged briefly to produce a "cluster" of 4×10^6 cells, as illustrated in Figure 1.

Clusters were incubated overnight, resuspended into single cell suspensions, and passed twice through MACS separation columns to produce two independent cell populations. The A_L fraction was plated for a 7-day expression period and subsequently subjected to the CD59 Antibody-Complement Cell Lysis Mutation Assay. These cells never incorporated the radioactive material, but were in close contact with cells that did. They constitute, therefore, a bystander population.

Role of reactive oxygen species in bystander mutagenesis

To determine whether reactive oxygen species contribute to bystander mutagenesis resulting from low LET exposure, the radical scavenger DMSO was incorporated into the clusters. As shown in Figure 2, 0.2% DMSO was not cytotoxic and nonmutagenic to the A_L cells. However, when DMSO was incorporated into the cells in the cluster and maintained throughout the incubation period, the bystander mutation frequency was reduced to about half. These data indicated that free radicals, mainly hydroxyl radicals, participate in the pathway leading to bystander mutagenesis.

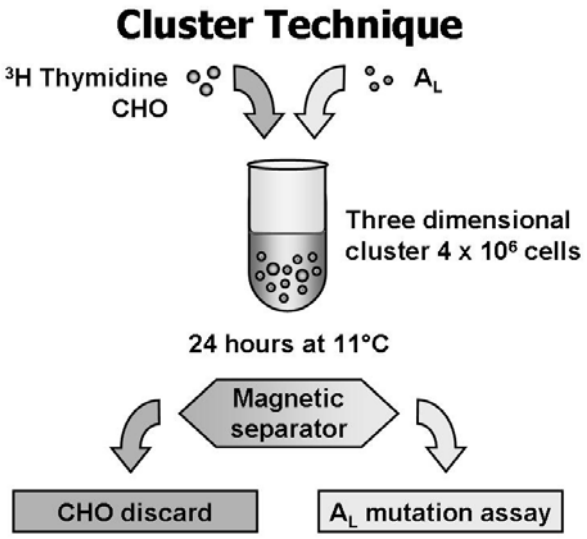

Fig. 1. CHO cells incorporating tritiated thymidine are mixed with A_L cells and centrifuged to form a three-dimensional cluster. Following overnight incubation, the two cell types are separated. The fraction of A_L cells showing a mutation is assessed using a standard assay.

Role of cell-to-cell communication in bystander mutagenesis

When experiments were repeated with connexin 43-deficient A_L cells, the bystander effect was essentially eliminated, as shown in Figure 3. This demonstrates the central role of gap-junction communication in the bystander effect.

In summary, the present study provides evidence that low LET electrons in directly labeled cells can illicit a mutagenic response in neighboring cells, that the signaling pathway involves reactive oxygen species and that gap junction communication is important. It appears that all of the basic features of the bystander effect characteristic of α-particles and cell monolayers are also true for low LET β-rays in a three-dimensional cluster model. ■

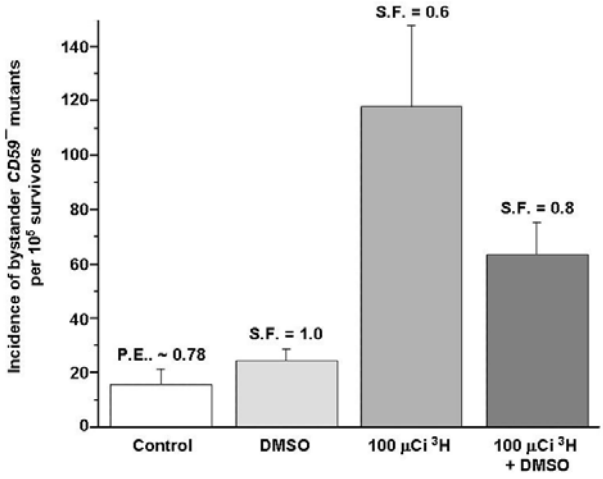

Fig. 2. Scavenging free radicals greatly reduces the magnitude of the bystander effect.

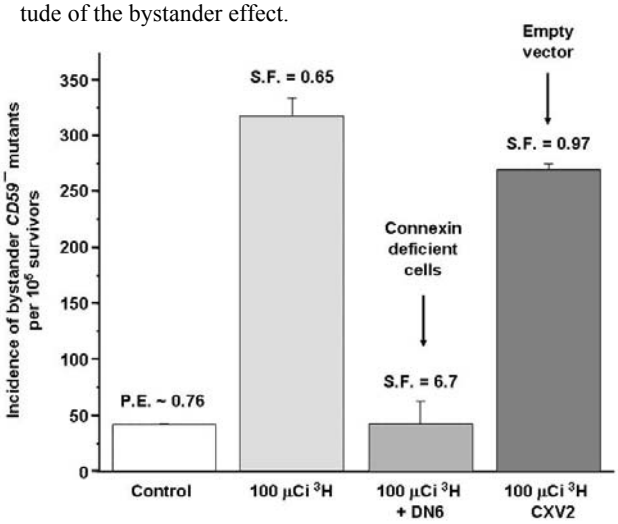

Fig. 3. If the A_L cells are connexin deficient, the bystander effect is eliminated.

Mechanism of Radiation-Induced Bystander Effect: Role of the Cyclooxygenase-2 Signaling Pathway

Hongning Zhou, Vladimir N. Ivanov, Joseph Gillespie and Tom K. Hei

Ionizing radiation is a well established human carcinogen. Established dogma has relied on the assumption that DNA of the nucleus is the main target for radiation induced genotoxicity and carcinogenesis. However, evidence accumulated over the past decade has indicated that both extranuclear targets and extracellular events may play an important role in determing the biological responses to ionizing radiation.[1-4] A major paradigm shift in radiation biology in the last decade has resulted from work involving the bystander effect,[5,6] which could have important impact on our thinking as well as immediate application in radiation protection.

Although bystander effects have been well described over the past decade, the mechanisms of the process remain unclear. In sub-confluent cultures, there is evidence that reactive oxygen species (ROS), nitric oxide, and cytokines such as TGFβ are involved in mediating the process.[7-9] On the other hand, gap junction-mediated cell-cell communications have been shown to be critical in mediating bystander effects in confluent cultures of either human[10] or rodent cells.[2,11] It is likely that a combination of pathways involving both primary and secondary signaling processes is involved in producing a bystander process.

Radiation-induced bystander effects have clear implications for low-dose radiation risk assessment. A better understanding of the cellular and molecular mechanisms of the phenomenon will allow us to formulate a more accurate assessment of the health effects of low doses of ionizing radiation.

In the present studies, the newly designed strip mylar dishes were used. Briefly, two concentric stainless steel rings were fitted with mylar bottoms with the outer and inner rings covered by a 6 μm- and 38 μm-thick mylar sheet, respectively. The thicker mylar sheet of the inner ring was sliced into strips. Exponentially growing normal human lung fibroblast (NHLF) cells were plated in the concentric strip dishes three days before irradiation to ensure a confluent state. Since the fibroblasts seeded on the 38 μm thick mylar strips would not be irradiated due to the short penetrating distance of the α-particles, these cells would effectively become the bystander cells, being seeded right next to the cells plated on the 6 μm mylar dishes that were directly irradiated. A 50 cGy dose of α-particles (120 keV/μm) was delivered to the NHLF cells using the 4 MV van de Graff accelerator at the Radiological Research Accelerator Facility of Columbia University, as previously described.[2,11-14] After irradiation, at selected time points, the inner and outer mylar dishes were separated and the cells from each growth surface were trypsinized and individually pooled for endpoint analysis. Figure 1 shows the cytotoxicity and mutagenesis at the *HPRT* locus for primary human lung fibroblasts that are either directly irradiated (seeded on the 6 μm mylar) or are bystander cells (seeded in the 38 μm mylar). Consistent with our previous findings, NHLF irradiated with a 0.5 Gy dose of α-particles resulted in a survival level of 0.21 ± 0.07 and a mutant fraction of 8.4 ± 2.2 mutants per 10^6 survivors. In contrast, the non-irradiated bystander cells showed a reduced surviving fraction of 0.76 ± 0.11, a level that was significantly different from the non-treated controls ($p < 0.05$). Similarly, non-irradiated bystander NHLF showed increased

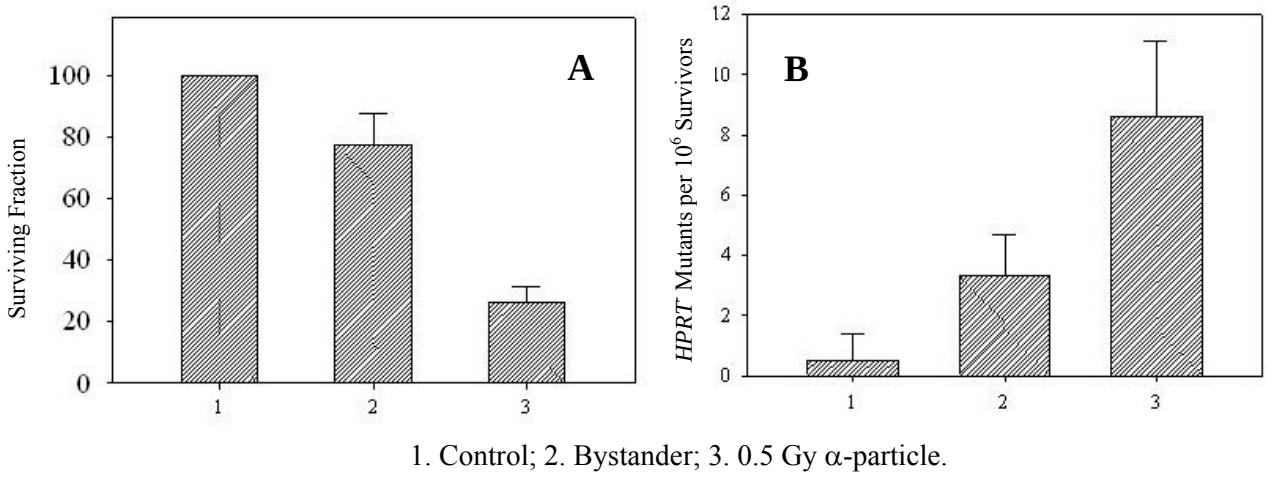

Fig. 1. Survival fraction **(A)** and *HPRT*⁻ mutations **(B)** in bystander and directly irradiated cells. Cultures were irradiated with a 0.5 Gy dose of α-particle radiation using the striped dishes. Data are pooled from six to eight independent experiments. Bars represents ± standard deviation (SD).

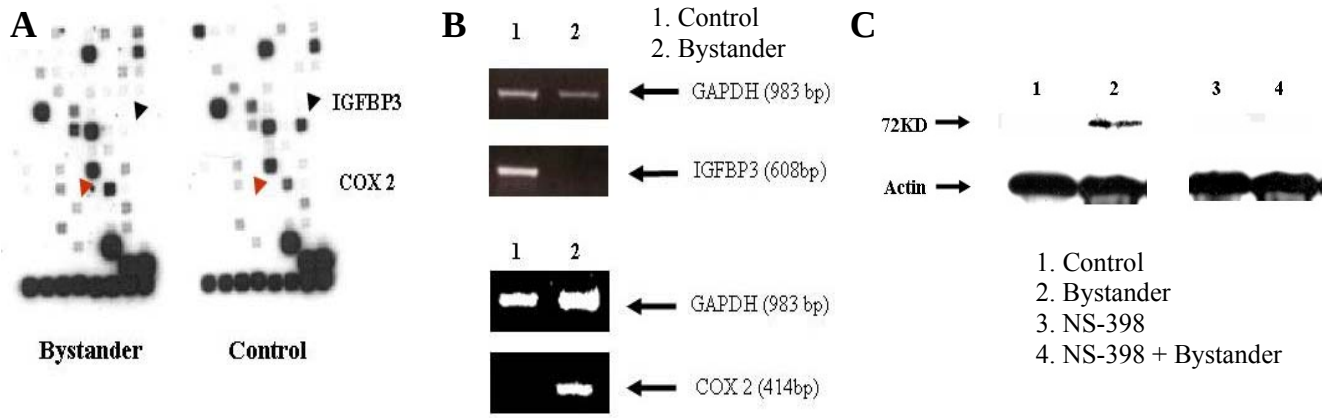

Fig. 2. A) Differentially expressed signaling genes in bystander and control normal human lung fibroblasts using the cDNA signal transduction pathway finder array (SuperArray). **B)** RT-PCR analysis and confirmation of the array data showing down-regulation. **C)** Western blotting of COX-2 protein in bystander and control cells with or without treatment with NS 398 (50 μM), a specific COX-2 inhibitor.

HPRT mutagenesis (3.2 ± 1.4 mutants per 10^6 survivors) at a level significantly higher than the background mutant fraction of 0.4 ± 1.1 ($p < 0.05$).

Using a signal transduction pathway specific SuperArray, we compared the differentially expressed genes among the non-irradiated control NHLF cells and the bystander cells (Fig. 2A). Among the 96 genes represented on the platform, the transcription level of one gene, cyclooxygenase-2 (*COX-2*), was found to be consistently up-regulated by more than three-fold, while the RNA level of insulin growth factor binding protein-3 (*IGFBP3*) was found to be consistently lower by more than seven-fold in multiple analyses of multiple bystander samples. Semi-quantitative reverse transcription (RT) PCR was used to confirm the expression levels of these two genes using the expression level of the glyceraldehyde 3-phosphate dehydrogenase (*GAPDH*) gene as an internal control (Fig. 2B). Expression of the COX-2 protein in the non-irradiated bystander cells was further confirmed by Western blotting (Fig. 2C). Addition of the COX-2 inhibitor NS-398 (50μM) suppressed the COX-2 level in NHLF cells. After 24 hours, the COX-2 protein in bystander cells was reduced to a non-detectable level (lane 2 versus lane 4). These results indicated that expression of *COX-2* is associated with the bystander effect. Since the *COX-2* gene plays an important role in arachidonic acid metabolism, the discovery is consistent with the finding that TGFβ may be linked to the bystander signaling cascade.[8]

If the *COX-2* gene is causally linked to the bystander signaling pathways, it should be possible to modulate the bystander response using a specific inhibitor of the COX-2 enzymatic activity. Figure 3 shows the effect of a non-cytotoxic and non-mutagenic dose of NS-398, a specific inhibitor of COX-2 activity, on bystander mutagenesis at the *HPRT* locus in NHLF cells irradiated with a 0.5 Gy dose of α-particles using the track segment beam. NHLF cells showed a bystander mutagenic yield of ~4.2 ± 1.2 mutants per 10^6 survivors. In contrast, in cultures co-treated with NS-398 (50 μM) that did not increase the spontaneous mutant yield by itself, the bystander mutant fraction was reduced by more than six-fold to a level of ~0.7 ± 0.2 mutants per 10^6 survivors. Although NS-398 treatment was able to reduce the *HPRT*$^-$ mutant fraction in the directly irradiated population as well, the magnitude of suppression, from 9.2 ± 3.5 to 5.9 ± 2.2 mutants per 10^6 survivors was only 36%. Similar findings were also obtained using cytotoxicity as an endpoint (data not shown).

Insulin growth factor and other cytokines activate the MAPK signaling cascade; and activation of ERK by phosphorylation is a critical upstream event preceding *COX-2* expression. Determination of ERK activity by Western blot analysis demonstrated strong up-regulation of phospho-ERK levels in both α-irradiated and bystander NHLF four hours after treatment (Fig. 4A). Increased levels of phospho-ERK could even be detected 16 hours after treatment, indicating a persistent response to the bystander signaling (data not shown). In contrast, activity of MAPK p38 kinase was found to be increased four hours after treatment (Fig. 4A) and was not detectable 16 hours after irradiation (data not shown). It should be noted that when compared with the controls, the

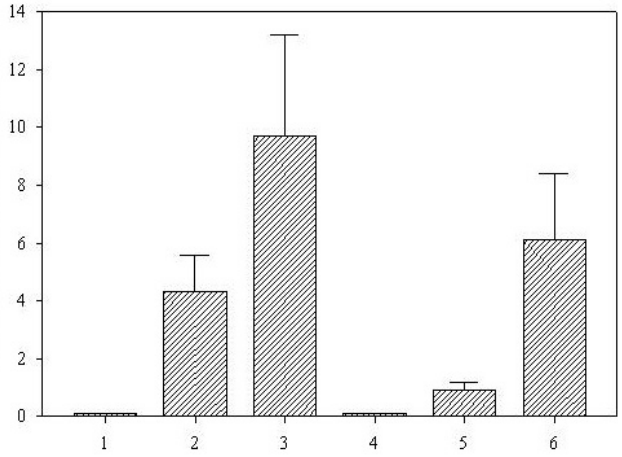

Fig. 3. Effect of NS 398 treatment (50 μM, 24 hr before and maintained overnight after irradiation), a specific COX-2 inhibitor, on *HPRT*$^-$ mutant fractions of NHLFs. Data are from three to four independent experiments. Error bars represent ± SD.

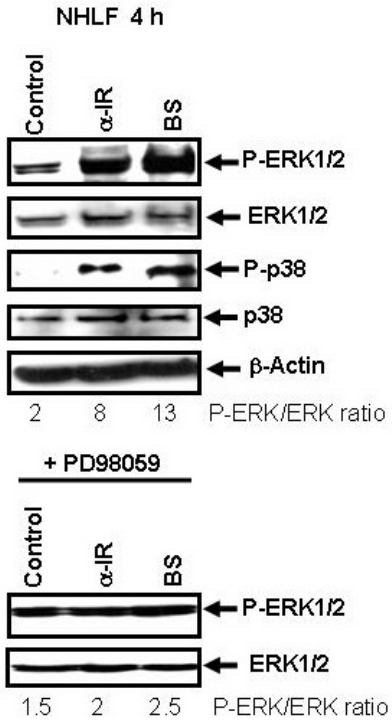

Fig. 4. Activation of the MAPK signaling pathways is involved in the radiation-induced bystander effects. Western blot analysis of phospho-ERK1/2, total ERK1/2, phospho-p38 and total p38 expression in control, α-irradiated and bystander NHLF cells four hours after irradiation with a 0.5 Gy dose of α-particles plated in striped dishes (**top panel**). β-actin was used as a loading control. Phospho-ERK /ERK ratio is indicated. PD98059 (50 μM), an inhibitor of MEK-ERK, was added to the cultures immediately after irradiation (**bottom panel**).

ratio of phosphorylated ERK over native ERK increased from 2 to 13 among the bystander cells. To further confirm the activation of ERK in bystander cells, we used PD98059 (50 μM), a specific inhibitor of MEK-ERK, which had been added to cell cultures immediately after irradiation for a period of four hours. In the presence of PD98059, the phosphorylated form of ERK and its activation were suppressed in both alpha particle irradiated and bystander cells (Fig. 4B).

If activation of the MAPK signaling cascade and ERK phosphorylation are essential in mediating the bystander effect, it should be possible to mitigate the later response by using a specific inhibitor of the MEK-ERK signaling cascade. Figure 5 shows the bystander toxicity in the presence or absence of a non-cytotoxic dose of PD98059 (50 μM) when added to cultures immediately after irradiation for a period of four hours as described above. The surviving fraction of the bystander cells was 0.72 ± 0.1 and treatment with PD98059 increased survival significantly to almost control level, 0.95 ± 0.12 ($p < 0.05$).

These results provide evidence that the COX-2 signaling pathway, which is essential in mediating a cellular inflammatory response, may be a critical signaling event for producing a bystander effect.

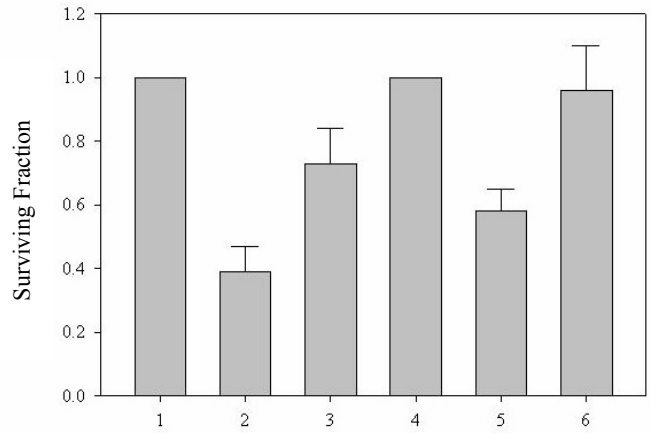

1. Control; 2. 0.5 Gy α-particle; 3. Bystander; 4. PD 98059; 5. PD 98059 + α-particle; 6. PD 98059 + Bystander

Fig. 5. Effect of PD98059 (an inhibitor of MEK-ERK, 50 μM) added immediately after and maintained overnight after irradiation), on surviving fractions of control, directly irradiated and bystander NHLF cells. Data are from three independent experiments. Error bars represent ± standard deviations (SD).

References

1. Nagasawa H and Little JB. Induction of sister chromatid exchanges by extremely low doses of alpha-particles. *Cancer Res* **52**:6394–6, 1992.
2. Zhou H, Suzuki M, Randers-Pehrson G, Vannais D, Chen G, Trosko JE, Waldren CA and Hei TK. Radiation risk to low fluences of alpha particles may be greater than we thought. *Proc Natl Acad Sci U S A* **98**:14410–5, 2001.
3. Azzam EI, De Toledo SM, Spitz DR and Little JB. Oxidative metabolism modulates signal transduction and micronucleus formation in bystander cells from alpha-particle-irradiated normal human fibroblast cultures. *Cancer Res* **62**:5436–42, 2002.
4. Hickman AW, Jaramillo RJ, Lechner JF and Johnson NF. Alpha-particle-induced p53 protein expression in a rat lung epithelial cell strain. *Cancer Res* **54**:5797–800, 1994.
5. Morgan WF. Non-targeted and delayed effects of exposure to ionizing radiation: I. Radiation-induced genomic instability and bystander effects in vitro. *Radiat Res* **159**:567–80, 2003.
6. Little JB. Genomic instability and bystander effects: a historical perspective. *Oncogene* **22**:6978–87, 2003.
7. Mothersill C and Seymour CB. Cell-cell contact during gamma irradiation is not required to induce a bystander effect in normal human keratinocytes: evidence for release during irradiation of a signal controlling survival into the medium. *Radiat Res* **149**:256–62, 1998.
8. Iyer R, Lehnert BE and Svensson R. Factors underlying the cell growth-related bystander responses to alpha particles. *Cancer Res* **60**:1290–8, 2000.
9. Matsumoto H, Hayashi S, Hatashita M, Ohnishi K, Shioura H, Ohtsubo T, Kitai R, Ohnishi T and Kano E.

Induction of radioresistance by a nitric oxide-mediated bystander effect. *Radiat Res* **155**:387–96, 2001.
10. Azzam EI, de Toledo SM and Little JB. Direct evidence for the participation of gap junction-mediated intercellular communication in the transmission of damage signals from alpha -particle irradiated to nonirradiated cells. *Proc Natl Acad Sci U S A* **98**:473–8, 2001.
11. Mitchell SA, Randers-Pehrson G, Brenner DJ and Hall EJ. The bystander response in C3H 10T1/2 cells: the influence of cell-to-cell contact. *Radiat Res* **161**:397–401, 2004.
12. Zhou H, Randers-Pehrson G, Waldren CA, Vannais D, Hall EJ and Hei TK. Induction of a bystander mutagenic effect of alpha particles in mammalian cells. *Proc Natl Acad Sci U S A* **97**:2099–104, 2000.
13. Ponnaiya B, Jenkins-Baker G, Bigelow A, Marino S and Geard CR. Detection of chromosomal instability in alpha-irradiated and bystander human fibroblasts. *Mutat Res* **568**:41–8, 2004.
14. Sawant SG, Randers-Pehrson G, Geard CR, Brenner DJ and Hall EJ. The bystander effect in radiation oncogenesis: I. Transformation in C3H 10T1/2 cells in vitro can be initiated in the unirradiated neighbors of irradiated cells. *Radiat Res* **155**:397–401, 2001. ■

Radiation-Induced Genomic Instability in Bystander Cells

Hongning Zhou, Shenbing Gu, and Tom K. Hei

There is considerable evidence that exposure to ionizing radiation may induce a heritable, genomic instability that leads to a persisting increased frequency of genetic and functional changes in the non-irradiated progeny of a wide variety of irradiated cells. Genomic instability is measured as chromosomal alterations, micronucleus formation, gene mutations, and decreased plating efficiency.[1-3] During the last decade, numerous studies have shown that radiation could induce a bystander effect in non-irradiated neighboring cells; similar endpoints were used as in genomic instability studies.[4,5] Both genomic instability and the bystander effect are phenomena that result in a paradigm shift in our understanding of radiation biology. In the past, it seemed reasonable to assume that the direct deposition of energy, by a charged particle crossing a cell nucleus, led to the production of single- and double-strand breaks in DNA, which are the basis for most radiation effects. It turns out that biology is not as simple as this.

Genomic instability and the bystander effect have one thing in common, namely that both involve nontargeted effects in unirradiated cells, exhibiting responses typically associated with direct radiation exposure, but occurring in one case in the progeny of irradiated cells and in the other case in the close neighbors of irradiated cells. In addition to this similarity, there is some evidence that they share a common mechanism; for example, a recent review article[5] makes a compelling case that both result from an inflammatory-type response to radiation-induced stress and injury. Although there is indication that genomic instability may occur in the progeny of bystander cells,[6-8] more evidence is still needed to establish this phenomenon.

Using the Columbia University charged particle microbeam and the highly sensitive A_L cell mutagenic assay, we reported previously that cells lethally irradiated with α-particles could induce mutagenesis in neighboring cells not directly hit by the particles.[9] These observations have been extended to cells traversed by a single α-particle, and it was seen that gap junction mediated cell-cell communication played an important role in mediating the process of bystander mutagenesis.[10] In the present study, 10% of the A_L cells were lethally irradiated with 30 α-particles to ensure that all irradiated cells are going to be killed by radiation. After overnight incubation, the bystander cells were replated in dishes for formatting the colonies that were picked up and expanded for further investigation. The experiments were conducted for 6 consecutive weeks to assess the plating efficiency and mutation frequency.

The preliminary results indicated that no significantly decreased plating efficiency in bystander colonies to compared with their parallel control was observed (Fig. 1). However, in the first two weeks, increased mutation frequency was observed in bystander colonies ($p<0.05$); these differ-

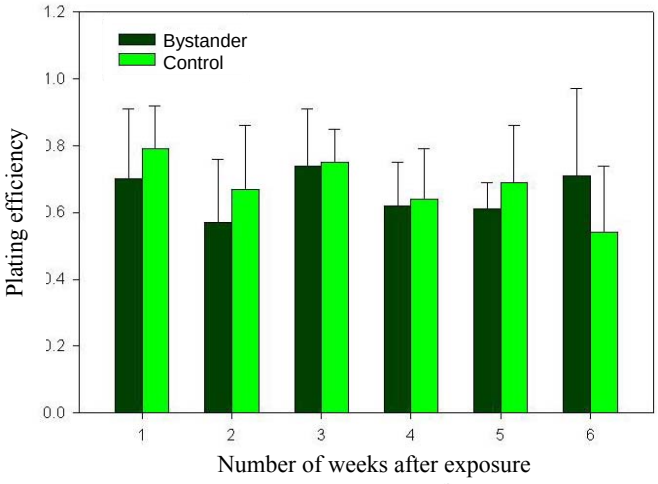

Fig. 1. Plating efficiency of bystander colonies and their parallel controls. Data are pooled from 15–17 colonies. Bars represent ± standard deviation (SD).

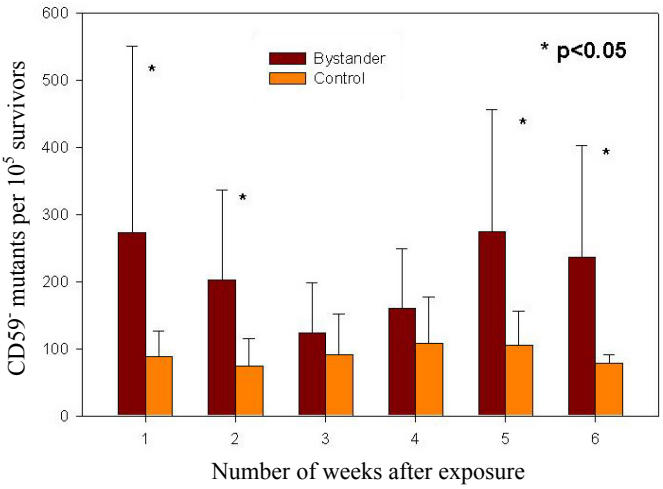

Fig. 2. *CD59*⁻ mutation frequency in bystander colonies and their parallel controls. Data are pooled from 15–17 colonies. Bars represent ± standard deviation (SD).

ences were decreased and became insignificant in the following two weeks before the significant difference reappeared in week 5 and 6 after radiation (Fig. 2). Further experiments are on going to confirm this interested finding.

Defining the bystander effect and genomic instability both contribute to our better understanding of radiation biology by allowing us to determine mechanisms of the biological effects of low doses. If phenomena demonstrated *in vitro* are applicable *in vivo*, then genomic instability and bystander effects imply that a linear extrapolation of risks from high to low doses may underestimate rather than overestimate low-dose risks.

References

1. Morgan WF. Non-targeted and delayed effects of exposure to ionizing radiation: I. Radiation-induced genomic instability and bystander effects in vitro. *Radiat Res* **159**:567–80, 2003.
2. Lorimore SA, Coates PJ and Wright EG. Radiation-induced genomic instability and bystander effects: inter-related nontargeted effects of exposure to ionizing radiation. *Oncogene* **22**:7058–69, 2003.
3. Lorimore SA and Wright EG. Radiation-induced genomic instability and bystander effects: related inflammatory-type responses to radiation-induced stress and injury? A review. *Int J Radiat Biol* **79**:15–25, 2003.
4. Little JB. Genomic instability and bystander effects: a historical perspective. *Oncogene* **22**:6978–87, 2003.
5. Hall EJ and Hei TK. Genomic instability and bystander effects induced by high-LET radiation. *Oncogene* **22**:7034–42, 2003.
6. Lorimore SA, Kadhim MA, Pocock DA, Papworth D, Stevens DL, Goodhead DT and Wright EG. Chromosomal instability in the descendants of unirradiated surviving cells after alpha-particle irradiation. *Proc Natl Acad Sci U S A* **95**:5730–3, 1998.
7. Watson GE, Lorimore SA, Macdonald DA and Wright EG. Chromosomal instability in unirradiated cells induced in vivo by a bystander effect of ionizing radiation. *Cancer Res* **60**:5608–11, 2000.
8. Lorimore SA, McIlrath JM, Coates PJ and Wright EG. Chromosomal instability in unirradiated hemopoietic cells resulting from a delayed in vivo bystander effect of gamma radiation. *Cancer Res* **65**:5668–73, 2005.
9. Zhou H, Randers-Pehrson G, Waldren CA, Vannais D, Hall EJ and Hei TK. Induction of a bystander mutagenic effect of alpha particles in mammalian cells. *Proc Natl Acad Sci U S A* **97**:2099–104, 2000.
10. Zhou H, Suzuki M, Randers-Pehrson G, Vannais D, Chen G, Trosko JE, Waldren CA and Hei TK. Radiation risk to low fluences of alpha particles may be greater than we thought. *Proc Natl Acad Sci U S A* **98**:14410–5, 2001. ■

Disassociation and Re-seeding of 3-D Sliced Tissues

Giuseppe Schettino, Gary W. Johnson and David J. Brenner

In order to fully appreciate the relevance of the bystander phenomenon on biological organisms, investigators in the Center for Radiological Research (CRR) are devoting particular effort in extending bystander studies to fully differentiated 3-dimentional tissue models.[1] The studies are using reconstructed normal human skin tissues (EPI-200) from MatTek. These tissues consist of fully differentiated normal, human-derived epidermal keratinocytes very similar to the human epidermis. The tissue samples are cultured in specially designed Millicell-CM culture inserts (Millipore) and fed with serum-free medium through the Millipore base membrane allowing the upper surface to be exposed to air, which stimulates differentiation.

For various biological end-points (such as micronuclei formation and chromosomal aberrations), it is essential to disassociate the tissue sample into single cells and allow them to go through one or more cell cycles. At the same time, it is mandatory for the bystander studies to have precise information regarding the distance of the examined cells from the irradiation site(s). At the CRR we have therefore focused on developing new tools and protocols to perform the above-mentioned experiments. Using a specifically de-

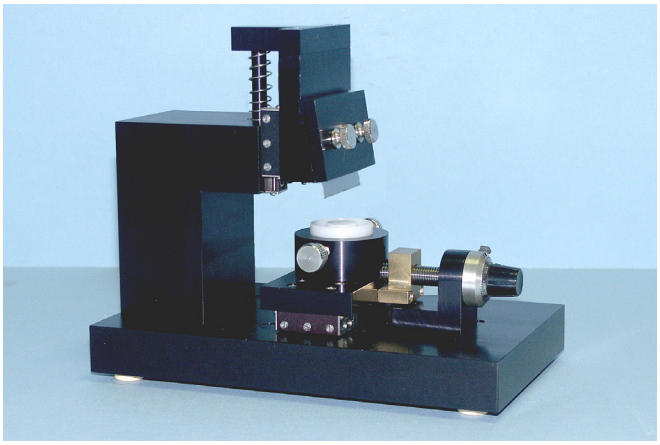

Fig. 1. Guillotine with micrometer to accurate cut tissue samples.

signed guillotine shown in Figure 1, it is possible to cut the tissue samples into slices of adjustable wideness down to few tens of microns. The slices can then be individually peeled off from the inset substrate for the disassociation process or other applications,[2] still preserving some information on their distance from the irradiation site. The slicing and peeling process takes only a few minutes per sample introducing negligible stress to the cells as confirmed by the same number of viable single cells obtained from whole or sliced tissues.

Two different chemical agents have been tested for the tissue disassociation procedure: trypsin and collagenase. Their concentration and incubation time have been closely monitored to maximize the number of viable single cells obtained from a single tissue as shown in Figure 2.

Cell-Tak and collagen have also been employed in a range of concentrations to coat the cell culture dishes and improve cell adhesion. Strangely, no improvement was measured following collagen coating (up to 10 μg/cm^2) while Cell-Tak coating (5 μg/cm^2) produced a small increase of the seeded cells (~10%).

Although producing a low number of viable cells per sample, the approach described appears to be successful and open to improvements, which could make it useful for cytogenetic studies of the bystander phenomenon in 3-D samples.

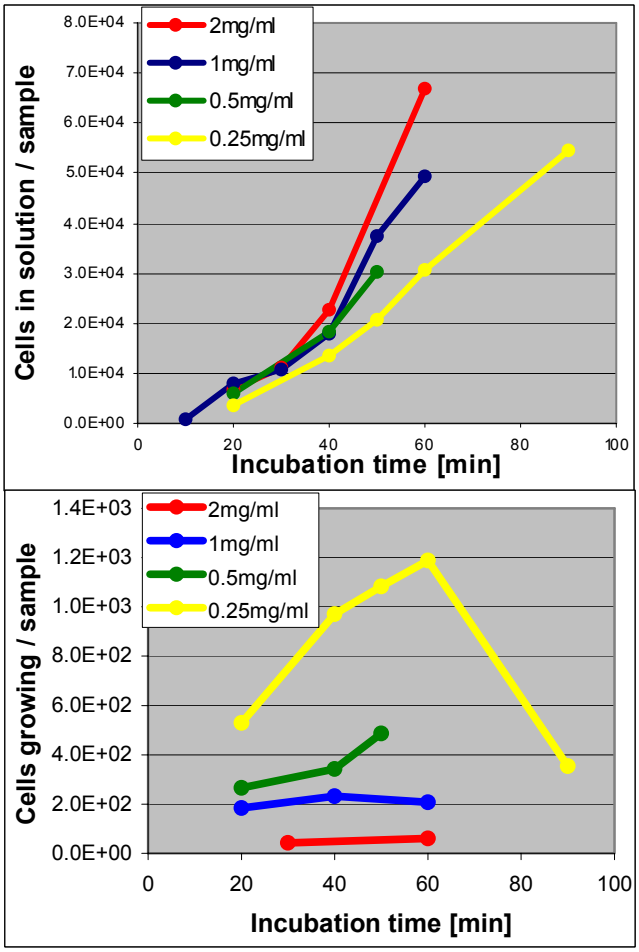

Fig. 2. Total number of cells per sample disassociated (**top**) and attached to plastic culture dishes (**bottom**) as a function of the incubation time in various collagenase concentrations.

References

1. Belyakov OV, Mitchell SA, Parikh D, Randers-Pehrson G, Marino SA, Amundson SA, Geard CR and Brenner DJ. Biological effects in unirradiated human tissue induced by radiation damage up to 1 mm away. *PNAS USA* **102**:14203-8, 2005.
2. Amundson SA and Schettino G. Isolation of RNA from sliced 3-dimensional tissue. Page 26 of this report. ■

(L–r): Giuseppe Schettino, Gary Johnson, and Gregory Ross.

Where Does the Bystander Effect Start?

Mykyta V. Sokolov,[1,2] Lubomir B. Smilenov, Eric J. Hall, Igor G. Panyutin,[1] William M. Bonner[3] and Olga A. Sedelnikova[3]

Introduction

The existence of bystander effects after low dose IR is well documented, but still the factors and the mechanisms involved in it are not known.[1-4] Most of the evidence supporting the bystander effect phenomena are based on directly measured endpoints, or partial molecular analysis of radiation response pathways in the bystander cells.[5-8] These evidence show that the response induced in the bystander cells is similar to the one in directly hit cells. A very important question is what is the magnitude of that response. Is it a mirror image of the one in the directly hit cells, or it is to some extent similar. To answer this question, we measured the induction of DNA double strand breaks (dsb) in bystander cells. Our results show that the bystander effect factors induce DNA double strand breaks in the bystander cells, indicating that the overall response in these cells should be very similar to the one in directly hit cells. However, the kinetics of the DNA double strand breaks formation is different. While in the directly hit cells the DNA double strand breaks could be detected almost immediately, the ones in the bystander cells appear much later – after 18 hours. This delay points out to a different mechanism of induction of DNA breaks in bystander cells. Most probably they are the result of the activation of stress response mechanisms.

Materials and methods

Cells

WI38 normal human lung fibroblasts were purchased from Coriell Cell Repositories (Camden, NJ, USA) and maintained according to recommended protocols. The cells were grown for 3–7 days prior to the experiments.

α-Particle irradiation studies

In this methodology cells were stained separately with 5 mM CellTracker CMRA dye and 1 mM Hoechst 33342 for 30 min. The two cell batches were mixed together in a 1:1 to 1:4 ratio and 500 cells of the mixture were seeded in a microbeam dish. The coordinates of each Hoechst-stained nucleus were automatically recorded using an imaging system and these cells were irradiated with two or 20 α-particles per cell. The CMRA dye identified the bystander cells. The cultures were fixed in 2% paraformaldehyde at 30 min, 18 or 48 h post-IR.

Cell mixing

Stained with CMRA cells were trypsinized and mixed with irradiated (0.2 Gy γ-rays) nonstained cells. The mixed cell cultures were incubated for either 18 or 48 h before fixation in 2% paraformaldehyde.

Threshold determination for scoring affected bystander cells

Preliminary γ-IR cell mixing experiments revealed that the increase in γ-H2AX focal incidence was not uniform in the bystander cell population, but rather limited to a fraction of the cell population. We found that using a threshold of four γ-H2AX foci per cell (fpc) was optimal for determining the fraction of the affected bystander cells. This value is high enough to exclude cells with foci numbers following the Poisson distribution.

Results

α-Particle irradiation studies

After irradiation with α-particles, the incidence of γ-H2AX foci in the targeted cells, followed kinetics similar to those previously reported. It increased at 30 min post-IR, returned to control values by 18 h and remained at initial levels at 48 h (Fig. 1). In marked contrast, the focal incidence in bystander cells remained at control values 30 min post-IR, increased by 18 h and remained elevated at 48 h.

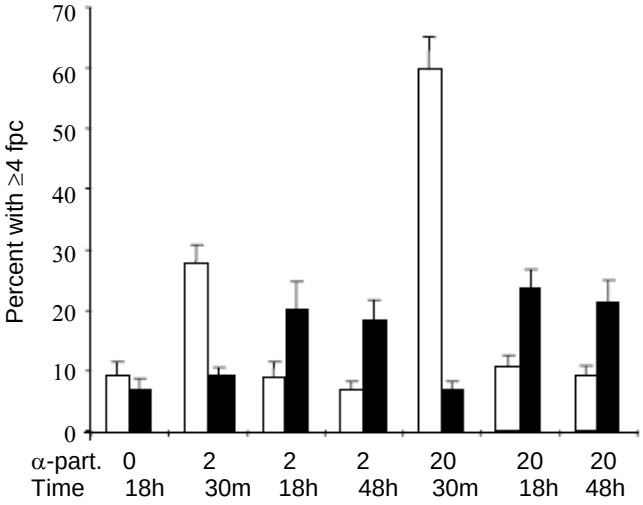

Fig. 1. Coculture studies: Target cells (white bars) received two or 20 α-particles. Black bars denote bystander cells. The bystander effect was evident at 18 and 48 h with two or 20 α-particles, but not at 30 min.

[1] *Department of Nuclear Medicine, Clinical Center, NIH, Bethesda, MD.*
[2] *Department of Radiation Biology and Biophysics, Institute of Cell Biology and Genetic Engineering, Ukraine.*
[3] *Laboratory of Molecular Pharmacology, Center for Cancer Research, National Cancer Institute, NIH, Bethesda, MD.*

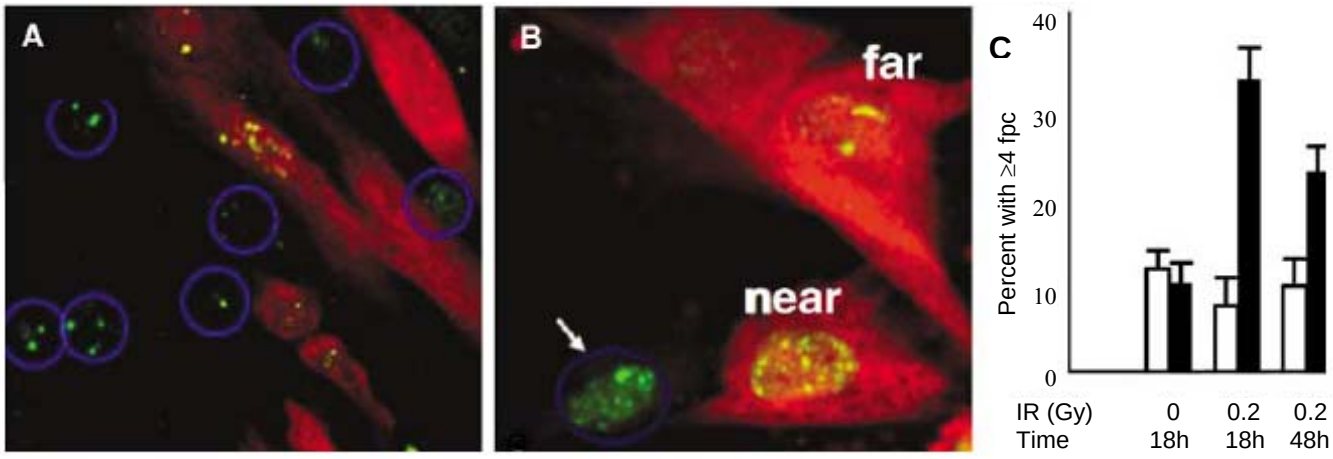

Fig. 2. Cell mixing studies. **(A)** Presence of γ-H2AX foci in mixed non-irradiated cells. **(B)** Irradiated non-stained cell (pointed with arrow) and bystander cells close to and distant from the irradiated cell. **(C)** The graph shows the bystander effect after 18 or 48 hours. White bars, irradiated cells; black bars, bystander cells.

Cell mixing

During these studies, we observed that greater numbers of bystander cells with more than 4 fpc were found next to targeted cells (see Fig. 2). This confirms the involvement of gap-junctions in the transmission of the bystander effect.

Characteristics of the bystander effect

The γ-H2AX foci observed in previous studies were found to serve as sites for the accumulation of DNA dsb repair proteins.[9,10] When bystander cells were examined, the proteins 53bp1, ATM (phospho S1981), Mre11, Rad50 and

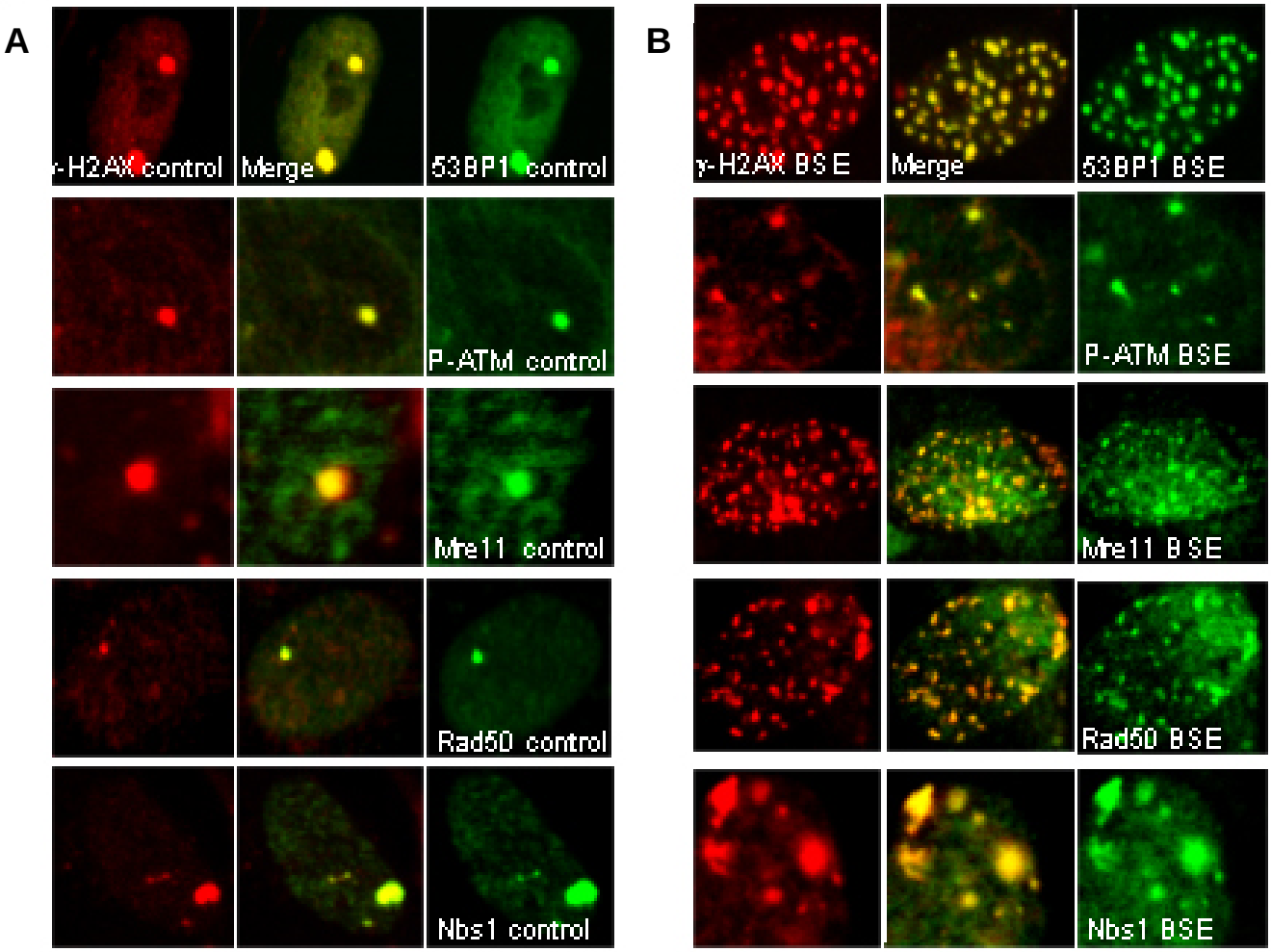

Fig. 3. Colocalization of DNA dsb repair proteins with γ-H2AX foci. **(A)** Unirradiated control cells. **(B)** Bystander cells from α-IR experiments.

Nbs1 were all found to accumulate at γ-H2AX foci in both the targeted and bystander cells (Fig. 3). This confirms that in both irradiated and bystander cells, the DNA lesions are recognized as DNA dsb, leading to the initiation of DNA dsb repair.

Discussion

We have shown here that γ-H2AX foci appear not only in cells targeted with IR but also in unirradiated bystander cells. Also, the γ-H2AX foci in bystander cells are sites of DNA dsb repair protein accumulation. These findings indicate that DNA dsb formation may be a major event in the manifestation of the bystander effect. If γ-H2AX foci have different origins in targeted and bystander cells, their formation may be expected to follow distinctly different kinetics, as we observed. In numerous studies including this one, γ-H2AX focus formation in targeted cells reaches maximum at approximately 30 min post-IR and returns to near pre-IR values by 18 h. In contrast, the γ-H2AX foci formation in bystander cells is low at 30 min post-IR, elevated by 18 h, and remains elevated at 48 h.

Additionally, our results indicate that γ-H2AX focus formation is limited to a subset of cells in the bystander population.

Further studies are needed to elucidate the factors involved in the signal transmission between targeted and bystander cells, and the characteristics that make some bystander cells vulnerable to these signals.

References

1. Brenner DJ, Little JB and Sachs RK. The bystander effect in radiation oncogenesis: II. A quantitative model. *Radiat Res* **155**:402–8, 2001.
2. Hall EJ and Hei TK. Genomic instability and bystander effects induced by high-LET radiation. *Oncogene* **22**:7034–42, 2003.
3. Bonner WM. Phenomena leading to cell survival values which deviate from linear-quadratic models. *Mutat Res* **568**:33–9, 2004.
4. Mothersill C and Seymour CB. Radiation-induced bystander effects--implications for cancer. *Nat Rev Cancer* **4**:158–64, 2004.
5. Nagasawa H and Little JB. Induction of sister chromatid exchanges by extremely low doses of alpha-particles. *Cancer Res* **52**:6394–6, 1992.
6. Wu LJ, Randers-Pehrson G, Xu A, Waldren CA, Geard CR, Yu Z and Hei TK. Targeted cytoplasmic irradiation with alpha particles induces mutations in mammalian cells. *Proc Natl Acad Sci U S A* **96**:4959–64, 1999.
7. Mothersill C, Seymour CB and Joiner MC. Relationship between radiation-induced low-dose hypersensitivity and the bystander effect. *Radiat Res* **157**:526–32, 2002.
8. Ponnaiya B, Jenkins-Baker G, Brenner DJ, Hall EJ, Randers-Pehrson G and Geard CR. Biological responses in known bystander cells relative to known microbeam-irradiated cells. *Radiat Res* **162**:426–32, 2004.
9. Paull TT, Rogakou EP, Yamazaki V, Kirchgessner CU, Gellert M and Bonner WM. A critical role for histone H2AX in recruitment of repair factors to nuclear foci after DNA damage. *Curr Biol* **10**:886–95, 2000.
10. Sedelnikova OA, Horikawa I, Zimonjic DB, Popescu NC, Bonner WM and Barrett JC. Senescing human cells and ageing mice accumulate DNA lesions with unrepairable double-strand breaks. *Nat Cell Biol* **6**:168–70, 2004.

■

Isolation of RNA from Sliced 3-Dimensional Tissues

Sally A. Amundson and Giuseppe Schettino

In a collaborative effort, members of the Center for Radiological Research have recently extended studies of bystander effects from standard 2-dimensional culture models to a 3-dimensional tissue model.[1] In order to enable the study of global gene expression as a tool for comparing signal transduction in 3D versus 2D models, we have developed methods for isolating high quality RNA from these artificial tissues.

For these optimization studies, we obtained EPI-200 reconstructed normal human skin tissues from MatTek. These tissues represent the human epidermis, and consist of fully differentiated epidermal keratinocytes. The tissues were cultured with an air-liquid interface tissue culture technique in which the tissue was grown on Millicell-CM culture inserts (Millipore) with a 28 μm hydrophilic PTFE membrane. The tissue was fed from below with proprietary serum-free medium from MatTek, while the upper surface was exposed to air, which stimulated differentiation.

Our ultimate goal is not only to be able to profile gene expression in the whole tissues, but also in tissue slices for bystander irradiation studies. Slicing the tissues can take several minutes, potentially enough time for degradation of the RNA to occur. Therefore, the first step was to investigate the effects of tissue slicing on RNA integrity, and to explore ways of stabilizing the RNA. We first tried immersing the tissue samples in RNAlater® from Ambion. This reagent rapidly permeates tissue samples and inactivates RNases, while preventing changes in the gene expression profile during processing. Once the test tissues were stabilized in the RNAlater, they were removed and sliced as described in

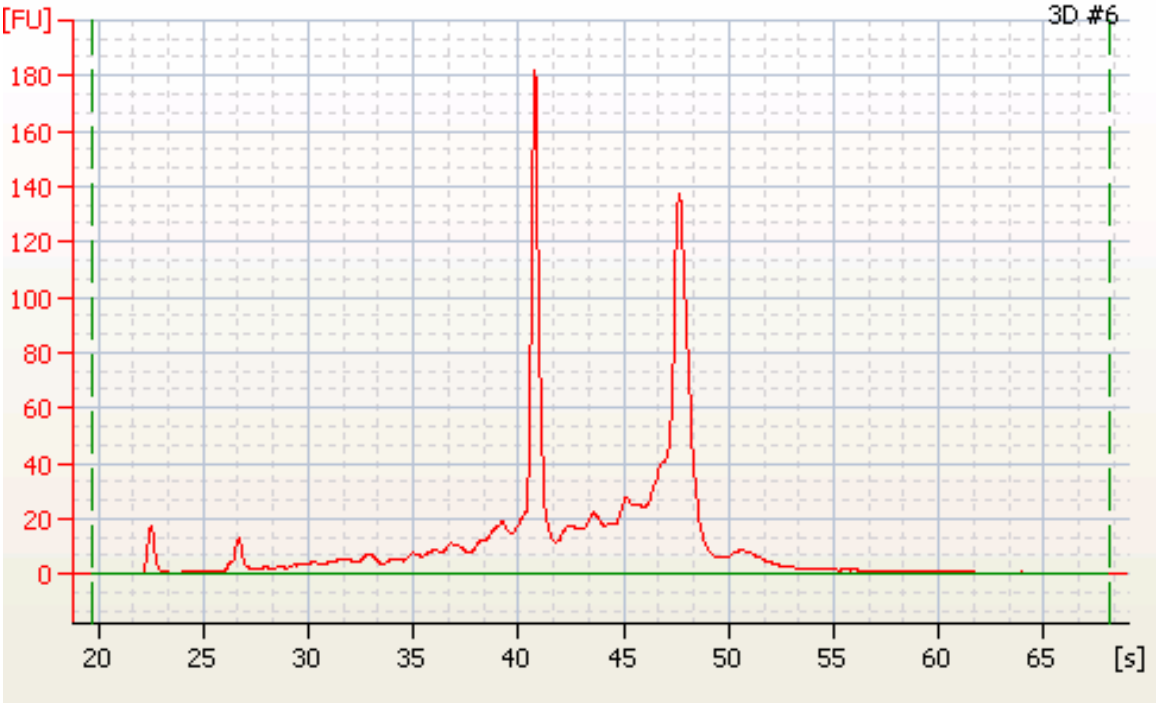

Fig. 1. Electropherogram of RNA from 3D tissue showing only minimal degradation.

reference 2, with 500, 250 and 100 μm thicknesses, then the slices were returned to RNAlater for storage. Unfortunately, the RNAlater treatment changed the texture of the tissues and made them extremely difficult to handle. The support membrane became very stiff and also curled up. Extra pressure was required to slice these tissues, and they frequently failed to separate from the membranes. Recovery of material and accuracy of slicing both appeared to be somewhat compromised by this treatment. As an alternative, we also tried slicing the tissues without pre-treatment in RNAlater. In this case, the individual tissue slices were placed into RNAlater solution as soon as they were cut.

We next extracted the RNA from these sliced tissues. First the tissues were ground in Trizol reagent using a disposable 15 ml tissue grinding tube. The aqueous phase from the Trizol extraction was further purified using NucleoSpin RNA II columns. The yields of purified RNA varied from 3 to 42 μg per tissue sample. The integrity of the recovered RNA was checked using the Agilent Bioanalyzer. While all samples showed varying amounts of RNA degradation, slicing tissues in RNAlater did not appear to improve the quality of the recovered RNA.

For subsequent experiments, the tissues were not presoaked in RNAlater, but the slices were placed immediately in the preservative solution. We next compared the disposable tissue grinders with reusable Teflon pestles. The Teflon pestles appeared to reduce the tissue much more efficiently, whereas the disposable grinders were very awkward for these small samples.

We then compared the two-step Trizol/NucleoSpin extraction with a simplified NucleoSpin only protocol, comparing the resulting RNA on the Bioanalyzer. Adding the Trizol extraction appeared to result in slightly lower yields, with no improvement in quality. More consistent yields were also obtained using the NucleoSpin purification alone (18–28 μg per sample).

When tissues were irradiated with 8 Gy gamma-rays prior to slicing and RNA extraction with the NucleoSpin protocol, no systematic increases in degradation or decreases in yield were observed. Thus the approach of standard tissue slicing with storage of slices in RNAlater, grinding in NucleoSpin lysis buffer with a Teflon pestle in an Eppendorf tube, and standard NucleoSpin extraction, appears to be relatively robust and amenable to future microarray profiling studies, including bystander experiments. A typical Bioanalyzer trace of RNA extracted from sliced EPI-200 tissue using this protocol is shown in Figure 1.

References

1. Belyakov, OV, SA Mitchell, D Parikh, G Randers-Pehrson, SA Marino, SA Amundson, CR Geard and DJ Brenner (2005) Biological effects in unirradiated human tissue induced by radiation damage up to 1 mm away. *PNAS (USA)* **102**:14203–8.
2. Schettino G, Johnson GW and Brenner DJ. Disassociation and re-seeding of 3-D sliced tissues. Page 22 of this annual report. ■

Investigation of Radiation-Induced Bystander Responses in Artificial Skin Tissues

Brian Ponnaiya, Stephen Marino and Charles R. Geard

We have previously demonstrated the induction of bystander responses in cellular monolayers as seen by induction of micronuclei and alterations in gene expression following exposure to ionizing radiation.[1] Here we report on the use of artificial skin tissues in the investigation of bystander responses.

EpiDerm (Mattek, MA) is an artificial skin tissue that consists of normal human epidermal keratinocytes which have been cultured to form a multilayered, highly differentiated model of the human epidermis (Fig. 1). These tissues exhibit in vivo-like morphological and growth characteristics and express all the markers of normal epidermis. They are provided in cell culture inserts and grow in serum free media at the liquid-air interphase. These tissues have previously been used to establish that bystander responses may be detected at up to 1 mm away from the site of irradiation.[2]

Tissues were irradiated inverted with 1 Gy α-particles (120 KeV/μm) using the Track Segment irradiation facility at RARAF. Given the limited penetration of the α-particles used, it was estimated that only about 25 μm of the tissue was actually traversed by a particle. Therefore the top two cell layers were irradiated and cells in the rest of the tissue were by definition bystanders (Fig. 1). Following irradiation tissues were fixed at 15, 30, 45 and 60 minutes post irradiation in 10% Neutral Buffered Formalin. Control samples were run in parallel. Tissues were paraffin-embedded and sectioned in the Core Histology Facility at the Columbia University Medical Center. Levels of specific proteins were assayed using specific antibodies (Santacruz, Cell Signaling Technologies) and immunohistochemical assay kits (CSA II, Dako USA). Stained samples were imaged with a Hamamatsu camera and individual nuclei were analyzed for densities and relative position from the surface using Image Pro Plus.

Since we have demonstrated that p21/WAF1 induction is one of the most robust bystander responses, initial studies looked at the expression of p21/WAF1 in irradiated tissues as a function of distance from the surface (Fig. 2, panels A, C, E and G [next page]). As can be seen, at the earliest time point, 15 minutes, both irradiated (up to 25 μm from the surface) and bystander cells (>25 μm from the surface) had higher levels of p21/WAF1 when compared to time-matched controls. These levels remained elevated up to 30 minutes post-irradiation but appeared to return to control levels at later time points (panels E and G).

Interestingly, phosphorylation of p53 at serine 15 showed similar patterns. Phosphorylation at serine 15 has been shown to occur following exposure to ionizing radiation as well as in response to other stresses.[3,4] Both irradiated and bystander cells had higher than control levels of serine 15 phosphorylation over the first 30 minutes post-irradiation. However, by 45 minutes these elevated levels had returned to those seen in cells in the control tissues.

In conclusion, the data presented here corroborate previous data of bystander responses observed in cellular monolayers and demonstrate the feasibility of using these 3-dimensional tissues to study the bystander phenomenon.

References

1. Ponnaiya B, Jenkins-Baker G, Brenner DJ, Hall EJ, Randers-Pehrson G and Geard CR. Biological responses in known bystander cells relative to known microbeam-irradiated cells. *Radiat Res* **162**:426–32, 2004.
2. Belyakov OV, Mitchell SA, Parikh D, Randers-Pehrson G, Marino SA, Amundson SA, Geard CR and Brenner DJ. Biological effects in unirradiated human tissue induced by radiation damage up to 1 mm away. *Proc Natl Acad Sci U S A* **102**:14203–8, 2005.
3. Levine AJ. p53, the cellular gatekeeper for growth and division. *Cell* **88**:323–31, 1997.
4. Shieh SY, Ikeda M, Taya Y and Prives C. DNA damage-induced phosphorylation of p53 alleviates inhibition by MDM2. *Cell* **91**:325–34, 1997. ■

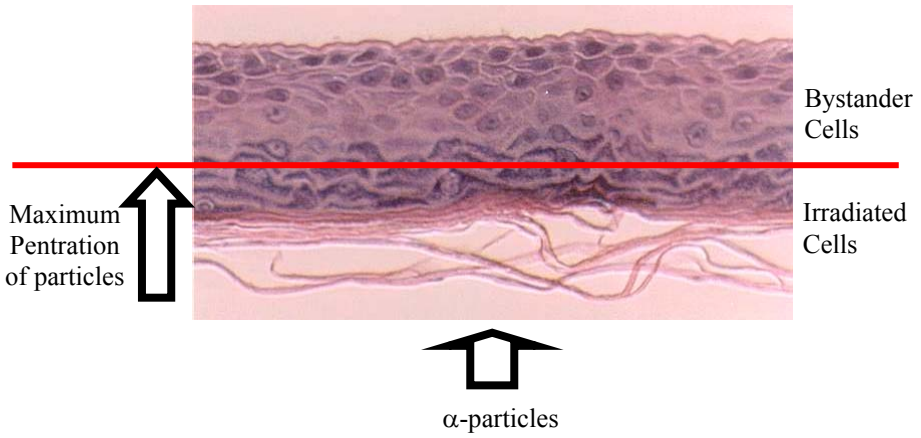

Fig. 1. H&E staining of section of EpiDerm tissue.

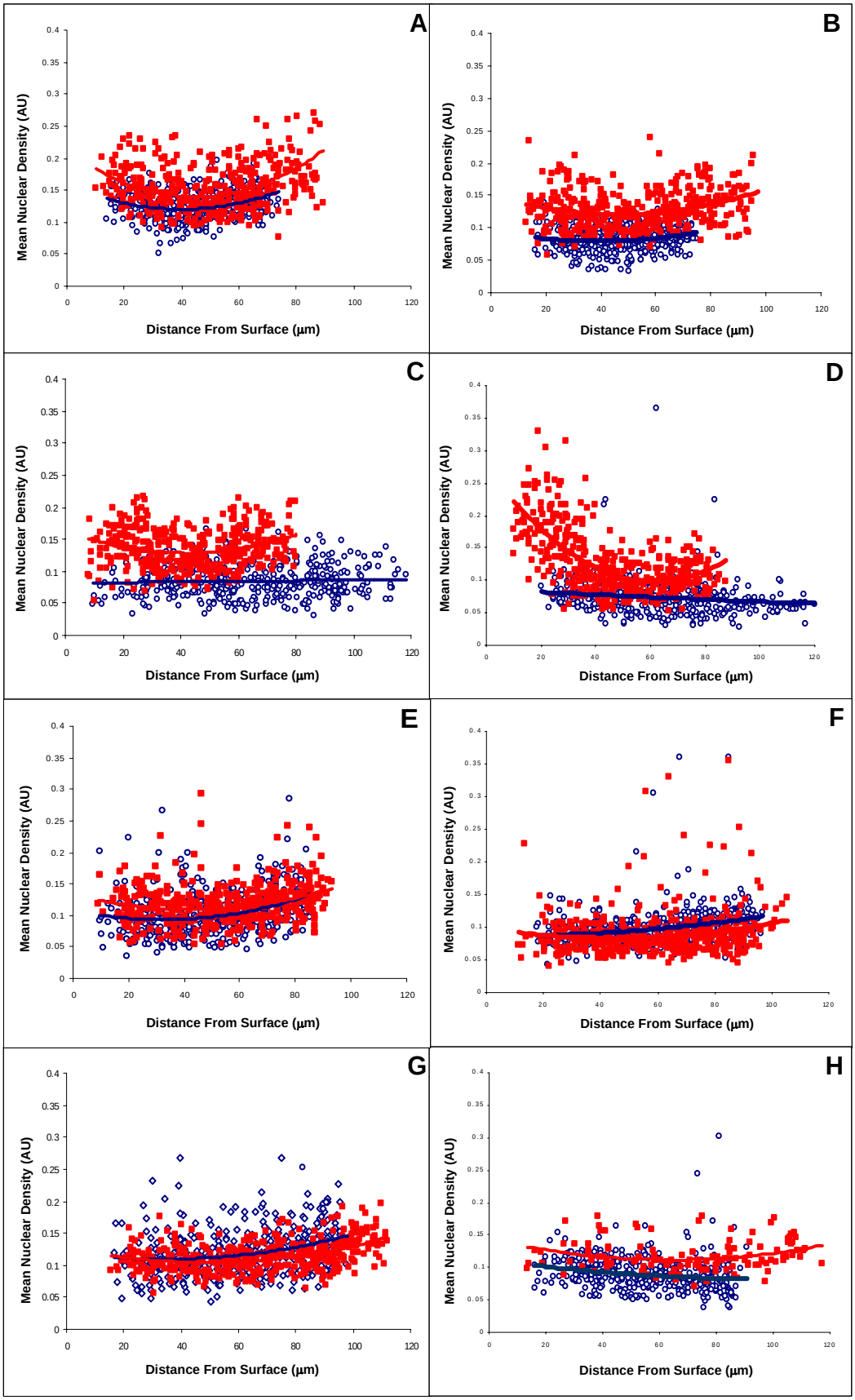

Fig. 2. Alterations in gene expression in EPI200 tissue as a function of distance from the surface. Induction of p21/WAF1 (panels A, C, E, G) and phosphorylation of p53 at serine 15 (panels B, D, F, H) at 15 minutes (A and B), 30 minutes (C and D), 45 minutes (E and F) and 60 minutes (G and H) following exposure to 1 Gy α-particles. Open circles are individual cells in control tissues while closed squares are individual cells in irradiated tissues.

The Role of MAP Kinase Pathways in Radiation-Induced Bystander Responses

Brian Ponnaiya, Stephen Marino and Charles R. Geard

While there is a significant amount of data demonstrating the appearance of bystander responses following exposure to ionizing radiation, very little is known of the mechanisms involved in the initiation and propagation of the phenomenon. One possible mechanism is the activation of MAP kinase pathways which may lead to expression of various other end points in bystander cells. MAP kinases are known to be activated by phosphorylation in response to ionizing radiation and other stresses.[1] Specifically, there is evidence that components of the JNK pathway are activated and may be involved in bystander responses.[2] Here we present data on the activation of two key proteins, JNK and Elk-1, in the bystander cells of a 3-dimensional artificial tissue system.

The artificial model used for this study was EpiDerm (Mattek, MA) which is an epidermis like tissue that consists of normal human epidermal keratinocytes cultured to form a multilayered, highly differentiated model of the human epidermis. These tissues exhibit in vivo-like morphological and growth characteristics and express all the markers of normal epidermis. They are provided in cell culture inserts and grow in serum-free media at the liquid-air interphase.

Tissues were irradiated inverted with 1 Gy α-particles (120 KeV/μm) using the Track Segment irradiation facility at RARAF. Control samples were run in parallel. Given the limited penetration of the α-particles used, it was estimated that only about 25% of the tissue was actually traversed by a particle. Therefore the top two cell layers were irradiated and cells in the rest of the tissue were by definition bystanders. Following irradiation tissues were fixed at 15, 30, 45 and 60 minutes post-irradiation in 10% Neutral Buffered Formalin. Tissues were paraffin-embedded and sectioned inthe Core Histology Facility at the Columbia University Medical Center. Levels of specific proteins were assayed using specific antibodies (Santacruz, Cell Signaling Technologies) and immunohistochemical assay kits (CSA II, Dako USA). Stained samples were imaged with a Hamamatsu camera and individual nuclei were analyzed for densities and relative position from the surface using Image Pro Plus.

The phosphorylation profiles of JNK (pJNK) and Elk-1 (pElk-1) as a function of time post-irradiation are given in Figure 1 [next page]. At 15 minutes post-irradiation, both irradiated cells (<25 μm from the surface) and bystander cells (>25 μm from the surface) had elevated levels of pJNK. However, control tissues seemed to show a similar pattern of expression, albeit at lower levels. This might be due to the inversion of the tissue samples during irradiation, or in the case of the controls, mock irradiation. Nevertheless, there was a clear elevation in the expression of pJNK in cells of the irradiated tissue (Fig. 1, panel A). Between 30 and 45 minutes post-irradiation it appeared that the bystander cells had greater levels of pJNK when compared to either irradiated cells (<25 μm) or cells in the control tissues. At 60 minutes irradiated tissues contained two populations of cells, one of which had pJNK levels similar to that of the controls, and the other which had elevated levels of pJNK. These two populations were spread over the entire thickness of the tissue. That is, there was no correlation between whether a cell had elevated levels of pJNK or not, and its distance from the surface of the tissue.

pJNK has been shown to activate the transcription factor Elk-1 by phosphorylation.[3,4] The patterns of pElk-1 expression were somewhat different. At 15 and 30 minutes postirradiation, both irradiated and bystander cells had elevated levels of pElk-1. However, unlike the patterns of expression of pJNK, pElk-1 levels were reduced to near control levels by 45 minutes post irradiation.

These data suggested that while JNK activation may have caused the enhanced phosphorylation of Elk-1 initially, there are additional cellular mechanisms that reduced the activation of Elk-1 in the presence of activated JNK. Studies are ongoing to further understand how MAP kinases may contribute to bystander responses.

References

1. Dent P, Yacoub A, Fisher PB, Hagan MP and Grant S. MAPK pathways in radiation responses. *Oncogene* **22**:5885–96, 2003.
2. Azzam EI, De Toledo SM, Spitz DR and Little JB. Oxidative metabolism modulates signal transduction and micronucleus formation in bystander cells from alpha-particle-irradiated normal human fibroblast cultures. *Cancer Res* **62**:5436–42, 2002.
3. Cavigelli M, Dolfi F, Claret FX and Karin M. Induction of c-fos expression through JNK-mediated TCF/Elk-1 phosphorylation. *Embo J* **14**:5957–64, 1995.
4. Whitmarsh AJ, Shore P, Sharrocks AD and Davis RJ. Integration of MAP kinase signal transduction pathways at the serum response element. *Science* **269**:403–7, 1995. ■

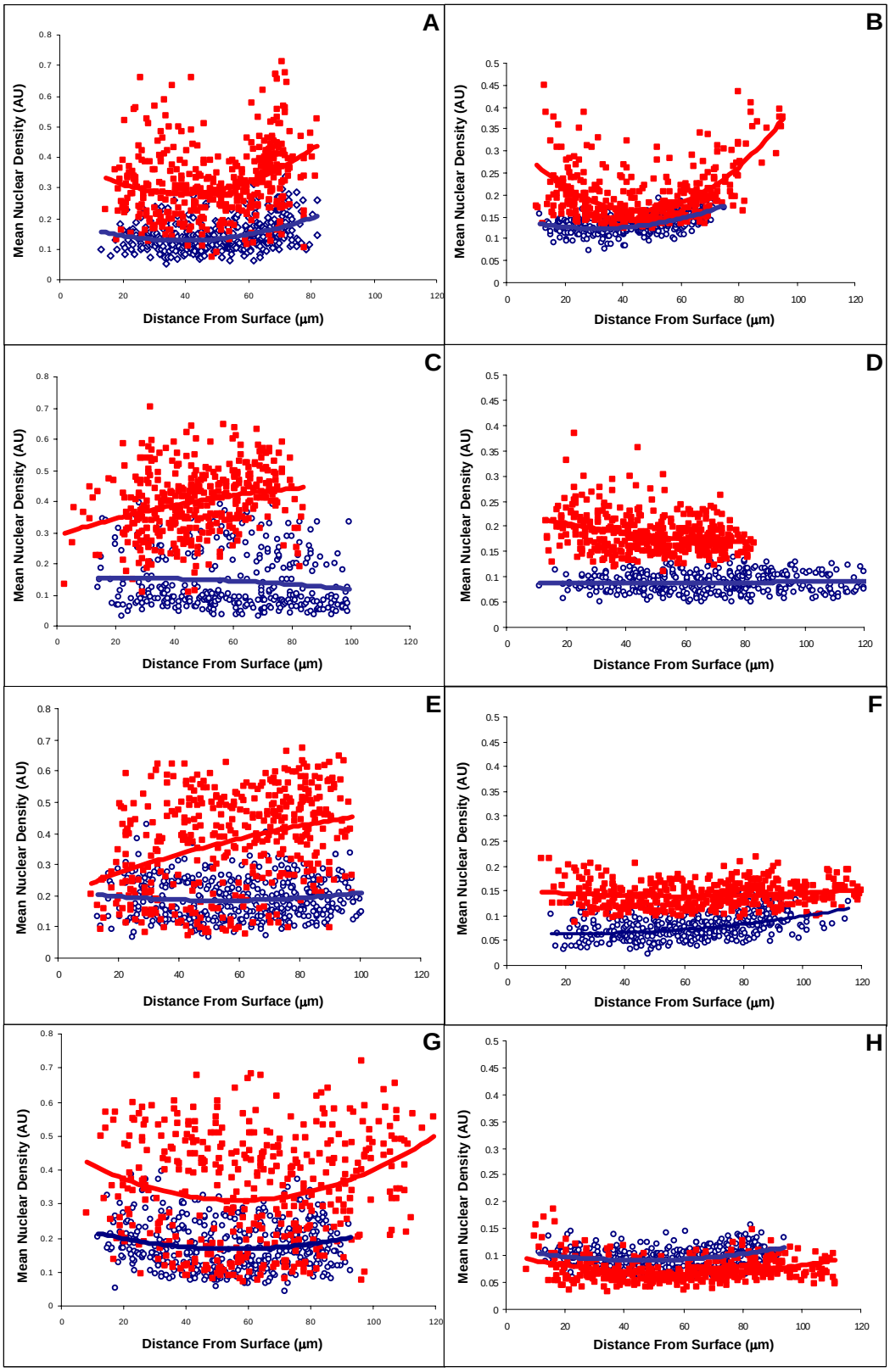

Fig. 1. Alterations in phosphorylation of specific MAP Kinase proteins in EPI200 tissue as a function of distance from the surface. Levels of phophorylated JNK (panels A, C, E, G) and phosphorylated Elk-1 (panels B, D, F, H) at 15 minutes (A and B), 30 minutes (C and D), 45 minutes (E and F) and 60 minutes (G and H) following exposure to 1 Gy α-particles. Open circles are individual cells in control tissues while closed squares are individual cells in irradiated tissues.

Rad9 Expression Is Aberrantly High in Human Prostate Cancer Cells

Howard B. Lieberman and Aiping Zhu

The *Schizosaccharomyces* pombe DNA damage resistance gene, *rad9*, is evolutionarily conserved. We identified human (*hRad9*) and mouse (*Mrad9*) orthologues[1,2] that share several features of the yeast gene. The mammalian versions promote resistance to radiation and certain chemicals, and can regulate the cell cycle response to DNA damage. In addition, the human and/or mouse genes maintain genomic stability, participate in embryonic development, can regulate transcription of *p21*, as well as other downstream target genes through recognition of promoter consensus sequences, and can function as a pro-apoptotic element. These and other activities are summarized in a recent review.[3]

The ability of *Rad9* to regulate genomic stability, and control the cell cycle response to DNA damage, in particular, suggest that the encoded protein might play a role in carcinogenesis. Several published studies support this idea. For example, combined haploinsufficiency for *Mrad9* and *Atm* lead to increased susceptibility of mouse embryo fibroblasts to radiation-induced transformation.[4] Furthermore, aberrant levels of Rad9 protein have been linked to nonsmall cell lung carcinoma[5] and breast cancer.[6]

In this report, we describe experiments designed to test the relationship between prostate cancer and *Rad9* expression. As can be seen in Figure 1, we used western blotting analysis to assess levels of Rad9 protein in normal and cancer cell lines derived from prostate tissue and in log phase growth. We found that all four cancer cell lines examined had aberrantly high levels of human Rad9 protein, when compared to the levels in normal prostate cells. Relative to internal beta-actin loading controls, the levels of human Rad9 protein were 14 to 22 fold higher in the cancer cells than in the PrEC normal controls.

This is the first report of a link between aberrant *Rad9* expression and prostate cancer. Ongoing studies are concerned with the extent to which high levels of Rad9 are found in human prostate tissue cancer samples, as well as the molecular mechanisms that are responsible for the high RNA and protein levels detected.

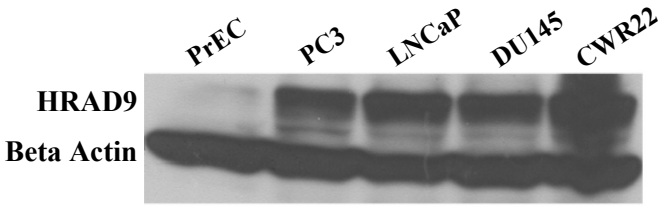

Fig. 1. Western analysis of human RAD9 protein levels in normal and cancer prostate cell lines.

References

1. Lieberman HB, Hopkins KM, Nass M, Demetrick D and Davey S. A human homolog of the *Schizosaccharomyces pombe rad9+* checkpoint control gene. *Proc Natl Acad Sci U S A* **93**:13890–5, 1996.
2. Hang H, Rauth SJ, Hopkins KM, Davey SK and Lieberman HB. Molecular cloning and tissue-specific expression of Mrad9, a murine orthologue of the *Schizosaccharomyces pombe rad9+* checkpoint control gene. *J Cell Physiol* **177**:241–7, 1998.
3. Lieberman HB. *Rad9*, an evolutionarily conserved gene with multiple functions for preserving genomic Integrity. *J Cell Biochem* **97**:690–7, 2006.
4. Smilenov LB, Lieberman HB, Mitchell SA, Baker RA, Hopkins KM and Hall EJ. Combined haploinsufficiency for ATM and RAD9 as a factor in cell transformation, apoptosis, and DNA lesion repair dynamics. *Cancer Res* **65**:933–8, 2005.
5. Maniwa Y, Yoshimura M, Bermudez VP, Yuki T, Okada K, Kanomata N, Ohbayashi C, Hayashi Y, Hurwitz J and Okita Y. Accumulation of hRad9 protein in the nuclei of nonsmall cell lung carcinoma cells. *Cancer* **103**:126–32, 2005.
6. Cheng CK, Chow LW, Loo WT, Chan TK and Chan V. The cell cycle checkpoint gene Rad9 is a novel oncogene activated by 11q13 amplification and DNA methylation in breast cancer. *Cancer Res* **65**:8646–54, 2005. ■

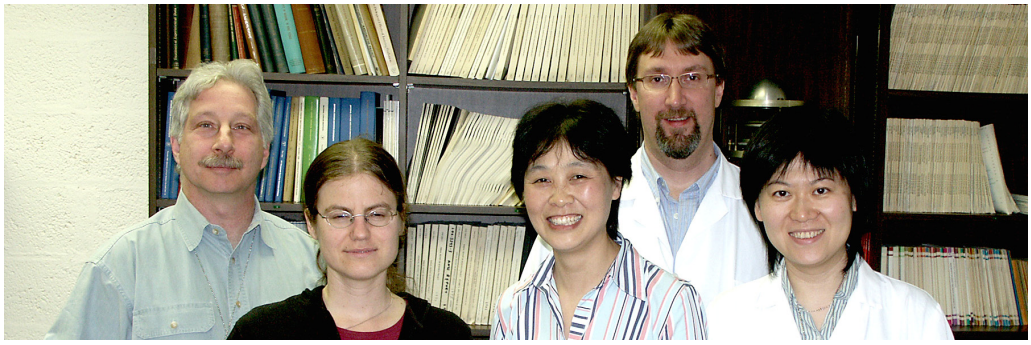

(*L–r*): Dr. Howard B. Lieberman and lab members Corinne Leloup, Aiping Zhu, Kevin Hopkins and Xiaojian Wang.

Human Rad9 Binds to the *p21* Promoter *in Vivo*

Xiaojian Wang, Kevin M. Hopkins, Koon Siew Lai[1] and Howard B. Lieberman

Introduction

Human RAD9 (hRAD9) was first identified as a homologue of yeast *Schizosaccharomyces pombe rad9* encoded protein.[1] It is a nuclear protein and has multiple functions in cells. hRAD9 is important for cell cycle checkpoint control after DNA damage is incurred; it also demonstrates a cell death mediator function and 3′ to 5′ exonuclease activity.[2]

It is widely believed that, in nuclei, hRad9, hHus1, and hRad1 proteins form a heterotrimer sharing structural similarity with PCNA. hRad17 and RecC form a complex, which facilitates the loading of this PCNA-like heterotrimer onto DNA.[2]

Recent EMSA and other studies have shown that hRAD9 acts as a positive transcriptional regulator of *p21*. hRAD9 can bind to two p53 DNA binding consensus sequences previously identified in the *p21* promoter. In the EMSA experiment, nuclear extracts from U937 cells were used as the source of hRAD9. The present study was designed to analyze the *in vivo* binding of hRAD9 to the more downstream p53 binding site in human cells.

The chromatin immunoprecipitation (ChIP) assay is a powerful technique to determine the *in vivo* interaction of proteins associated with specific regions of the genome. ChIP allows detection of the recruitment of a particular transcription factor to a promoter region, or the analysis of the interaction of any protein with any DNA sequence.[3] The assay is illustrated in Figure 1.

Material and Methods

Cell culture

Hela and H1299 (lacking p53) cells were cultured in DMEM and MEM (Invitrogen), respectively, with 10% FBS at 37°C, in a 5% CO_2 atmosphere.

Chromatin Immunoprecipitation (ChIP) assay

ChIP assays were performed according to the manufacturer's protocol,[3] with some modifications.[4,5] In brief, one 100 mm dish of Hela or H1299 cells was fixed with 0.5% formaldehyde at room temperature for 10 min, followed by washing twice with cold PBS containing protease inhibitors. As a result, DNA and protein were cross-linked. After cells and nuclei were lysed, DNA was sheared by sonication in a cold room. Samples were placed on ice during the procedure. Sonication conditions were determined experimentally to get most DNA fragments between 200 and 1000 bp. Each sample was then split into two. The first half of sheared chromatin complexes were treated to reverse crosslinks. DNA was purified by phenol/chloroform extraction and was used as input DNA. The second half of the sample was diluted 10-fold with ChIP dilution buffer, followed by preclearing with Salmon Sperm DNA/protein A/G agarose for 1.5 hours. Samples were then incubated overnight at 4°C with monoclonal Rad9 antibody (BD Transduction Laboratory). Mock ChIP samples did not undergo this step. The next day, immunoprecipitated chromatin was purified from the chromatin/antibody mixtures by incubating with the same agarose beads for an hour, followed by several washing steps. The DNA was then eluted in 0.1 M $NaHCO_3$ and 1% SDS. After reversing the crosslink and removal of proteins by proteinase K digestion, DNA was purified and examined by PCR with primer pairs flanking the p53 DNA binding consensus sequence site. The primer sequences used were forward: 5′-GTATAGGAGCGAAGGTGCAGCA-3′; reverse: 5′-CTCCTTTCTGTCCCTGAAACAT-3′ (Invitrogen).

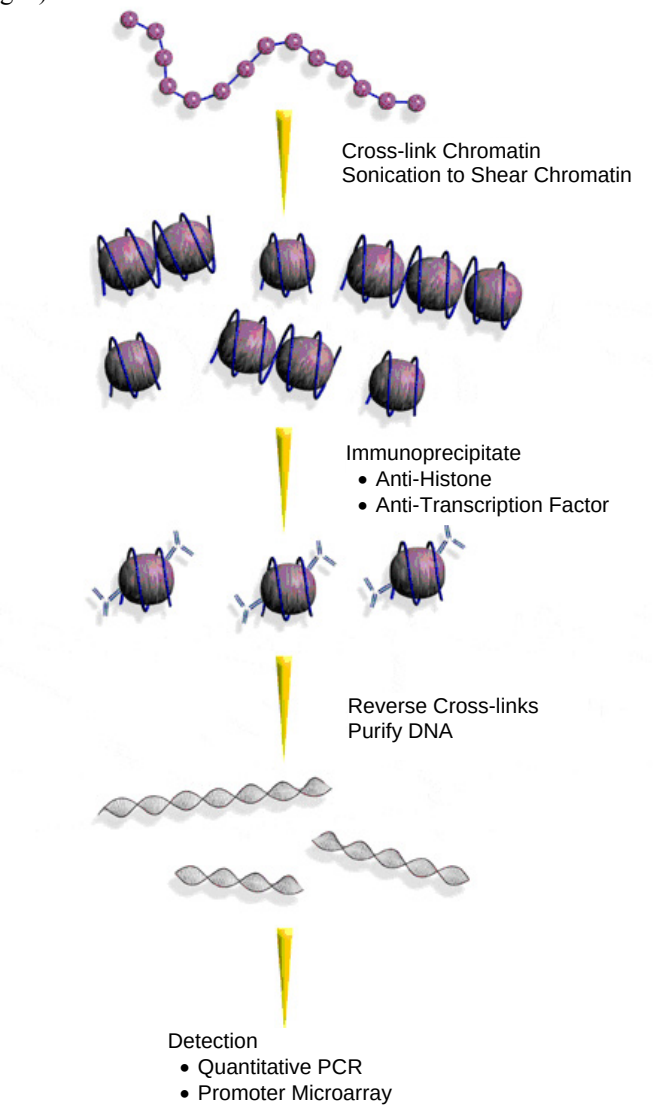

Fig. 1. Diagram of the ChIP assay.

[1] *Massachusetts General Hospital, Boston, MA.*

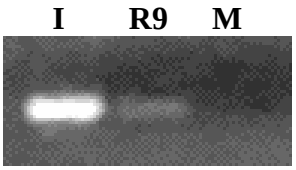

Fig. 2. *p21* promoter region containing p53 DNA binding consensus sequence site is a target for hRAD9 protein binding. For the ChIP assay, genomic DNA from Hela cells was cross-linked and sheared, then immunopreciptiated with monoclonal antibody against human Rad9 (R9) or without antibody as a mock (M) experiment. After reversing the cross-links, PCR was performed. The size of the PCR product corresponds to the length of the p53 DNA binding consensus sequence. Input DNA (I) was the positive control for PCR.

Result and Discussion

hRAD9 binds to the *p21* promoter *in vivo*

To determine whether hRAD9 can bind to the *p21* promoter *in vivo* since we have shown it can bind *in vitro* by EMSA, we performed the ChIP assay in Hela and H1299 cells. As shown in Figure 2, hRAD9 can bind to the *p21* promoter region containing the downstream p53 DNA binding consensus sequences in Hela cells. This binding is specific since no band was obtained by PCR of mock ChIP processed samples. We also used H1299 cells to perform ChIP assays and the results were also positive (data not shown), suggesting that hRAD9 binding to this promoter was independent of p53.

References

1. Lieberman HB, Hopkins KM, Nass M, Demetrick D and Davey S. A human homolog of the Schizosaccharomyces pombe rad9+ checkpoint control gene. *Proc Natl Acad Sci U S A* **93**:13890–5, 1996.
2. Yin Y, Zhu A, Jin YJ, Liu YX, Zhang X, Hopkins KM and Lieberman HB. Human RAD9 checkpoint control/proapoptotic protein can activate transcription of p21. *Proc Natl Acad Sci USA* **101**:8864–9, 2004.
3. See the Upstate online catalog for ChIP assay kits (www.upstate.com).
4. Wende AR, Huss JM, Schaeffer PJ, Giguere V and Kelly DP. PGC-1alpha coactivates PDK4 gene expression via the orphan nuclear receptor ERRalpha: a mechanism for transcriptional control of muscle glucose metabolism. *Mol Cell Biol* **25**:10684–94, 2005.
5. Li CM, Margolin AA, Salas M, Memeo L, Mansukhani M, Hibshoosh H, Szabolcs M, Klinakis A and Tycko B. PEG10 is a c-MYC target gene in cancer cells. *Cancer Res* **66**:665–72, 2006. ■

Human Rad9 Regulates Radiation-Induced Expression of *p21* and *Cox-2*

Aiping Zhu, Yuxin Yin, Tom K. Hei and Howard B. Lieberman

Human checkpoint control protein, HRAD9, has many cellular functions: it participates in promoting DNA damage resistance, cell cycle checkpoint control, DNA repair and apoptosis. It also serves as a negative regulator of androgen-induced transactivity of androgen receptor in prostate cancer cells, and as a transactivator of multiple downstream target genes including *p21* (for review see reference 1). p21 is a universal inhibitor of cyclin/cyclin-dependent kinases and functions as a brake for cell cycle progression. The regulation of *p21* is a critical element in controlling the cell cycle in response to DNA damage induced by radiation and other types of environmental stress.

Recently, it was reported that expression of *HRAD9* was increased in nonsmall cell lung carcinoma[2] and breast cancer.[3] Cox-2 is a member of the COX gene family that plays an important role in mediating cellular immune response and modulating cellular inflammation, carcinogenesis and genomic instability. It is also inducible by radiation and likely important for mediating radiation-induced bystander effects.[4]

We were interested in testing whether there are functional relationships among HRAD9, p21 and COX-2 in cells exposed to radiation. To begin to address this question, a *HRAD9* siRNA construct was made using the pSilencer 1.0 U6 vector. *HRAD9* siRNA plasmid and a U6 empty vector control were cotransfected separately with pcDNA into H1299 cells. H1299 is derived from p53 mutated lung cancer cells. Stable clones were selected using 700μg/ml G418. Positive clones were identified using HRAD9 monoclonal antibody through Western-blotting. As shown in Figures 1 and 2, while p21 and COX-2 protein levels in U6 empty vector control and H1299 cells were increased following gamma-irradiation, p21 and COX-2 levels remained unchanged in the HRAD9 siRNA stable clones. Time course experiments also showed that p21 protein levels in control cells increased 16 hours after gamma irradiation, and COX-2 levels also increased 8 hours post-irradiation. But, there were almost no changes in p21 and COX-2 protein levels in the *HRAD9* siRNA clones after irradiation.

Gamma-ray sensitivity was examined to demonstrate that

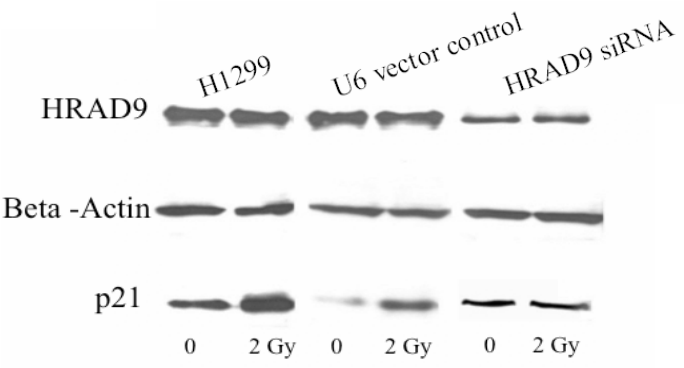

Fig. 1. Western-blotting analysis of HRAD9, p21 and beta actin proteins in H1299 cells mock irradiated or exposed to 2 Gy of gamma-rays. Cells were either the original H1299 population or those bearing a U6 insertless vector control or a plasmid containing *HRAD9* siRNA stable clone cells. The level of HRAD9 protein in the *HRAD9* siRNA cells was much lower than in the control cells. The results show that HRAD9 gene expression was successfully knocked down. Beta actin levels serves to monitor protein-loading levels. p21 level in control cells was increased after 2 Gy gamma irradiation, but there was no change in *HRAD9* siRNA containing cells after irradiation.

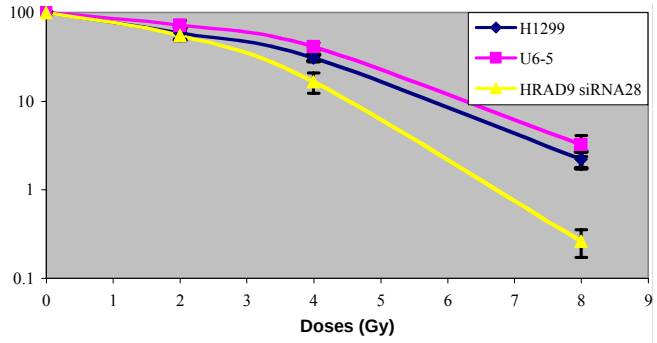

Fig. 3. Sensitivity of H1299 cells containing *HRAD9* siRNA or a control vector. Experiments were carried out in triplicate. The experimental points are the means ± standard deviation of the values from three independent experiments.

the *HRAD9* siRNA was effective, and should thus predictably make cells radiosensitive. As shown in Figure 3, H1299 cells containing *HRAD9* siRNA are more radiosensitive than the control cells, confirming that the reduction in HRAD9 protein levels achieved is biologically significant.

In summary, we demonstrate that HRAD9 is essential for radiation to induce expression of p21 and COX2, even in the absence of p53. Additional studies are underway to help define the precise molecular mechanisms involved.

References

1. Lieberman HB. Rad9, an evolutionarily conserved gene with multiple functions for preserving genomic Integrity. *J Cell Biochem* **97**:690–7, 2006.

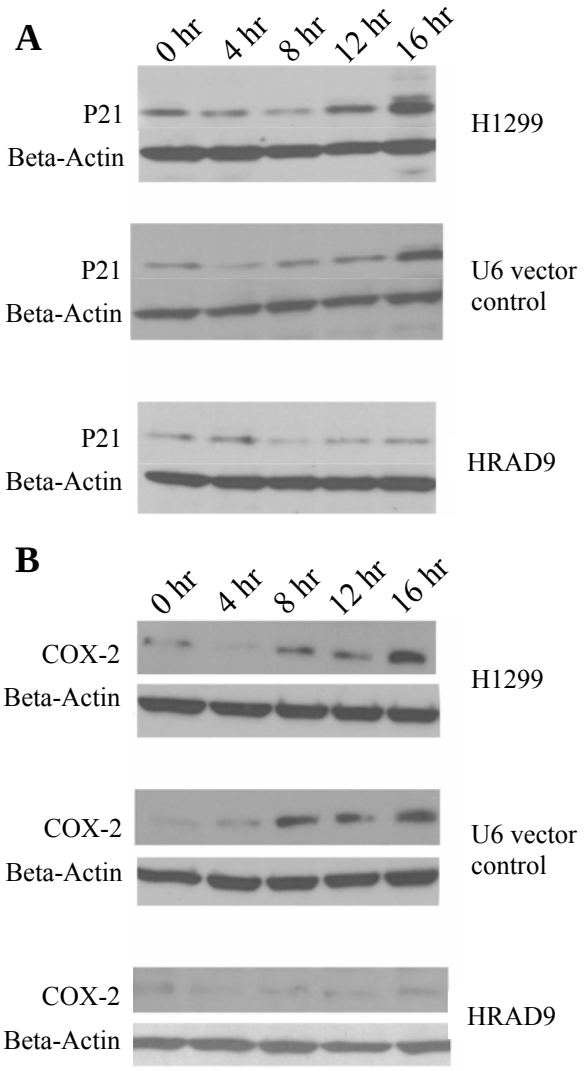

Fig. 2. Western blotting analysis of p21, COX-2 and beta actin protein levels. Cell lysate was collected at different times after gamma irradiation. **A.** Levels of p21 protein were increased 16 hours after irradiation in the control cells, and there was no change in cells containing *HRAD9* siRNA post-irradiation. **B.** Levels of COX2 protein were increased 8 hours after irradiation in the control cells, but there was no change in *HRAD9* siRNA containing cells after irradiation.

2. Maniwa Y, Yoshimura M, Bermudez VP, Yuki T, Okada K, Kanomata N, Ohbayashi C, Hayashi Y, Hurwitz J and Okita Y. Accumulation of hRad9 protein in the nuclei of nonsmall cell lung carcinoma cells. *Cancer* **103**:126–32, 2005.
3. Cheng CK, Chow LW, Loo WT, Chan TK and Chan V. The cell cycle checkpoint gene Rad9 is a novel oncogene activated by 11q13 amplification and DNA methylation in breast cancer. *Cancer Res* **65**:8646–54, 2005.
4. Zhou H, Ivanov VN, Gillespie J, Geard CR, Amundson SA, Brenner DJ, Yu Z, Lieberman HB and Hei TK. Mechanism of radiation-induced bystander effect: role of the cyclooxygenase-2 signaling pathway. *Proc Natl Acad Sci USA* **102**:14641–6, 2005. ■

Histone H2AX Is Phosphorylated in Mitotic Cells in the Absence of Exogenous DNA Damage

Adayabalam S. Balajee and Charles R. Geard

Histones play a crucial role in chromatin remodeling by undergoing post-translational modifications and chromatin remodeling occurs during the cellular processes of DNA replication, transcription, recombination and repair. H2AX, a variant form of histone H2A, is rapidly phosphorylated at serine 139 in response to DNA double strand breaks (DSB) originating from exogenous DNA damage, replication fork collision, shortened telomeres, apoptosis and transcription inhibition. Phosphorylated histone H2AX, designated as γ-H2AX, forms distinct nuclear foci at or near the DSB sites[1,2] and γ-H2AX foci co-localize with many DNA damage signaling components including ATM, BRCA1, 53BP1, MDC1, Rad51 and Mre11/Nbs1/Rad50 complex. γ-H2AX is considered important for recruitment and retention of DSB repair factors such as Nbs1 (Nijmegen breakage syndrome gene product) and 53BP1 (53 binding protein 1) during the late hours after ionizing radiation as cells deficient in H2AX failed to show both 53BP1 and Nbs1 foci formation. Additionally, physical interactions between Nbs1 and γ-H2AX suggest that Nbs1 recruitment to the damaged DNA sites may be dependent on its direct binding to γ-H2AX. H2AX phosphorylation in response to DSB is mediated by four kinases[3] belonging to a super family of phosphatidylinositol kinase-like kinases (PIKK). These include ataxia telangiectasia mutated (ATM), ATM- and Rad3-related (ATR), ATM related kinase (ATX) and DNA dependent protein kinase (DNA-PK). H2AX phosphorylation is detectable to varying degrees in cells deficient in these kinases, suggestive of a functional redundancy among different pathways that activate H2AX. While ATM and DNA-PK are involved in H2AX phosphorylation in an overlapping manner after ionizing radiation induced DSB, H2AX phosphorylation after replicative stress is mediated mainly by ATR. In our earlier study, we demonstrated the assembly of both replication protein A (p32 subunit) and γ-H2AX foci in response to DSB generated by ionizing radiation and stalled replication forks suggestive of their involvement in both DNA damage response and cell cycle checkpoint regulation.[4]

Cells deficient in H2AX display spontaneous chromosomal instability and increased radiosensitivity.[5,6] Chromosomal instability can arise from defects either in cell cycle checkpoints or DNA repair pathways or both. It is presently unclear whether histone H2AX phosphorylation is cell cycle specific or DNA damage specific and whether or not H2AX phosphorylation is critical for chromosome stability. To address these issues, histone H2AX phosphorylation was analyzed in human fibroblast cells in the absence of exogenous DNA damage. In the majority of cells, γ-H2AX foci appeared very faint but 12–15% of the cells displayed intense homogenous staining of γ-H2AX throughout the nucleoplasm. Further, bright homogeneous γ-H2AX staining was observed in morphologically distinguishable cells that were in metaphase, anaphase and telophase. This observation prompted us to verify whether the histone H2AX phosphorylation preferentially occurs in mitotic cells. Since phosphorylated histone H3 is considered to be an excellent marker for mitotic cells, cells were simultaneously immunostained with γ-H2AX and phosphorylated histone H3. As expected, all cells with intense γ-H2AX staining were also found to be positive for phosphorylated histone H3 (Fig. 1).

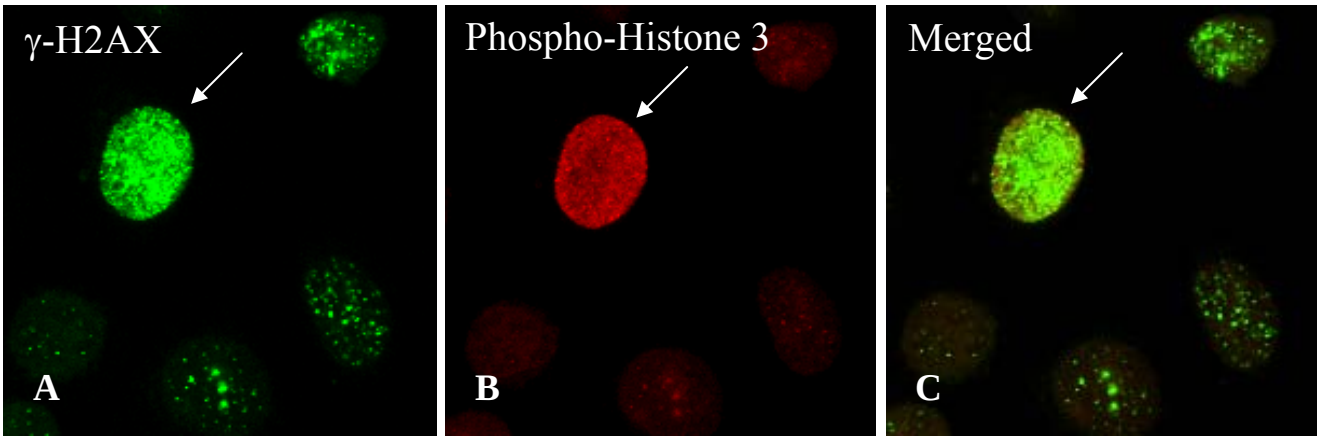

Fig. 1. GM637H cells in exponential growth phase were fixed in acetone:methanol (1:1) and immunostained using antibodies specific for **(A)** phosphorylated histone H2AX (FITC, Upstate Biotechnology) and **(B)** histone H3 (Texas Red, Upstate Biotechnology). Histone H2AX was detected using anti-mouse secondary antibody conjugated with FITC and histone H3 was detected using anti-rabbit Texas red conjugated secondary antibody. **(C)** Merged images. Arrows indicate the mitotic cell positive for phosphorylated forms of both H2AX and histone H3.

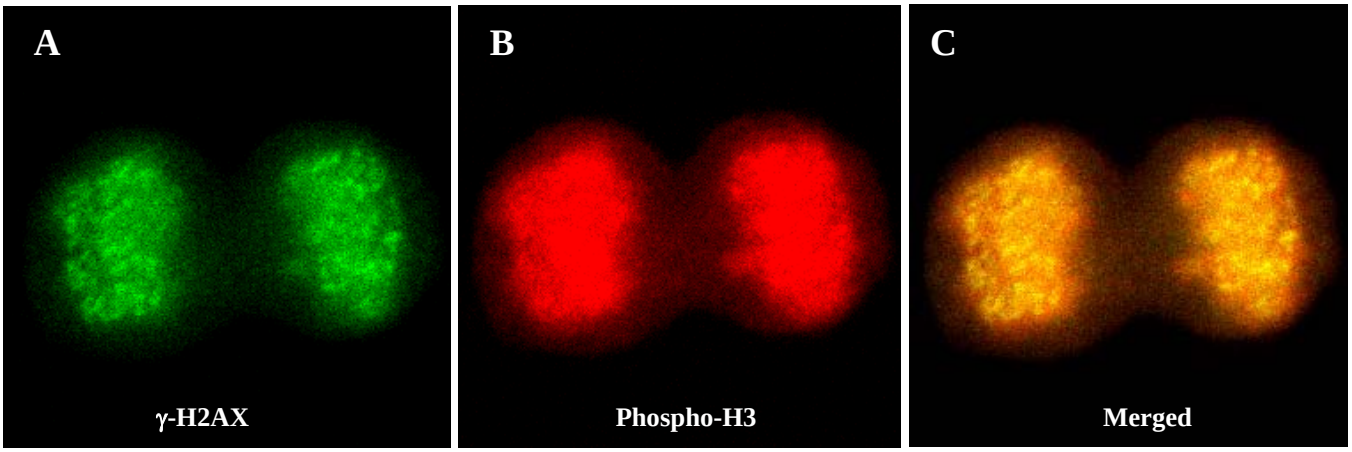

Fig. 2. GM637H cells in exponential growth phase were fixed in acetone:methanol (1:1) and immunostained using antibodies specific for **(A)** phosphorylated histone H2AX (FITC, Upstate Biotechnology) and **(B)** phosphorylated histone H3 (Texas Red, Upstate Biotechnology). **(C)** Merged images.

Intense staining of γ-H2AX and phosphorylated H3 was observed in all the stages of mitotic cells and an anaphase cell positive for both is shown in Figure 2.

In order to verify this observation, histone H2AX phosphorylation was analyzed in both primary and SV-40 immortalized human fibroblasts (MRC5 and GM637H) synchronized at mitosis following treatment with nocodazole and demecolcine (Sigma). Treatment of human fibroblast cells with nocodazole and demecolcine for 16 hrs yielded more than 80% of the cells in mitosis. Histone H2AX phosphorylation was analyzed both by immunofluorescence and Western blot analyses. In corroboration with earlier observations, intense H2AX phosphorylation was observed in the synchronized mitotic cells of both cell lines. Human gliobalstoma cells deficient (MO59J) and proficient in DNA dependent protein kinase (DNA-PK) also showed H2AX phosphorylation in mitosis indicating that kinases other than DNA-PK are responsible for H2AX phosphorylation. The specific phosphorylation of histone H2AX in mitotic cells suggests that H2AX plays an important role in the organization of the mitotic apparatus.

It is interesting to note that the pattern of γ-H2AX staining observed in mitotic cells was different from that of irradiated cells. In irradiated cells, numerous distinct γ-H2AX foci were observed while the mitotic cells especially in metaphase, anaphase and telophase showed an intense homogeneous staining. In an earlier study,[7] histone H2AX has been demonstrated to be critical for the transient G_2 arrest after low doses of low LET radiation. It is likely that histone H2AX phosphorylation is critical for the integrity of the mitotic apparatus to prevent chromosomal abnormalities. In addition to histone H2AX, we also found the enrichment of phosphorylated forms of ATM kinase and replication protein A (p32 subunit) in mitotic cells.

Experiments are in progress to characterize the kinase(s) that are responsible for the phosphorylation of histone H2AX and to understand the functional significance of H2AX phosphorylation in mitosis.

References

1. Rogakou EP, Pilch DR, Orr AH, Ivanova VS and Bonner WM. DNA double-stranded breaks induce histone H2AX phosphorylation on serine 139. *J Biol Chem* **273**:5858–68, 1998.
2. Rogakou EP, Boon C, Redon C, Bonner WM, Pilch DR, Orr AH and Ivanova VS. Mega base chromatin domains involved in DNA double-strand breaks in vivo. *J Cell Biol* **146**:905–16, 1999.
3. Wang H, Wang M, Bocker W and Iliakis G. Complex H2AX phosphorylation patterns by multiple kinases including ATM and DNA-PK in human cells exposed to ionizing radiation and treated with kinase inhibitors. *J Cell Physiol* **202**:492–502, 2005.
4. Balajee AS and Geard CR. Replication protein A and gamma-H2AX foci assembly is triggered by cellular response to DNA double-strand breaks. *Exp Cell Res* **300**:320–34, 2004.
5. Celeste A, Petersen S, Romanienko PJ, Fernandez-Capetillo O, Chen HT, Sedelnikova OA, Reina-San-Martin B, Coppola V, Meffre E, Difilippantonio MJ, Redon C, Pilch DR, Olaru A, Eckhaus M, Camerini-Otero RD, Tessarollo L, Livak F, Manova K, Bonner WM, Nussenzweig MC and Nussenzweig A. Genomic instability in mice lacking histone H2AX. *Science* **296**:922–7, 2002.
6. Bassing CH, Chua KF, Sekiguchi J, Suh H, Whitlow SR, Fleming JC, Monroe BC, Ciccone DN, Yan C, Vlasakova K, Livingston DM, Ferguson DO, Scully R and Alt FW. Increased ionizing radiation sensitivity and genomic instability in the absence of histone H2AX. *Proc Natl Acad Sci U S A* **99**:8173–8, 2002.
7. Fernandez-Capetillo O, Chen HT, Celeste A, Ward I, Romanienko PJ, Morales JC, Naka K, Xia Z, Camerini-Otero RD, Motoyama N, Carpenter PB, Bonner WM, Chen J and Nussenzweig A. DNA damage-induced G2-M checkpoint activation by histone H2AX and 53BP1. *Nat Cell Biol* **4**:993–7, 2002. ■

Expression of Human Drug Metabolism Genes Altered by Organophosphorous Pesticides and Estrogen of Human Breast Epithelial Cells

Gloria M. Calaf,[1] Debasish Roy,[2] Adayabalam Balajee and Tom K. Hei

Environmental chemicals may be involved in the etiology of breast cancer.[1] Organophosphorous compounds are the most widely used pesticides by virtue of their biodegradable nature and short persistence. Such compounds are of great interest because of the extensive use in agriculture, medicine and industry. Breast cancer risk is associated with prolonged exposure to female hormones. Among these hormonal influences a leading role is attributed to estradiol since prolonged stimulation by steroid hormones may increase cell division, increasing the risk of breast cancer.[2]

Methods to define patterns of gene expression have applications in a wide range of biological systems. Several molecular biological techniques are used to study gene expression patterns during the neoplastic progression of breast epithelial cells. The aim of the present study was to identify differentially expressed human drug metabolism genes altered by organophosphorous pesticides and estrogen in human breast epithelial cell lines using cDNA arrays.

MCF-l0F, an immortalized human breast epithelial cell line, was treated with the pesticide, parathion, either alone or in combination with estrogen. Malignant cell lines were developed through a series of sequential steps. Previous studies have shown that parathion and a combination of parathion and 17β estradiol induced malignant transformation of MCF-l0F, as indicated by increased cell proliferation, invasive capabilities and increased mutant p53, BRCA1, ErbB2, c-Ha ras, β catenin, transforming factor RhoA, Ezrin [villin2], Notch 4, Trio, Rac protein expression in the transformed cell lines in comparison to control MCF-10F, cells as detected by immunofluorescent staining and quantified by confocal microscopy.[3]

Expression of drug metabolism in the parental MCF-10F and in the transformed cells induced by the various treatments were ascertained using the 96 gene human drug metabolism gene array (from Super Array, Bioscience Corporation, MD). By using the experimental RNA samples of MCF-10F cells treated with estrogen, parathion and parathion plus estrogen in comparison to control MCF-10F the array was able to simultaneously quantify and analyze the expression profile of 96 genes involved in human drug metabolism regulation.

Human cytochrome P450 2E1 (CYP 2E1) is a phase I metabolizing enzyme. It is involved in the biotransformation of xenobiotics and endogenous substrates. Inter-individual genetic polymorphisms of the CYP 2E1 gene are associated with different cancer diseases.[4]

Mammalian cytosolic GST forms a super family consisting of four distinct families, named alpha, mu, pi and theta. The mu (GSTM1) and theta (GSTT1) members of the GST multigene family are candidate cancer susceptibility genes because of their ability to regulate the conjugation of carcinogenic compounds to excretable hydrophilic metabolites.[5]

The organo(thio)phosphate esters are one of the most widely used classes of insecticides. Worldwide, organophosphate insecticides result in numerous poisonings each year. In insects, glutathione S-transferases (GSTs) play an important role in insecticide resistance. GST enzymes mediate exposure to cytotoxic and genotoxic agents and may be involved in cancer susceptibility.[6] The high frequency of the GSSTT1 null genotype in patients diagnosed with breast cancer before the age of 60 years suggests that this genotype could influence the age of disease onset.

Table 1 shows the anchorage independence capability of treated cells as well as the invasive characteristics of control and irradiated MCF-10F cells scored 20 h after plating onto matrigel basement membranes using modified Boyden's chambers constructed with multi-well cell culture plates and

Table 1.
Origin and phenotypic characteristics of cell lines.

Cell lines	Anchorage Independence	Invasion	Tumorigenicity
MCF-10F	-	-	-
MCF10F + E	-	-	-
Parathion	+	+	-
Parathion + E	+	+	ND

Anchorage Independence: colony-forming efficiency in soft agar fluctuated from 1–3%.
Invasion: invasive characteristics of control and treated MCF-10F cells scored 20 h after plating onto matrigel basement membranes using modified Boyden's chambers constructed with multi-well cell culture plates and cell culture inserts.
Tumorigenicity: tumors formed in nude mice. Average of 6 animals/group.
Positive signs (+): represent the results in relation to anchorage independent growth and number of cells that crossed the filters.
Negative signs (-): lack of anchorage independent growth, invasiveness or formation of tumors in the nude mice.
E: 17β estradiol (10^{-8} M).
ND: not determined.

[1] *Also affiliated with University of Tarapaca and Research Center for the Man in the Desert, Arica, Chile.*
[2] *Brookhaven National Laboratory, Biology Department, Upton, New York.*

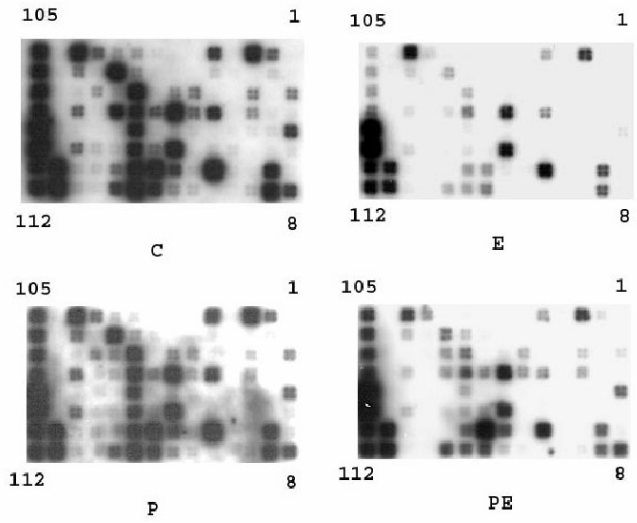

Fig. 1. Expression of human drug metabolism genes in the parental MCF-10F (top left), MCF-10F + Estrogen (top right), MCF-10F + Parathion (bottom left) and MCF-10F + Parathion + Estrogen (bottom right) cell lines.

cell culture inserts.

Results indicated that among the various genes that regulate the human drug metabolism, 17 were found to be altered either by estrogen alone, parathion or a combination of both (Fig. 1). The altered genes included those that related to Cytochrome P450, subfamily IIF, polypeptd1, Cytochrome P450, subfamily IIIA, polpeptd 7, Cytochrome P450, subfamily IVF, polypeptd3, that is CYP2F1, CYP3A7, CYP4F3. The gene expression was increased 2–5 fold in the parathion-treated group in comparison to control whereas gene expression was decreased 2–5 fold in the estrogen and parathion plus estrogen-treated cells (Table 2).

Table 2.
Human Drug Metabolism Gene Array*

Position in Array	Gene Name	Gene Symbol	MCF-10F	MCF-10F + Estrogen (E)	MCF-10F + Parathion (P)	MCF-10F (P + E)
3	ATP-binding cassette,subfam-C,member-1	ABCC1		↓	-	-
5	ATP-binding cassette,subfam-C,member-3	MOAT-D		↓	-	-
8	Acetyl-CoenzymeA acetyl-transferase	ACAT1		↓	↑	↑
15	Carbohydrate(N-acetylglucosamine6-0) Sulphotransferase 5	CHST5		↓	↑	↓
16	Carbohydrate(N-acetylglucosamine6-0) Sulphotransferase 6	CHST6		↓	↑	↓
17	Carbohydrate(N-acetylglucosamine6-0) Sulphotransferase 7	CHST7		↓	↑	↓
33	Cytochrome P450,subfamily IIF,polypeptd1	CYP2F1		↓	↑	↓
36	Cytochrome P450,subfamily IIIA,polpeptd7	CYP3A7		↓	↑	-
39	Cytochrome P450,subfamily IVF,polypeptd3	CYP4F3		↓	↑	↓
44	Epoxide hydrolase 1,microsomal(xenobiotic)	EPHX1		↓	-	-
52	Glutathione S-transferase Pi 1	GSTP1		↓	↑	↑
54	Glutathione S-transferase theta 2	GSTT2		↓	↑	↑
55	Histone acetyltransferase 1	HAT1		↓		↑
60	N-ter acetyltransf. Complex ard1 subunit	LOC51126		↓	-	-
63	Glutathione S-transferase microsomal	MGST1		↓	↑	↑
64	Microsomal glutathione S-transferase 2	MGST2		-	↑	-
67	Metallothionein 1A (functional)	MT1A		↓	-	↓
68	Metallothionein 1E (functional)	hMT-1e		↓	-	↓
69	Metallothionein 1G	MT1G		↓	-	↓
70	Metallothionein 1H	MT1H		↓	-	↓
71	Metallothionein 1L	MT1L		↓	-	↓
72	Metallothionein 2A	MT2A		↓	-	↓
74	Metallothionein 1X	MT1X		↓	↑	↓
76	Homo sapience nicotinamide N-methyltransf.	NNMT		↓	↓	↓
80	Sulfotransferase family,cystolic1A,member1	SULT1A1		↓	-	-
81	Sulfotransferase family,cystolic1A,member2	SULT1A2		↓	-	-
89	Thiopurine S-methyltransferase	TPMT		↓	↑	↓
90	Tyrosylprotein sulfotransferase 1	TPST1		-	↑	-
92	UDP glycosyltransf. 1 fam.,polypeptide A1	UGT1A1		↓	↑	-
94	UDP glycosyltransf. 2 fam.,polypeptide B	UGT2B		↓	↑	-

* All the upregulated and downregulated genes are two fold or more differentially expressed with respect to control.

Metallothioneins (MTs) belong to a family of cysteinrich, metal-binding intracellular proteins, which have been linked with cell proliferation.[7] In this study, gene expression level of MT1A functional isoform was only increased in parathion-treated cells. This isoform has been found to be increased in human invasive ductal breast cancer specimens when determined by RT-PCR. The finding that MT1 appears to be associated with cell proliferation in parathion-treated cells and invasive ductal carcinoma may have therapeutic implications.

It can be concluded that pesticides in the presence of estradiol were capable of inducing transformation of human breast epithelial cells and altered drug metabolism gene expression. These studies suggest that organophosphorous pesticides and estradiol induced changes in gene expression in the human breast epithelium can influence the carcinogenesis process.

References

1. Falck A Jr, Ricci A Jr, Wolff MS, Godbold J and Deckers P. Pesticides and polychlorinated biphenyl residues in human breast lipids and their relation to breast cancer. *Arch Environ Health* **47**:143–6, 1992.
2. Dickson RB and Lipman MF(eds): Control of human breast cancer by estrogen, growth factors and oncogenes. In Breast Cancer: Cellular and Molecular Biology, Kluwer Academic Nonwell, MA, pp 119–66, 1988.
3. Calaf GM. Critical approach to the malignant transformation of human breast epithelial cells with physical and chemical carcinogens. 10th World Congress on Advances in Oncology and 8th International Symposium on Molecular Medicine in Hersonissos, Creta, Greece. Oct. 13, 2005.
4. Bauer M, Herbarth, Aust G and Graebsch C. Molecular cloning and expression of novel alternatively spliced cytochrome P450 2E1 mRNAs in humans. Mol Cell Biochem **280**:201–7, 2005
5. Nascimiento H, Coy CS, Teori MT, Boin IF, Goes JR, Costa LL and Lima CS. Possible influence of glutathione S-transferases GSTTI null genotype on age of onset of sporadic colorectal adenocarcinoma. *Dis Colon Rectum* **46**:510–5, 2003.
6. Rebbeck TR. Molecular epidemiology of the human glutathione S-transferase genotypes GSTM1 and GSTT1 in cancer susceptibility. *Cancer Epidemiol Biomarkers Prev* **6**:733–43, 1997.
7. Jin R, Chow VT, Tan PH, Dheen ST, Duan W and Bay BH. Metallothionein 2A expression is associated with cell proliferation in breast cancer. *Carcinogenesis* **23**:81–6, 2002. ■

Mutagenicity of Chrysotile Fibers in Primary *gpt* Delta Transgenic Mouse Embryo Fibroblast Cells

An Xu, Lubomir Smilenov, Peng He, Ronald Baker and Tom K. Hei

Asbestos fibers are carcinogenic to both humans and experimental animals. The continued discoveries of exposure routes whereby the general public is exposed to asbestos suggest a long-term, low dose exposure for a large number of people.[1] In the last few years, several mutagenicity assays that are proficient in detecting either large deletions, homologous recombinations, or score mutations located on non-essential genes have been used successfully to demonstrate the mutagenic potential of various fiber types, suggesting a close relationship between chromosomal abnormalities that have occurred frequently in fiber-exposed human and rodent cells and carcinogenicity that has occurred *in vivo*.[2-4] However, the molecular mechanism(s) by which asbestos induces mutagenicity *in vivo* are not entirely understood.

In the past decades, several transgenic mutation systems have been developed to detect gene and/or chromosomal mutations in multiple organs of mice or rats including the Muta Mouse and Big Blue mice.[5] Although the coding size of *lacZ*, *lacI* and *cII* in the transgenic mice are different, they all have high backgrounds of base substitution mutations, which results in the underestimation of deletion mutations. *gpt* delta transgenic mice were created by microinjection of λEG10 phage DNA into the fertilized eggs of C57BL/6J mice and carried about 80 copies of the transgene tandem in chromosome 17.[6] The novel merit of this transgenic model is to detect both deletion mutations by Spi^- selection (sensitive to P2 interference) and point mutations by 6-thioguanine selection. To establish this transgenic model to better understand asbestos mutagenicity, the mutant frequency and mutation spectrum induced by chrysotile asbestos were evaluated in primary *gpt* delta transgenic mouse embryo fibroblast (MEF) cells.

The Spi^- assays were performed as described previously.[7] Briefly, the rescued phages were infected to E.coli XL1-Blue MRA or P2 and incubated at 37°C with molten soft agar containing $MgSO_4$. The plaques on agar plates were treated as Spi^- candidates and confirmed by infection to WL95. The numbers of mutants that made clear spit on both XL1-Blue

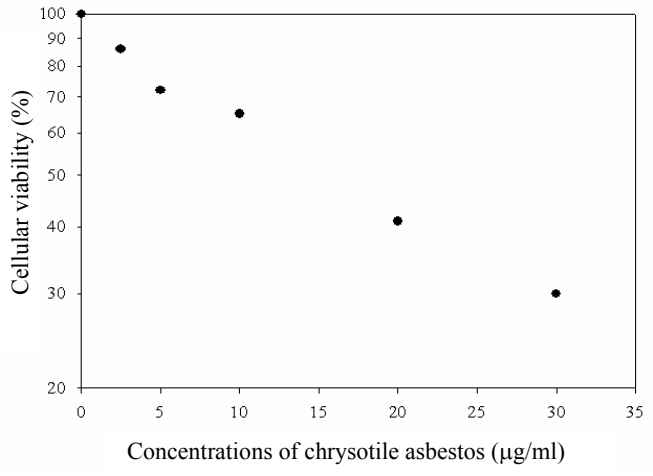

Fig. 1. Cellular viability of MEF cells treated with chrysotile asbestos.

P2 and WL95 were counted as confirmed Spi$^-$ mutants.

As shown in Figure 1 treatment with chrysotile asbestos resulted in a dose-dependent decrease of viability in MEF cells. The background mutation frequency of MEF cells used in the present study was 3.75 per 10^6 plaques. Our preliminary result showed that the mutation frequencies increased with the doses of chrysotile and reached a level that was approximately 1.9-fold higher than background at a 5 μg/ml dose of chrysotile in MEF cells (Table 1). Although these data were consistent with our previous findings, the molecular characteristics of deletion mutations induced by chrysotile asbestos in MEF cells need to be evaluated.

Table 1.
The Spi$^-$ mutant frequencies in MEF cells exposed to chrysotile asbestos.

Chrysotile concentrations (μg/ml)	Total plaque	Spi$^-$ plaque	MEF/10^6	Fold increase over the control
control	4,000,000	15	3.75	1
2.5	1,700,000	10	5.88	1.6
5	1,960,000	14	7.14	1.9

References

1. Virta RL. Worldwide asbestos supply and consumption trends from 1900 to 2000. *USGS Survey* 2003.
2. Both K, Turner DR, Henderson DW. Loss of heterozygosity in asbestos-induced mutations in a human mesothelioma cell line. *Environ Mol Mutagen* **26**:67–71, 1995.
3. Hei TK, Piao CQ, He ZY, Vanneis D, Waldren CA. Chrysotile fiber is a strong mutagen in mammalian cells. *Cancer Res* **52**:6305–9, 1992.
4. Unfried K, Schurkes C, Abel J. Distinct spectrum of mutations induced by crocidolite asbestos: clue for 8-hydroxydeoxyguanosine-dependent mutagenesis in vivo. *Cancer Res* **62**:99–104, 2002.
5. Gossen JA, de Leeuw WJ, Tan CH, Zwarthoff EC, Berends F, Lohman PH, Knook DL, Vijg J. Efficient rescue of integrated shuttle vectors from transgenic mice: a model for studying mutations in vivo. *Proc Natl Acad Sci USA* **86**(20):7971–5, 1989.
6. Nohmi T, Masumura KI. Gpt delta transgenic mouse: A novel approach for molecular dissection of deletion mutations in vivo. *Adv Biophy.* **38**:97–121, 2004.
7. Hayashi H, Kondo H, Masumura K, Shindo Y, Nohmi T. Novel transgenic rat for in vivo genotoxicity assays using 6-thioguanine and Spi$^-$ selection. *Environ Mol Mutagen* **41**:253–9, 2003. ■

MKP2 Is a Novel Transcription Target of p53 in Signaling Apoptosis

Wen Hong Shen, Jianli Wang, Victor Zhurkin[1] and Yuxin Yin

The p53 tumor suppressor plays critical regulatory roles in diverse cellular responses such as cell cycle arrest, senescence and apoptosis through transcriptional control of its target genes. Identification and characterization of new p53 target genes will advance our understanding of how p53 exerts its multiple regulatory functions. In this report, we demonstrate that mitogen-activated protein kinase phosphatase 2 (MKP2) is a novel transcription target of p53 in mediating apoptosis. Induction of MKP2 is highly responsive to oxidative stress in a p53-dependent manner. Interestingly, the p53-dependent induction of MKP2 is prominent only in the cellular response to stimuli leading to apoptosis, but not to cell cycle arrest. In response to oxidative stress, MKP2 is not only required for p53-mediated apoptosis, but

[1] *Laboratory of Experimental and Computational Biology, National Cancer Institute, National Institutes of Health, Bethesda, MD.*

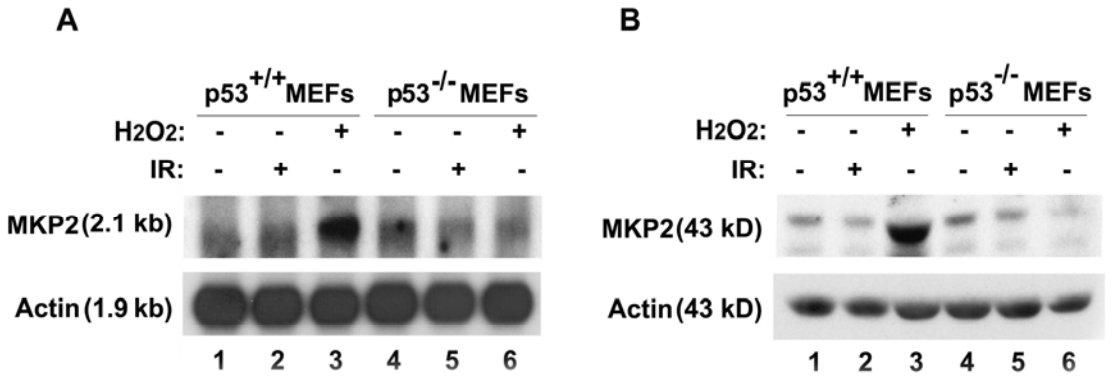

Fig. 1. Induction of MKP2 expression during p53-dependent apoptosis, tested with a mouse embryo fibroblast (MEF) cell system in which γ-irradiation causes cell cycle arrest whereas oxidative stress causes apoptosis. **(A)** MKP2 mRNA expression was detected with Northern blotting in MEFs with either $p53^{+/+}$ or $p53^{-/-}$ genotype exposed to either 6 Gy of γ-irradiation (IR) or 100 μM of H_2O_2 for 3 h. **(B)** Protein levels of MKP2 were analyzed by Western blotting in MEFs stimulated as in (A) for 4 h. GAPDH and actin were used as loading controls for Northern (A) and Western (B) blotting.

ectopic MKP2 expression can also enhance apoptotic responses even independently of p53. These data suggest that p53 regulates distinct genes via different binding mechanisms and that MKP2 is an essential target of p53 in signaling apoptosis.

Mitogen-activated protein kinase phosphatase 2 (MKP2) is a dual-specificity phosphatase known to inactivate mitogen-activated protein (MAP) kinases.[1] We have recently discovered a palindromic site in the promoter of PAC1, a p53-targeted gene, as a p53 binding motif to induce transcription of the PAC1 gene.[2] In order to identify more p53-target genes with palindromes in their regulatory regions, we conducted a genome-wide search for potential p53-targets using palindromic information. A new 10-bp perfect palindromic sequence was found to reside in the promoter region of MKP2, a homologue of PAC1. The perfect palindromic feature implies that it has a potential role as a new site for p53 to bind and activate MKP2 transcription. To test the ability of p53 to induce MKP2, and to investigate whether MKP2 participates in p53-dependent apoptotic cell death, we measured both mRNA and protein levels of MKP2 in a MEF cell system. As shown in (Fig. 1), in normal MEF cells with wild-type p53, MKP2 expression at both mRNA and protein levels was significantly increased by oxidative damage (H_2O_2, lane 3 in both Fig. 1A–Northern and Fig. 1B–Western blots), but not by γ-irradiation (IR, lane 2 in both Fig. 1A and 1B). These observations suggest that, in the presence of p53, MKP2 selectively responds to stimuli leading to apoptosis, but not to cell cycle arrest. To further determine whether p53 is required for the MKP2 response to different cellular stresses, p53-null MEFs ($p53^{-/-}$MEFs) were treated with both γ-irradiation and H_2O_2. Consistent with $p53^{+/+}$MEFs, γ-irradiation failed to stimulate MKP2 expression. Different from the MKP2 response to oxidative stress

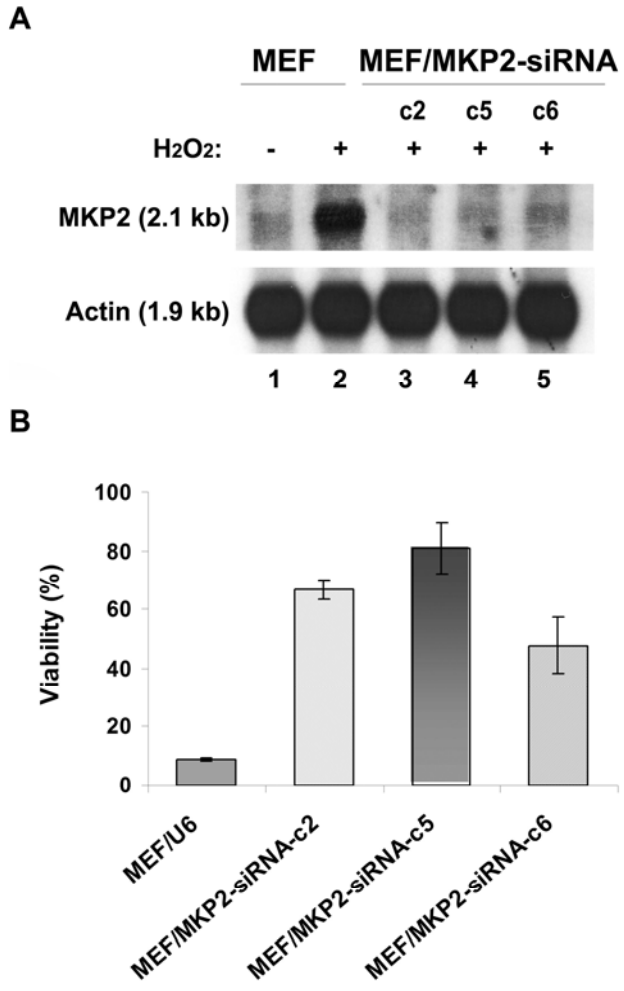

Fig. 2. MKP2 is required for p53-mediated apoptotic responses to oxidative stress. **(A)** MKP2 siRNA eliminated p53-dependent MKP2 expression in MEFs under oxidative stress. $p53^{+/+}$MEFs were transfected with either pSilencer 1.0 U6 vector or U6/MKP2 siRNA, and stable clones were selected. Northern blotting was performed to detect MKP2 expression in these cell clones exposed to 3 h treatment with 100 μM H_2O_2. Equal mRNA levels of actin were shown in each lane. **(B)** Knocking-down MKP2 endowed resistance to H_2O_2-induced cell death in $p53^{+/+}$MEFs. Exponentially growing MEFs containing either pSilencer U6 vector or U6/MKP2 siRNA were stimulated with 100 μM H_2O_2 for 24h, followed by treatment with trypan blue exclusion to measure cell viability. The results are presented as means ± SE of three independent experiments.

in $p53^{+/+}$MEFs, the induction of MKP2 in response to H_2O_2 was undetectable in $p53^{-/-}$MEFs. These data provide clear evidence that MKP2 responds to oxidative stress in a p53-dependent fashion, which places MKP2 in the p53 pathway specifically leading to apoptotic cell death.

To assess the essential role of MKP2 in p53-dependent apoptosis, we examined the change of cell viability of $p53^{+/+}$MEFs in response to oxidative stress when MKP2 is knocked down with small interfering RNA (siRNA). We constructed a mouse MKP2 siRNA vector, U6/MKP2-siRNA, and obtained a set of stable transfected clones (c2, c5 and c6) from $p53^{+/+}$MEFs. Northern blotting (Fig. 2A) confirmed the induction of MKP2, but not β-actin, by H_2O_2 in parental $p53^{+/+}$MEFs. In contrast, the same oxidative stimulus failed to increase MKP2 mRNA in $p53^{+/+}$MEFs containing MKP2-siRNA, indicating that the siRNA specifically blocked MKP2 accumulation in response to oxidative stress. As a consequence, these stable $p53^{+/+}$MEF clones with U6/MKP2-siRNA became resistant to H_2O_2 and resulted in an increased number of viable cells (>50%), com-

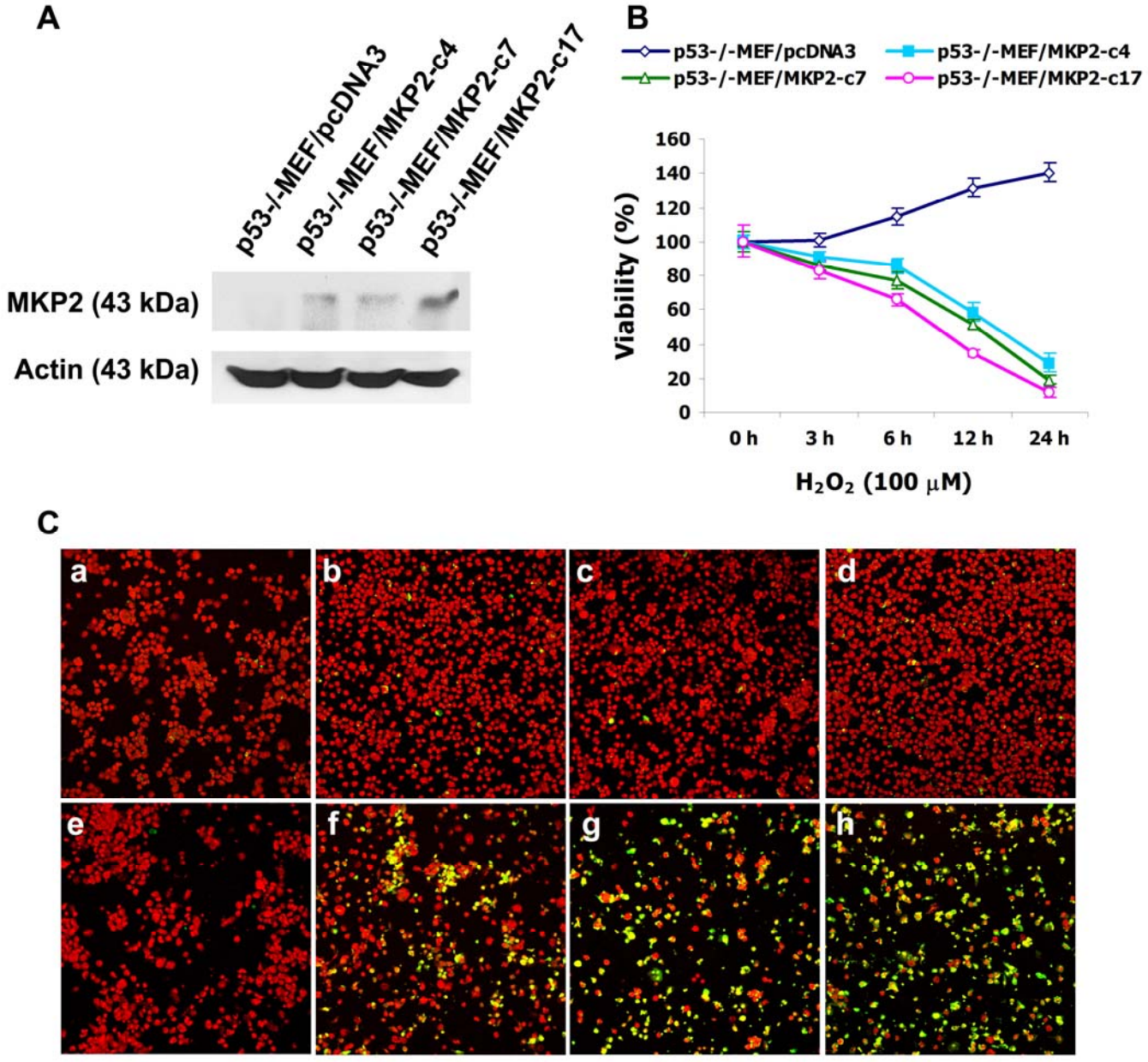

Fig. 3. MKP2 elevates cellular apoptotic responses to oxidative stress in the absence of p53. **(A)** $p53^{-/-}$MEFs were transfected with a mouse MKP2 expression plasmid, pcDNA3-mMKP2. MKP2 expression was analyzed by Western blotting in $p53^{-/-}$MEFs with or without ectopic MKP2. **(B)** Ectopic expression of MKP2 sensitizes $p53^{-/-}$MEFs to oxidative stress-induced apoptosis. Selected $p53^{-/-}$MEF/MKP2 clones, as well as $p53^{-/-}$MEFs transfected with the control vector, were stimulated with H_2O_2 (100 μM) for 24 h. Cell viability was analyzed by trypan blue exclusion. The means ± SE of three independent experiments are shown in the graph. **(C)** The in situ staining of apoptotic cells (a-d, untreated; and e-h, 24 h treatment with 100 μM H_2O_2) detected by the TUNEL assay is shown in the pictures. (a and e) $p53^{-/-}$MEF/pcDNA3; (b and f) p53-/-MEF/MKP2-c4; (c and g) $p53^{-/-}$MEF/MKP2-c7; (d and h) $p53^{-/-}$MEF/MKP2-c17.

pared to the low cell viability (<10%) found in control $p53^{+/+}$MEFs transfected with the empty U6 vector (Fig. 2B). These data suggest that blockage of MKP2 expression offers a signal barrier in a p53-dependent cell death pathway and results in resistance to H_2O_2, demonstrating the essential role of MKP2 in mediating the p53-triggered apoptotic response to oxidative stress. Given its essential role in the p53 apoptotic pathway, MKP2 may elicit an apoptotic response to oxidative stress even in the absence of p53. In order to test this idea, we transfected $p53^{-/-}$MEFs with a mouse MKP2 expression plasmid, pcDNA3-mMKP2, and isolated stable clones (c4, c7 and c17) expressing ectopic MKP2. As shown in Figure 3A, increased expression of MKP2 was observed in $p53^{-/-}$MEFs transfected with pcDNA3-mMKP2, compared to $p53^{-/-}$MEFs transfected with the empty pcDNA3 vector. Ectopic expression of MKP2 greatly augmented the sensitivity of these $p53^{-/-}$MEF cells to oxidative stimulation and resulted in a dramatic reduction of cell viability (Fig. 3B). The apoptotic feature of the oxidation-induced cell death in MKP2-expressing $p53^{-/-}$MEFs is shown by the TUNEL assay (Fig. 3C). These findings provide a p53-independent link between MKP2 and apoptosis, and demonstrate the capability of MKP2 in responding to oxidative stress and provoking apoptotic cell death through a pathway similar to but independent of p53.

In this report, we show that p53 responds to oxidative damage through transcriptional induction of an important MAP kinase phosphatase, MKP2, leading to apoptotic cell death. Residing in the p53 apoptotic pathway, MKP2 can initiate a cellular apoptotic response to oxidative stress even in the absence of p53. Although p53 is well known to signal various cellular responses to stresses and damages,[3] MKP2 is induced by p53 only after the application of stimuli that lead to apoptotic cell death. Our results shed light on how p53 responds to different stresses by selectively inducing distinct categories of target genes, directing diverse cellular outcomes. The important role of MKP2 as a critical mediator of p53 function in signaling apoptosis is demonstrated by its essentiality and sufficiency in provoking p53-dependent cell death under oxidative damage. This work may stimulate subsequent studies that elucidate the molecular mechanism by which p53 regulates the suppression of cancer.

References

1. Theodosiou A and Ashworth A. MAP kinase phosphatases. *Genome Biol* **3**:REVIEWS3009, 2002.
2. Yin Y, Liu YX, Jin YJ, Hall EJ and Barrett JC. PAC1 phosphatase is a transcription target of p53 in signalling apoptosis and growth suppression. *Nature* **422**:527–31, 2003.
3. Vogelstein B, Lane D and Levine AJ. Surfing the p53 network. *Nature* **408**:307–10, 2000. ■

Dr. Eric Hall receives a plaque from Dr. Wendy Bines, OBE, President of the Society for Radiological Protection, in June 2005, at their annual meeting in Cardiff, U.K. Dr. Hall was made an Honorary Fellow of the Society in view of "significant contributions to our understanding of radiobiology and to education, and thereby to radiation protection."

Dr. Hall poses with Dr. Frank Ellis, in September, 2005, on the occasion when Dr. Hall delivered the inaugural Frank Ellis lecture organized by the Royal College of Radiologists, in London, U.K., in honor of Dr. Ellis' 100th birthday. In his long career Dr. Ellis became recognized as Britain's most eminent radiation oncologists and a world leader in cancer radiotherapy.

Deletion of Mouse *Rad9* Leads to High Frequencies of Sister Chromatid Exchange

Kevin M. Hopkins, Adayabalam S. Balajee and Howard B. Lieberman

Mouse embryonic stem cells deleted for *Mrad9* were generated to determine the role of the gene in the response of cells to DNA damaging agents.[1] We found that these cells are very sensitive to a number of DNA damaging agents, including gamma rays, ultraviolet light and hydroxyurea.

To understand the function of Mrad9 in promoting cell survival after exposure to these DNA damaging agents, we initiated a study to examine the role of the protein in homologous recombination. To do this, we started by determining the level of sister chromatid exchange (SCE) in cells differing in the status of *Mrad9*, including populations that were *Mrad9*$^{+/+}$, *Mrad9*$^{+/-}$, *Mrad9*$^{-/-}$, and the latter ectopically expressing *HRAD9* or *Mrad9*. We found that cells devoid of Mrad9 protein have a two-fold increase in the level of SCE, relative to that observed in wild-type *Mrad9* cells (Fig. 1). This higher level was reflected both in terms of exchanges per cell and per chromosome (Table 1). In addition, the range of SCEs per cell for the *Mrad9*$^{+/+}$ population was 1–16, whereas the range for *Mrad9*$^{-/-}$ was 4–24 (Table 2).

The method to determine SCE uses Fluorodeoxyuridine (FudR) as part of the procedure. Treatment of cells with FudR can lead to the incorporation of uracil into DNA.[2] Interestingly, *Mrad9*$^{-/-}$ cells are sensitive to FudR relative to *Mrad9*$^{+/+}$ cells (Fig. 2). By using an *in vitro* base excision repair (BER) assay, we show that *Mrad9*$^{-/-}$ protein cell extracts show up to a three fold reduction of incision at sites of uracil in a DNA oligonucleotide when compared to *Mrad9*$^{+/+}$ cell-free protein extracts (Fig. 3). These results suggest that the high levels of SCE in *Mrad9* mutant cells might in fact be due to their inability to remove uracil from genomic DNA by BER.

Additional studies are underway to understand how mutations in *Mrad9* lead to the formation of high levels of SCEs, and how these results relate to cellular resistance to DNA damage.

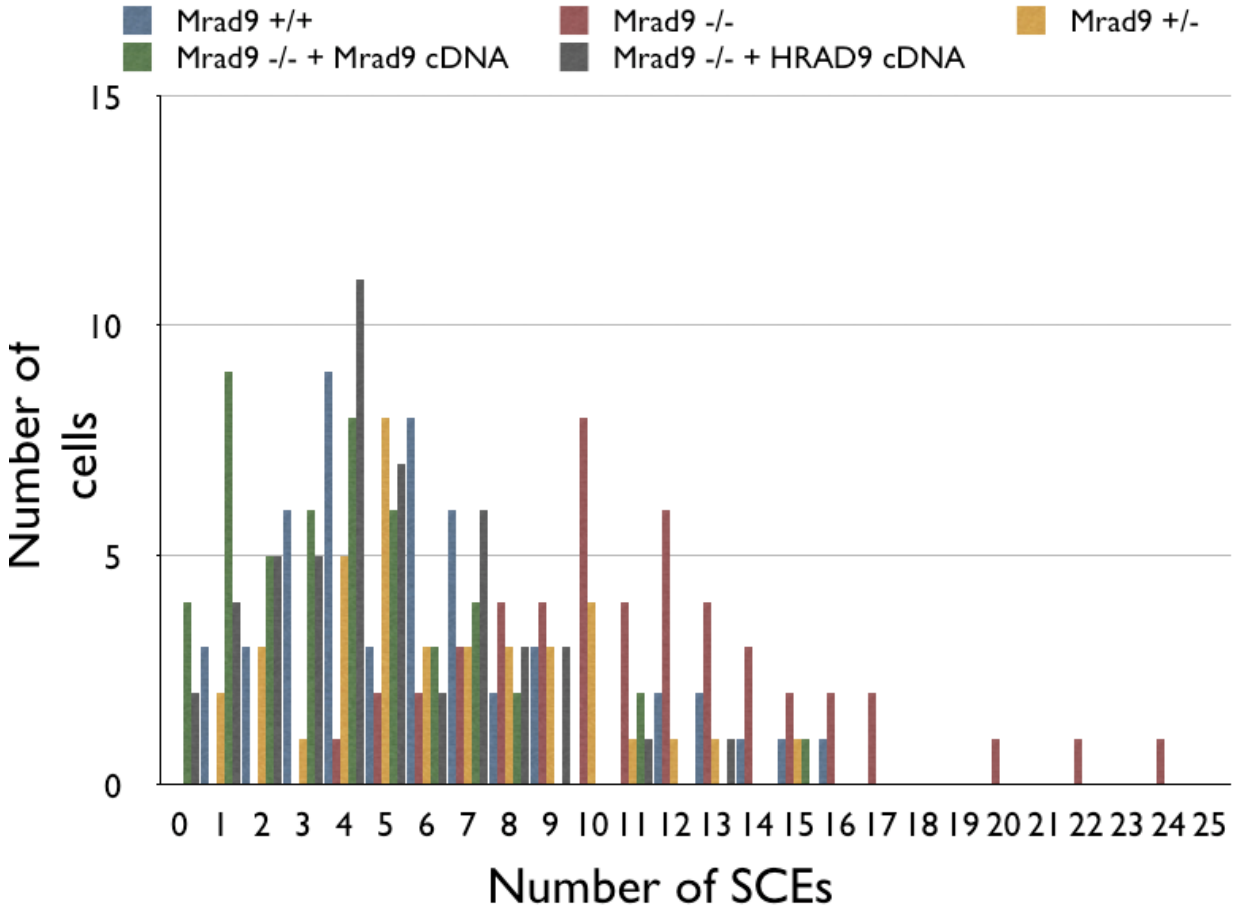

Fig. 1. Frequencies of sister chromatid exchange (SCE) in mouse embryonic stem cells differing in the status of *Mrad9*.

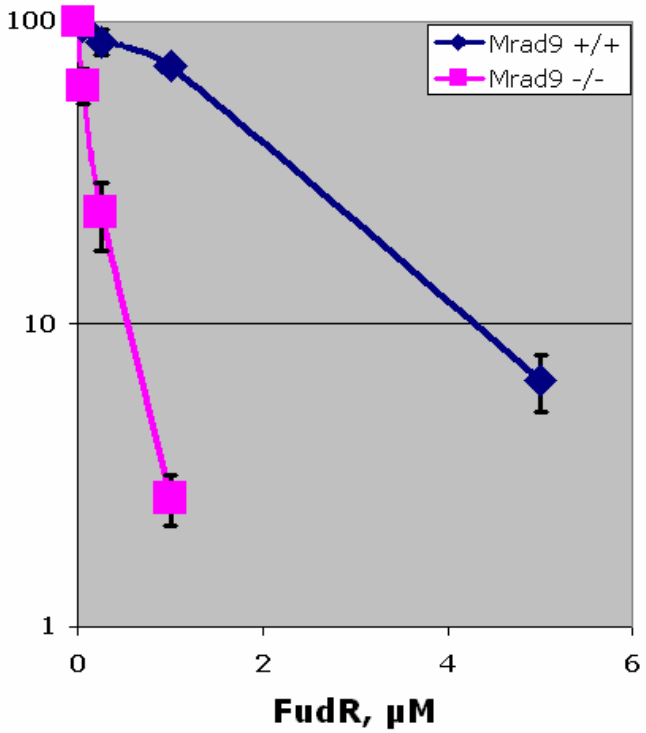

Fig. 2. Fluorodeoxyuridine (FudR) sensitivity of *Mrad9*$^{+/+}$ and *Mrad9*$^{-/-}$ mouse embryonic stem cells.

Table 1.
Effect of *Mrad9* status on SCE per cell and per chromosome.

SCEs per Cell and Chromosome.

Cell Line	Exchange/ Cell	Exchange/ Chromosome
Mrad9$^{+/+}$	6.12	.154
Mrad9$^{+/-}$	6.46	.158
Mrad9$^{-/-}$	11.34	.281
Mrad9$^{-/-}$ + Mrad9 cDNA	3.96	.099
Mrad9$^{-/-}$ + HRAD9 cDNA	4.74	.118

Table 2.
Effect of *Mrad9* status on range of SCE per cell.

Range of SCEs per Cell.

Cell Line	SCEs
Mrad9$^{+/+}$	1-16
Mrad9$^{+/-}$	1-15
Mrad9$^{-/-}$	4-24
Mrad9$^{-/-}$ + Mrad9 cDNA	0-15
Mrad9$^{-/-}$ + HRAD9 cDNA	0-13

References

1. Hopkins KM, Auerbach W, Wang XY, Hande MP, Hang H, Wolgemuth DJ, Joyner AL, Lieberman HB. Deletion of mouse rad9 causes abnormal cellular responses to DNA damage, genomic instability, and embryonic lethality. *Mol Cell Biol* **24**:7235–48, 2004.
2. Mishina Y, Ayusawa D, Seno T and Koyama H. Thymidylate stress induces homologous recombination activity in mammalian cells. *Mutat Res* **246**:215–20, 1991. ■

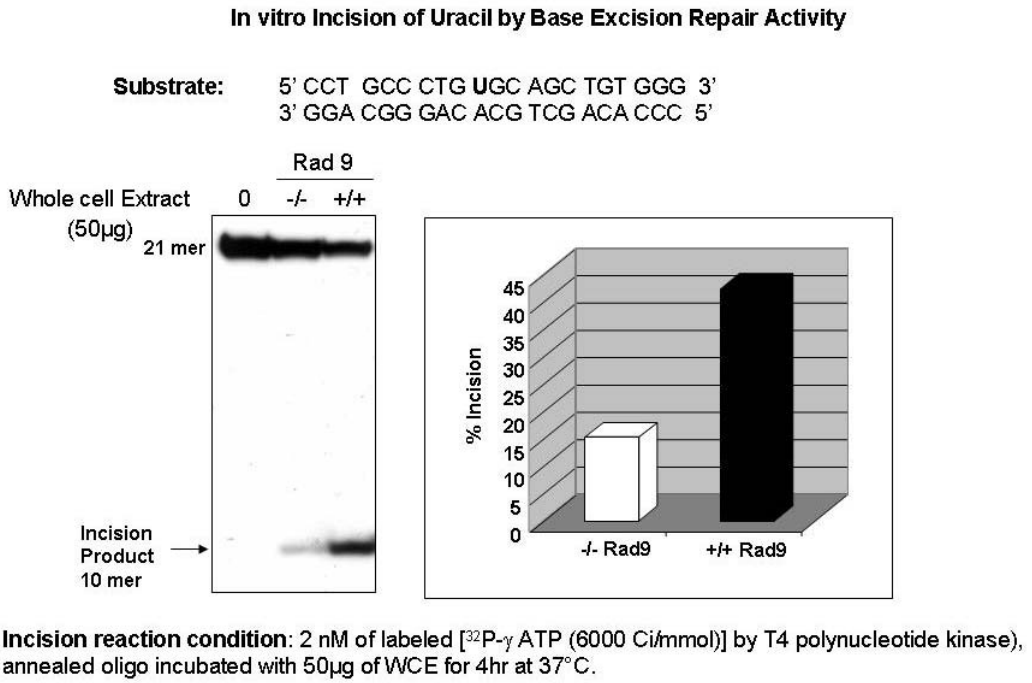

Fig. 3. Base excision repair assay for incision at sites of Uracil in DNA by *Mrad9*$^{+/+}$ and *Mrad9*$^{-/-}$ cell-free protein extracts.

Characterization of *Mrad9B*$^{-/-}$ Mouse ES Cells and Generation of *Mrad9B*$^{-/-}$ Mice

Corinne Leloup, Aiping Zhu, Kevin M. Hopkins and Howard B. Lieberman

Introduction

Human *HRAD9B* and mouse *Mrad9B* were identified in our laboratory as paralogs of the cell cycle checkpoint control genes *HRAD9* and *Mrad9*, respectively.[1]

RAD9, which shares 35% identity and 50% similarity with *RAD9B,* plays a key role in maintaining genomic stability. It is involved in G1 and G2/M checkpoint control[2,3] possibly by inducing p21 transcription[4] and by detecting DNA damage as a member of the 9-1-1 (hRAD9-hRAD1-hHUS1) complex.[5] It is essential for embryonic development. It is also involved in base damage repair and reduces death induced by UV, γ-irradiation, hydroxyurea and mitomycin C (3, unpublished results). RAD9 is expressed in many tissues in mammals, both in human and mouse, while RAD9B is predominantly localized in the testis.

In order to determine the function of *Mrad9B*, the first two exons of that gene were knocked out by homologous recombination in mouse embryonic stem (ES) cells, thereby inactivating *Mrad9B*. Mouse ES cells heterozygous and homozygous deleted for *Mrad9B* were generated. Those cells are being compared to WT (wild type) cells in regard to cell cycle and DNA repair characteristics.

In order to study the role of Mrad9B in development and especially in relation to testis, the generation of knock-out mice is being pursued.

Moreover, since RAD9B seems to share some RAD9 functions, we are investigating whether the proteins have truly redundant functions.

Sensitivity of *Mrad9B*$^{-/-}$ cells to various DNA damaging agents

Mrad9B$^{-/-}$ and wild type ES cells were seeded at low density and treated with various DNA damaging agents. One week later, colonies originating from surviving cells were counted. As shown in Table 1, *Mrad9B*$^{-/-}$ cells are sensitive to UV, γ-irradiation and mitomycin C.

The knockout ES cells were not clearly sensitive to hydroxyurea, cisplatin and ethyl methane-sulfonate relative to the WT control.

Table 1.
Percent survival for WT and *Mrad9B*$^{-/-}$ (mt) cells after treatment with 254 nm UV-light (UV), ^{137}Cesium (γ-rays) or mitomycin C (mit. C).*

	UV (25 J/m^2)	γ-rays (8 Gy)	mit. C (0.9 μg/ml)
WT	8 ± 1.3	4.4± 0.8	47.1± 6.5
mt	2 ± 0.6	1.7± 0.1	21± 5.5

* The data are presented as mean ± S.E.M. Percent survival is calculated as the number of colonies formed in treated versus untreated populations times 100.

Complementation between Rad9 and Rad9B.

In order to assess whether Mrad9 and HRAD9 can make up for loss of Mrad9B function in the presence of DNA damaging agents, *Mrad9B*$^{-/-}$ ES cells were stably transfected with *HRAD9* and *Mrad9* cDNAs in expression vectors. Similarly, *Mrad9*$^{-/-}$ cells were stably transfected with *HRAD9B* and *Mrad9B* cDNAs in appropriate vectors. Clones were isolated and the expression of the transfected genes is currently under investigation.

Generation of knock-out mice.

Heterozygous *Mrad9B*$^{-/-}$ ES cells were injected into C57BL/6J mouse blastocysts. Chimeric offspring were born and the males were mated with C57BL/6J wild type females. Forty mice were born and will be assessed by southern blotting for germline transmission of the mutated allele. If successful, the heterozygous mice will be bred to produce homozygous mutant animals.

References

1. Hopkins KM, Wang X, Berlin A, Hang H, Thaker HM, Lieberman HB. Expression of Mammalian Paralogues of HRAD9 and Mrad9 Checkpoint Control Genes in Normal and Cancerous Testicular Tissue. *Cancer Res* **63**:5291–8, 2003.
2. Chen MJ, Lin YT, Lieberman HB, Chen G, Lee EY. ATM-dependent phosphorylation of human Rad9 is required for ionizing radiation-induced checkpoint activation. *J Biol Chem* **276**:16580–6, 2001.
3. Hopkins, KM, Auerbach, W, Wang, XY, Hande, MP, Hang, H, Wolgemuth, DJ, Joyne, AL, and Lieberman, HB. Deletion of mouse *Rad9* causes abnormal cellular responses to DNA damage, genomic instability and embryonic lethality. *Mol Biol* **24**:7235–48, 2004.
4. Yin Y, Zhu A, Jin YJ, Liu YX, Zhang X, Hopkins KM, Lieberman HB. Human RAD9 checkpoint control/ proapoptotic protein can activate transcription of p21. *Proc Natl Acad Sci USA* **101**:8864–9, 2004.
5. Hang H, Lieberman HB. Physical interactions among human checkpoint control proteins HUS1p, RAD1p, and RAD9p, and implications for the regulation of cell cycle progression. *Genomics* **65**:24–33, 2000. ■

Human Chromosome 11-Encoded Antigens Expressed on A_L Cells: Flow Cytometry Analysis for Detecting Mutations Induced by Arsenic and Asbestos

Michael A. Partridge, SiYuan Yao,[1] An Xu, Hongning Zhou and Tom K. Hei

Introduction

The quantification of chromosomal mutations generated by treating cells with chemical or radiological mutagens has been a critical research tool in the laboratory for a number of years. The principal cell line used for these studies was the human-hamster hybrid A_L cells. A_L cells are Chinese hamster ovary (CHO) cells with human chromosome 11 stably incorporated into the nucleus. The quantification of DNA mutations in these cells has, until recently, been accomplished with the complement-antibody cell lysis assay. The assay measures absence of a human chromosome 11-encoded antigen, CD59, on the surface of the cells. In the presence of anti-CD59 antibody and complement, wild type cells are lysed while mutated cells (which have lost the marker) survive to form colonies.[1-3]

Recently, an alternative technique for quantitating the number of cells expressing CD59 has been developed which utilizes flow cytometry.[4,5] This method permits a more precise determination of the level of *CD59* mutagenesis because it eliminates a number of variables inherent in the traditional complement-antibody cytotoxicity assay; non-specific toxicity of complement, differences in plating efficiency, and counting and pipetting errors, to name a few. Interestingly, flow cytometry analysis may provide a tool for detecting deletions in other regions of human chromosome 11 in A_L cells, as the chromosome encodes genes for at least 19 other cell surface antigens. We first wanted to determine which of these proteins were expressed on the surface of A_L cells (i.e., could be detected with commercially available antibodies by flow cytometry) and, subsequently, we wanted to know whether flow cytometry with these antibodies could be used to quantify gene deletions after mutagenic treatment, as has been established at the *CD59* locus.[5] Finally we wondered whether flow cytometry could be used to detect multilocus deletions in CD59-negative clones isolated from the complement-antibody lysis assay. Previously, deletions at different loci on human chromosome 11 had been detected using multiplex PCR, revealing the spectrum of mutations induced by exposure to mutagens.[6,7] Although PCR is a relatively rapid diagnostic technique, flow cytometry is an even faster procedure. Furthermore, there is no need to extract DNA as there is with PCR and, in addition, multiple antigens (encoded at different loci) can be detected in a single sample by using antibodies conjugated to different fluorophores.

In this report we have identified five additional chromosome 11-encoded antigens that are expressed on the surface of A_L cells. Furthermore, we have determined that these antigen-antibody combinations can be used to quantitate the level of mutation induced by treatment of A_L cells with two known mutagens, asbestos and arsenic. Finally, we have analyzed *CD59* negative clones isolated from the complement-antibody lysis assay and confirmed that they can be used as an alternative to multiplex PCR for the detection of multilocus deletions on human chromosome 11 in A_L cells.

Results

Human antigens expressed on A_L cells

Initially we wanted to determine which of the putative surface antigens encoded by human chromosome 11 were expressed on A_L cells. Examination of the commercial and academic literature identified 19 cell surface markers encoded on the chromosome and more than half of these markers had commercially available antibodies that recognized the antigen.[8,9] In addition to anti-CD59, we selected 8 antibodies to be tested based on two criteria; we required probes for gene products that were encoded at a range of loci on both the short and long arms of chromosome 11, and we wanted antibodies to detect proteins encoded at loci that were unique and not closely linked. We first determined whether A_L cells expressed the antigen at the cell surface and found that most of the antibodies positively stained A_L cells (Table 1). One antibody, CD82, stained A_L cells very weakly, even at very high antibody dilutions (1:4). Only 2 of the antibodies tested were unable to detect antigens on A_L cells, anti-CD3 and anti-CD20. Even when cells were detached from culture dishes with 1 mM EDTA alone before flow cytometry analysis, CD3 and CD20 still could not be detected, and CD82 remained only weakly positive, confirming that these negative results were not due to trypsinization of the antigen. CD3 and CD20 are only expressed in T-cells and B-cells, respectively, so it was not surprising that they were not expressed in the human-hamster hybrid cell line. All antibodies that positively stained A_L cells were subsequently tested with CHO cells to confirm that the antibody was recognizing human chromosome 11 encoded proteins and not cross-reacting with hamster antigens. Anti-CD81 antibody was the only antibody to have a minor positive reaction to CHO cells (average fluorescence increase ± SE = 2.9 ± 0.2, [Ab] = 1:100), but this could largely be eliminated by using the antibody at a lower dilution (1.1 ± 0.1, 1:200).

The second step in identifying probes that could be used for flow cytometry analysis of mutations was establishing the correct antibody dilution for staining. This was important

[1] *Student from Okayama University Medical School, Okayama, Japan.*

Table 1.
Human antigens expressed on A_L cells.

Human Chromosome 11 Cell Surface Antigens on A_L cells				
Name	**Fluor.***	**Location**	**Antibody (dilution)**	**Reaction#**
		Short Arm		
CD151	PE	p15.5	BD (1:50)	++
CD81	PE	p15	BD (1:200)	++
CD59	FITC	p13	BD (1:400)	++
CD44R		p13		n.d.
CD44	FITC	p13	BD (1:10)	+
CD148		p11.2		n.d.
CD82	FITC	p11.2	eBioscience (1:4)	weak
		Long Arm		
CD20	APC	q12-q13.1	BD	-
CD57		q12	Sigma, eBioscience	n.d.
CD5		q13	BD, Sigma	n.d.
CD6		q13	BD	n.d.
CD98	PE	q13	BD (1:100)	++
CD90	APC	q22.3-q23	BD (1:100)	++
CD3	PE	q23	BD	-
CD146		q23.3	BD, Chemicon	n.d.
CD56	APC	q23-q24	BD (1:4)	+
CD111		q23-q24		n.d.
		Unknown		
CDw210				n.d.
CD225				n.d.

* Fluorophore: FITC, Fluorescein Isothiocyanate; PE, Phycoerythrin; APC, Allophycocyanin.
# Average response at least one (+) or two (++) orders of magnitude above background.

because we anticipated that only a small percentage of the population of treated cells would incur a DNA mutation in the gene being tested. Thus, we needed to use the antibody at a concentration that maximized its sensitivity to change in antigen concentration, while still exhibiting a strong response. This analysis was performed for all 5 antibodies that positively stained A_L cells and the appropriate concentrations for use in flow cytometry are given in Table 1.

Flow Cytometry for detecting mutagenesis of chromosome 11-encoded genes

It has been previously established that flow cytometry could be used as an alternative to the complement-antibody cytotoxicity assay for detecting deletions at the *CD59* locus in A_L cells.[5] Having established a suite of antibodies that recognized different antigens encoded on human chromosome 11 which were expressed on A_L cells, we wanted to determine whether they could be used as probes for detecting gene deletions after treatment with mutagenic agents. To accomplish this we treated cells with asbestos and arsenic, two substances known to cause mutations at the *CD59* locus in A_L cells.[1,6] We first confirmed that the treatments resulted in a dose-dependent increase in mutation/deletions using both the complement-antibody cytotoxicity assay and flow cytometry analysis (Table 2). Next we analyzed by flow cytometry each of the newly identified antibody probes that could detect human antigens on the surface of A_L cells. Using pools of cells that had been allowed to recover for 7–10 days after treatment, we stained the cells with each antibody and compared the results to those obtained with untreated cells. For each antibody, gates were set to ensure that >95% of unstained cells were considered negative. Using these parameters, we were able to identify a dose-dependent increase in antigen-negative cells after treatment with both arsenic and asbestos (Table 3). This confirmed that, in addition to *CD59*, flow cytometry could be used to detect deletions at a number of other loci on human chromosome 11.

Table 3.
Increase in human antigen-negative cells after arsenic or asbestos treatment.

	Proportionate Increase in Antigen-Negative A_L Cells*					
	Arsenic (ng/mL)			Asbestos (μg/mL)		
Locus	0	250	500	0	10	20
CD56	1	1.30	2.61	1	1.47	1.68
CD81	1	1.83	2.32	1	0.92	1.72
CD90	1	1.37	1.49	1	n.d.	2.60
CD98	1	1.48	1.78	1	n.d.	5.71
CD151	1	1.20	3.43	1	1.22	1.54

* Samples were normalized around the number of antigen-negative events in untreated cells and the percentage increase after treatment expressed as a proportion of that figure.

Having established that flow cytometry could detect mutations at several individual loci in pools of arsenic and asbestos treated A_L cells, we wanted to determine whether this technique could be used as an alternative to multiplex PCR for analyzing the deletion spectrum in CD59 negative clones. To accomplish this we isolated clones from sister plates of those used in the initial analysis of mutation frequency with the complement-antibody cytotoxicity assay. Clones were then expanded until sufficient cells were available for flow cytometry using each of the available antibodies. The results for 19 clones isolated from arsenic treatment, and 9 clones from asbestos treatment, are presented in Table 4. As expected, CD59 was not expressed in any of the clones tested. In addition, 13 clones from both treatments did not express antigens encoded by the *CD90* and *CD98* genes,

Table 2.
CD59 mutation fraction after arsenic or asbestos treatment of A_L cells.

	Mutation Fraction (10^{-5} Survivors)					
	Arsenic (ng/mL)			Asbestos (μg/mL)		
	0	250	500	0	10	20
Complement-Antibody Assay	34 ± 23	87 ± 59	154 ± 33	163 ± 37	288 ± 44	598 ± 49
Flow Cytometry	135 ± 49	212 ± 53	244 ± 68	247 ± 112	565 ± 179	709 ± 187

both of which are located on the long arm of human chromosome 11 (Table 1). These results clearly show that flow cytometry is readily applicable to determining mutation spectrums and may provide a simple and rapid alternative to multiplex PCR for this analysis.

Interestingly, the antibody to one of the human chromosome 11-encoded antigens expressed on A_L cells, CD151, did not detect mutations in any of the clones from either arsenic or asbestos treatment. All of the other antibodies tested had identified at least one clone in which the corresponding gene had been mutated (Table 4). Importantly, CD151 is encoded at the distal end of the short arm, tightly linked to the gene encoding the small guanosine triphosphatase (GTPase), Ras (11p15.5). Ras expression is essential for the stable incorporation of human chromosome 11 into CHO cells[6,10] and so it is likely that mutations in the linked *CD151* gene may also affect Ras expression, rendering the clone inviable. Two other antibodies detected only one clone in which the corresponding protein was not expressed, CD56 and CD81. Like, CD151, CD81 is encoded at the distal end of the short arm of chromosome 11 and mutations in this region are likely to also affect Ras expression. CD56 is encoded at the other end of chromosome 11 at the distal end of the long arm. Although not linked to any genes essential for A_L cell survival, it is possible that deletions/mutations in this gene may also affect the telomere region causing instability in the chromosome and consequently decrease the viability of A_L cells.

Discussion

Flow cytometry is a technique routinely used in cell biology to analyze processes such as apoptosis, cell differentiation and cell cycle progression.[11-13] Recently, it has been used as an alternative to the complement-antibody cytotoxicity assay for detecting mutations in the human-hamster hybrid A_L cells. We wanted to expand the applicability of flow cytometry for mutation analysis in the A_L cell line by identifying antibodies that recognized other antigens expressed on the cell surface. We have now established that five probes, in addition to anti-CD59, can be used to detect mutations at loci spanning the short and long arms of human chromosome 11. This may permit a more precise analysis of the regions of human chromosome 11 that different mutagens act on, and, as a consequence, may allow identification of mutations that occur primarily in regions other than the *CD59* locus, which would have otherwise been missed in the traditional anti-CD59-based mutation assays.

In addition to their utility in detecting mutations in pools of treated cells, the suite of antibody probes identified here also provides an alternative to multiplex PCR for assaying

Table 4.
Mutation spectrum of CD59⁻ negative clones after arsenic or asbestos treatment.

		Cell Surface Antigen					
Treatment	**Clone**	**CD56**	**CD90**	**CD98**	**CD59**	**CD81**	**CD151**
Arsenic-νg/mL							
0	0.1	+	-	-	-	+	+
0	0.2	+	+	+	-	+	+
0	0.3	+	+	+	-	+	+
0	0.4	+	+	+	-	+	+
0	0.5	+	-	-	-	+	+
0	0.6	+	-	-	-	+	+
250	25.1	+	+	+	-	+	+
250	25.2	+	+	+	-	+	+
250	25.4	+	+	+	-	+	+
250	25.5	+	+	+	-	+	+
500	50.1	+	-	-	-	+	+
500	50.2	+	-	-	-	+	+
500	50.3	+	+	+	-	+	+
500	50.4	+	-	-	-	+	+
500	50.5	+	-	-	-	+	+
500	50.6	+	-	-	-	+	+
500	50.7	+	+	+	-	+	+
500	50.8	+	-	-	-	+	+
500	50.9	+	+	+	-	+	+
Asbestos-μg/mL							
0	0.1	+	+	+	-	+	+
0	0.2	+	+	+	-	+	+
0	0.3	+	+	+	-	+	+
10	10.1	+	-	-	-	+	+
10	10.2	+	+	+	-	+	+
10	10.3	+	-	-	-	+	+
20	20.1	+	-	-	-	+	+
20	20.2	-	-	-	-	-	+
20	20.3	+	+	+	-	+	+

the mutagenic spectrum in CD59 negative clones. Flow cytometry has some limitations in comparison to PCR for this purpose because only genes that express cell surface antigens can be analyzed. In addition, PCR assays the presence of the gene itself whereas flow cytometry (and the complement-antibody lysis assay) measure the presence of the gene product. However, flow cytometry is a more rapid technique than PCR for identifying clones that have deletions on both the long and short arms of human chromosome 11. Consequently, flow cytometry provides a high-speed screening tool for determination of important CD59-negative clones for additional analysis.

References

1. Hei TK, Piao CQ, He ZY, Vannais D and Waldren CA. Chrysotile fiber is a strong mutagen in mammalian cells. *Cancer Res* **52**:6305–9, 1992.
2. Waldren C, Jones C and Puck TT. Measurement of mutagenesis in mammalian cells. *Proc Natl Acad Sci U S A* **76**:1358–62, 1979.
3. Waldren C, Correll L, Sognier MA and Puck TT. Measurement of low levels of x-ray mutagenesis in relation to human disease. *Proc Natl Acad Sci U S A* **83**:4839–43, 1986.
4. Wedemeyer N, Greve B, Uthe D, Potter T, Denklau D, Severin E, Hacker-Klom U, Kohnlein W and Gohde W. Frequency of CD59 mutations induced in human-hamster hybrid $A(_L)$ cells by low-dose X-irradiation. *Mutat Res* **473**:73–84, 2001.
5. Zhou H, Xu A, Gillispie JA, Waldren CA and Hei TK. Quantification of CD59(-) mutants in human-hamster hybrid ($A(_L)$) cells by flow cytometry. *Mutat Res* 2005.
6. Hei TK, Liu SX and Waldren C. Mutagenicity of arsenic in mammalian cells: role of reactive oxygen species. *Proc Natl Acad Sci U S A* **95**:8103–7, 1998.
7. Hei TK, Wu LJ, Liu SX, Vannais D, Waldren CA and Randers-Pehrson G. Mutagenic effects of a single and an exact number of alpha particles in mammalian cells. *Proc Natl Acad Sci U S A* **94**:3765–70, 1997.
8. BD Biosciences, Official Poster of the 8th International Workshop on Human Leukocyte Differentiation Antigens, Adelaide, Australia, Dec. 12–16, 2004: http://www.bdbiosciences.com/pdfs/other/05-810095-3A_HLDA.pdf.
9. eBioscience; Human CD and other surface antigens: http://www.ebioscience.com/ebioscience/whatsnew/humancdchart.htm.
10. McGuinness SM, Shibuya ML, Ueno AM, Vannais DB and Waldren CA. Mutant quantity and quality in mammalian cells (A_L) exposed to cesium-137 gamma radiation: effect of caffeine. *Radiat Res* **142**:247–55, 1995.
11. Nicoletti I, Migliorati G, Pagliacci MC, Grignani F and Riccardi C. A rapid and simple method for measuring thymocyte apoptosis by propidium iodide staining and flow cytometry. *J Immunol Methods* **139**:271–9, 1991.
12. Guadagno TM and Assoian RK. G1/S control of anchorage-independent growth in the fibroblast cell cycle. *J Cell Biol* **115**:1419–25, 1991.
13. Schmeissner PJ, Xie H, Smilenov LB, Shu F and Marcantonio EE. Integrin functions play a key role in the differentiation of thymocytes in vivo. *J Immunol* **167**:3715–24, 2001. ■

Cellular Responses of Lymphoblasts to 1 GeV ^{56}Fe Ions

Sally A. Amundson and Jaeyong Ahn

Introduction

Exposure to heavy ions from galactic cosmic rays poses a serious radiological health concern for extended space missions. ^{56}Fe ions are a major component of Galactic Cosmic Rays and at 1 GeV/amu, have a LET of approximately 148 keV/μm. This is within the range of maximum RBE for cell killing, and many studies have focused on these particles. To date, studies of cellular endpoints, including toxicity, cytogenetic changes, and mutagenesis, have formed the basis of our understanding of biological responses to the unique space radiation environment. Studies of molecular signaling responses can further our mechanistic understanding, and lead to biomarker identification, improved risk assessment, and more targeted design of intervention and radiation protection measures.

This study utilized the well-characterized p53 wild-type human TK6 cell line, and its p53-null derivative, NH32.[1] Three independent irradiations with 1 GeV ^{56}Fe ions were completed at the NASA Space Radiation Laboratory during two runs (NSRL-5 and NSRL-6). Cellular parameters and preliminary gene expression data are reported here, while profiling by microarray analysis is ongoing.

Survival

Irradiation with high-charge high-energy particles, such as 1 GeV ^{56}Fe ions, temporarily activates the tissue culture medium, making it an additional source of ionizing radiation in these experiments. Since the lower LET radiation from the activated medium could contribute to cellular responses, all experiments utilized an "activated medium control." Culturing unexposed cells in the presence of activated medium that was exposed to 250 cGy ^{56}Fe ions did not alter cloning

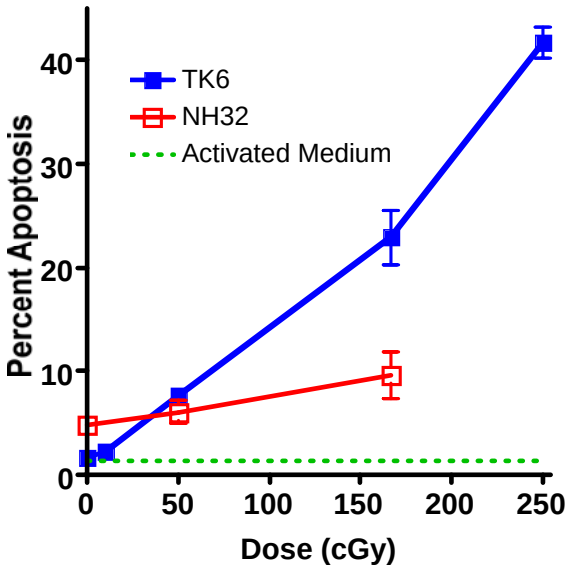

Fig. 1. Percentage of apoptotic cells by DAPI staining 2 days after irradiation with 1 GeV ^{56}Fe ions, the peak of TK6 apoptosis.

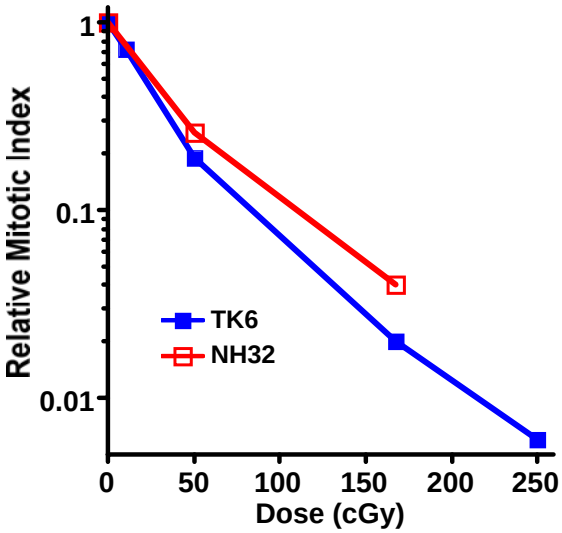

Fig. 2. Relative mitotic index 3 hours after irradiation as measured by phospho-histone H3 staining and flow cytometry. Percentage of cells in mitosis in treated cells was normalized to that in controls.

efficiency. The lowest particle exposure used, equivalent to 10 cGy, did result in a nearly 20% decrease in cell survival, however. TK6 survival decreased linearly with increasing dose, with observed survival levels in agreement with what was predicted from the literature. The NH32 cells were treated with only two doses of iron ions, so the shape of the survival curve could not be accurately determined. Survival of the p53 knock-out cells was similar to that of the parental TK6, with perhaps a slightly enhanced survival evident at the higher dose.

Apoptosis

Nuclear morphology was scored in DAPI-stained cells as a measure of apoptosis at 3 hours after irradiation, and at 24-hour intervals for the first week after exposure. Activated medium alone did not produce any significant deviations from the level of apoptosis in the unirradiated controls. The 10 cGy dose produced a slight, transient elevation of apoptosis. Induction of apoptosis increased with increasing dose, and returned to near-baseline levels by one week after exposure. No further elevation in apoptosis was observed at later times. Interestingly, the p53 knock-out cells showed nearly the same peak levels of apoptosis as the p53 wild-type parent cell line, but with different kinetics of expression. Apoptotic morphology took longer to manifest in the absence of p53 protein, and apoptotic cells then persisted in culture somewhat longer. Peak levels of apoptosis in TK6 were observed around two days after irradiation (Fig. 1), while apoptosis did not peak in NH32 cells until a day or two later, when apoptosis levels in TK6 were already declining.

Cell cycle and mitotic index

Irradiation from culturing cells in the presence of activated medium did not alter cell cycle distribution or mitotic index. In contrast, the lowest exposure, 10 cGy, did induce a cell cycle disturbance, reflected as a decrease in mitotic index. This decrease was transient, with the cultures recovering normal levels of mitosis by 24 hours. Increasing doses resulted in more profound and more prolonged loss of cells from M-phase. The dose-response for relative mitotic index 3 hours after irradiation is illustrated in Figure 2. Although the initial effects were quite similar with or without p53, the knock-out cell line appeared to resume normal cell cycle progression more rapidly than the wild-type TK6. All cultures had recovered normal levels of mitosis by one week post-exposure, and further disturbances were not noted at later times.

Gene expression

CDKN1A is generally one of the most robustly radiation-responsive genes in cells expressing wild-type p53. Expression of this "sentinel" gene was measured at multiple times after irradiation. Incubation of cells in activated medium did not result in any measurable change in *CDKN1A* expression at any time-point assayed. Peak expression in TK6 cells exposed to ^{56}Fe ions occurred between 3 and 4 hours post-irradiation, consistent with results from low LET experiments. However, in contrast to the rapid return to near normal gene expression levels expected with low LET, ^{56}Fe ion exposure yielded a prolonged elevation of *CDKN1A* expression, with little decrease from maximum levels during the first 24 hours. By one week after treatment, levels had returned to normal, and did not increase further through week three. This protracted elevation was observed even at the lowest dose, 10 cGy.

The dose response remained fairly linear at all times between 2 and 24 hours. There was a slight flattening of the dose-response curve at the highest dose, as is typically seen for highly toxic treatments. Interestingly, there is also a discontinuity evident at the low end of the dose-response curve. This mirrors the response we have seen previously with low LET, where gene induction responses for several genes were

found to be linear, but did not extrapolate back to baseline levels at zero dose.[2] These results indicate that expected gene expression responses were seen, and that the 167 cGy dose may yield maximum magnitudes of gene expression changes in the microarray analyses.

The ionizing radiation response of *CDKN1A* is dependent on TP53, and as expected, no induction was observed at early times in NH32, the p53 knock-out cell line. At 24 hours, there was a slight elevation in *CDKN1A* levels in the ^{56}Fe ion treated NH32 cultures, however. This was significant at the 167 cGy dose, although the magnitude of induction remained far below that in TK6, the TP53 wild-type cell line (Fig. 3).

Conclusion

The measured survival and apoptosis responses to 1 GeV ^{56}Fe ions in these experiments were in line with predictions based on prior publications, indicating the robustness of our experimental protocols. The induction of apoptotic cells in the p53 knock-out cell line after irradiation with ^{56}Fe ions has precedence in the response to γ-rays, where delayed onset apoptosis has also been reported.

Interestingly, the cell cycle response of the p53 wild-type TK6 differed between γ-rays and ^{56}Fe ions. While TK6 manifests no immediate G_1 block in response to γ-rays, exposure to ^{56}Fe ions did not result in the characteristic rapid loss of cells from G_1. This may indicate an altered regulation of cell cycle delay in response to high-charge high-energy particle irradiation, which could impact on the biological response to space radiation at many levels. This aspect warrants further investigation, and will be of high interest as the signaling pathways revealed by our ongoing microarray analysis are unraveled.

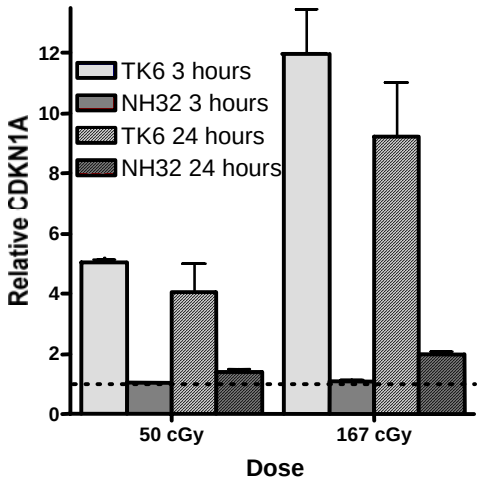

Fig. 3. Induction by 1 GeV ^{56}Fe ions relative to control levels (dashed line) of *CDKN1A* mRNA measured by quantitative hybridization.[3]

References

1. Chuang YY, Chen Q, Brown JP, Sedivy JM and Liber HL. Radiation-induced mutations at the autosomal thymidine kinase locus are not elevated in p53-null cells. *Cancer Research* **59:**3073–6, 1999.
2. Amundson SA, Do KT and Fornace AJ Jr. Stress gene induction by low doses of gamma-rays. *Radiation Research* **152**:225–31, 1999.
3. Koch-Paiz CA, Momenan R, Amundson SA, Lamoreaux E and Fornace AJ Jr. Estimation of relative mRNA content by filter hybridization to a polyuridylic probe. *Biotechniques* **29**:706–14, 2000. ■

Regulation of the Susceptibility of Cancer Cells to Apoptosis through the Inhibition of Dynamin-2 Expression

Vladimir N. Ivanov, Sangsoo Kim and Tom K. Hei

Melanoma, the most aggressive form of skin cancer, is largely curable at early stages of tumor development. However, at advanced and metastatic stages, human malignant melanoma responds poorly to both radiotherapy and chemotherapy. The common underlying aim of anti-cancer therapy involves the inhibition of cancer cell proliferation and induction of cancer cell death by apoptosis using different approaches, such as stimulation of a cellular stress response, which may initiate a complex cascade of stress-inducible signaling molecules and finally activate the mitochondrial apoptotic pathway.[1] An alternative approach is the induction of the TNF-TNFR, FasL-Fas or TRAIL-TRAILR death signaling pathways. Since combined chemotherapy to treat different forms of cancer is much more effective than monotherapy, it is important to use ligands of death receptors in different combinations with the specific inhibitors of cell signaling pathways, which are both effective and low in toxicity for melanoma treatment.[2,3] This methodology requires efficient expression of death receptors on the surface of cancer cells. However, death receptor translocation from the cytoplasm to the cell surface could sometimes be disturbed in cancer cells via different pathways. Studying mechanisms

of receptor translocation in normal and cancer cells will allow finding precise targets for acceleration or down-regulation of death receptor surface expression.

Dynamin, a large GTPase and an essential regulatory protein, is connected with several cellular functions, such as the formation of phagosomes, the control of endocytotic pathways, protein translocation from the Golgi complex to the plasma membrane and regulation of the cytoskeleton assembly.[4] With respect to apoptosis, GTPase dynamin-2 has the potential to act as a regulator of the transcription factor p53. Indeed, increased expression of dynamin-2 may induce p53-dependent apoptosis and reduced proliferation in some cell systems.[5] Furthermore, NS-398, a selective cyclo-oxygenase-2 inhibitor, affects colon carcinoma cells through modulating expression of different genes (including dynamin-2), which regulate programmed cell death, cell proliferation and cell-cell communication.[6]

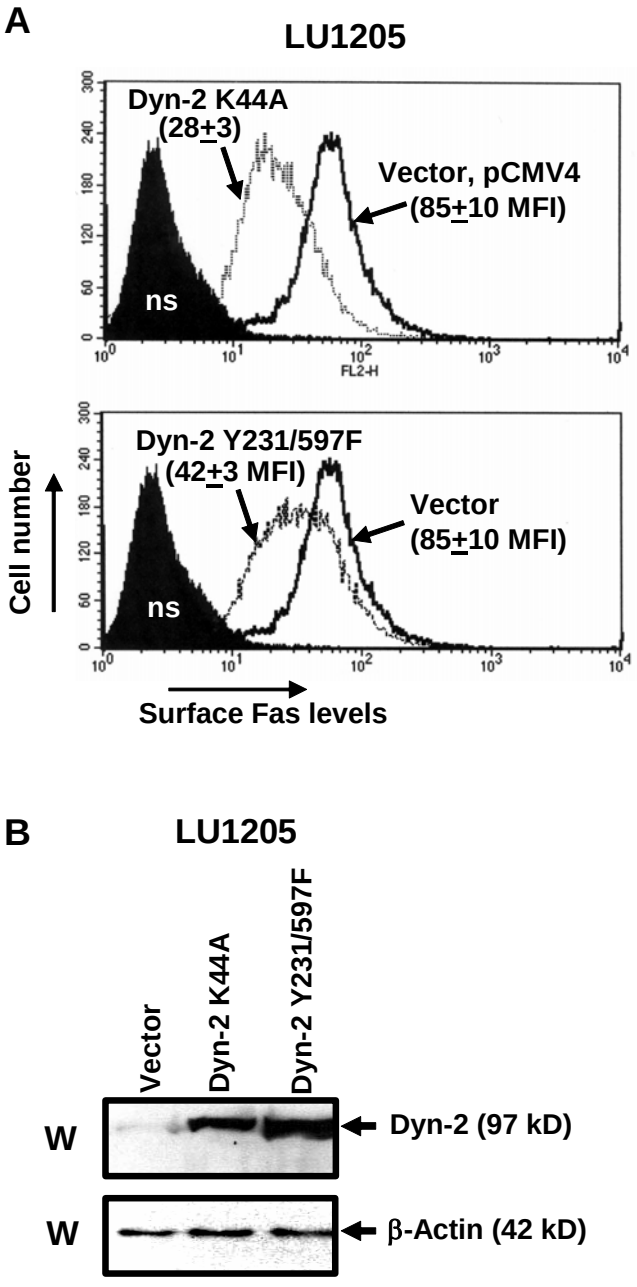

Fig. 1. Regulation of surface Fas expression and susceptibility to the Fas-mediated apoptosis by dynamin-2 in melanoma cells. **(A)** LU1205 melanoma cells were stably transfected with either the empty vector pCMV4 or Dyn-2 K44A or Dyn-2 Y231F/Y597F expression constructs; surface Fas expression in transfected cell lines was determined by FACS analysis; MFI is indicated. **(B)** Western blot analysis of Dyn-2 levels in indicated transfected cell lines using anti-Dyn-2 mAb.

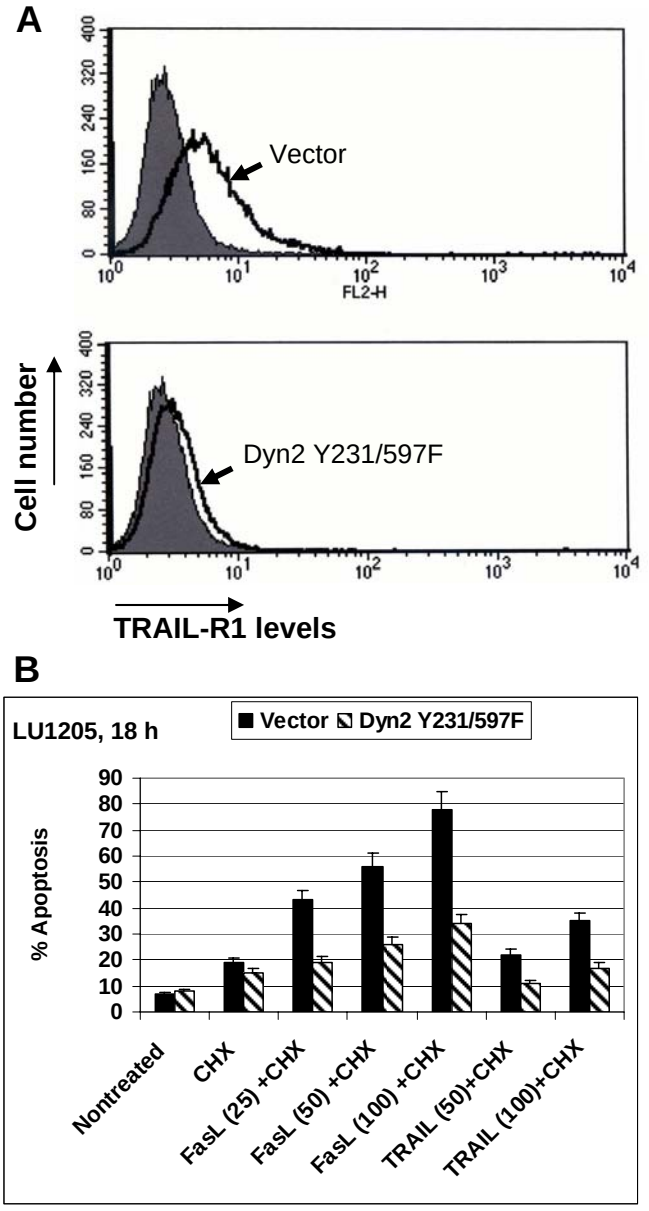

Fig. 2. Regulation of surface TRAIL-R1 expression and susceptibility to the Fas- and TRAIL-R1-mediated apoptosis by dynamin-2 in melanoma cells. **(A)** Surface TRAIL-R1 expression in transfected cell lines was determined by FACS analysis; MFI is indicated. **(B)** Apoptosis levels were determined 18 hours after treatments with recombinant FasL (25–100 ng/ml) and recombinant TRAIL (50–100 ng/ml) together with CHX (1 μg/mL) using PI-staining DNA and the flow cytometry. *Error bars* represent mean ± S.D. from three independent experiments.

The present study was conducted in order to determine the degree of susceptibility of highly metastatic LU1205 human melanoma cells to FasL- or TRAIL-mediated apoptosis through the suppression of functions of the endogenous dynamin by dynamin-2 dominant-negative construct. The hypothesis formulated was that the melanoma cells transfected by a dominant-negative dynamin-2 (with suppression of endogenous dynamin-2) would be much less susceptible to treatment of recombinant FasL or TRAIL than control melanoma cells. Through these experiments, the degree to which endogenous dynamin sensitizes highly metastatic cancer cells to anti-cancer treatment may be further elucidated, while opening the possibility of more effective anti-cancer treatments with dynamin-2 overexpression.

Regulation of surface Fas levels and FasL-mediated apoptosis in melanoma via dynamin-2

To find physiological consequences of Fas export regulation by dynamin, we established LU1205 human melanoma cell lines (mass cultures) that have been stably transfected either with dominant-negative Dyn-2 K44A or Dyn-2 Y231/597F. Control cells were transfected by the empty vector pCMV. Melanoma cells transfected with dominant-negative Dyn-1 K44A showed a substantial decrease of endogenous surface Fas expression (Fig. 1A, B). Established LU1205 melanoma lines respectively responded to recombinant FasL (25 ng/mL–100 ng/ml) and cycloheximide (1 μg/mL) treatment by the induction of apoptosis, which was proportional to preexisting Fas levels (Fig. 2B).

Regulation of surface TRAIL-R1 levels and TRAIL-mediated apoptosis in melanoma via dynamin-2

As expected, dynamin-2 plays a more universal role in the regulation of death receptor translocation to the cell sur-

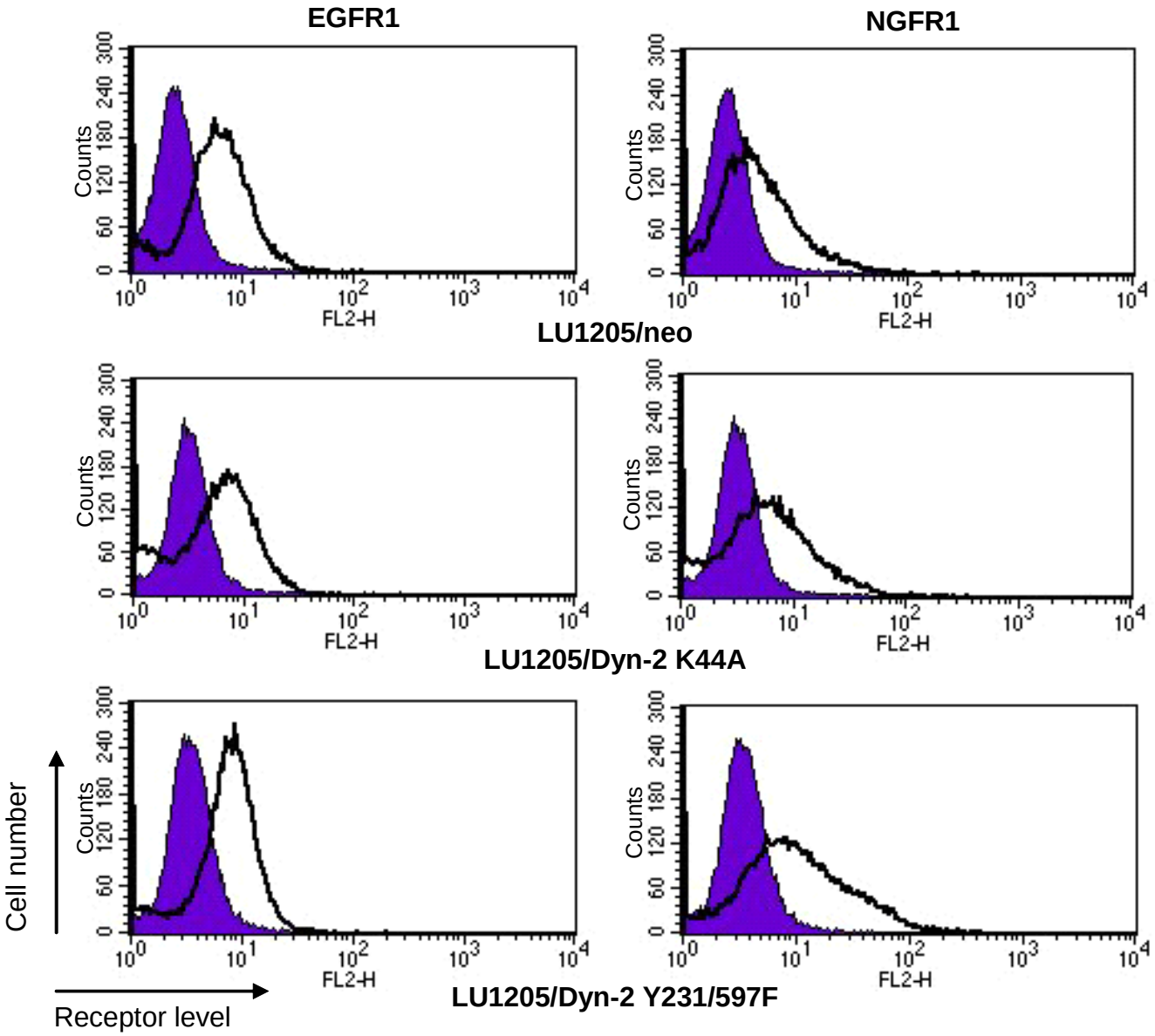

Fig. 3. Dominant-negative dynamin-2 did not suppress surface expression of EGFR1 and NGFR1 in LU1205 melanoma cells. Surface receptor levels were determined using FACS analysis.

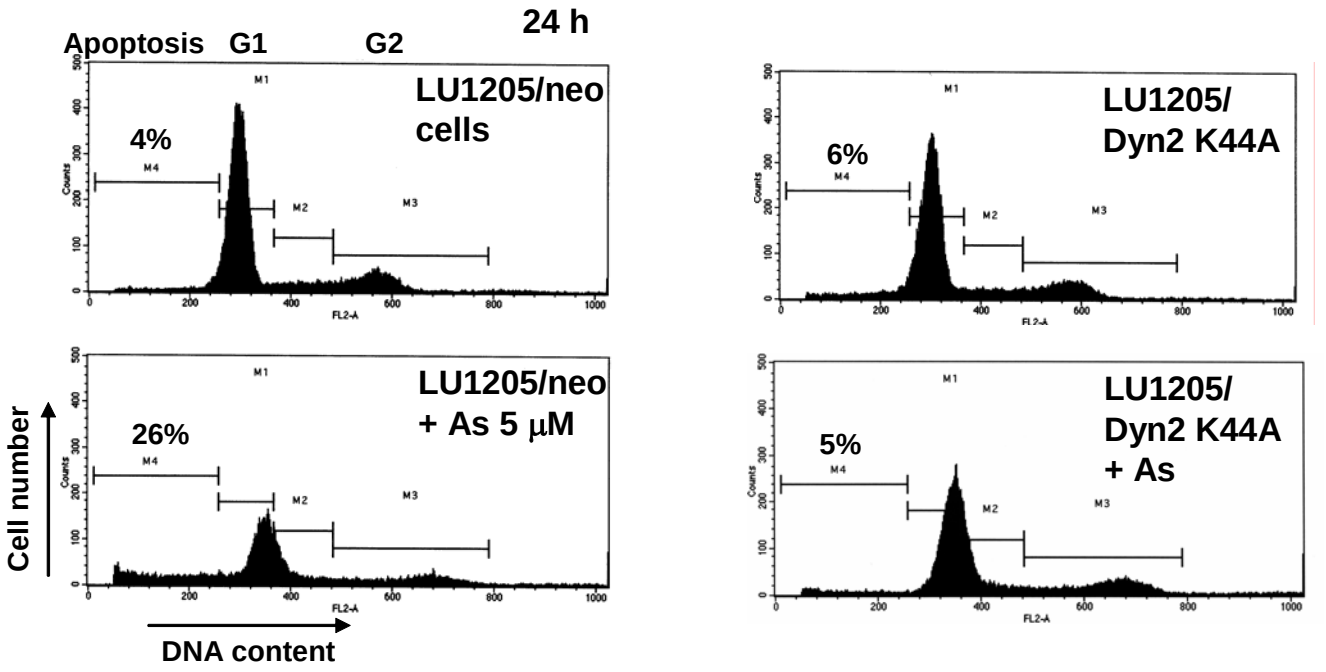

face, Indeed, LU1205 cells stably transfected with either Dyn-2 K44A or Dyn-2 Y231/597F demonstrated negative regulation of surface expression of both death receptors, Fas (Fig. 1) and TRAIL-R1; even the basal levels of surface TRAIL-R1 were relatively low (Fig. 2A). Treatment of established melanoma lines with recombinant TRAIL (50–100 ng/ml) (in combination with CHX, 1 μM) induced apoptosis, which was proportional to the surface level of the death receptor (Fig. 2B). However, there was certain specificity in dynamin-2-dependent control of surface expression since levels of both EGFR1 and NGFR1 on the surface of LU1205 cells have not been affected by suppression of dynamin-2 (Fig. 3).

Arsenite treatment induced the TRAIL promoter activity and TRAIL expression in human melanoma cells (our unpublished observations). Dominant-negative suppression of dynamin-2 protected melanoma cells against arsenite-induced apoptosis (Fig. 4). Taken together, results of the present study demonstrated a new control function of dynamin-2 in the regulation of surface expression of two major death receptors, Fas and TRAIL-R1, and established dynamin-2 as an important target for elucidating the effects of potential anti-cancer treatments.

References

1. Debatin KM and Krammer PH. Death receptors in chemotherapy and cancer. *Oncogene* **23**:2950–66, 2004.
2. Perlis C and Herlyn M. Recent advances in melanoma biology. *Oncologist* **9**:182–7, 2004.
3. Satyamoorthy K, DeJesus E, Linnenbach AJ, Kraj B, Kornreich DL, Rendle S, Elder DE and Herlyn M. Melanoma cell lines from different stages of progression and their biological and molecular analyses. *Melanoma Res* **7:**35–42, 1997.
4. Schlunck G, Damke H, Kiosses WB, Rusk N, Symons MH, Waterman-Storer CM, Schmid SL and Schwartz MA. Modulation of Rac localization and function by dynamin. *Mol Biol Cell* **15**:256–67, 2004.
5. Fish KN, Schmid SL and Damke H. Evidence that dynamin-2 functions as a signal-transducing GTPase. *J Cell Biol* **150**:145–54, 2000.
6. Zhang Z and DuBois RN. Detection of differentially expressed genes in human colon carcinoma cells treated with a selective COX-2 inhibitor. *Oncogene* **20**:4450–6, 2001. ■

Combined Treatment with COX-2 Inhibitor and Sodium Arsenite Leads to Induction of Surface Fas Ligand Expression and Fas Ligand-Mediated Apoptosis in Human Cancer Cells

Vladimir N. Ivanov and Tom K. Hei

Death receptor Fas (CD95/APO-1), and TRAIL receptors-1 and -2 (DR4 and DR5) are present in a variety of tissues and play an important role in the regulation of general homeostasis.[1,2] Cancer development is often accompanied by the suppression of the surface Fas receptor expression and/or inactivation of the Fas-mediated signaling potentially resulting in suppression of immunological anti-cancer surveillance *in vivo*.[3] However, in some highly metastatic cancer cells, including Fas-negative melanomas, Fas Ligand (FasL) surface expression is restored; this could be used as an additional mechanism to suppress anti-cancer immune effector cells (the so called "tumor counterattack").[4,5] Although a role of FasL in the "tumor counterattack" hypothesis is still under active investigation,[3,6,7] experimental data certainly demonstrated FasL expression in some cancer cell lines, including melanomas[8-11] Taken together, these observations illustrate important aspects of the general problem of resistance of cancer cells to the induction of programmed cell death. Many recent investigations in the area of cancer therapy have been focused on the problem of overcoming resistance to programmed cell death and to restore the ability of cancer cells to undergo apoptosis.[12,13] An effective approach was *FasL* gene transfer for induction of apoptosis in Fas-positive cancer cells and tumor regression *in vivo*.[14-16]

Cyclooxygenase (COX) enzymes catalyze the synthesis of prostaglandins from arachidonic acid,[17,18] which are involved in numerous survival functions of cells. The cyclooxygenase-2 (*COX-2*) gene promoter contains κB- and CRE sites and its activity is critically dependent on NF-κB, AP-1 and CREB/ATF2 transcription factors.[19] In normal cells, the *COX-2* gene is highly inducible by signals that activate the IKKβ-NF-κB pathway. In contrast, many types of cancer cells possess high basal levels of COX-2, due to permanent activation of NF-κB in these cells followed by expression of the *COX-2* gene.[17,20] The downstream product of COX-2 enzymatic activity is prostaglandin E_2 (PGE_2), which serves as an important stimulus for induction of several cell signaling pathways, including the NF-κB pathway that subsequently regulates cell proliferation and motility. Indeed, inhibition of COX-2 enzymatic activity by specific pharmacological inhibitors is an effective tool for controlling both inflammation and, in some cases, cancer development.[17,20]

The aim of the present study was to test whether restoration of endogenous surface expression of FasL in Fas-positive melanomas could facilitate apoptosis of these cancer cells. We found that the combined treatment of melanoma cells with sodium arsenite, an IKKβ-NF-κB inhibitor, and NS398, an inhibitor of COX-2, would be an effective tool for induction of cancer cell apoptosis. Surprisingly, such combined treatment did not activate the *FasL* promoter activity and *FasL* transcription in melanomas, but dramatically affected FasL translocation and expression on the cell surface.

COX-2 inhibition up-regulated arsenite-induced apoptosis in Fas-positive melanomas

We and others have previously demonstrated that simultaneous treatment of cancer cells with sodium arsenite in addition to specific inhibitors of cell survival pathways may dramatically increase apoptosis. It has been established that many types of cancer cells, including melanomas, contain high levels of COX-2 activity. Active anti-apoptotic functions of COX-2 in cancer cells have been widely reported.[21-23] Western blot analysis indeed demonstrated high basal levels of COX-2 protein in several melanoma lines (Fig. 1A). Normal human lung fibroblasts, which were treated with IL-1β and TNFα, served as a positive control of COX-2 induction at the protein level in the normal, non-cancerous, cells (Fig. 1A). Furthermore, determination of the total COX-2 levels (after cell permeabilization) by FACS analysis in several melanoma cell lines confirmed the presence of high levels of COX-2 in WM9 and LOX cells, and average levels in LU1205 and WM793 cells (Fig. 1B). Specific inhibition of COX-2 activity by NS398 (50 μM) alone had no considerable effects on induction of apoptosis in melanoma cells. However, combined treatment with sodium arsenite (5 μM) and NS398 (50 μM) synergistically increased apoptosis in Fas-positive melanomas WM793, LU1205, WM9 and LOX 16 h after treatment (Fig. 1C, and data not shown). Total levels of cell death of melanomas induced by combined treatment with sodium arsenite and NS398 were somewhat higher than apoptotic levels due to secondary necrosis.

Role of surface FasL expression in apoptosis induced by NS398 and arsenite

To evaluate a probable role of the FasL-Fas-mediated death in arsenite and NS398-treated melanomas, we first determined levels of surface expression of Fas and FasL following such treatment. We observed a marginal effect on the surface Fas receptor levels after treatment of melanomas

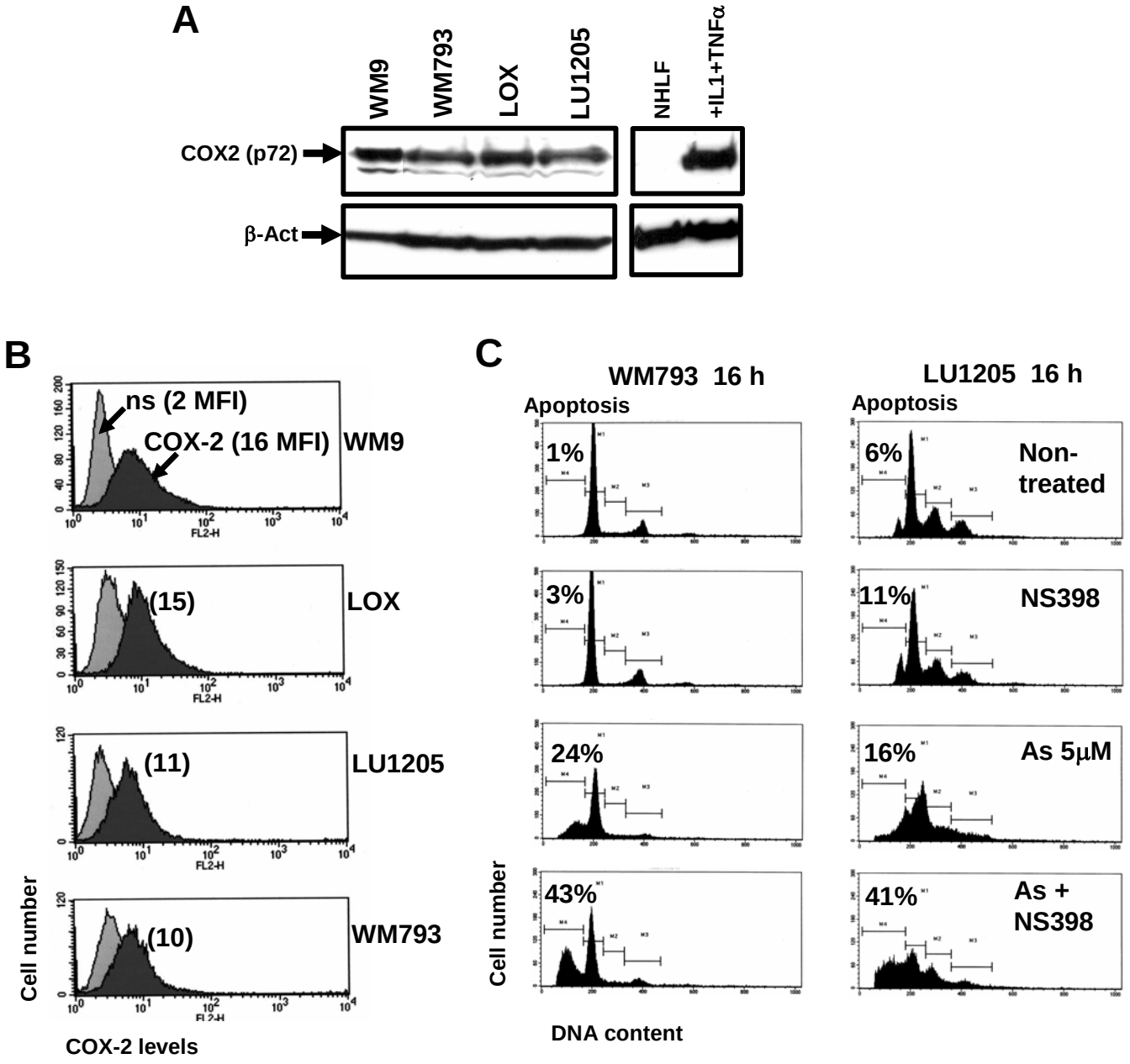

Fig. 1. COX-2 expression in human melanomas. (A) Western blot analysis of COX-2 levels in the indicated cell lines. Normal human lung fibroblasts were untreated or treated with IL-1 (2 ng/ml) and TNFα (10 ng/ml) for 4 h. **(B)** Total COX-2 levels in human melanomas have been determined by FACS analysis after cell permeabilization and staining using mAb against COX-2, PE-conjugated goat anti-mouse secondary Ab and the flow cytometry. Non-specific (ns) staining; Medium fluorescence intensity (MFI) is indicated in brackets. **(C)** Inhibition of COX-2 activity by NS398 (50 μM) had synergistic effects on arsenite-induced apoptosis in COX-2-positive human melanomas. Levels of apoptosis have been determined by FACS analysis of PI stained melanoma cells 16 h after treatment with sodium arsenite (5 μM), NS398 (50 μM), or a combination of the two.

with arsenite and NS398. TNFα stimulation was used as a positive control for up-regulation of Fas levels (Fig. 2A). In contrast, the surface levels of FasL were notably increased 16 h after combined treatment with sodium arsenite and NS398 in WM9, LU1205 (Fig. 2B), WM793 and LOX melanoma cells (data not shown). Arsenite or NS398 alone did not induce notable expression of FasL on the cell surface (Fig. 2B). Anti-FasL inhibitory mAb (NOK-1) partially suppressed apoptosis induced with arsenite and NS398 in all melanoma lines tested, while the effect of anti-TNFα mAb was pronounced only in WM793 cells (Fig. 2C)**.** This effect was likely due to inhibition of arsenite-induced TNFα-mediated apoptosis in these cells. To demonstrate a dependence of apoptosis induced by arsenite and NS398 on caspase activities, we used specific inhibitors of caspases. Both Ac-IETD-CHO (an inhibitor of caspase-8 and caspase-6) and Ac-LEHD-CHO (an inhibitor of caspase-9) partially suppressed arsenite and NS398-induced apoptosis, although

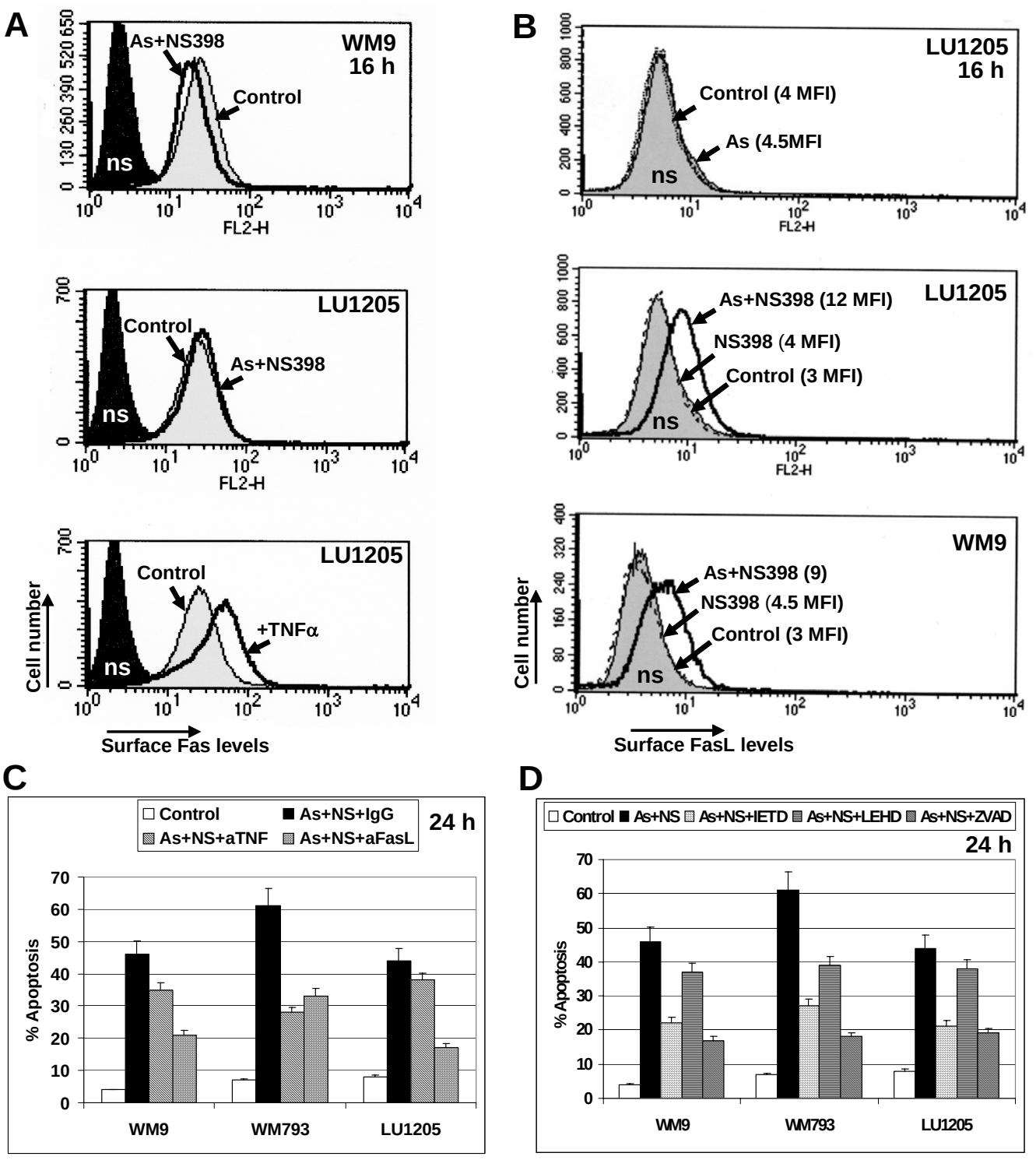

Fig. 2. Upregulation of the surface FasL levels after treatment of melanoma cells with a combination of NS398 and sodium arsenite. (A) Surface Fas levels after treatment of indicated melanomas with arsenite and NS398. TNFα was used as a positive regulator of Fas expression. Control non-treated cells (Control) and non-specific (ns) staining cells with IgG-PE are indicated. **(B)** Surface FasL levels were determined using anti-FasL mAb (NOK-1), PE-conjugated secondary Ab in flow cytometry. Control (untreated) levels of FasL were the same as non-specific (ns) staining. **(C)** Pretreatment of the cell cultures with anti-FasL inhibitory mAb (NOK-1) or with anti-TNFα mAb partially suppressed apoptosis in the indicated melanoma cell lines, which was induced by dual treatment with arsenite and NS398. **(D)** Effects of caspase inhibitors on apoptosis in melanoma cells.

Ac-IETD-CHO was more effective (Fig. 2D), indicating that the death-receptor/caspase-8-mediated cascade operated during apoptosis. A general caspase inhibitor, zVAD-fmk (5 μM), was quite efficient for suppression of apoptosis, although this suppression was not complete, likely due to secondary necrosis (Fig. 2D).

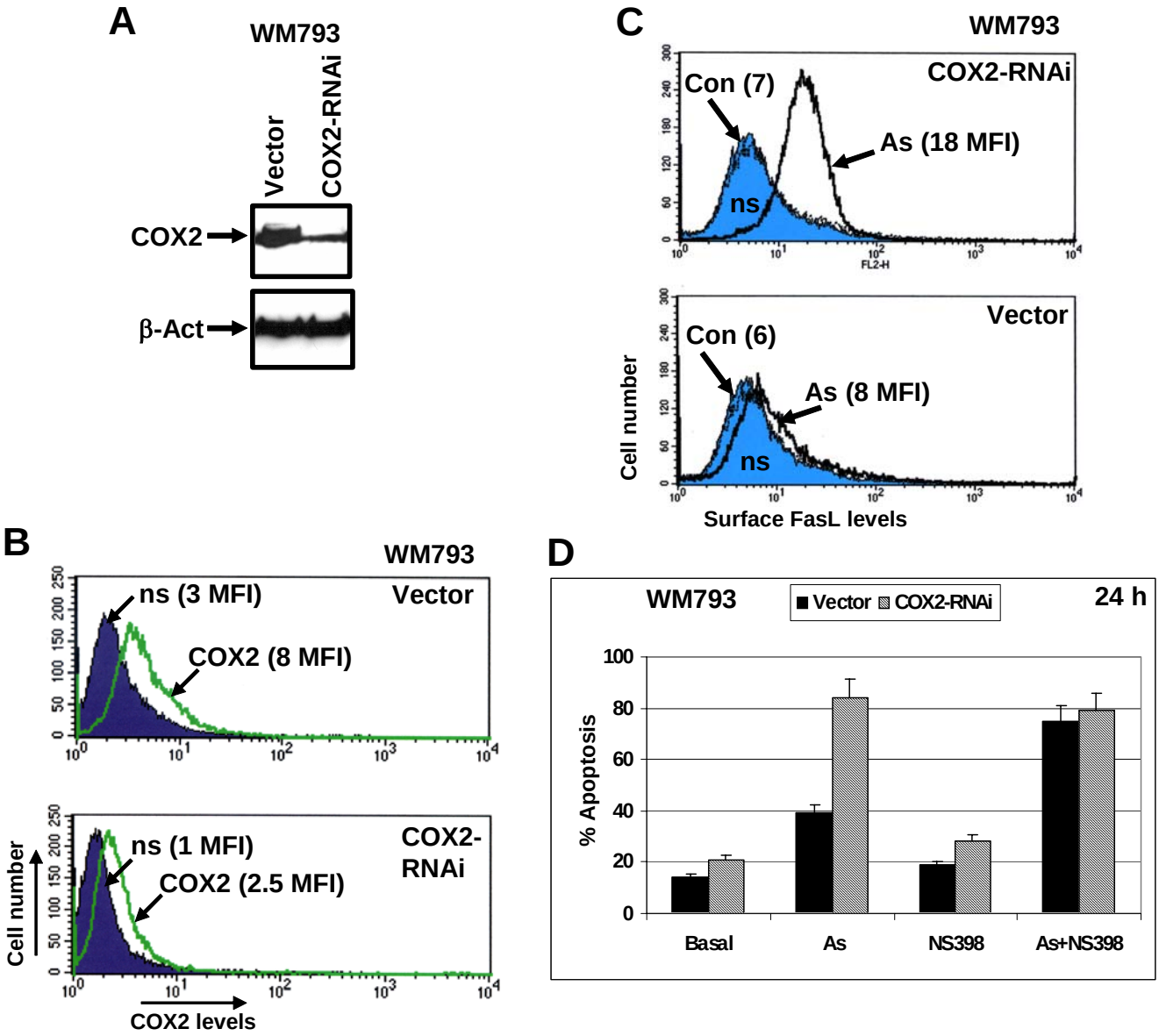

Fig. 3. Down-regulation of COX-2 protein levels by targeting of COX-2 mRNA with specific RNAi of 19 nucleotides leads to upregulation of FasL expression and accelatation of arsenite-induced apoptosis in human melanoma WM793. RNAi, designed to target human COX-2 mRNA within nucleotides 354-372 was expressed using pSR-GFP/Neo (COX-2-RNAi) vector, which also produced a marker GFP protein. Human melanoma WM793 cell line has been used for COX-2 silencing. Two mass cultures of WM793 cells were obtained after transfection with the empty vector or with the COX-2 RNAi expression construct and subsequently selected in the presence of G418. **(A)** Total protein levels of COX-2 expression in selected cultures were detected by Western analysis. **(B)** FACS analysis of transfected and selected cells using monoclonal anti-COX-2 antibody and the secondary anti-mouse Ab labeled with PE confirmed a down-regulation of COX-2 levels in WM793/COX2 RNAi cells from 8 MFI to 2 MFI. **(C)** Sodium arsenite (As, 5 mM) treatment of control (Vector) and COX-2 knockdown cells dramatically increased surface expression of FasL. FACS analysis was performed as indicated in the legend to Fig. 4. **(D)** Percentage of Annexin-V-PE-positive (red) apoptotic cells among transfected GFP-positive cells was determined using FACS analysis. Treatment of WM793 cells with arsenite, NS398, or both was performed for 12 h.

Taken together, these data demonstrated that the upregulation of the surface FasL expression in several melanoma lines following the combined treatment with arsenite and COX-2 inhibitor could potentially explain an increase in the apoptotic response. Hence, in addition to basal apoptosis driven by sodium arsenite (which was TNFα-mediated in WM793 cells), combined treatment with sodium arsenite and NS398-induced FasL-Fas-mediated apoptosis in melanoma cells.

COX-2 downregulation by specific RNAi

As an alternative approach for suppression of COX-2, silencing COX-2 expression with COX-2 RNAi has been used. We designed and created a COX-2 RNAi expression construct based on the pSR-GFP/Neo vector from Oligoengine (Seattle, WA). Following transfection by COX-2 RNAi or the empty vector and subsequent selection in the presence of G418, two mass cultures of WM793 melanoma enriched with COX-2 RNAi/GFP or vector/GFP were established. In

both types of transfected cells, GFP was localized in the cytoplasm and in the nucleus. Determination of COX-2 protein levels by Western or FACS analysis demonstrated a down-regulation of basal COX-2 protein levels by COX-2 RNAi expression in WM793 cells (Fig. 3A and B). Interestingly, this was accompanied by up-regulation of the surface FasL levels in transfected cells after arsenite treatment (Fig. 3C). The percentage of Annexin-V-PE positive (red) apoptotic cells substantially increased after treatment of WM793/COX-2-RNAi (green) cells by sodium arsenite (Fig. 3D). A combination of arsenite and NS398 increased levels of apoptosis in control cells, which were transfected with the empty pSR-GFP/Neo vector. Taken together, these data demonstrated relatively similar effects on FasL surface expression and arsenite-induced apoptosis either after pharmacological inhibition of COX-2 activity by NS398, or after silencing *COX-2* expression by RNAi. RNAi also effectively increased surface FasL expression following arsenite treatment.

Upregulation of the surface FasL levels was based on an increase in the efficiency of translocation to the cell surface, and stabilization of FasL protein on the cell surface, rather than on acceleration of *FasL* gene transcription (data not shown). Results obtained demonstrate that the combination of arsenite with inhibitors of COX-2 may affect the target cancer cells via induction of FasL-mediated death signaling.

References

1. Debatin KM and Krammer PH. Death receptors in chemotherapy and cancer. *Oncogene* **23**:2950–66, 2004.
2. Nagata S. Fas ligand-induced apoptosis. *Annu Rev Genet* **33**:29–55, 1999.
3. French LE and Tschopp J. Defective death receptor signaling as a cause of tumor immune escape. *Semin Cancer Biol* **12**:51–5, 2002.
4. Hahne M, Rimoldi D, Schroter M, Romero P, Schreier M, French LE, Schneider P, Bornand T, Fontana A, Lienard D, Cerottini J and Tschopp J. Melanoma cell expression of Fas(Apo-1/CD95) ligand: implications for tumor immune escape. *Science* **274**:1363–6, 1996.
5. Igney FH and Krammer PH. Immune escape of tumors: apoptosis resistance and tumor counterattack. *J Leukoc Biol* **71**:907–20, 2002.
6. Kurooka M, Nuovo GJ, Caligiuri MA and Nabel GJ. Cellular localization and function of Fas ligand (CD95L) in tumors. *Cancer Res* **62**:1261–5, 2002.
7. Chappell DB, Zaks TZ, Rosenberg SA and Restifo NP. Human melanoma cells do not express Fas (Apo-1/CD95) ligand. *Cancer Res* **59**:59–62, 1999.
8. Hallermalm K, De Geer A, Kiessling R, Levitsky V and Levitskaya J. Autocrine secretion of Fas ligand shields tumor cells from Fas-mediated killing by cytotoxic lymphocytes. *Cancer Res* **64**:6775–82, 2004.
9. Ivanov VN and Ronai Z. Down-regulation of tumor necrosis factor alpha expression by activating transcription factor 2 increases UVC-induced apoptosis of late-stage melanoma cells. *J Biol Chem* **274**:14079–89, 1999.
10. Repp AC, Mayhew ES, Howard K, Alizadeh H and Niederkorn JY. Role of fas ligand in uveal melanoma-induced liver damage. *Graefes Arch Clin Exp Ophthalmol* **239**:752–8, 2001.
11. Andreola G, Rivoltini L, Castelli C, Huber V, Perego P, Deho P, Squarcina P, Accornero P, Lozupone F, Lugini L, Stringaro A, Molinari A, Arancia G, Gentile M, Parmiani G and Fais S. Induction of lymphocyte apoptosis by tumor cell secretion of FasL-bearing microvesicles. *J Exp Med* **195**:1303–16, 2002.
12. Schulze-Bergkamen H and Krammer PH. Apoptosis in cancer--implications for therapy. *Semin Oncol* **31**:90–119, 2004.
13. Soengas MS and Lowe SW. Apoptosis and melanoma chemoresistance. *Oncogene* **22**:3138–51, 2003.
14. Aoki K, Akyurek LM, San H, Leung K, Parmacek MS, Nabel EG and Nabel GJ. Restricted expression of an adenoviral vector encoding Fas ligand (CD95L) enhances safety for cancer gene therapy. *Mol Ther* **1**:555–65, 2000.
15. Arai H, Gordon D, Nabel EG and Nabel GJ. Gene transfer of Fas ligand induces tumor regression in vivo. *Proc Natl Acad Sci U S A* **94**:13862–7, 1997.
16. Eberle J, Fecker LF, Hossini AM, Wieder T, Daniel PT, Orfanos CE and Geilen CC. CD95/Fas signaling in human melanoma cells: conditional expression of CD95L/FasL overcomes the intrinsic apoptosis resistance of malignant melanoma and inhibits growth and progression of human melanoma xenotransplants. *Oncogene* **22**:9131–41, 2003.
17. Williams CS, Mann M and DuBois RN. The role of cyclooxygenases in inflammation, cancer, and development. *Oncogene* **18**:7908–16, 1999.
18. Dannenberg AJ, Lippman SM, Mann JR, Subbaramaiah K and DuBois RN. Cyclooxygenase-2 and epidermal growth factor receptor: pharmacologic targets for chemoprevention. *J Clin Oncol* **23**:254–66, 2005.
19. Kanekura T, Goorha S, Kirtikara K and Ballou LR. The involvement of NF-kappaB in the constitutive overexpression of cyclooxygenase-2 in cyclooxygenase-1 null cells. *Biochim Biophys Acta* **1542**:14–22, 2002.
20. Tsujii M, Kawano S and DuBois RN. Cyclooxygenase-2 expression in human colon cancer cells increases metastatic potential. *Proc Natl Acad Sci U S A* **94**:3336–40, 1997.
21. Shishodia S, Koul D and Aggarwal BB. Cyclooxygenase (COX)-2 inhibitor celecoxib abrogates TNF-induced NF-kappa B activation through inhibition of activation of I kappa B alpha kinase and Akt in human non-small cell lung carcinoma: correlation with suppression of COX-2 synthesis. *J Immunol* **173**:2011–22, 2004.
22. Hsu AL, Ching TT, Wang DS, Song X, Rangnekar VM and Chen CS. The cyclooxygenase-2 inhibitor celecoxib induces apoptosis by blocking Akt activation in human prostate cancer cells independently of Bcl-2. *J Biol Chem* **275**:11397–403, 2000.
23. Martey CA, Pollock SJ, Turner CK, O'Reilly KM, Bag-

lole CJ, Phipps RP and Sime PJ. Cigarette smoke induces cyclooxygenase-2 and microsomal prostaglandin E2 synthase in human lung fibroblasts: implications for lung inflammation and cancer. *Am J Physiol Lung Cell Mol Physiol* **287**:L981–91, 2004. ■

Epigenetic Inactivation of the *Betaig-h3* Gene in Human Cancer Cells

Genze Shao, Tom K. Hei and Yongliang Zhao

CpG islands located in the promoter regions of certain tumor suppressor genes undergo aberrant hypermethylation in cancer cells, which is an important mechanism responsible for gene silencing.[1] It has been well-documented that some known tumor suppressor genes, such as cell cycle inhibitor (*p16INK4a*) and DNA repair genes (*hMLH1* and *BRCA1*), are modified and transcriptionally silenced by promoter hypermethylation.[2] We have previously shown that *Betaig-h3* possesses an anti-tumor function in malignantly transformed human bronchial epithelial cells.[3,4] It is expressed ubiquitously in a variety of normal human tissues but downregulated or inactivated in many human tumor cell lines.[3,4] As DNA methylation of CpG islands play an important role in regulation of gene expression in human cancers,[5,6] methylation patterns of the promoter region and the first exon of *Betaig-h3* gene were investigated in 17 cell lines derived from lung, prostate, mammary and kidney using a bisulfite sequencing method. Reactivation of the *Betaig-h3* promoter was further investigated in *Betaig-h3*-silenced cells by treatment with demethylating chemical 5-Aza-CdR.

As shown in Figure 1, the real-time PCR was employed to quantify the expression of *Betaig-h3* gene in a series of normal, immortalized and tumor cell lines derived from lung, prostate and mammary as well as from kidney. The results showed that the *Betaig-h3* gene was expressed at a relatively high level in normal and immortalized cell lines, whereas it was downregulated in most of the tumor cell lines. Interestingly, *Betaig-h3* expression was undetectable in three lung cancer cell lines (H522, H810, and H1417) and one kidney cell line 293T.

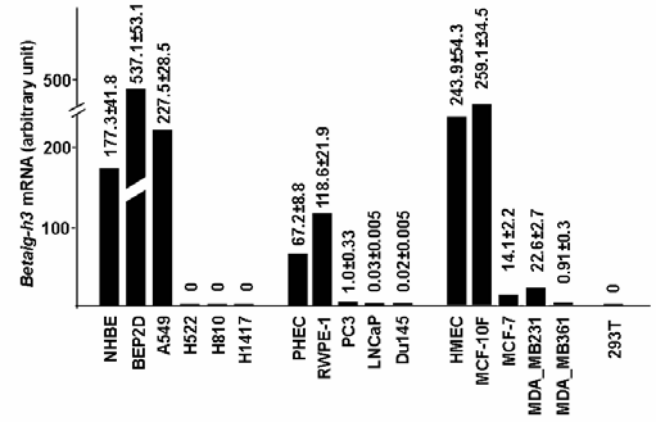

Fig. 1. Expression of *Betaig-h3* in normal, immortalized and cancer cell lines of lung, prostate and mammary origin, as well as 293T. Relative quantification of *Betaig-h3* expression was performed by using real-time PCR, calibrated and normalized to its expression in PC3 cells.

To determine whether loss of *Betaig-h3* expression resulted from promoter hypermethylation, methylation status of a total of 49 CpGs across 0.6 kb of the *Betaig-h3* locus in these cell lines was characterized by bisulfite genomic sequencing. Most of the CpG islands of the *Betaig-h3* gene were selected for DNA methylation analysis. The data have shown that most of the CpG sites of the *Betaig-h3* promoter were not methylated in normal NHBE, immortalized BEP2D and A549 tumor cells that expressed a relatively high level of *Betaig-h3* gene. Although several methylated CpG sites were identified, they were randomly distributed and limited to one methylated site per clone. In contrast, *Betaig-h3*-negative cell lines, including H522, H810, and H1417 showed dense methylation in the *Betaig-h3* promoter. Among all of the CpG sites examined, only two sites (-147, -40) were found to be unmethylated in the clones obtained from H522 tumor cells. Similarly, H810 cells showed 1-3 sites and H1417 showed 5-8 sites that were not methylated and randomly distributed in each clone. These results clearly demonstrate that the *Betaig-h3* promoter was hypermethylated in these three tumor cell lines that lack of *Betaig-h3* expression (Fig. 2).

To determine the correlation between DNA methylation and *Betaig-h3* silencing, the tumor cell lines that showed hypermethylation of the *Betaig-h3* promoter were treated with the demethylating agent, 5-Aza-CdR. The expression levels of the *Betaig-h3* gene were then quantified by real-time PCR. As shown in Figure 3, 5-Aza-CdR treatment resulted in the re-expression of *Betaig-h3* in all of the *Betaigh3*-negative cell lines, including H522, H810, H1417 and 293T. Significantly increased expression of *Betaig-h3* was also detected in two *Betaig-h3*-positive cell lines, including LNCaP and Du145. To confirm the demethylation effect of 5-Aza-CdR, bisulfite sequencing was performed on treated cell lines and the results clearly showed that the pro-

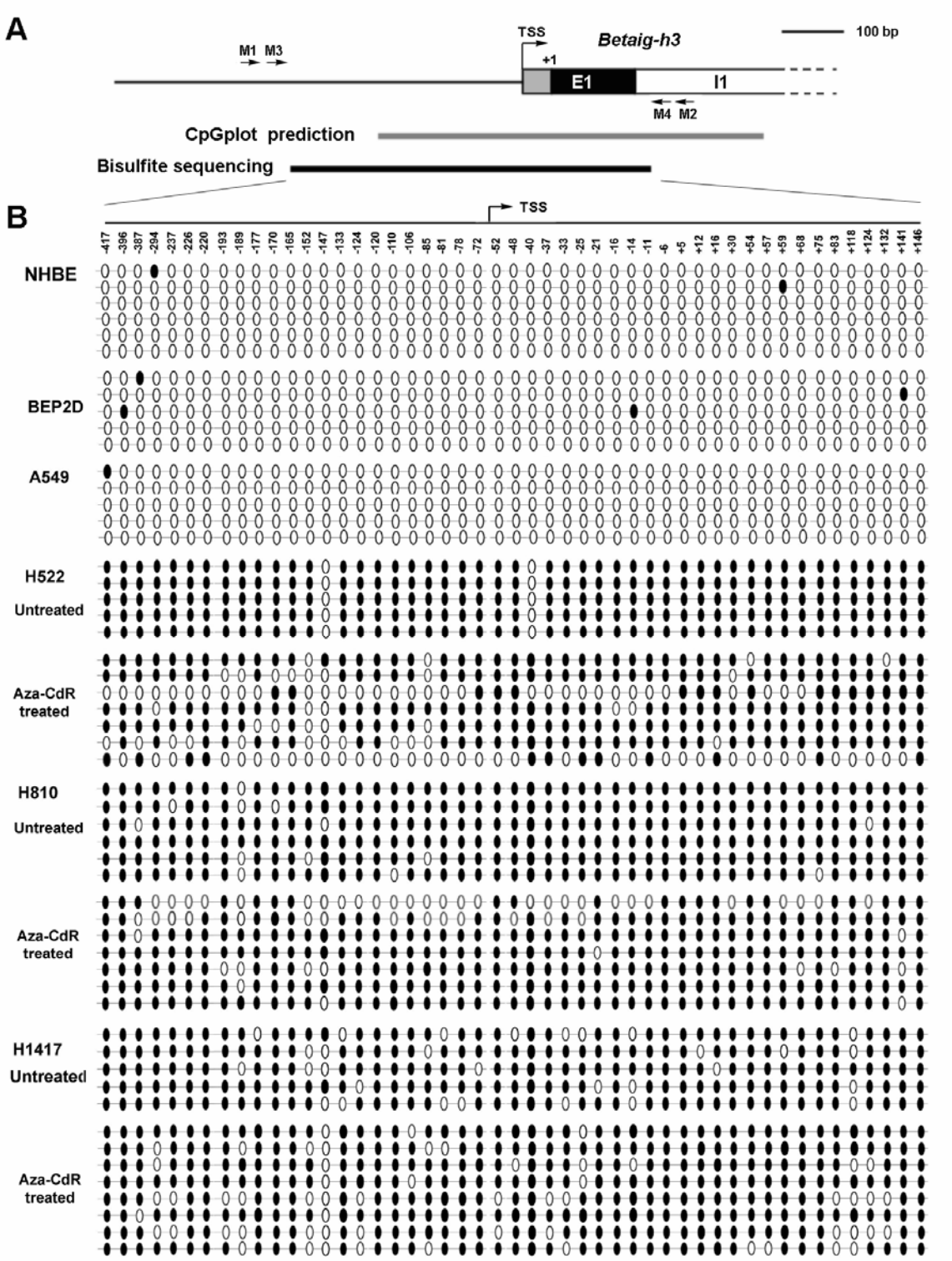

Fig. 2. (A) Schematic diagram indicating CpG island on the *Betaig-h3* promoter region. Transcription start site (TSS) is located at -65 in relation to the ATG start codon (+1). The bisulfite sequencing fragment containing the promoter region and the first exon is indicated as a black bar. **(B)** Fine methylation mapping of 49 CpG sites of the *Betaig-h3* promoter region obtained from bisulfite sequencing in lung cell lines. Open circles, unmethylated CpG sites; closed circles, methylated CpGs.

moter was truly demethylated (Fig. 3). These data strongly suggest that hypermethylation was responsible for *Betaig-h3* gene silencing.

To further verify whether promoter methylation plays a pivotal role in the regulation of *Betaig-h3* expression, we cloned the promoter region of the *Betaig-h3* gene and analyzed its activity under methylated or unmethylated conditions in 293T cells using the promoter luciferase assay. The

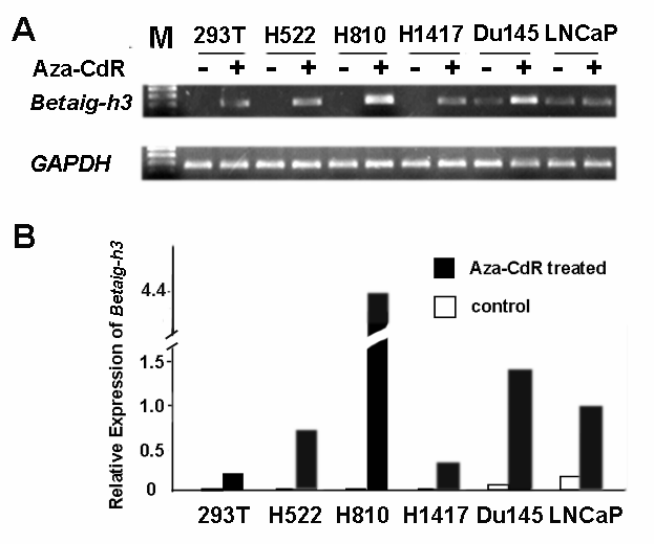

Fig. 3. Re-expression of *Betaig-h3* following treatment with 5-aza-2-deoxycytidine (Aza-CdR). **(A)** Levels of *Betaig-h3* expression in tumor cell lines after Aza-CdR treatment analyzed by agarose gel electrophoresis. **(B)** Levels of *Betaig-h3* expression were quantified by Real time PCR and normalized to its expression in Aza-CdR treated LNCaP tumor cells.

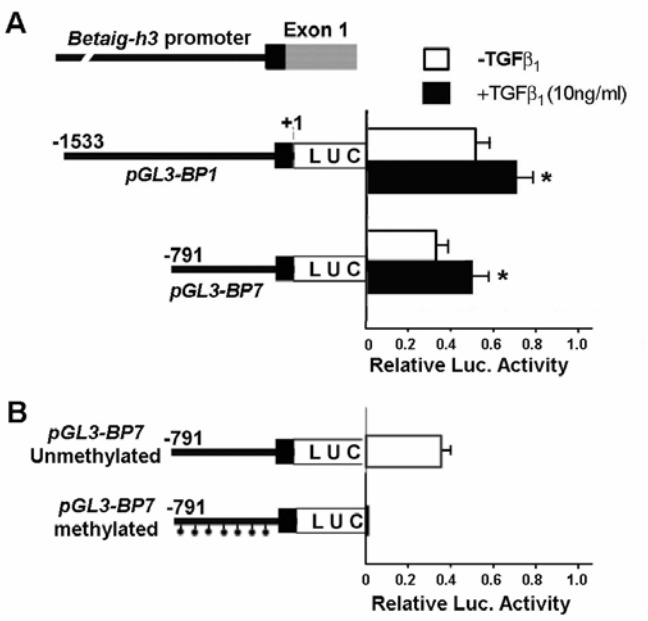

Fig. 4. Effect of methylation on activity of the *Betaig-h3* promoter. **(A)** Relative luciferase activity of 293T cells after transfection of *Betaig-h3* promoter-luciferase construct and treatment with 10 ng/ml of TGF-β1. Transfection efficiency was normalized based on the luciferase activity after transfection of the *pGL3-Promoter* vector. **(B)** Methylation-dependent repression of the *Betaig-h3* promoter. Data are presented as the mean ± standard deviation of triplicate experiments. * $p<0.01$ when compared with *Betaig-h3* promoter-luciferase construct transfected cells without TGF-β1 treatment.

293T tumor cells were chosen because the *Betaig-h3* promoter in these cells is demonstrated to be hypermethylated and completely silenced. Additionally, 293T cells have high transfection efficiency. Two different fragments of the promoter sequence were constructed into a luciferase reporter vector and transfected into 293T cells. Luciferase activity was measured as an indicator of *Betaig-h3* promoter activity. As shown in Figure 4, high luciferase activities were detected in 293T cells when transfected with *Betaig-h3* fragments *pGL3-BP1* or *pGL3-BP7*. Furthermore, a significant increase in luciferase activities were found in cells treated with TGFβ1 (10 ng/ml) when compared with untreated cells ($p<0.01$). *In vitro* methylation of *pGL3-BP7* with M. *Sss* I methylase resulted in a complete abrogation of luciferase activity when transfected into 293T cells. These results indicate that promoter methylation is sufficient for the silencing of *Betaig-h3* promoter.

Taken together, the present study demonstrates for the first time that hypermethylation of the *Betaig-h3* gene correlates with silencing of the *Betaig-h3* promoter in lung, prostate and 293T tumor cell lines and occurs in primary lung tumors. Further studies of methylation profiles of a large number of primary tumor samples will provide important insight in the role of CpG island hypermethylation of the *Betaig-h3* promoter in tumor progression.

References

1. Das PM and Singal R. DNA methylation and cancer. *J Clin Oncol* **22**:4632–42, 2004.
2. Esteller M. CpG island hypermethylation and tumor suppressor genes: a booming present, a brighter future. *Oncogene* **21**:5427–40, 2002.
3. Zhao Y, Shao G, Piao CQ, Berenguer J and Hei TK. Down-regulation of Betaig-h3 gene is involved in the tumorigenesis in human bronchial epithelial cells induced by heavy-ion radiation. *Radiat Res* **162**:655–9, 2004.
4. Zhao YL, Piao CQ and Hei TK. Downregulation of Betaig-h3 gene is causally linked to tumorigenic phenotype in asbestos treated immortalized human bronchial epithelial cells. *Oncogene* **21**:7471–7, 2002.
5. Belinsky SA, Nikula KJ, Palmisano WA, Michels R, Saccomanno G, Gabrielson E, Baylin SB and Herman JG. Aberrant methylation of p16(INK4a) is an early event in lung cancer and a potential biomarker for early diagnosis. *Proc Natl Acad Sci U S A* **95**:11891–6, 1998.
6. Pulling LC, Divine KK, Klinge DM, Gilliland FD, Kang T, Schwartz AG, Bocklage TJ and Belinsky SA. Promoter hypermethylation of the O6-methylguanine-DNA methyltransferase gene: more common in lung adenocarcinomas from never-smokers than smokers and associated with tumor progression. *Cancer Res* **63**:4842–8, 2003. ■

Loss of Betaig-h3 Protein Is Frequent in Primary Lung Carcinoma and Related to Tumorigenic Phenotype in Lung Cancer Cells

Yongliang Zhao and Tom K. Hei

The *Betaig-h3* gene product is a secreted protein that can be induced by transforming growth factor beta in human adenocarcinoma cells as well as other human cell types.[1] This gene is located at chromosome 5q31 and encodes a highly conserved 683 amino-acid protein that contains a secretary signal sequence and four internal homologous domains of 140 amino-acids, the last of which contains an Arg-Gly-Asp (RGD) sequence which can serve as a ligand recognition site for several integrins.[1] Recent studies have shown that the *Betaig-h3* gene is a component of the lung extracellular matrix (ECM) and present in normal skin which can promote the adhesion and spreading of dermal fibroblasts *in vitro*.[2] Using papillomavirus-immortalized human bronchial epithelial cells, we have previously found that the *Betaig-h3* gene was markedly downregulated in malignantly transformed cells induced by radiation or asbestos fibers. Meanwhile, ectopic expression of this gene in transformed cells significantly suppresses their tumorigenicity.[3,4] However, physiological functions of the *Betaig-h3* gene in primary human lung cancer are not well understood. The present study investigated whether loss of *Betaig-h3* expression plays a role in the development of human lung cancer by studying Betaig-h3 protein levels in primary lung carcinomas using immunohistochemical methods. We further delineated the effects of vector-transduced Betaig-h3 protein expression in lung adenocarcinoma-derived H522 cells that lack endogenous Betaig-h3 protein.

Positive staining with brown color was found in the nucleus and cytoplasm of Betaig-h3-transfected cells and lung bronchial epithelia (data not shown). In addition, strong staining was found in the stroma of normal lung tissues. No staining was found in *Betaig-h3*-transfected H522 cells when incubating with either IgG or anti-Betaig-h3 antibody plus neutralizing peptide.

To estimate the staining of Betaig-h3 protein expression in lung cancers, the average values of integrated optical density (IOD 611) and percentage of stained area (PS 75.9%) from 24 cases of normal lung bronchial epithelia quantified by MetaVue software were used as the standards. Tumor samples with more than a 7-fold decrease in IOD and PS relative to normal tissues are categorized as the low staining group. This standard will enable the low-staining group to have at least a 2-fold decrease of staining value than the normal bronchial epithelia when the later has the lowest reading (IOD 228). We used the following standards to divide the stained tumor samples into three groups: 1)low staining: 0–76 (IOD) and 0–11% (PS); 2) medium staining: 76–218 and 12–34%; and 3) high staining: >218 and >34%. If the two values for one sample only meet one standard, this sample will be graded into the following group. As summarized in Table 1, low staining of Betaig-h3 protein occurred in 34.6% (45/130) of lung cancers with different histological types, including 24 of 43 squamous carcinomas, 12 of 49 adenocarcinomas and 9 of 38 other tissue types of cancers such as large cell carcinomas. No correlation was found between *Betaig-h3* expression and the pathological parameters tested. By statistical analysis, the average value of IOD and PS in the tumors with low Betaig-h3 staining were significantly lower than that in normal bronchial epithelia ($P<0.01$) (Figs. 1A and B).

Table 1.
Summary of immunohistochemical staining analysis in lung tumors.

	Betaig-h3 staining			
Histological types	Low	Medium	High	Total
Squamous carcinomas	24 (55.8%)*	11 (25.6%)	8 (18.6%)	43
Adenocarcinomas	12 (24.5%)	13 (26.5%)	24 (49.0%)	49
Anaplastic bronchogenic carcinomas	1	2	1	4
Carcinomas	1	1	5	7
Bronchioloalveolar carcinomas	4	1	4	9
Large cell carcinomas	1	3	2	6
Small cell carcinomas	0	3	1	4
Mesotheliomas	1	1	1	3
Mucoepidermoid carcinomas	1	2	2	5
	45 (34.6%)	37 (28.5%)	48 (36.9%)	130

*$P<0.01$ compared with adenocarcinomas.

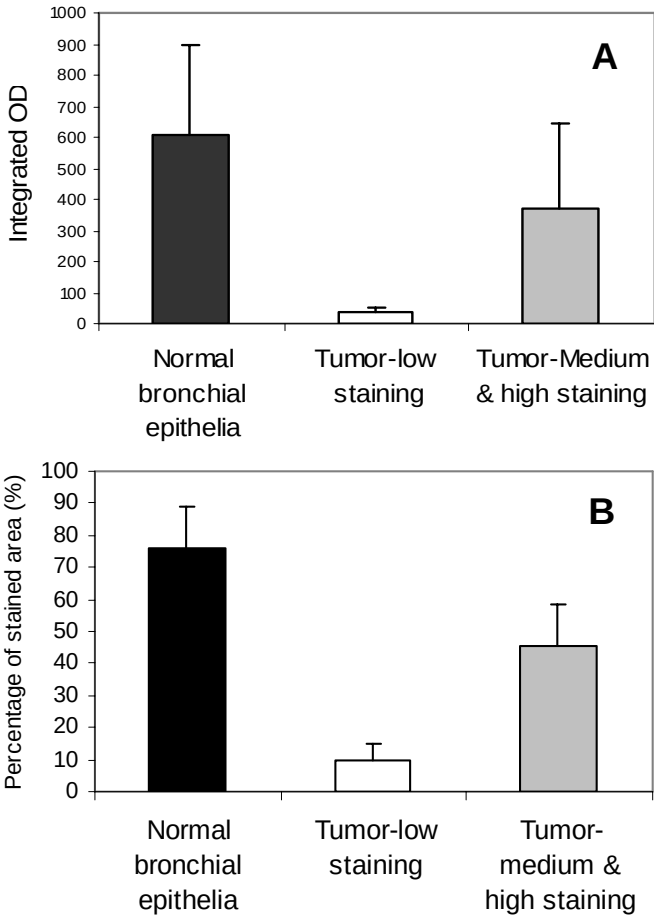

Fig. 1. The average value of integrated optical density (IOD) (**A**) and percentage of stained area (PS) (**B**) for Betaig-h3 protein quantified by MetaVue computerized image software in lung cancers and normal bronchial epithelia (n=24). Mean ± SD. Significantly decreased values of IOD and PS were found in the tumors with low Betaig-h3 staining (P<0.01, n=45). No significant decrease was found in the tumors with medium and high staining (n=85).

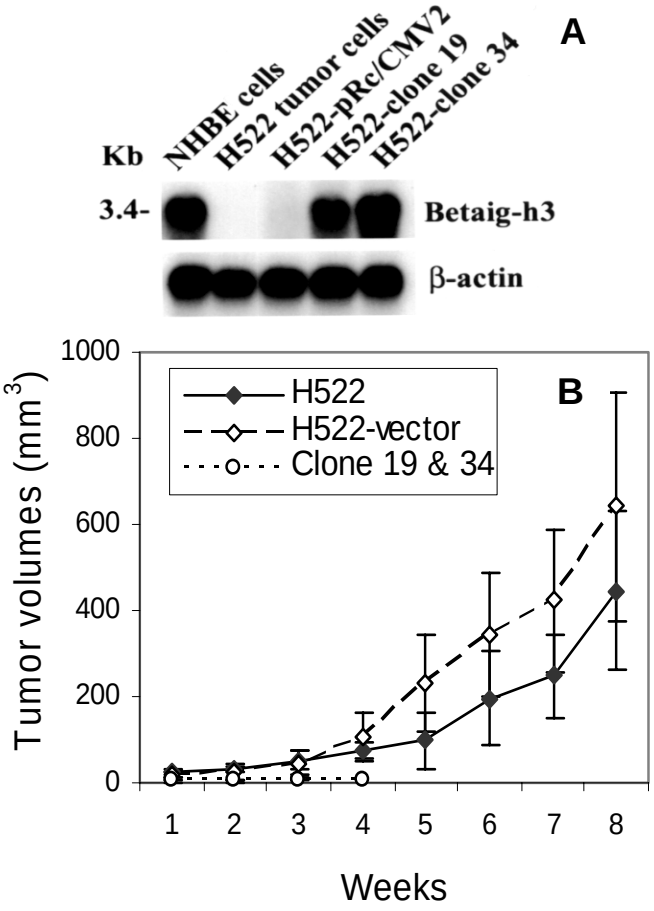

Fig. 2. (A) Expression of the *Betaig-h3* gene determined by Northern analyses in NHBE, parental H522, vector and pRc/CMV2-Betaig-h3 transfected H522 clone 19 and 34 cells. **(B)** *In vivo* tumor growth of *Betaig-h3* transfected H522 lung tumor cells. Tumor volume was calculated using the formula (longest diameter × shortest diameter^2) × 0.5. Results are expressed as the mean ± s.d. from three independent experiments. At each timepoint, the tumor volumes of *Betaig-h3* transfected cells were significantly smaller than parental H522 lung tumor cells (P<0.01).

To ascertain the significance of loss of *Betaig-h3* expression in lung carcinogenesis, the wild type *Betaig-h3* gene was ectopically re-expressed in H522 tumor cells using thepRc/CMV2-Betaig-h3 expression vector. Two G418 resistant colonies (clone 19 and 34) that expressed recovered levels of the *Betaig-h3* gene were chosen for further studies. As shown in Figure 2A, the mRNA and protein levels of the *Betaig-h3* gene were absent in parental and empty vector-transfected H522 cells. After transfection, the expression of *Betaig-h3* in H522-clone 19 and 34 were restored to a level similar to that of control NHBE cells. Immunobloting results showed that two sizes of Betaig-h3 protein exist in NHBE cells due to post-translational modification.

To determine whether ectopic expression of the *Betaig-h3* gene in H522 tumor cells suppresses tumor formation *in vivo*, we inoculated parental and *Betaig-h3*-transfected tumor cells subcutaneously into nude mice for a tumorigenicity assay. As summarized in Table 2, mice injected with H522

Table 2.
Suppression of *in vivo* tumor growth by ectopic expression of the *Betaig-h3* gene in H522 lung cancer cells.

Cell type	Tumors/ total mice		Tumor volume at 8 weeks (mm^3)
H522 cells	12/12		446.75 ± 186.10
H522-pRc/CMV2	12/12		641.80 ± 266.46
Betaig-h3-clone 19	0/12	}0/24*	0*
Betai-gh3-clone 34	0/12		

The tumor volumes were calculated using the formula (longest diameter × shortest diameter^2) × 0.5.

* P<0.01 compared with parental and empty vector-transfected tumor cells.

(12/12 mice) and vector-transfected cells (12/12 mice) produced progressively growing tumors at 2 months, with the average tumor volume of 446.75 mm^3 and 641.8 mm^3, respectively. In contrast, half of the sites injected with H522-clone 19 and 34 formed small nodules at 1–2 weeks after inoculation. All of these nodules regressed in one month and no tumors were formed at two months (0/24 mice, $P<0.01$ compared with parental tumor cells). In addition, tumor growth at each time point was significantly suppressed in *Betaig-h3*-transfected H522 cells (Fig. 2B)

Sensitivity to apoptosis after *Betaig-h3* transfection was further determined by treatment of cells with etoposide, a chemotherapeutic drug. Control NHBE, parental and *Betaig-h3*-transfected H522 cells were treated with etoposide (45 μM) for 8 h. After treatment, all cells, including floating ones in the medium, were collected and the percentage of apoptotic cells in the culture was analyzed by Flow cytometry. As shown in Figure 3, the percentage of apoptotic cells in etoposide-treated NHBE cells was 3.5-fold higher than untreated cells. However, apoptosis induction was not significantly increased in parental and vector-transfected H522 tumor cells after etoposide treatment, and the level was significantly lower than that in NHBE cells. In contrast, recovery of *Betaig-h3* expression in H522-clone 19 and 34 cells resulted in a significant increase of apoptosis induction ($P<0.01$), which was about 2.5-fold higher than untreated cells or etoposide-treated parental tumor cells.

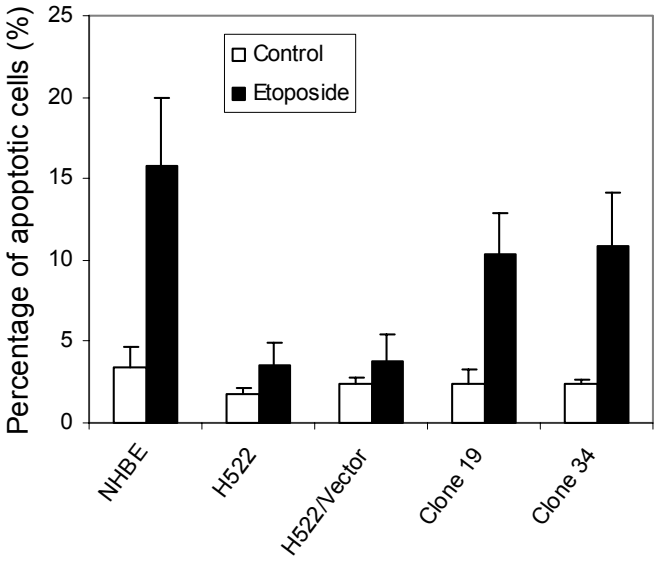

Fig. 3. Apoptotic induction by 45 μM of etoposide determined by APO-BR DU™ kit. Significant lower apoptotic induction in parental H522 tumor cells compared with NHBE cells ($P<0.01$). *Betaig-h3*-transfected H522 clone 19 and 34 cells had increased apoptotic induction, compared to parental tumor cells ($P<0.01$). Data represent mean ± s.d. from three independent experiments.

References

1. Skonier J, Neubauer M, Madisen L, Bennett K, Plowman GD and Purchio AF. cDNA cloning and sequence analysis of *betaig-h3*, a novel gene induced in a human adenocarcinoma cell line after treatment with transforming growth factor-beta. *DNA Cell Biol* **11**:511–22, 1992.
2. Billings PC, Herrick DJ, Kucich U, Engelsberg BN, Abrams WR, Macarak EJ, Rosenbloom J and Howard PS. Extracellular matrix and nuclear localization of beta ig-h3 in human bladder smooth muscle and fibroblast cells. *J Cell Biochem* **79**:261–73, 2000.
3. Zhao YL, Piao CQ and Hei TK. Downregulation of *Betaig-h3* gene is causally linked to tumorigenic phenotype in asbestos treated immortalized human bronchial epithelial cells. *Oncogene* **21**:7471–7, 2002.
4. Zhao YL, Piao CQ and Hei TK. Overexpression of *Betaig-h3* gene downregulates integrin alpha5beta1 and suppresses tumorigenicity in radiation-induced tumorigenic human bronchial epithelial cells. *Br J Cancer* **86**:1923–8, 2002. ■

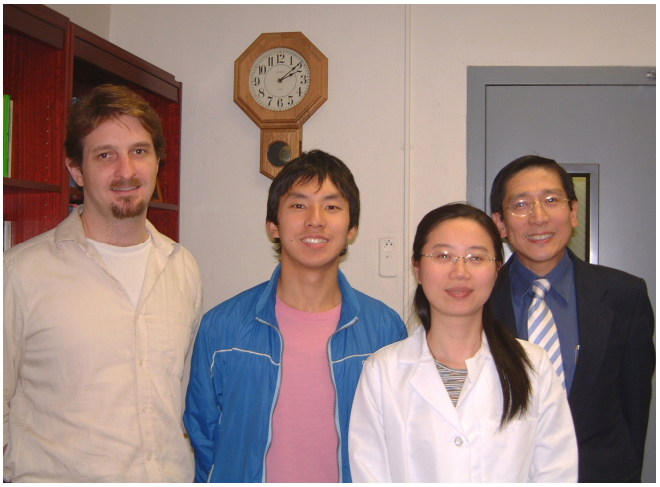

Dr. Hei and Mr. Si-Yuan Yao, a third year trainee from the Okayama Medical University with his mentors, Drs. An Xu and Michael Partridge.

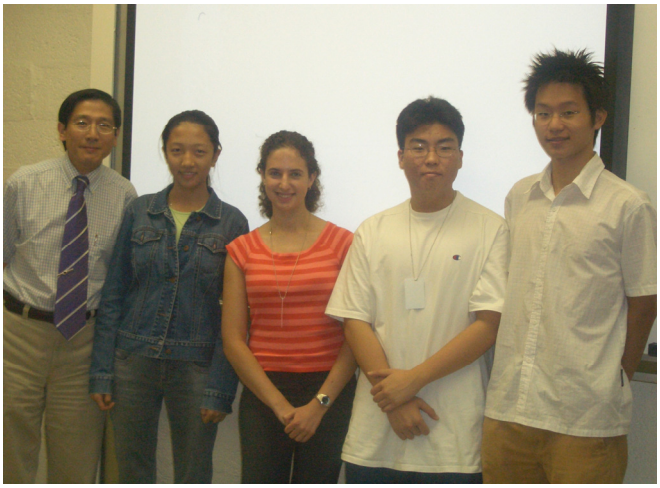

Dr. Hei poses with a group of high school summer students that he is teaching, the next generation of radiation scientists.

IMRT, Protons and the Risk of Second Cancers

Eric J. Hall

Intensity modulated radiation therapy (IMRT) allows dose to be concentrated in the tumor volume while sparing normal tissues. However, the downside to IMRT is the potential to increase the number of radiation-induced second cancers. There are two reasons for this. First, there will be more monitor units and therefore a larger total body dose due to leakage radiation. Second, since IMRT involves more fields, a bigger volume of normal tissue will be exposed to lower radiation doses.

It has been estimated that IMRT may double the incidence of solid cancers in long-term survivors. Table 1 shows the earlier estimates of Hall and Wuu,[1] as well as the more recent estimates from M.D. Anderson Cancer Center.[2] Some machines leak a little more than others, but the overall conclusion is that IMRT may approximately double the induced cancer rate compared with conventional treatment. This may be acceptable in older patients if balanced by an improvement in local tumor control and reduced acute toxicity. On the other hand, the incidence of second cancers is much higher in children, so that doubling it may not be acceptable.

The use of IMRT with children represents a special case. There are three reasons. First, children are more sensitive to radiation induced cancer than adults by a factor of at least 10. Second, radiation scattered from the treatment volume is more important and more significant in the small body of the child than in the larger body of an adult. Put another way, nearby radiogenic organs are closer in a child than in an adult. This is illustrated in Figure 1. Third, there is the question of genetic susceptibility. Many of the cases of childhood cancer involve a germline mutation which may confer susceptibility to radiation-induced cancer for example. The study of Hodgkin's patients treated with radiation, which resulted in an incidence of breast cancer, included the suggestion that they were more sensitive to the induction of breast cancer than children with other malignancies such as Wilms' tumor or neuroblastoma.

Table 1.
Risk of fatal radiation-induced malignancies after RT for prostate cancer (%/Sv)

Hall & Wu, 2003	
Conventional 6 MV	**1.5**
IMRT 6 MV	**3.0**
Kry et al., 2005	
Conventional 18 MV Varian	**1.7**
IMRT 6 MV Varian	**2.9**
Siemens	**3.7**
IMRT 10 MV Varian	**2.1**
IMRT 15 MV Varian	**3.4**
Siemens	**4.0**
IMRT 18 MV Varian	**5.1**

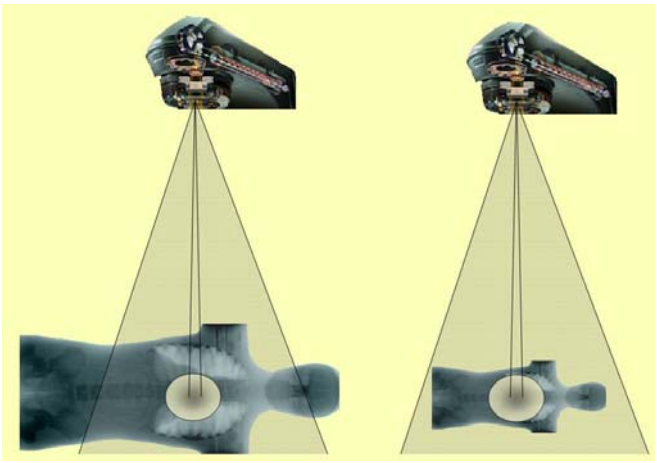

Fig. 1. There is the same leakage for adult RT vs. pediatric RT, but scattered radiation from the treatment volume is more important in the small body of a child because nearby radiogenic organs are closer in a child.

The levels of leakage radiation in current Linacs are not inevitable. Leakage can be reduced, but at substantial cost. For example, the leakage from multi-leaf collimators is 1 to 3% (Fig. 2). This was considered adequate at the time that MLCs were introduced since they replace Cerebend blocks, which were characterized by a leakage of about 5%. However, it can be much reduced by the addition of more shielding material.

An alternative strategy to reduce the volume of normal tissue exposed to radiation would be to replace x-rays with protons. However, this is an advantage only if the proton machine employs a pencil scanning beam. Most facilities in

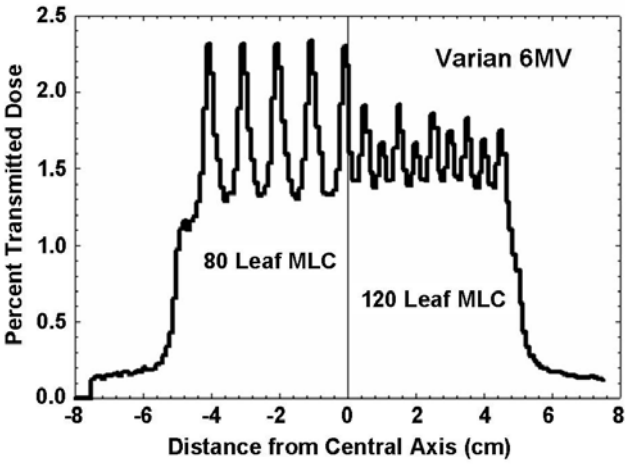

Fig. 2. Illustrating the leakage radiation through multi-leaf collimators (MLCs) for a 6 MV Linac. (Figure courtesy of Dr. Paul Keall.)

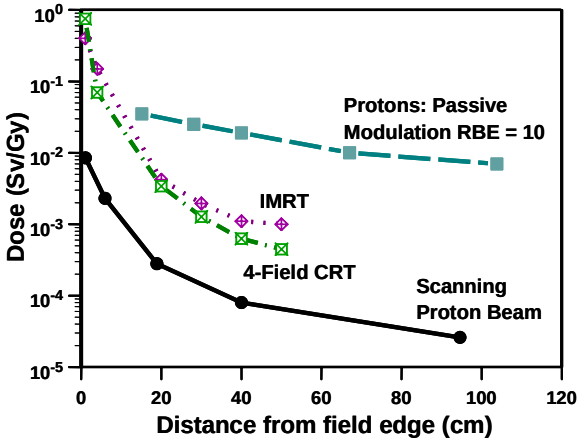

Fig. 3. The equivalent dose outside the edge of the treatment field as a fraction of the dose at the isocenter for protons with passive modulation, for a scanning proton beam and for 6 MV x-rays, either 4 field CRT or IMRT. (Neutron data due to Harald Paganetti, Massachusetts General Hospital, Boston.)

the U.S. use passive modulation in order to produce a field of adequate size, but a scattering foil becomes a source of neutrons which result in a total body dose to the patient. The consequences are illustrated in Figure 3.

Passive modulation results in doses distances from the field edge that are an order of magnitude higher than those characteristic of IMRT with x-rays. The full benefit of protons is achieved only if a scanning beam is used in which case doses are an order of magnitude lower than is the case with x-rays.

References

1. Hall EJ and Wuu CS. Radiation-induced second cancers: the impact of 3D-CRT and IMRT (Review). *Int J Radiat Oncol Biol Phys* **56**:83-8, 2003.
2. Kry SF, Salehpour M, Followill DS, Stovall M, Kuban DA, White RA, Rosen II. The calculated risk of fatal secondary malignancies from intensity-modulated radiation therapy. *Int J Rad Oncol Biol Phys* **62**:1195-203, 2005. ■

Center for High-Throughput Minimally-Invasive Radiation Biodosimetry

David J. Brenner and Sally A. Amundson

The Office of Science and Technology Policy and the Homeland Security Council recently assessed and prioritized the nation's needs in terms of a response to a terrorist attack using radiological or nuclear devices. Among the most critical needs identified were development of biomarkers and devices for biodosimetry, and automation of biodosimetry assays. The Center for High-Throughput Minimally-Invasive Radiation Biodosimetry is a research consortium devoted to developing high-throughput radiation dose assessment techniques. This Consortium represents a multidisciplinary balance between radiation biologists, radiation physicists, radiation chemists, mechanical engineers, software engineers, product development experts, commercial companies in the field, and end users. The three areas that we have identified as having the highest potential for high-throughput biodosimetry are cytogenetics, functional genomics, and metabolomics. Each area has its own project, supported by a bioinformatics core, a functional genomics core, a fabrication core and, crucially, a product development core. In addition, our Consortium has a training and education component built around the two premier programs in the U.S. currently involved in the training and education of radiation biologists (Columbia University and the Harvard School of Public Health).

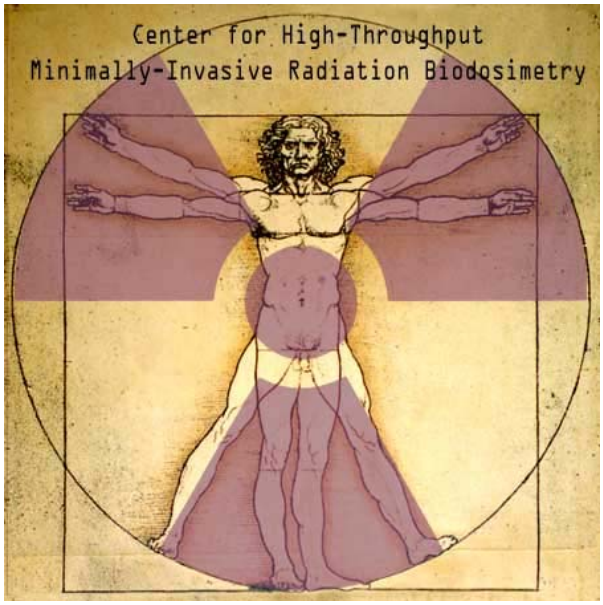

The need for high throughput rapid biodosimetry can be well illustrated by reference to the 1987 radiation incident in Goiânia, Brazil, a city with about the same population as Manhattan. In the first few days after the incident became known, about 130,000 people (roughly 10% of the population) came for screening, of whom 20 required treatment. In response to a RDD (radiological dispersal device) event in a U.S. city, one would anticipate a similar scenario. Tens or possibly hundreds of thousands of individuals will need to be screened within a few days for radiation exposure both because they will demand it, and because of the medical necessity to perform radiological triage.

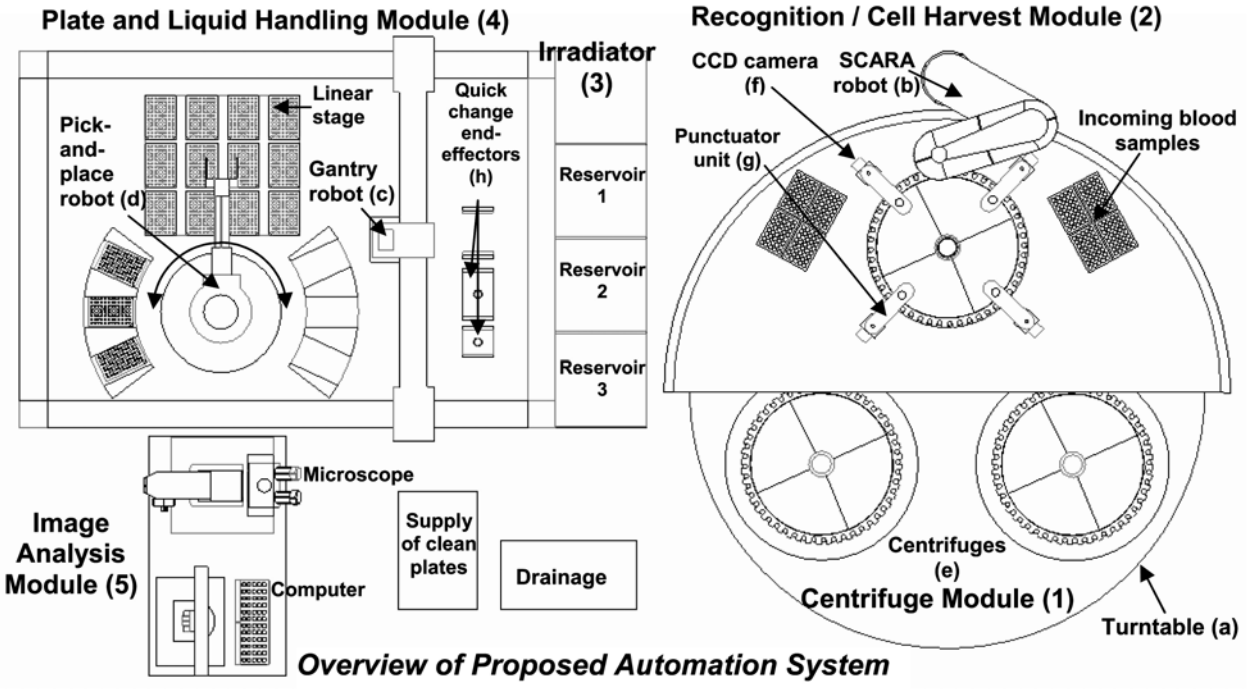

Fig. 1. Overall design for Project 1 device.

Mass radiological triage will be critical after a large-scale event because of the need to identify, at an early stage, those individuals who will benefit from medical intervention, and those who will not. Individuals who actually received whole-body doses above, say, 1.5 Gy can benefit from antibiotics, platelet and cytokine treatment. At higher doses, say between 5 and 12 Gy, there is also a critical need for biodosimetry. This is because there is only a quite narrow dose window (approximately 7–10 Gy) in which bone-marrow transplantation is a useful option (below 7 Gy, survival rates are good solely with medication, while above 10 Gy patients will generally have lethal gastrointestinal damage). Thus it is critical to ascertain, through biodosimetry, whether a patient's dose is within this dose window, such that a bone marrow transplant is a useful option.

Eliminating and reassuring those patients who do not need medical intervention will, of course, be crucial in what will certainly be a highly resource-limited scenario.

Many variables can impact on the effectiveness of a biodosimetry approach. These include the dose range, time since exposure, individual variability and confounding exposures. Such considerations led us to conclude that different biodosimetric endpoints may be needed for different situations. Thus each of the three central projects in this Center represent a different approach to high-throughput biodosimetry.

Project 1: Automated Robotically-Based High Throughput Radiation Biodosimetry

Lead by Dr. David Brenner, this project involves the design and construction of a new device that will use advanced, high-speed automated image analysis and robotics to rapidly examine tissue samples (e.g., a fingerstick of blood) for quantitative indicators of radiation exposure (e.g., fragments of DNA; DNA repair complexes). Our goal is to develop a fully automated ultra-high throughput radiation biodosimetry workstation, using purpose-built robotics and advanced high-speed automated image acquisition (Fig. 1).

Target throughput will be 30,000 samples/day, compared with throughputs in current devices of a few hundred samples/day.

The basic system involves the well-characterized micronucleus assay in lymphocytes, with all the assays being carried out *in-situ* in multi-well plates. By calling up pre-programmed options in timing, liquid handling, and image analysis, the device will also measure γ-H2AX foci yields, and micronucleus yields in reticulocytes, both providing "same-day answer" dose estimates. By calling up pre-programmed options in liquid handling steps, the device will also measure micronuclei in other readily-accessible tissues, such as exfoliated cells from urine or buccal smears.

A key option of this system will be that each lymphocyte sample will be split in two, with one of the two split samples being irradiated before being analyzed. This will allow a positive control for each individual, providing an internal calibration to take into account inter-individual variability in radiosensitivity.

This project will involve collaborations with the Department of Mechanical Engineering at Columbia University, The National Cancer Institute, the University of Pittsburgh Medical Center, and the City of New York Department of Health and Mental Hygiene.

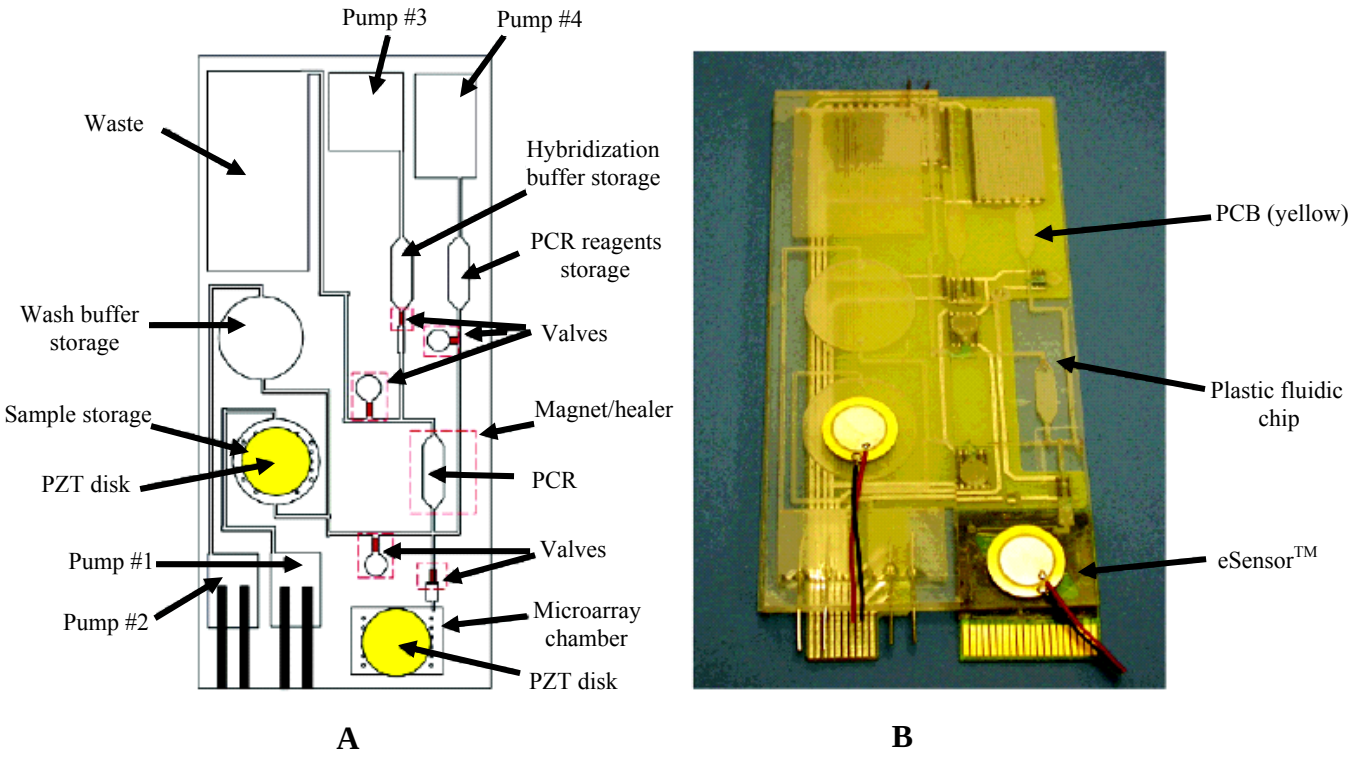

Fig. 2. Prototype of fully integrated self contained biochip for radiation biodosimetry, Project 2.

Project 2: Biodosimetry with a Fully Integrated Biochip Using Gene Expression Signatures

Lead by Dr. Frederic Zenhausern at the Arizona State University Center for Applied Nanobioscience, this project will develop self-contained biochip-based cassettes capable of rapidly measuring expression levels of a set of genes that we will establish as quantitatively and specifically defining a radiation exposure. This approach will only require a drop of blood and will be readily deployable for large-scale population screening.

Exposure to ionizing radiation produces dose-dependent changes in the expression of many genes, potentially providing a means to assess both radiation exposure and to quantify dose. We have recently developed a completely self-contained biochip that consists of microfluidic mixers, valves, pumps, channels, chambers, heaters, and DNA microarray sensors to perform DNA analysis of complex biological sample solutions, such as blood (Fig. 2). We will develop this device into a self-contained radiation biodosimeter suitable for large scale screening.

While the technology exists to perform highly sensitive and accurate gene-expression analysis using bench-top instrumentation and skilled technicians, the goal of this project is to fabricate a self-contained, fully integrated cartridge that autonomously performs the complete bio-assay. The cartridge will contain its own power source, control electronics, functional microfluidic components and reagents. After assay completion, the cartridge is inserted into a commercial fluorescence reader where the signal is read out within seconds.

Thousands of such cartridges can be stockpiled to be used in parallel after a radiological incident, for high-throughput screening of affected populations.

This project will involve close collaboration with the Functional Genomics Core in the Center for Radiological Research, as well as the Bioinformatics Core at Translational Genomics, and the University of Pittsburgh Medical Center.

Project 3: Rapid Non-Invasive Radiation Biodosimetry Through Metabolomics

This project is centered at the Harvard University School of Public Health under the leadership of Dr. Albert J. Fornace Jr. The ultimate goal for this project is to design and construct a completely non-invasive screening tool for radiation exposure. We hope to avoid even the smallest finger prick for a blood sample. The team will analyze sweat, urine or saliva samples for unique changes in metabolites that indicate radiation exposure. This project will combine metabolomics and stress-signaling expertise with the sensor-chip expertise of Sionex Corporation, to develop instrumentation for rapid non-invasive assessment of radiation exposure and injury using metabolic markers, thus addressing the overall theme of the Consortium.

Irradiation *in vivo* triggers the expression of many genes involved in intercellular signaling. The proteins coded for by these genes can have wide-ranging effects on cellular metabolism. Our preliminary data from a modern metabolomics approach indicate that these changes are reflected in alterations in the spectrum of metabolites in urine and sputum. Such metabolomic analyses offer several key advantages

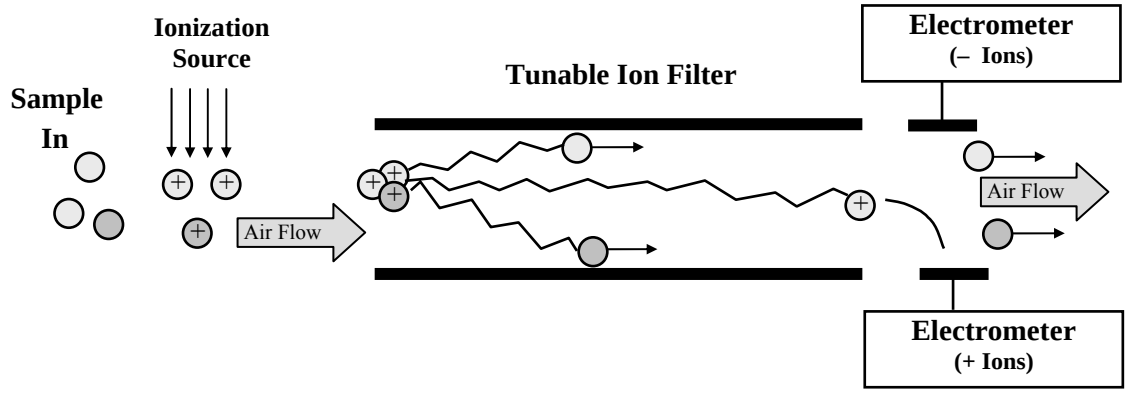

Fig. 3. Schematic of radio-frequency differential ion mobility spectrometer (DMS), Project 3.

including simple, non-invasive collection, and thus the potential for very high-throughput biodosimetry screening. We will also investigate the potential for using a metabolomic signature in sweat, which would increase throughput still further.

Basic supporting studies will include expression profiling and metabolite analyses carried out in mouse model systems, to determine the tissues and signaling pathways, which are reflected in metabolomics changes. Cutting-edge informatics analyses, in collaboration with the Bioinformatics Core, will be used to select thoroughly characterized metabolomics markers to develop an optimal radiation metabolomics signature. Translational studies will extend these signatures into humans using samples from patients having total body irradiation.

In the discovery phase, we are identifying and characterizing metabolomics signatures of radiation responses. The initial work is on the urinary metabolome of the mouse, and other metabolomes (blood, sweat, and saliva) will also be analyzed. This work is being done at the NCI using a state-of-the-art UPLC-MS(TOF) system, which is able to analyze the entire metabolome.

The technology that we have chosen for the biodosimetry device is radio-frequency differential ion mobility spectrometer (DMS, schematized in Fig. 3), which operates like a gas chromatograph, in that a carrier gas (air) is employed in the separation, but it is ions that are separated and detected, as in a mass spectrometer. This chip is the underlying technology currently used in the Thermo Electron EGIS™ Defender trace explosive and drug detection system, used in U.S. airports.

DMS is quantitative and has extremely sensitive detection limits, down to the parts-per-trillion range. The DMS method uses the non-linear mobility dependence of ions on high strength RF electric fields for ion filtering, and operates in air at atmospheric pressure. This novel method enables the rapid detection and identification of compounds that cannot be resolved by other analytical techniques. The DMS scales down well in size, while preserving sensitivity and resolution. This makes DMS attractive as a quantitative detector that is portable and comparatively low cost.

This project will involve collaborators from Harvard University School of Public Health, the University of Bern, Switzerland, the National Cancer Institute, the University of Pittsburgh Medical Center, and Sionex Corporation. ■

Estimating Radiation-Induced Cancer Risks at Very Low Doses: Rationale for Using a Linear No-Threshold Approach

David J. Brenner and Rainer K. Sachs[1]

Introduction

The possible excess cancer risks caused by ionizing radiation doses of ~1 mSv or less are probably too small to be estimated directly from epidemiological data, being buried in the noise of the background cancer risk. The linear no-threshold (LNT) approach to estimating such risks involves using epidemiological data at higher (but still low) doses to establish an "anchor point," and then extrapolating the excess cancer risk linearly down from this point to the very low doses of interest. A French Academy of Sciences (FAS) report,[1] provides arguments, which we here critically evaluate, that such LNT extrapolations systematically give substantial overestimates of the excess cancer risk at very low doses.

[1] *University of California, Berkeley.*

Microdosimetric argument for the LNT approach

One of the main lines of argument in support of LNT, and one which is strongly criticized in FAS, is the so-called "microdosimetric argument": Consider a low dose D_1 which corresponds to a mean of about one photon passing through a cell nucleus. Let us assume (see below) that there is evidence that this radiation dose causes an increased cancer risk in a human population. Next, suppose that radiation carcinogenesis involves *single-cell action*, i.e., that radiation effects on separate cells and subsequent development of independent cell lineages dominate, with inter-cellular interactions acting only as comparatively small perturbations of dominant one-lineage effects (the implications of dropping this assumption are discussed later). With these assumptions, of an increased cancer risk at dose D_1 and of single-cell action, the same basic biological responses to the radiation damage must operate at, say, a dose of $D_1/10$, as compared with a dose of D_1; this follows from the fact that those proportionately fewer cells that were damaged at dose $D_1/10$ would each be subject to the same (single photon) damage as the larger number of cells damaged at dose D_1. In other words, at dose $D_1/10$, ten times fewer cells would be damaged, but the nature of damage to those cells would be the same as at dose D_1. Given this, the excess risk must simply decrease by the same factor of 10 over the dose range from D_1 to $D_1/10$, i.e., linearity would hold.

This microdosimetric argument underlying LNT extrapolations requires, as an anchor point, evidence for a radiation-induced cancer risk in humans at a dose D_1, sufficiently low that most exposed cell nuclei are subjected to no more than one energy deposition event. We argue that the studies of childhood cancer after *in-utero* exposure of about 6 mGy, as reported, for example, by Mole,[2] fulfill the criterion. First, a dose of 6 mGy of 80-kVp x-rays does indeed correspond to a mean of about one photon passing through a cell nucleus; second, this dose does indeed result in a statistically-significant increase in childhood cancer risk.

FAS has criticized this instance of the microdosimetric argument on three grounds:

1. They suggested that the dose of 6 mGy, reported by Mole in the *in-utero* study, corresponds to about 10 energy depositions per nucleus. This is not correct for the 80-kVp x-rays used in the *in-utero* examinations. Based on microdosimetric measurements, 6 mGy of 80-kVp x-rays corresponds to a mean of about 1 energy deposition in a spherical cell nucleus with a diameter of 7 μm.
2. They suggested that there may not be a causal relationship between the radiation dose and the observed increased cancer risk in the children exposed *in utero*. Doll and Wakeford[3] reviewed in detail the relationship between the increase in childhood cancer risk and the low-dose radiation exposure, and concluded: "…*on review, the evidence against bias and confounding as alternative explanations for the association is strong. Scrutiny of the objections to causality suggests that they are not, or may not be, valid. A causal explanation is supported by evidence indicating an appropriate dose-response relationship and by animal experiments. It is concluded that radiation doses of the order of 10 mGy received by the fetus in utero produce a consequent increase in the risk of childhood cancer.*"
3. They questioned the extrapolation from ante- to post-partum exposure; however, they do not give a convincing reason why the same dose that causes an increase in cancer risk when delivered *in utero*, would produce no cancer risk when delivered after birth.

Based on the arguments above, we suggest that these three objections by FAS to the basis of LNT are not valid – and thus *if single-cell action dominates*, a linear extrapolation of excess cancer risk from low to very low doses is appropriate for most radiation-induced carcinomas.

Significance of inter-cellular interactions

As we have discussed, the microdosimetric argument in which the LNT model is derived depends on the assumption that a radiation-induced cancer can develop from a single damaged cell, independently of other damaged cells in the tissue of interest. Of course it is known that inter-cellular interactions, and interactions of cells with the extra-cellular matrix, do play a role in radiation carcinogenesis; for example, epithelial cancer cells in an organ interact with cells of their own type, with fibroblasts, with inflammatory cells including immune-system cells, and with endothelial cells responsible for vasculature. If inter-cellular interactions among radiation-damaged cells play a dominant role during carcinogenesis, rather than being comparatively small modulations of single-cell action, the microdosimetric argument becomes inapplicable, to the extent that the low-dose "anchor-point" dose in the argument now involves many hits to a population of interacting cells, even though any one cell nucleus is unlikely to be hit more than once. Thus a central theoretical underpinning for LNT extrapolation would be called into question. But it would still remain to be determined whether LNT was underestimating or overestimating cancer risks at very low doses.

Specifically, the case made in FAS, is that if inter-cellular interactions are important factors in radiation carcinogenesis, such interactions necessarily imply *decreased* excess cancer risks per unit dose at very low doses compared to higher doses. But the fact that multi-cellular repair mechanisms are complex and may well control the development of pre-malignant cells, does not necessarily imply decreased excess cancer risk per unit dose at very low doses. Many different complex cellular interaction scenarios can be hypothesized, some of which would indeed involve decreased cancer risks per unit dose at low doses (or even zero or negative excess risk), but one can equally well hypothesize inter-cellular carcinogenesis mechanisms that would increase the low dose risks.

Our understanding of the effect of inter-cellular interactions is still in its infancy, but those multi-cellular effects which have been investigated at low doses, such as bystander responses, often show an *increased* mutagenic or oncogenic risk per surviving cell, compared with what would be estimated using LNT. For example, there is evidence that some bystander effects saturate at quite low doses, in which case the first hit to any cell in a communicating population of cells could be more dangerous to the popu-

lation than subsequent hits to other cells in that population – implying that LNT would *underestimate risks* at very low doses.

Even for comparatively simple *in-vitro* endpoints such as DNA double strand breaks, often implicitly considered by FAS to be mechanistic surrogates for carcinogenesis, we know little about inter-cellular interactions after very low doses of radiation, so it is not surprising that we know little about the quantitative significance of such interactions for low-dose radiation carcinogenesis *in vivo.*

Significance of immune surveillance

FAS speculated that, at very small doses, immune surveillance or some other mechanism would eliminate, with 100% efficiency, all of the small number of pre-malignantly damaged cells: "*at a dose of a few mSv [mGy], lesions are eliminated by disappearance or senescence of the cells*." Such a mechanism would indeed lead to a threshold in dose, below which radiation-induced cancer risks are zero. However the notion that small numbers of radiation-induced pre-malignant cells can always be highly efficiently "mopped up" seems unlikely for several reasons: Firstly, it is well established that we always carry a significant burden of pre-malignant cells which have therefore not been eliminated through immune surveillance or any other mechanism. Secondly, what quantitative evidence there is about the dose-dependence of immune surveillance suggests that it is often much less effective when the number of relevant cells is small: this is the well documented phenomenon of "dilution escape"[4] or "sneaking through,"[5] in which small numbers of tumor cells are not recognized and can "sneak through" immune surveillance, while somewhat larger numbers of tumor cells are recognized and are rejected, whereas large numbers of tumor cells can break through immune elimination. Thirdly, a mechanism which is completely effective in removing small numbers of pre-malignant cells would seem to imply that, regardless of radiation exposure, no clonal cancers could ever arise, because pre-malignant clones would always be eliminated when they are still very small in number – in clear contrast to the overwhelming evidence that most cancers are clonal in origin.

Conclusions

The critiques presented by FAS to the microdosimetric arguments which support LNT do not seem to be valid. It is, however, certainly true that if inter-cellular interactions among radiation-damaged cells dominate carcinogenesis, rather than being small perturbations of the carcinogenesis process, one would expect deviations from LNT. But it would still remain to be determined whether LNT was underestimating or overestimating cancer risks at very low doses, and whether such deviations from linearity were small or large. There is no convincing evidence to support the suggestion that immune surveillance will differentially decrease cancer risks at very low doses, and there is some evidence to the contrary.[4,5]

As we start to learn more about the main mechanisms of inter-cellular communication during carcinogenesis, it will be possible to incorporate this information into quantitative cancer risk models. However, the data summarized in the French Academy Report, and also in the corresponding U.S. National Academy Report, BEIR VII, both suggest that we currently know little of the magnitude inter-cellular communication effects on radiation carcinogenesis *in vivo*, whether these effects have similar consequences for different cancer types, or even whether these effects would increase or decrease very low-dose cancer risks compared with the predictions of LNT. In this light it seems premature to use arguments about inter-cellular interactions to justify replacing linearity in cancer risk at very low doses with any non-linear dose-response relationship.

References

1. Tubiana M, Aurengo A, Averbeck D, Bonnin A, Le Guen B, Masse R, Monier R, Valleron AJ and de Vathaire F. Dose-effect relationships and estimation of the carcinogenic effects of low doses of ionizing radiation, Institut de France Académie des Sciences (www.academie-sciences.fr/publications/rapports/pdf/dose_effet_07_04_05_gb.pdf), Paris, 2005.
2. Mole RH. Childhood cancer after prenatal exposure to diagnostic X-ray examinations in Britain. *Br J Cancer* **62**:152–68, 1990.
3. Doll R and Wakeford R. Risk of childhood cancer from fetal irradiation. *Br J Radiol* **70**:130–9, 1997.
4. Bonmassar E, Menconi E, Goldin A and Cudkowicz G. Escape of small numbers of allogeneic lymphoma cells from immune surveillance. *J Natl Cancer Inst* **53**:475–9, 1974.
5. De Boer RJ and Hogeweg P. Tumor escape from immune elimination: simplified precursor bound cytotoxicity models. *J Theor Biol* **113**:719–36, 1985. ■

RARAF – Table of Contents

RARAF Professional Staff and Picture 71
Introduction 72
Research Using RARAF 72
Development of Facilities 74
Van de Graaff Utilization and Operation 77
Training 77
Personnel 77
Recent Publications of Work Performed at RARAF (2004–2005) 78
SPECIAL REPORT: Replacement of the RARAF Accelerator 83

RARAF PROFESSIONAL STAFF

RARAF Staff *(l–r)*: Bottom row: Guy Garty and Alan Bigelow; *2nd row*: Gerhard Randers-Pehrson, Stephen Marino and Gregory Ross; *3rd row*: Gary Johnson, David Brenner and Giuseppe Schettino; *top row*: Charles Geard and Brian Ponnaiya. *Not shown*: Gloria Jenkins-Baker.

David J. Brenner, Ph.D., D.Sc. **–** RARAF Director
Stephen A. Marino, M.S. **–** RARAF Manager
Gerhard Randers-Pehrson, Ph.D. **–** RARAF Associate Director, Chief Physicist
Charles R. Geard, Ph.D. – CRR Associate Director, Senior Biologist
Alan Bigelow, Ph.D. – Associate Research Scientist
Brian Ponnaiya, Ph.D. – Associate Research Scientist
Guy Y. Garty, Ph.D. – Staff Associate
Gregory Ross, M.S. – Programmer Analyst
Giuseppe Schettino, Ph.D. – Post-Doctoral Research Scientist
Gloria Jenkins-Baker, B.A. – Biology Technician

The Radiological Research Accelerator Facility

AN NIH-SUPPORTED RESOURCE CENTER – WWW.RARAF.ORG

Director: David J. Brenner, Ph.D., D.Sc.
Manager: Stephen A. Marino, M.S.
Chief Physicist: Gerhard Randers-Pehrson, Ph.D.

Introduction

This was a major year for RARAF. The Van de Graaff accelerator, which was 55 years old and provided us with charged particle beams for over 38 years, was decommissioned in June, 2005. We have installed a new Singletron from High Voltage Engineering (HVE) that will provide us with increased voltage and stability. A detailed description of the removal of the Van de Graaff and the installation of the Singletron are given in a section elsewhere in the CRR Annual Report.

In addition, over 2000 square feet of office and (mostly) laboratory space have been commissioned for the third floor, which until the stand-alone microbeam development had been used only for storage. The construction is funded by a Homeland Security grant obtained by David Brenner.

Research Using RARAF

As has been the case for more than 5 years, the focus of most of the biology experiments at RARAF has been the "bystander" effect, in which cells that are not irradiated show a response to radiation when in close contact with or even only in the presence of irradiated cells. Several experiments examining this effect were continued this year and new ones were initiated, observing a variety of endpoints to determine the size of the effect and the mechanism(s) by which it is transmitted. Evidence continues to be obtained for both direct gap junction communication through cell membrane contact and indirect, long-range communication through media transfer. Both the microbeam and the track segment facilities continue to be utilized in various investigations of this phenomenon. The single-particle microbeam facility provides precise control of the number and location of particles so that irradiated and bystander cells may be distinguished but is somewhat limited in the number of cells that can be irradiated. The track segment facility provides broad beam irradiation that has a random pattern of charged particles but allows large numbers of cells to be irradiated and multiple users in a single day.

Two special types of track segment dishes are being used to investigate the bystander effect using the track segment facility: double-sided dishes and "strip" dishes. Double-sided dishes have Mylar foils glued on both sides of a stainless steel ring, with cells plated on the inside surfaces of both foils. The interior is completely filled with medium. This type of dish is used for investigation of the non-contact, long-range bystander effect since the cells on the two surfaces are not in direct contact, can only communicate through the culture medium, and only the cells on one surface are irradiated. "Strip" dishes consist of a stainless steel ring with Mylar foil glued to one side in which a second dish is inserted. The Mylar foil glued to the inner dish has alternate strips of the Mylar removed. Cells are plated over the combined surface and are in contact. The Mylar on the inner dish is thick enough to stop the charged particles (usually ^{4}He ions) and the cells plated on it are not irradiated. These dishes are used for bystander experiments involving cell-to-cell communication.

In Table 1 are listed the experiments performed at RARAF from November 1, 2004 through June 11, 2005 (when the Van de Graaff was run for the last time) and the number of days each was run in this period. Use of the accelerator for experiments was over 53% of the normal available time, 6% higher than last year and the highest we have attained at Nevis Labs. Fourteen different experiments were run during this period, a little less than the average for 2000–2004; however the accelerator was only available for 8 months instead of 12, as in other years. Eight experiments were undertaken by members of the CRR, supported by grants from the National Institutes of Health (NIH) and the Department of Energy (DOE). Six experiments were performed by outside users, supported by grants and awards from the National Aeronautics and Space Administration (NASA), the Ministry of Education, Science, Sports and Culture of Japan, the NIH and a private corporation. Brief descriptions of these experiments follow.

An experiment on the production of chromosome aberrations in human cell lines was resumed by Charles Geard and Adayabalm Balajee of the CRR (Exp. 71). Normal human fibroblasts and Ataxia telengectasia (AT) cells were irradiated with ^{4}He ions using the track segment facility. The cells were examined for chromosome aberrations using the techniques of MFISH and MBAND.

Development of a method to detect explosives in baggage (Exp. 82) was resumed this year. Gerhard Randers-Pehrson of the CRR continued measurements of neutron spectra and yield from the $Be^9(p,n)$ reaction using a very thin beryllium target. The detection system is based on resonant scattering of 0.43 MeV neutrons by nitrogen and oxygen. Measurements were made for several combinations of reaction angle and incident proton energy that produce 0.43 MeV neutrons to determine parameters producing the highest yield and the spectrum that contains the highest percentage of neutrons of the desired energy.

Richard Maurer, David Roth and James Kinnison of Johns Hopkins University continued the calibration of a neutron spectrometry system that may be used on the International Space Station and possibly the manned mission to Mars (Exp. 89). Measurements of pulse rise times for the

Table 1.
Experiments Run at RARAF, November 1, 2004–June 11, 2005

Exp. No.	Experimenter	Institution	Exp. Type	Experiment Title	No. Days Run
71	A Balajee, CR Geard	CRR	Biology	Chromosome aberration and micronucleus production in human cell lines by α-particles	0.7
82	G Randers-Pehrson	CRR	Physics	Detection of explosives	1.0
89	RH Maurer, J Kinnison	Johns Hopkins University	Physics	Calibration of a portable real-time neutron spectrometry system	4.8
92	S Amundson	CRR	Biology	Functional genomics of cellular response to high-LET radiation	15.1
103	G Jenkins, CR Geard	CRR	Biology	Damage induction and characterization in known hit versus non-hit human cells	3.5
106	B Ponnaiya, CR Geard	CRR	Biology	Track segment α-particles, cell co-cultures and the bystander effect	1.7
110	H Zhou, TK Hei	CRR	Biology	Identification of molecular signals of α-particle-induced by-stander mutagenesis	24.8
121	A Zhu, H Lieberman	CRR	Biology	The bystander effect in mouse embryo stem cells with mutant Mrad9 gene	5.3
125	M Suzuki (H Zhou)	Nat. Inst. of Radiological Science, Japan	Biology	Chromatid fragment induction detected with the PCR technique by cytoplasmic irradiation in normal human bronchial cells	3.0
126	O Sedelnikova (S Mitchell)	NIH	Biology	γ-H2AX foci formation in directly irradiated and bystander cells	1.8
127	E Tucker	Baruch Col-lege, CCNY	Biology	The effect of high-LET radiation on blue/UV-A signaling	4.8
128	M Salasky, M Akselrod	Landauer, Inc.	Physics	Radiation response of Al2O3 dosimeters	11.0
130	B Ponnaiya, C Geard	CRR	Biology	Investigation of bystander responses in 3-dimensional systems	2.0
132	S Meyn	U. of Toronto	Biology	Observation of localization of TRF2 in bystander cells	1.3

Note: Names in parentheses are members of the CRR who collaborated with outside experimenters.

Bicron scintillation detector were made for a series or neutron energies ranging from 0.8 to 14 MeV in order to refine the discrimination of gamma-ray pulses from neutron pulses.

Sally Amundson of the CRR continued two types of experiments concerning the radiation-induced gene expression profiles in human cell lines using cDNA microarray hybridization and other methods (Exp. 92). One involves track segment irradiation for comparison of gene expression responses to direct and bystander irradiation. In these experiments, gene expression at 4 and 24 hours post treatment are compared. Early experiments worked well and are being repeated to establish reproducibility and to obtain sufficient data to begin informatic analysis. The other type of irradiation involves use of the microbeam to irradiate either cell nuclei or cytoplasm. These experiments require cDNA amplification techniques to produce sufficient material for microarray hybridization from the small number of cells irradiated. RNA from single microbeam dishes has been isolated successfully and amplification and hybridization results are highly encouraging. Gene expression profiles have been obtained after both nuclear and cytoplasmic irradiation at 4 and 24 hours post-treatment. These experiments are being repeated to obtain reproducible data that can be analyzed to reveal gene expression trends.

Charles Geard and Gloria Jenkins of the CRR continued their studies of the bystander effect in several cell lines using the microbeam facility (Exp. 103). Normal human fibroblasts were irradiated with helium ions, targeting 10% and 100% of the cell nuclei. Endpoints for various experiments included micronucleus production in S phase and production of p21, p53 and H2AX.

A study investigating the bystander effect was continued by Brian Ponnaiya and Charles Geard of the CRR and another was initiated. One study uses the track segment facility for broad-beam charged particle irradiations of normal human fibroblasts plated on double-sided dishes (Exp. 106). These studies were expanded to irradiations using the microbeam facility. A line of cells was irradiated across the center of the microbeam dish using either ^{4}He ions or protons. Analyses of cellular signaling pathways in both irradiated and bystander cells were made at both the protein and mRNA levels. The proteins examined by immunofluorescence techniques include p21/WAF1 and members of the MAP kinase signaling pathway whose phosphorrylation status have been shown to be altered in both irradiated and bystander cells. Levels of mRNA from early response genes, including c-fos, c-jun, junB and p21/WAF1 were also assayed using RT-PCR protocols. A study of the bystander

effect in artificial tissue systems has also been initiated (Exp. 130). EPI-200 epithelial tissue samples from MatTek Corp. were irradiated with ^{4}He ions using the track segment facility. Because the thickness of the tissues is much greater than the range of the ions, only about 25% of the cells are irradiated and about 75% are unirradiated bystander cells. Both irradiated and bystander cells are examined for MAP kinase using immuno-histochemistry.

Hongning Zhou and Tom Hei of the CRR continued to use the single-particle microbeam facility to try to identify the signaling transduction pathways involved in radiation-induced bystander mutagenesis (Exp. 110). A fraction of A_L cells is irradiated with alpha particles in the nucleus or the cytoplasm with doses that kill most of these irradiated cells. The surviving, predominantly unirradiated cells are observed for mutation. In addition, experiments have been performed using the track segment facility employing "strip" dishes for at least 8 different cell lines including normal human fibroblasts, lung fibroblasts and DNA-PK deficient cells. The cells are kept *in situ* for 2, 6, 24 or 48 hours after irradiation, thereby increasing the number of cells and the time for interaction. The mRNA extracted from the cells is analyzed using micro-arrays. Preliminary data show some changes in gene expression in the bystander cells.

Howard Lieberman and Aiping Zhu of the CRR have completed experiments investigating the bystander effect in mouse embryo stem cells with a mutation in the Mrad9 gene (Exp. 121), which promotes radiation resistance and helps regulate the cell cycle and apoptosis. Cells plated on the special "strip" dishes were irradiated with 1 to 10 Gy of helium ions using the track segment facility and observed for cell survival, micronucleus production and apoptosis. Cells with the mutated gene show an enhanced bystander effect. The study was expanded to observe the survival of directly irradiated cells for LETs in the range 12 to 180 keV/μm. The cells with the mutated gene had significantly lower survival than normal cells for 12 keV/μm protons but there was little or no difference for 125 keV/μm helium ions.

Masao Suzuki of the National Institute of Radiological Science, Japan, in collaboration with Hongning Zhou of the CRR, continued his efforts to determine whether alpha particle irradiation can induce a bystander response in primary human bronchial epithelial (NHBE) cells (Exp. 125), extending the study to bystanders of cytoplasmic irradiation. Either all or ten percent of the cells were irradiated in the cytoplasm with helium ions using the microbeam facility. The cells were then accumulated in the G2 phase of the cell cycle and the process of premature chromosome condensation (G2PCC) was used to observe chromatin aberrations. Preliminary data indicate cytoplasmic alpha particle irradiation can induce a bystander effect, however more irradiated cells as well as non-irradiated bystander cells are needed to confirm the results.

The occurrence of non-targeted effects calls into question the use of simple linear extrapolations of cancer risk to low doses from data taken at higher doses. Olga Sedelnikova of the NIH, in collaboration with Stephen Mitchell of the CRR, is investigating a model for bystander effects that would be potentially applicable to radiation risk estimation (Exp. 126). They are evaluating the lesions that are introduced into DNA by alpha particles and the resulting non-targeted bystander effect. These lesions, and particularly the most dangerous – the double strand breaks (DSBs), can be revealed by phosphorylation of histone H2AX. This investigation has expanded to the irradiation of 3-D tissue systems from MatTek Corp. EpiAirwy and EpiDermFT (full thickness). Tissue samples were irradiated in a single line across the diameter with ^{4}He ions using the microbeam facility. Irradiated and unirradiated (bystander) cells were incubated for various times up to a week. Fluorescent confocal microscopy was used to observe H2AX foci, apoptosis, micronuclei, proliferation indices, telomere FISH and SA β-gal staining. The results from these experiments as well as from experiments from other labs will be used to make an overall best assessment of the public health significance of bystander-mediated responses.

Ed Tucker, of Baruch College of the City College of New York (CCNY) is investigating the effect of high-LET radiation on the blue/ultraviolet A signaling in *P. patens* moss cells (Exp. 127). The cells are grown on cellophane with a thin layer of agar. The plastic cell dishes in which the moss cells were grown were placed upside down in a track segment irradiation wheel and irradiated with ^{4}He ions. Irradiations were made in the dark since the moss cells irreversibly start forming side-branches when stimulated by blue/UV-A light. The cells are exposed to blue/UV-A light at various times after irradiation and. gravitropic response and side-branch formation are quantified.

Mark Salasky and Mark Akselrod of Landauer, Inc. initiated an experiment to investigate the radiation response of a novel, completely optical, non-destructive technique of imaging tracks in fluorescent crystals using confocal microscopy (Exp. 128). Irradiations of the fluorescence nuclear track detectors were performed using 0.2 to 3.0 MeV protons produced by the track segment facility and with monoenergetic neutrons with energies from 0.2 to 6.0 MeV. Standard CR-39 track-etch detectors were irradiated in parallel for comparison.

Stephen Meyn of the University of Toronto has begun an experiment to observe localization of the protein TRF2 in irradiated cells (Exp. 131). Human fibroblasts were irradiated with different numbers of ^{4}He ions using the microbeam facility and TRF2 was visualized using immunofluorescence techniques.

Development of Facilities

This year our development effort increased considerably over last year, primarily for the stand-alone microbeam facility. Development continued on a number of extensions of capabilities:

- Development of focused accelerator microbeams
- Source-based (stand-alone) microbeam
- Non-scattering particle detector
- Advanced imaging systems
- Focused x-ray microbeam
- New accelerator

Development of focused accelerator microbeams

The first quadrupole triplet for the double quadrupole lens, installed in 2003, continues to produce a beam spot for helium ions 3.5 μm in diameter. It has been very reliable, with very few sparks. The parts for the second quadrupole triplet have been constructed in our shop and will be inserted into a separate alignment tube for testing, in place of the present lens once construction on the third floor is completed and the permanent magnet (stand-alone) microbeam is reinstalled and available for biological irradiations. When the voltages on this second lens have been adjusted to produce the smallest beam spot attainable, the two lenses will be mounted in a single tube for testing of the compound lens system that will produce a sub-micron beam spot. After using this sub-micron beam for biological irradiations for a suitable period, the testing process will be repeated with two more triplet lenses so that we will eventually have two complete compound lenses, one of which will be used as a spare.

For the focused microbeam, a high voltage amplifier with a very high slew rate was connected to two of the electrodes in the electrostatic quadrupole doublet at the exit of the Van de Graaff. Switching the voltage on the electrodes rapidly diverted the beam to end each cell irradiation and resulted in no "dark" current, i.e., no particles at the exit window of the microbeam system. This is not possible with the quadrupole triplet of the new Singletron (especially during the warranty period), so the high voltage amplifier is now connected to two of the adjustable slits in front of the main beam stop. This new configuration provides the same response as the previous one.

Source-based microbeam

A stand-alone microbeam (SAM) has been designed based on a small, relatively low activity radioactive alpha-particle emitter (5 mCi ^{210}Po) plated on the tip of a 1-mm diameter wire. Alpha particles emitted from the source will be focused into a spot 10 μm in diameter using a compound quadrupole lens made from commercially available permanent magnets, since only a single type and energy of particle will be focused. The pair of quadrupole triplets is similar to the one designed for the sub-micron microbeam, the only difference being that it uses magnetic lenses, rather than electrostatic lenses. A small stepping motor rotating a disc with holes will be placed just above the source to chop the beam, enabling single particle irradiations. The end station for the original microbeam will be used to perform microbeam irradiations.

To test the system and adjust the lenses, we used a helium beam from the Van de Graaff incident on a thin aluminum foil to produce an energy and energy spread that match those calculated for the polonium source. The beam was collimated to 1 mm diameter, to simulate the size of the polonium source. The endstation for our original microbeam was moved to the floor above (3rd floor) because additional room for the lens structure was required between the focal point and the final bending magnet. After alignment of the lenses and adjustment of the quadrupole magnet strengths using micrometric screws to retract and extend the individual magnets of each quadrupole, a beam spot 20 μm in diameter was obtained.

The required polonium source is not available commercially, so a method of producing one was developed. Sources of 0.1 and 50 μCi have been created by electroplating polonium in solution onto the tip of a 1-mm diameter platinum rod. A thin layer of gold plated over the source will be used to contain the polonium. A 5-mCi source has not yet been manufactured, in part because the upper part of the stand alone microbeam system has had to be removed because of the impending construction on the 3rd floor.

Since we have already replaced the Van de Graaff with the Singletron, when the SAM is reinstalled after construction the aluminum foil will be removed and the collimator size will be reduced. A ^{4}He ion beam from the accelerator will be used instead of the polonium source. The greatly reduced energy spread and the smaller collimator should produce a beam spot less than 10 μm in diameter. Because the ion beam is much more intense than the alpha source, the particle fluence will be increased from less than 1 per second to thousands per second. This system will be used for irradiations when the electrostatic system is unavailable because of development.

Non-scattering particle detector

To irradiate thick samples, such as model tissue systems or oocytes, to use particles with very short ranges such as the heavy ions from the laser ion source, and to allow irradiation of cell monolayers without removing the culture medium, a completely non-scattering particle detector is necessary upstream of the samples. A novel particle detector has been designed on the basis of a long series of inductive cells coupled together into a delay line. The Lumped Delay Line Detector (LD^2) will consist of 300 silver cylinders 3 mm long with a 2.2 mm inside diameter connected by inductors and capacitively coupled to ground. The cylinders are glued to a semi-cylindrical tube of dielectric material 1 m long for mechanical support. The dielectric has a semi-cylindrical metal tube around it that can be rotated about its axis to adjust the capacitance. If the individual segment delays are set (by adjustment of the capacitance) such that the propagation velocity of the pulse equals the projectile velocity, the pulses capacitively induced in all segments by the passage of a single charged particle will add coherently, giving a fast electron pulse at one end of the delay line that is 150 times larger than the charge induced on a single cylinder. This easily detectable charge of at least 150 electrons will be amplified to provide the detection pulse for the particle counter. It is anticipated that this detector will become the standard detector for all microbeam irradiations.

Advanced imaging systems

Development continued on new imaging techniques to view cells without using stain and to obtain three-dimensional images of unstained cells. Two different techniques are being investigated: quantitative non-interference phase microscopy (QPm) and interference microscopy.

QPm and immersion-based Mirau interferometry (IMI) have both been integrated into the microbeam facility and are under continued testing for applicability to rapid location

and targeting of cells for microbeam irradiation without use of stain. QPm is a non-interferometric approach in which light reflected from the sample is used to obtain images in focus and also with the focus set slightly above and below the sample plane. These images are used to approximately solve the light transport equation using a Fourier transform method. The resulting phase-contrast image is then fed back into the normal microbeam automated imaging and locating routines. This technique is in direct competition with IMI, which uses a novel immersion-based Mirau objective that is currently under construction. For testing IMI, we are using an interim liquid-filled Mirau lens that can behave as an immersion lens for about 30 minutes before it needs to be disassembled, refilled with cell medium, and reassembled. This technique has produced several preliminary images, missing none of the cells and producing no false positives (as compared with a regular, stained image). IMI is therefore presently showing more promise than the QPm technique, which still misses some cells and suffers some false positives. Both of these techniques require rapid automated motion in the X-Y plane for locating the cells as well as in Z for changing the focal plane, which is readily supplied by the Mad City stage.

We are keeping both techniques available for now since the final permanent IMI lens is not yet completed and tested. By continuing to isolate and correct possible causes of the QPm errors, either technique eventually could be the "winner." Both techniques will result in an approximately 10% reduction in throughput due to the extra motions required in Z for obtaining multiple images and also due to some additional computing time.

We are also developing a multi-photon microscope for our single-cell single-particle microbeam facility to detect and observe the short-term molecular kinetics of radiation response in living cells. The multi-photon capability is being built into the Nikon Eclipse E600-FN research fluorescence microscope of the microbeam irradiation system and will provide three-dimensional imaging. We have purchased and installed a Chameleon (Coherent Inc.) tunable titanium sapphire laser (140 fs pulses at a 90 MHz repetition rate) as the source for multi-photon excitation. The scan head will incorporate commercial scanners and the incident laser beam will enter the microscope through the side of the trinocular tube of the microscope. A switch mirror will allow us to choose between multi-photon microscopy and standard fluorescence microscopy. To control the multi-photon microscope, we are adopting design and software from Karel Svoboda, Cold Spring Harbor. We anticipate that this imaging technique will be operational in the summer of 2006.

Focused x-ray microbeam

We have investigated expanding the microbeam to include soft x-rays. Microbeam studies with focused high-energy x-rays or gamma-rays are not feasible due to Compton scattering effects, so we are limited to x-ray energies where the predominant mode of interaction is photo-electron absorption.

The present proposal is to employ Zone Plate (ZP) lenses to de-magnify to a micron or sub-micron size spot, a small x-ray source (i.e., ~100 μm D) produced by bombarding a thin solid target with high-energy protons using the microbeam triplet lens. We investigated the production of characteristic x-rays (K_α line) as a function of the proton energy for aluminum and titanium (K_α x-rays of 1.45 and 4.5 keV respectively). According to the literature, the best cross section for characteristic K_α x-ray production in thick targets is achieved at proton energies of 2.86 MeV for Al and 9.1 MeV for Ti. For protons of 5 MeV (the maximum energy achievable with the new accelerator), the Ti K_α cross-section is only 60% of the maximum value and the penetration in the target is 135 μm. Based on these calculations, a target thickness of about 100 μm would represent an ideal initial choice. Such a thickness will assure a nearly optimum x-ray production efficiency (i.e., maximum energy deposited into the target by incident particles and small x-ray self-absorption) although it will result in the x-ray source being elongated along the Z-axis (direction of the proton beam). An extended depth of focus is to be expected as a result of the elongated x-ray source. This effect has been simulated using an x-ray tracing program (SHADOW) and estimated to be approximately ±10 μm, with the depth of focus defined as the distance from the focal point at which the beam size increases by 20%. The relatively thin target will also allow us to use it in transmission mode (i.e., x-rays extracted from the side opposite to the proton bombardment) as this will better suit the present charged particle microbeam configuration (vertical alignment).

The final microbeam system will allow rapid switching between charged particles (with ions directly focused into the biological samples) and soft x-rays (with protons focused onto a solid target and x-rays probing the cells). Assuming a target thickness of 50–60 μm, the maximum power that is possible to be dissipated by the target for an extended period of time is related to the specific design of the target and the area of the proton beam spot (i.e., x-ray source size). Extended simulations performed using a finite element analysis program (ANSYS) have provided indication on the x-ray source size and the maximum power with which is possible to bombard the target. The present design consists of 3 thin Al or Ti foils 15–20 μm thick separated by 5 μm gaps through which cooled He is blown. Such a target is able to cope with a substantial amount of power from the proton beam, providing an x-ray dose rate suitable for many radiobiological experiments (~0.05 Gy/sec), even with a sub-micron diameter photon beam.

New accelerator

The capabilities of the Singletron from HVE in general exceed those for the Van de Graaff it replaced. The maximum terminal voltage is 5 MV with less than 100 V at 3 MV. The maximum voltage ever attained by the Van de Graaff was 4.4 MV and the ripple was never less than 1–2 kV. The maximum beam currents for the Singletron are 200 μA of protons, 100 μA of deuterons and 1 μA of helium ions, similar to or greater than those of the Van de Graaff.

We began the process of disconnecting the Van de Graaff wiring and plumbing on June 13. The Van de Graaff was removed from the building on August 2 and the new

Singletron arrived on August 10. The Singletron was installed by an engineer and technician from High Voltage Engineering with considerable assistance from the RARAF staff. After testing to determine that the accelerator achieved the specified voltage, voltage stability and ion beam currents, it was accepted on December 2. The entire process took just under 6 months, within the 5–6 month time period that had been projected. A more detailed description of the removal of the Van de Graaff and installation of the Singletron is presented elsewhere in the CRR Annual Report.

Van de Graaff Utilization and Operation

Accelerator usage is summarized in Table 2. The Van de Graaff was started at 7:30 AM on most days, run into the evening on many nights and run on many weekends for experiments, development and repair. This has resulted in a total use (121%, including repairs) that considerably exceeds the nominal accelerator availability of one 8-hour shift per weekday and is the highest we have had at Nevis Labs, exceeding last year's record use by 5%.

Use of the accelerator for radiobiology and associated dosimetry increased about 15% over 2003–2004 and was about the same as the average for 2000 to 2004. Over half the accelerator use for all experiments was for microbeam irradiations and 30% for track segment irradiations. The microbeam facility is in great demand because it enables selective irradiation of individual cell nuclei or cytoplasm. In addition, because of the relatively low number of cells that can be irradiated in a day, microbeam experiments usually require considerably more beam time than broad beam irradiations to obtain sufficient biological material, especially for low probability events such as transformation, mutation and bystander effects.

Radiological physics utilization of the accelerator decreased somewhat this past year, consisting mainly of experiments from Landauer Inc. and Johns Hopkins University.

Approximately 1/3 of the experiment time was used for experiments proposed by outside users, down from last year's record 52% use but still more than 20% higher than the average for the last four years..

Use of the accelerator for online development increased by about 30% over last year to more than 50% of all available time. For several months, many more than the usual number of extra shifts was worked in the evening, on weekends and holidays developing the stand-alone microbeam system.

Table 2.
Accelerator Use, November 2004–June 2005
Percent Usage of Available Days

Radiobiology and associated dosimetry	42%
Radiological physics and chemistry	11%
On-line facility development and testing	55%
Safety system	2%
Accelerator related repairs/maintenance	10%
Other repairs and maintenance	1%
Off-line facility development	15%

Accelerator maintenance and repair time decreased by almost half relative to last year, returning to the level of 1998–2001, as the problem with the power supply in the terminal used to spray negative charge on the charging belt was solved. We anticipate much less accelerator maintenance, not only because the Singletron is new, but also because it is charged electronically (similar to a Cockroft-Walton) and has few moving parts (no belt or chains). It has an RF ion source that also should require less maintenance than the Duoplasmatron source we were using, although we have had accelerator openings in December 2005 and January 2006 to replace RF tubes in the ion source. We believe repositioning the electrodes on the ion source has solved the problem and haven't had a problem for over 2 months.

Training

We continued our Small Group Apprenticeship Program, where we had seven students from Stuyvesant High School in Manhattan spend at least two half-days each week for six weeks during the summer working on projects in biology (3) or physics (4). This is a school specializing in science that is open to students throughout New York City by competitive admission. Following suggestions from the previous group of students, we condensed the orientation phase of this program so that the students and their chosen mentors would have an earlier start with their projects. The students gave professional PowerPoint presentations to our group at the end of the program. Below is a list of the titles of the work presented followed by the name of the student and the name of his or her mentor:

1. Micronucleus Induction in Bystander Cells Following Microbeam Irradiation of 3D Tissues II – Deep Parikh (Brian Ponnaiya)
2. The Role of Mitogen-Activated Protein Kinase Pathways in the Bystander Effect – Jessica Chen (Brian Ponnaiya)
3. Lumped Delay Line Detector (LD2) – Kevin Wu (Guy Garty)
4. Multi-photon Microscope – Shar Rafi (Alan Bigelow)
5. Flash chip programming – Flora Ng (Greg Ross)
6. Personal Dosimeter – Jessie Wang (Gerhard Randers-Pehrson)
7. Disassociation and Reseeding of Tissue Samples – Tina Varkey (Giuseppe Schettino)

Dr. Tomoo Funayama of the Japan Atomic Energy Agency arrived in November for a one-year visit at RARAF. He is working with Charles Geard and will learn to perform experiments using the microbeam facility.

Personnel

The Director of RARAF is Dr. David Brenner. The accelerator facility is operated by Mr. Stephen Marino and Dr. Gerhard Randers-Pehrson. Our ranks remain at a total of seven physicists.

Dr. Alan Bigelow, an Associate Research Scientist, is continuing the development of the laser ion source and has

begun the development of a two-photon microscopy system using a fast laser.

Dr. Guy Garty, a Staff Associate, worked on the development of a stand alone microbeam, and continues to develop the secondary emission ion microscope (SEIM) and an inductive detector (LD^2) for single ions.

Mr. Greg Ross is a Programmer/Analyst, assisting with various programming tasks. He worked on the development of a stand alone microbeam and is presently working on new methods of imaging cells without stain.

Dr. Giuseppe Schettino, a Postdoctoral Fellow, is working primarily on the development of the x-ray microbeam.

Several biologists from the Center for Radiological Research are stationed at the facility in order to perform experiments:

- Dr. Charles Geard, the Associate Director of the CRR, continues to spend most of each working day at RARAF. In addition to his own research, he collaborates with some of the outside users on experiments using the single-particle microbeam facility.
- Dr. Brian Ponnaiya is an Associate Research Scientist performing experiments using the track segment and microbeam irradiation facilities.
- Ms. Gloria Jenkins, a biology technician, performed experiments on the microbeam facility for Dr. Geard. She has been working at the CRR since June, 2005, when the accelerator was shut down for removal.
- Dr. Stephen Mitchell, a Postdoctoral Fellow, returned to Great Britain in June, 2005.

Recent Publications of Work Performed at RARAF (2004–2005)

1. Aprile E, Giboni KL, Majewski P, Ni K, Yamashita M, Hasty R, Manzur A and McKinsey DN. Scintillation Response of Liquid Xenon to Low Energy Nuclear Recoils. *Phys Rev D* **72**:072006, 2005.

2. Belyakov OV, Mitchell SA, Parikh D, Randers-Pehrson G, Marino SA, Amundson SA, Geard CR and Brenner DJ. Biological effects in unirradiated human tissue induced by radiation damage up to 1 mm away. *PNAS (USA)* **102**:14203–8, 2005.

3. Persaud R, Zhou H, Baker SE, Hei TK, Hall EJ. Assessment of low linear energy transfer radiation-induced bystander mutagenesis in a three-dimensional culture model. *Cancer Res* **65**:9876–82, 2005.

4. Ross GJ, Bigelow AW, Randers-Pehrson G, Peng CC, Brenner DJ. Phase-based cell imaging techniques for microbeam irradiations. *Nucl Instrum Meth B* **241**:387–91, 2005.

5. Smilenov LB, Hall EJ, Bonner WM and Sedelnikova OA. DNA double-strand breaks in bystander cells: A microbeam study. *Rad Protec Dosim* (submitted 2005).

6. Smilenov LB, Lieberman HB, Mitchell SA, Baker R, Hopkins KM and Hall EJ. Combined haploinsufficiency for ATM and RAD9 as a factor in cell transformation, apoptosis and DNA lesion repair dynamics. *Cancer Res* **65**:933–8, 2005.

7. Sokolov MV, Smilenov LB, Hall EJ, Panyutin IG, Bonner WM, Sedelnikova OA. Ionizing radiation induces DNA double-strand breaks in bystander primary human fibroblasts. *Oncogene* **24**:7257–65, 2005.

8. Suzuki M, Zhou H, Hei TK, Tsuruoka C and Fujitaka K. Effects of irradiated medium on chromatid aberrations in mammalian cells using double mylar dishes. *Biol Sci Space* **18**:110-1, 2004.

9. Zhou HN, Ivanov V, Gillespie J, Geard CR, Amundson SA, Brenner DJ, Yu Z, Lieberman HB and Hei TK. Mechanism of radiation induced bystander effect: role of COX-2 signaling pathway. *PNAS (USA)* **102**:14641–6, 2005.

10. Zhou H, Suzuki M, Persaud R, Gillispie J, Randers-Pehrson G and Hei TK. Contribution of bystander effects in radiation induced genotoxicity. *Acta Med Nagasaki* **50**:73–7, 2005.

11. Zhu A, Zhou H, Marino SA, Leloup C, Geard CR, Hei TK and Lieberman HB. Differential impact of mouse rad9 deletion on ionizing radiation-induced bystander effects. *Rad Res* **164**:655–61, 2005. ■

Replacement of the RARAF Accelerator

Stephen A. Marino, Gerhard Randers-Pehrson, Alan Bigelow, Guy Y. Garty, Greg Ross, Giusseppe Schettino and David J. Brenner

This has been an historic year for the Radiological Research Accelerator Facility (RARAF) and the CRR. The 4.2-MV Van de Graaff accelerator that since 1967 produced charged particle beams at RARAF for neutron irradiations, track segment experiments and the microbeam facilities was replaced this year with a 5-MV coaxial Singletron from High Voltage Engineering Europa (HVEE). As noted in the Annual Reports for the past several years, the reliability of the Van de Graaff had been declining. In addition to requiring a major overhaul of many of its components in order to operate more stably and reliably, the custom acceleration tube had a vacuum leak that would require us to build new sections and suitable charging belts were no longer being manufactured anywhere in the world.

The Van de Graaff was purchased in 1949 from the High Voltage Engineering Corporation (originally the parent company of HVEE but now no longer in business) by Brookhaven National Laboratory (BNL) as the injector for the Cosmotron (Fig. 1), the first GeV proton accelerator in the world. It was probably the first commercial product from the company founded by Robert J. Van de Graaff, the inventor of the accelerator that bears his name. For this purpose the accelerator was run in pulsed beam mode.

When the Cosmotron was decommissioned, Dr. Harald Rossi of the CRR and Dr. Victor Bond of the Medical Department of BNL obtained control of the accelerator to use for radiobiology and formed RARAF in 1967. Dr. Clarence Turner, who had been in charge of Van de Graaff operations for the Cosmotron, converted the accelerator to produce constant beams of protons and deuterons. Initial use of the accelerator was to produce monoenergetic neutrons by bombardment of targets containing tritium or deuterium for irradiation of biological specimens, from plants and cells to mice and rats. In the 1970's, beams of protons, deuterons, and helium ions were used to directly irradiate cells using the Molecular Ion Beam and Track Segment facilities.

In 1980, RARAF was forced out of its BNL location by the ill-fated proton intersecting storage ring project, Isabelle. The Van de Graaff was dismantled in April of that year and the entire facility was shipped to the Nevis Laboratories of Columbia University. The accelerator was reassembled (Fig. 2), the RARAF facility rebuilt, and operations resumed in 1984. In the 1990's, a collimated microbeam was developed and added to the available irradiation facilities. In 2004, a focused microbeam was established.

The last use of the Van de Graaff was on June 11, 2005. On June 13, we began to dismantle the accelerator for removal. Although there were a few inquiries by people interested in obtaining it, they declined when informed of the acceleration and charging belt problems. One person with a small company was interested in the internal parts of the accelerator and he has taken much of them. We removed (Figs. 3 and 4) the terminal shell, the equipotential rings, the charging system, the terminal, the acceleration tube and insulating column. The belt drive motor and all other components in the ground plane area were also removed, leaving little but the pressure tank and baseplate.

When the Van de Graaff was installed at Nevis Labs, it was moved using a 50-ton overhead building crane. Afterward the Van de Graaff was positioned, the area over the accelerator was covered with long shield blocks 2-foot thick. Later, the Microbeam II lab was built on top of these shield blocks. Since it couldn't be removed the way it was brought into the building, a 10' wide by 11' high opening was made

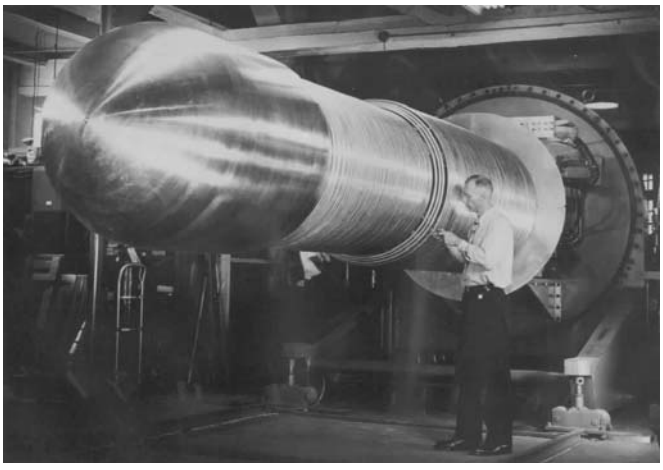

Fig. 1. The Van de Graaff at BNL circa 1949. Visible are the terminal shell on the left and the more than 100 equipotential rings. The interior looked almost the same in 2005.

Fig. 2. The exterior of the Van de Graaff shortly before decommissioning.

Fig. 3. Starting to dismantle the Van de Graaff. The equipotential rings have been removed. The red charging belt can be seen hanging from the terminal pulley on the left.

Fig. 4. The accelerator mostly dismantled. The terminal shell is right of the center; the terminal in front of the tank; the acceleration tube is on the left on its cradle and the insulating column on the floor in the middle. The baseplate is on the right.

Fig. 5. The accelerator tank being lifted by 90-ton crane to be placed on a truck. The storage tank for the accelerator insulating gas is seen on the left.

Fig. 6. The Van de Graaff baseplate being dragged out by a forklift.

in the 1'-thick solid concrete wall behind the Van de Graaff in which to remove it and bring in the Singletron. On August 2 the tank was rolled back on its rails then pulled out of the building on rollers with the aid of a large forklift. A 90-ton crane was then used to lift the tank onto a trailer (Fig. 5). The baseplate was placed on rollers, dragged out of the building using the forklift (Fig. 6), lifted with the crane, and placed on a trailer. These items were taken to a scrap yard (Fig. 7).

The Singletron arrived from The Netherlands in three shipments, two by water and one by air. The pressure vessel arrived first, on August 10, with the insulating column attached. In the reverse of the procedure for the removal of the Van de Graaff, the tank was lifted off the trailer on which it arrived (Fig. 8), placed on rollers and pushed into the building using a large forklift (Fig. 9). The delivery was observed by an engineer from HVEE. The baseplate, gas transfer system, resonant coil tank, column electrodes and other parts arrived in three crates inside a roll-on-roll-off shipping con-

Fig. 7. The Van de Graaff tank leaving Nevis Labs.

Fig. 8. The Singletron on a trailer about to be lifted by crane.

Fig. 9. The Singletron being pushed by a large forklift into the building through the new opening in the building wall.

tainer. After some difficulties, the crates were moved into the building. The acceleration tube arrived by air in two boxes.

Because of the differences between the Van de Graaff and the Singletron in handling the accelerator insulating gas, modifications to the piping to the storage tank (large silver double-sphere seen on the left of Fig. 5) had to be made. The Singletron and the computer used to control it require European voltages, so transformers had to be installed in addition to a new power distribution rack and wiring from the rack to the accelerator and gas-handling system.

On September 20, after necessary modifications to the building were essentially completed, HVEE sent an engineer and a technician to install and test the Singletron. It took about 3 weeks to install the Singletron. It was aligned with the existing beam line system, the rails for the tank were placed under it, the baseplate and rails anchored to the floor, the acceleration tube installed and evacuated, and the column electrodes installed (Figs. 10–13). The ion source was tested with three of the supply gases. The accelerator was then evacuated and filled sulfur heaxafluoride (SF_6) insulating gas and voltage conditioning of the acceleration tube began, finally reaching 5.5 MV. The ripple of the accelerator voltage was certified to be less than 100 V at 3.75 MV and the beam currents for protons and helium ions were measured and found to exceed the guaranteed values. The accelerator was accepted on December 2.

The Van de Graaff and the Singletron are both linear electrostatic accelerators; however they differ significantly in how the terminal voltage is achieved. A Van de Graaff has a belt driven by a motor. Charge is sprayed onto the belt and carried mechanically to the terminal. Charge of the op-

Fig. 10. The interior of the Singletron. The top and bottom curved pieces along the column are electrodes. Along the side of the column there is a string of diodes, a resistor and a spark gap for each electrode.

Fig. 11. The Singletron terminal and terminal cap. The cylinders of source gas can be seen on the upper part of the terminal plate. The terminal is much less complicated than on the Van de Graaff since it doesn't require a downcharge power supply, has no analog gauges, has thermo-mechanical controls for the gas rather than large mechanical valves, and uses opto-electronics to control the gas valves and power supplies rather than pulleys and Variacs. The generator can be seen on the lower right of the terminal.

Fig. 12. The HVEE people putting the acceleration tube into the accelerator.

Fig. 13. The Singletron positioned and assembled. The cylinder on the right is the resonant coil container. The accelerator control rack is on the far right. The section of pipe at the front of the accelerator contains an electrostatic quadrupole triplet. The dark gray "H" at the front of the accelerator is the "baseplate" – much less massive than the 8'-diameter, 8"-thick plate used for the Van de Graaff.

Fig. 14. The Singletron tank, showing the "dees" at the top and bottom of the tank. Each dee is connected to the resonant coil by the copper tubing.

posite polarity can be sprayed onto the belt at the terminal and carried back to the ground end of the machine, doubling the charging capacity. The Singletron is purely electronic and has no belt. A resonant coil operating at 35 kHz and up to 40 kV is connected to a pair of "dees" inside the tank (Fig. 14). The dees are capacitively coupled to the electrodes at the top and bottom of the column and induce a current in them. This current is rectified by the diodes on each electrode, producing a voltage. The voltage on the terminal is the sum of the voltages on the electrodes. The only moving parts in the Singletron are a shaft driven by an external motor that runs a generator to provide power to the terminal. In the Van de Graaff, the generator was driven by the terminal belt pulley.

There are other differences between the Singletron and the old Van de Graaff. One is that all the controls and readouts on the Singletron are accomplished using fiber optics; on the Van de Graaff control was accomplished with electric motors, strings and pulleys and read-out was performed by viewing an analog gauge in the terminal with a monocular or camera. Another difference is that the Singletron is controlled by a PC whereas the Van de Graaff was controlled by custom electronics and consequently didn't have many of the display, reporting and recording features provided by the PC software. A third difference is that the Singletron uses an RF ion source rather then the Duoplasmatron ion source in the Van de Graaff, which employed a filament with a sometimes all-too-limited lifetime. ■

RSO – TABLE OF CONTENTS

RADIATION SAFETY OFFICE STAFF & STAFF PICTURE 88
INTRODUCTION 89
OVERVIEW OF RADIATION SAFETY OFFICE RESPONSIBILITIES 89
SUMMARY OF RADIATION SAFETY OFFICE OPERATIONS FOR 2005 90
Maintenance of New York City Department of Health and Mental Hygiene, Office of Radiological Health Licenses, Registrations, Permits, and Audits and Inspections 90
Maintenance of New York State Department of Environmental Conservation Permits, Audits and Inspections 92
Administration of Radioactive Material: Receipt, Distribution, and Radioactive Waste Disposal 93
Personnel Dosimetry, Bioassay, and Area Monitoring 94
Routine Radiation Safety Compliance – Internal Inspections and Audits 95
Training 95
Professional Radiation Safety and Health Physics Support 96
Professional Radiation Safety and Medical Physics Support for Non-Radiology X-ray Activities 98
Radiation Safety Office Personnel and Facilities 98

Sample Images from the RSO's Picture Archives

(*R–l*): Roman Tarasyuk, David Rubinstein and Dae-In Kim.

Ahmad Hatami discusses security concerns with an irradiator user.

Dae In Kim (*l*) and Shinkyu Park (*r*) perform a radiation safety survey of the Leksell Gamma Knife.

James Dolan performs a radiation safety survey of an I-131 therapy patient.

RADIATION SAFETY OFFICE

The RSO Staff (s*tanding l-r):* Ahmad Hatami, Roman Tarasyuk, David Rubinstein, Salmen Loksen, Shinkyu Park and Thomas Juchnewicz; (s*eated l-r):* James Dolan, Yvette Acevedo, Milvia Perez, Raquel Garcia and Jacob Kamen; *not pictured:* Bruce Emmer, Dae In Kim and Jennifer Curiel.

PROFESSIONAL STAFF

Salmen Loksen, M.S., CHP, DABR; Director, Radiation Safety Officer
Ahmad Hatami, M.S., DABR, DABMP; Assistant Director
Thomas Juchnewicz, M.S., DABR; Assistant Radiation Safety Officer
Jacob Kamen, Ph.D., NRRPT, CHP; Assistant Radiation Safety Officer
Bruce Emmer, M.S., DABMP, DABR; Physicist
Dae In Kim, M.S., Health Physicist
James Dolan, M.S., Junior Physicist
Shinkyu Park, M.S., Radiation Protection Supervisor

TECHNICAL STAFF

Roman Tarasyuk, Technician B
Dong Michelle Kang, M.S.; Chief Technician (resigned as of 1/2006)
David Rubinstein, B.S., Technician B

ADMINISTRATIVE AND SUPPORT STAFF

Diana Morrison, Administrative Assistant, assigned to the JRSC
Yvette Acevedo, A.A.S.; Administrative Aide
Raquel Garcia, Senior Clerk
Milvia Perez, A.A.S.; Clerk B
Stephen Benson, B.A.; Administrative Assistant (resigned as of 11/2005)
Jennifer Curiel, Administrative Staff

RADIATION SAFETY OFFICE

INTRODUCTION

On May 19, 1957, the President of Columbia University distributed a memo entitled "Directive to All University Departments Having a Source of Ionizing Radiation," advising all parties of the expanded function of the Radiation Safety Committee.

Later, a notice entitled "Radiation Safety Guide for Columbia University," dated February 10, 1959, named Philip M. Lorio as the Health Physics Officer for University Departments and Laboratories other than the College of Physicians & Surgeons, where Dr. Edgar Watts was the named Health Physics Officer. The Chairman of the Radiation Safety Committee was Dr. Gioacchino Failla, who initiated the Radiological Research Laboratory in the Department of Radiology of Columbia University Medical Center.

By agreement between the Presbyterian Hospital in the City of New York and Columbia University, the Radiation Safety Office was established as an autonomous unit in 1962 for the purpose of maintaining radiation safety. The Joint Radiation Safety Committee (JRSC), appointed by the Medical Board of the Presbyterian Hospital in the City of New York and the Vice President for Health Sciences of Columbia University, is charged with the responsibility of defining and ensuring enforcement of proper safeguards in the use of sources of ionizing radiation.

Dr. Herald H. Rossi, Director of the Radiological Research Laboratories, was appointed Chairman of the Joint Radiation Safety Committee. Under his direction, this committee developed a "Radiation Safety Code and Guide," the administration of which is assigned to the Radiation Safety Officer. Dr. Eric J. Hall, the present Director of the Center for Radiological Research, now chairs the JRSC.

The present Joint Radiation Safety Committee of the Columbia University Medical Center, New York Presbyterian Hospital and the New York State Psychiatric Institute came into existence through an agreement made on February 12, 1991 between New York State Psychiatric Institute, the College of Physicians and Surgeons of Columbia University, and The Presbyterian Hospital in the City of New York. This agreement combined several overlapping clinical and educational programs, including all programs for ensuring radiation safety. The current Director of the Radiation Safety Office and Radiation Safety Officer, Salmen Loksen, CHP, DABR, was appointed on December 16, 1996.

The Radiation Safety Office reports to and advises the Joint Radiation Safety Committee of Columbia University Medical Center, New York Presbyterian Hospital, and New York State Psychiatric Institute. The Committee meets on a quarterly basis. The Radiation Safety Officer reports on professional and technical matters to Dr. Eric J. Hall, Chair of the JRSC and on budgetary matters to Dr. Robert Lewy, who represents Dr. Gerald D. Fischbach, the Dean of the Columbia University Medical Center. In addition, the Radiation Safety Office participates in the review of research protocols for the Radioactive Drug Research Committee (RDRC) under the jurisdiction of the U.S. Food and Drug Administration.

Radiation Safety Office staff are Columbia University Medical Center employees. Columbia University Medical Center (CUMC), New York Presbyterian Hospital (NYPH), and the New York State Psychiatric Institute (NYSPI) fund the Radiation Safety Office budget via a cost sharing payback arrangement.

OVERVIEW OF RADIATION SAFETY OFFICE RESPONSIBILITIES

Collectively, Columbia University Medical Center, New York Presbyterian Hospital and New York State Psychiatric Institute form a large health sciences complex with extensive teaching, research, and clinical facilities. The basic goal of the Radiation Safety Office is to ensure the implementation of all protective measures necessary to ensure that the dose from ionizing radiation to patients, visitors, students, faculty and staff on campus, as well as to the general community at large, is As Low As Reasonably Achievable (ALARA). Major entities supported by the Radiation Safety Office include:

- Columbia University Medical Center
- New York Presbyterian Hospital
- New York State Psychiatric Institute
- Columbia Presbyterian Eastside
- New York Presbyterian Hospital, Allen Pavilion
- CUMC Cyclotron Facility.
- Dental Facilities throughout CUMC and elsewhere as described later in this report.

The projected completion of several additional buildings, as well as the Columbia University Medical Center Integrated Imaging Center will add to the responsibilities of the Radiation Safety Office in the near future. For the purposes of this report, this collection of entities will hereafter be referred to as CUMC/NYPH/NYSPI.

Reporting to the Joint Radiation Safety Committee of CUMC/NYPH/NYSPI, the Radiation Safety Officer and the staff of the Radiation Safety Office are responsible for obtaining and maintaining licenses authorizing the possession and use of radioactive materials and obtaining and maintaining registrations and permits for the operation of radiation producing equipment. In addition, the Radiation Safety Office is responsible for obtaining and maintaining those permits necessary for the safe disposal or controlled release of research and medical wastes containing radioactivity.

The Radiation Safety Office ensures compliance of authorized users of radioactive materials or radiation producing equipment with all governmental regulatory requirements and guidelines by means of: training, education, consultation, and by a program of internal audits and inspec-

tions of facilities. Regulatory agencies charged with overseeing the possession, use, or disposal of radioactive materials or radiation producing machines include:

- United States Food and Drug Administration
- United States Nuclear Regulatory Commission
- United States Environmental Protection Agency
- New York State Department of Environmental Conservation
- New York State Department of Health
- New York City Department of Health and Mental Hygiene, Office of Radiological Health

The New York City Department of Health and Mental Hygiene (NYCDOHMH), the New York State Department of Environmental Conservation, and the United States Food and Drug Administration conduct periodic inspections and audits of the Columbia University Medical Center, New York Presbyterian, and the New York State Psychiatric Institute, Hospital facilities operating under their licenses or permits. The Radiation Safety Office works continuously to prevent regulatory violations and swiftly implement any regulatory recommendations.

The Radiation Safety Office also ensures compliance with institutional policies and procedures published in the "Radiation Code and Guide of Columbia Presbyterian Medical Center and New York State Psychiatric Institute."

SUMMARY OF RADIATION SAFETY OFFICE OPERATIONS FOR 2005

A summary of activities performed and services provided by the Radiation Safety Office is presented below. While inclusive of most major activities and services, the summary is by no means exhaustive, but is intended to provide a representative overview of departmental operations. An unabridged compilation of Radiation Safety Office activities and services may be found in the Minutes of the Quarterly Meetings of the Joint Radiation Safety Committee of Columbia University Medical Center, New York Presbyterian Hospital, and the New York State Psychiatric Institute.

Statistical data presented are from the calendar year, January 1, 2005 through December 30, 2005. Activities are covered up to March 9, 2006.

Maintenance of New York City Department of Health and Mental Hygiene, Office of Radiological Health Licenses, Registrations, Permits, and Audits and Inspections

A primary activity of the Radiation Safety Office is the continued maintenance of the City of New York Radioactive Materials Licenses, the Certified Linac Registrations, and the X-Ray Permits**.** Currently this includes:

- Radioactive Materials License No. 75-2878-01 (Broad Scope Human Use)
- Radioactive Materials License No. 92-2878-02 (Teletherapy)
- Radioactive Materials License No. 74-2878-03 (Non-Human Use)
- Radioactive License No. 52-2878-04 (Cyclotron Facility)
- Radioactive Materials License No. 93-2878-05 (Gamma Knife)
- City of New York Therapeutic Radiation LINAC Unit Certified Registration No. 77-0000019.
- City of New York Therapeutic Radiation LINAC Unit Certified Registration No. 77-0000019.
- Columbia-Presbyterian Hospital Radiation Installation Permit H96 0076353 86
- Columbia-Presbyterian-Allen Pavilion Radiation Installation Permit H96 0076383 86
- Columbia University Gymnasium, Morningside Campus or Baker Field Radiation Installation Permit H98 1005495
- Columbia University Physicians Metabolic Diseases Unit, Bone Density Permit H90 1162695

Significant activities performed in 2005 to maintain the City of New York Licenses, Registrations and Permits include:

1. The Radiation Safety Office provided health physics assistance with two teletherapy source transfer operations that took place in the Department of Radiation Oncology. These were complex projects that involved the cooperation of the Department of Radiation Oncology, NYPH Security, the NYPH Offices of Design and Construction, Facilities Management, and Biomedical Engineering, the NYCDOHMH, the NYPD, the Department of Homeland Security, Los Alamos National Laboratory, and the Radiation Safety Office. The Radiation Safety Office provided assistance with regulatory considerations during the planning phases of the operations and maintained a continuous presence during the actual source transfers in order to monitor ambient dose rates, distribute personal dosimeters, perform exit surveys, and expedite the processing of required paperwork.

- Between May 27, 2005 and May 29, 2005, the Phoenix #23 Co-60 Teletherapy unit located in the Department of Radiation Oncology was decommissioned by MDS Nordion (Ottawa, Ontario). The source was removed from the CUMC/NYPH campus. Upon completion of the project, Radiation Safety Office staff performed the required exit survey.
- Between August 26, 2005 and August 30, 2005, a source exchange was performed for the Leksell Gamma Knife located in the CUMC/NYPH Center for Radiosurgery. The source exchange itself was performed by Alpha Omega Services, Inc while the reconnection of the hydraulic system of the Gamma Knife was performed by Elekta, Inc. A radiation safety survey was performed following completion of the project. Radiation levels were measured at 16 locations throughout the Department of Radiation Oncology and the first floor of the Children's Hospital, directly above the Gamma Knife. All public doses and dose rates were found to be within the limits specified by Rules of the City of New York Article 175 and the conditions of Radioactive Materials License No. 93-2878-05.

2. On March 29, 2005, the Radiation Safety Office submitted a request to the New York City Department of Health, Office of Radiological Health to amend Radioactive

Materials License No. 74-2878-03 (Non-Human Use) in order to permit the possession of 44.4 TBq of Cs-137 to be used for irradiating animals. This source will be housed on the 11th floor of the Irving Cancer Center, Room 1125A. The Amendment was approved by the New York City Department of Health, Office of Radiological Health on April 21, 2005.

3. On December 6, 2005, the Radiation Safety Office received an Order of the Commissioner from Thomas R. Frieden, M.D., M.P.H., Commissioner, New York City Department of Health and Mental Hygiene. The Order requires the implementation of increased security controls over radioactive sources which exceed certain "quantities of concern." There are several sources throughout CUMC and NYPH which require these additional controls. As of January 16, 2006, the following actions have been taken in response to the Order:

- On October 20, 2005, Radiation Safety Office staff attended a lecture devoted to the increased security requirements given by Tobias Lickerman, Head, Radioactive Materials Division, New York City Department of Health and Mental Hygiene.
- On November 29, 2005, Radiation Safety Office staff were accompanied by Detective Gail Ballanntyne, member, NYPD Counter Terrorism Division, and Thomas Taylor, NYPH Security, on a walkthrough of all departments affected by the Order.
- On January 11, 2006, the Radiation Safety Office held a meeting with all departments affected by the Order in which the implementation of the increased controls was discussed.

4. The Radiation Safety Office reported to the Joint Radiation Safety Committee regarding several procedural and administrative requirements. The specifics of these requirements may be found in the quarterly reports of the Radiation Safety Office. Briefly, some of the topics covered were:

- Authorized Users need to report to the Radiation Safety Office any changes in the following: (1) handling or experimental procedures related to the use of radionuclides; (2) quantities and chemical/physical forms of radionuclides used; or (3) therapy physicists, authorized technicians, and radiation safety managers who use or oversee the use of radioactive materials.
- Human-use research protocols require IRB review at least once a year.
- The U.S. Food and Drug Administration recommends, as good practice, that all DMFs be updated annually.
- Certain conditions of the Radioactive Materials Licenses and Certified LINAC Registrations require that certain function procedures be performed only by and/or in the physical presence of specific individuals.
- Medical Physicists practicing in New York State are required to obtain professional licensure from the New York State Department of Education. At present, all senior officers of the Radiation Safety Office are certified either by the American Board of Health Physics, the American Board of Medical Physics, and/or the American Board of Radiology and are licensed to practice as Medical Physicists by the State of New York.
- RCNY 175.103(2) requires that: "(ii) The radiation safety officer shall: (A) investigate overexposures, misadministrations, accidents, spills, losses, thefts, unauthorized receipts, uses, transfers, and disposals, and other deviations from approved radiation safety practice and implement corrective actions as necessary."

5. The NYCDOHMH conducts periodic audits of records and inspections of facilities at CUMC/NYPH/NYSPI operating under the Radioactive Material Licenses, the Certified Linac Registration, and the X-ray Permits. In 2005, these audits and inspections included:

- December 15, 2004, No. 92-2878-02 (Teletherapy)
- January 14, 2005, No. 77-0000019 (Certified LINAC Registration)
- June 27–July 6, 2005, No. 75-2878-01 (Human Use)
- February 9–February 23, 2006, No. 74-2878-03 (Non-Human Use)
- February 2006, No. 77-0000019 (Certified LINAC Registration)
- February 2006, Nos. H96 0076383 86, H96 0076383 86, and H90 1162695 (X-ray Permits)

No deficiencies were cited during any of these inspections. However, a safety interlock on the door of a linear accelerator room was repaired as a result of the January 14, 2005 inspection.

6. During 2005, David Wilson, R.Ph. was named as a Pharmacist for the Cyclotron/Radiopharmacy Facility (Radioactive Materials License No. 52-2878-04: Cyclotron).

7. In response to issues raised by the JRSC and the Radioactive Drug Research Committee with regard to human subject research using PET radioisotopes, Radiation Safety Office staff performed an in-depth review and analysis of the specific regulatory requirements governing Authorized Users and Supervised Individual Physicians responsible for the administration of radioisotopes and radiation for diagnosis, therapy and human subject research. In addition, Radiation Safety Office staff consulted directly with the New York City Department of Health and Mental Hygiene, Office of Radiological Health, which confirmed that *"...your institution's Radiation Safety Committee has both the authority and responsibility of determining and ruling on whether 'the supervised clinical experience requirements of Section 175.103(j)(4)(ii)(C) have been met.'"* The Radiation Safety Office's regulatory review and analysis and the New York City Department of Health and Mental Hygiene's comments were presented at the quarterly Joint Radiation Safety Committee meeting of March 9, 2005. On August 3, 2005, the Executive Committee of the Joint Radiation Safety Committee approved a motion that *"the PET program should have a centralized group of Responsible Investigators (RI's) who are Board Certified Nuclear Medicine Physicians, and that until this can be implemented, the committee will not re-instate previous RI's or approve new RI's in this area."* At the quarterly Joint Radiation Safety Committee meeting of January 5, 2006, the Radiation Safety Office followed up with a detailed review of the Licensee's responsibilities regarding "Supervised Individuals," as required by RCNY 175.103(b) and the recent revisions of 10 CFR 35 effective October 2005.

Maintenance of New York State Department of Environmental Conservation Permits, and Audits and Inspections

Another primary activity of the Radiation Safety Office is the continued maintenance of New York State Department of Environmental Conservation Radiation Control Permit No. 2-6201-00005/00006.

CUMC/NYPH/NYSPI conducts medical research and clinical activities that discharge limited and controlled quantities of radioisotopes to the atmosphere and to sewage systems as per the Conditions of the Radiation Control Permit and in compliance with New York State 6 NYCRR Part 380, Rules and Regulations for Prevention and Control of Environmental Pollution by Radioactive Materials.

The entities served by the Radiation Safety Office are situated within a densely populated urban area. The quantities of radioisotopes discharged and the resulting public radiation dose are closely regulated by the New York State Department of Environmental Conservation. Radiation doses to the general public resulting from atmospheric discharges of radioisotopes are required not to exceed the USNRC Constraint Limit of 10 mrem per year.

CUMC/NYPH/NYSPI are currently permitted a total of fifteen (15) atmospheric emission points from which radionuclides are discharged to the atmosphere. Monitoring, analyzing, reporting, and minimizing discharges from these emission points, in order to ensure compliance with the Conditions of the Radiation Control Permit, is one of the major continuing activities of the Radiation Safety Office.

Significant activities performed in 2005 to maintain the New York State Department of Environmental Conservation Radiation Control Permit include:

1. As required by New York State 6 NYCRR Part 380 and the Conditions of the New York State Department of Environmental Conservation Radiation Control Permit, the Radiation Safety Office will be submitting an Annual Report summarizing Discharges of Radioactive Effluents to the Environment from the fifteen atmospheric emission points and by controlled sewer disposal by the end of March 2006. For the calendar year 2005, all atmospheric discharges were within the quantities authorized by the Radiation Control Permit, and the resulting public dose was within the U.S.N.R.C. constraint limit of 10 millirems per year. All discharges to sewers were well below the Effluent Concentration Limits as required by 6 NYCRR Part 380-11.7, Table of Concentrations.

2. The Radiation Safety Office evaluated emission data from Radioligand and Cyclotron stacks for the years 2001 – 2004 and found that the activity of F-18 released to the atmosphere does not necessarily increase if the amount F-18 produced increases. It was also found that large annual releases of N-13, C-11 and O-15 were most strongly associated with catastrophic events, such as target breaks.

3. As required by the Conditions of NYSDEC Radiation Control Permit 2-6201-0005/0006, on December 21, 2005, annual calibrations were performed on the monitoring systems of the Radioligand and Cyclotron exhaust stacks.

4. On May 5, 2005, the Radiation Safety Office received a Modified Radiation Control Permit. The Modified Permit included new release limits and the following new requirements:

- That the Annual Discharge Report includes results from fixed environmental dosimeters.
- That any emissions exceeding the annual discharge limits be reported to the Radiation Control Section in writing by the following business day.
- That the effluent monitoring system be recalibrated whenever changes are made in system deployment or electronics.

5. In response to the recommendations of an October 2004 inspection, the following training sessions were attended by Radiation Safety Office Staff:

- March 22–24, 2005: Jacob Kamen attended the RDS-112 Cyclotron Operations Course provided by CTI (Knoxville, Tn).
- May 5–6: Salmen Loksen attended the PETNET facility RSO training program (Knoxville, Tn).

6. Members of the Radiation Safety Office continued to attend the scheduled Design Meetings for the CUMC Integrated Imaging Center (see pictures below). Significant activities performed in this area in 2005 include the following:

- A cost estimate was obtained for the relocation of the RDS-112 cyclotron from its current location on the

Foreground: A view of the proposed stack location for the new CUMC Integrated Imaging Center. *Background*: Milstein Hospital.

Salmen Loksen and Thomas Juchnewicz pose with Cyclotron, Radioligand, and NYSDEC staff during a visit to the construction site of the CUMC Integrated Imaging Center.

basement of Milstein Hospital to a new location on the basement level of the Mailman School of Public Health Building.
- Shielding specifications (based on different possible workloads) were proposed for the new cyclotron vault, new radiopharmacy and new radioligand laboratory to be located on the basement level of the Mailman School of Public Health Building and for the new PET and PET/CT imaging center to be located on the ground level of the Mailman School of Public Health Building.
- It was decided that the RDS-112 could be replaced by a RDS-111 with no additional shielding requirements.

7. As required by the Conditions of the NYSDED Radiation Control Permit 2-6201-00005/00006, on May 8, 2005, all filters in the Cyclotron, Radioligand, PET Suite, and Nuclear Medicine stacks were replaced.

8. On August 4, 2005, the Radiation Safety Office submitted a permit modification application for Radiation Control Permit No. 2-6201-00005/00006 to the NYSDEC. The purpose of the permit modification was to add an additional atmospheric effluent point, located on the rooftop of Irving Cancer Research Center. On September 23, 2005, Radiation Safety Office staff contacted the NYSDEC to request expedition of the permit amendment. As per the recommendations of the NYSDEC, a charcoal filter has since been installed in the hood.

9. On August 22, 2005, the Radiation Safety Office was invited to comment on proposed amendments to Part 621 of the State Uniform Procedures Act. The proposed amendments will set time limits for the NYSDEC to act on permit applications and also define a time frame in which a radiation control permit application will be subject to public notice. No comments were made.

10. On November 8 and 9, 2005, representatives of the NYSDEC, Radiation Section conducted an unannounced audit of records and inspection of facilities operating under NYSDEC Radiation Control Permit No. 2-6201-00005/00006. The inspection also included the Integrated Imaging Center, which is currently under construction. During the November 9, 2005 exit interview, the NYSDEC inspectors complimented the competency and professionalism of the Radiation Safety Office staff. Adequacy of staffing was the sole area with which the NYSDEC inspectors expressed concern. This area was particularly stressed because the same issue had been previously addressed following a 2004 inspection. In response to the 2004 inspection, the University authorized that several positions within the Radiation Safety Office be filled. During 2005, two new employees were hired. However, the staffing level has not increased because of the departure of two other staff members.

Administration of Radioactive Material: Receipt, Distribution, and Radioactive Waste Disposal

A major program of the Radiation Safety Office is the centralized administration of all authorized radioactive materials used at CUMC/NYPH/NYSPI. The use of radioisotopes by individual investigators is authorized by the Joint Radiation Safety Committee and controlled by the Radiation Safety Office. Human Use of radioactive materials is carried out by Authorized User Physicians. Authorized User status is granted following a review of credentials and a majority vote by a quorum of the Joint Radiation Safety Committee. Non-Human Use of radioactive materials by Responsible Investigators is granted after a review of applications and written permission of the Chairman of the Joint Radiation Safety Commission and the Radiation Safety Officer. In 2005, 8 new Responsible Investigators were reviewed and approved for non-human use of radioactive materials, and 82 current Responsible Investigators received renewal of their authorizations.

Significant activities in 2005 to administer, receive, distribute, and dispose of radioactive materials included:

1. 1045 purchase orders for materials that contain radioisotopes were approved. 2020 packages containing radioactive material, excluding shipments to the Nuclear Medicine and Radiation Oncology, departments were received. Prior approval was given for all received shipments. Package surveys and wipe tests were also conducted to ensure that none of the packages were contaminated.

2. The Radiation Safety Office maintains inventory control of all radioactive materials received and distributed through the use of a computerized database. The orders referred to in Item 1 of this section resulted in the purchase of a total of approximately 1.9 Curies of activity. ^{35}S, ^{3}H, and ^{32}P were the isotopes purchased with the highest activities.

3. 2297 liters of low-level aqueous radioactive waste were disposed of through sewer disposal. The total activity of sewer-disposal aqueous radioactive waste was 121 mCi, of which 29 mCi was tritium (^{3}H), 76 mCi was ^{35}S, and 16 mCi was other radionuclides. As required by 6 NYCRR Part 380 and the conditions of our NYSDEC Radiation Control Permit, the controlled sewer disposal of aqueous radionuclides was reviewed. The discharge for all isotopes was well below the concentration limits of 6NYCRR Part 380-11.7 Table II.

4. Approximately 5000 gallons of fully decayed short half-life radioactive waste that had been stored for more than ten half-lives was disposed. All containers were surveyed and analyzed to ensure that there was no detectable radiation prior to disposal of this waste as ordinary waste.

5. Approximately 1600 waste cans were picked up from and/or delivered to research laboratories. 150 bags of patient waste were picked up from clinical areas and placed in Decay-in-Storage.

6. On October 3, 2005, the Radiation Safety Office notified the New York State Department of Energy Conservation, Bureau of Hazardous Waste Regulation that CUMC/NYPH/NYSPI was claiming the conditional storage and treatment exemption for Low Level Mixed Waste outlined in 40 CFR 266 Subpart N and adopted by New York State on September 2, 2005. Claiming the exemption allows for greater flexibility in the way mixed waste is managed. This flexibility will increase the ease with which the current mixed waste policy is implemented for both laboratory and radiation safety personnel.

7. Under current CUMC/NYPH/NYSPI mixed waste policy, short-lived liquid mixed wastes are held in storage for decay. Once the contained radioactivity is decayed to

background levels, the wastes are transferred to the Environmental Health and Safety Office for disposal as non-radioactive hazardous waste. The following waste transfers took place during 2005:

- May 11, 2005: 60 L of waste from the labs of Dr. Papaioannou, Dr. Marks, Dr. Kandel, and Dr. Wardlaw.
- December 20, 2005: 80 L of waste from the labs of Dr. Connelly, Dr. Lieberman, Dr. Wolgemuth, Dr. Goldberg, Dr. Gunderson, and Dr. Marks.

8. On August 25, 2005, the Radiation Safety Office shipped nineteen 30-gallon drums of Liquid Scintillation Vials (LSV) and 19-gallons of long half-life low level liquid mixed waste for disposal by NSSI Source and Services, Tx. The licensed shipper was Radiac Research Corporation. The total volume of the LSV shipment was 76 cubic feet, the total weight was 2550 lbs., and the total activity shipped was 26 mCi. The total activity of the mixed waste shipment was 10.7 mCi and the primary hazardous components were chloroform, methanol and heptanes.

9. A number of older, unused sources were transferred from rooms 11-203 and 11-204 of the Vanderbilt Clinic to the Radiation Safety Office's Storage and Redistribution rooms in B-419 of the Physicians and Surgeons Building and SC-17 of the Russ Berrie Building. Among the transferred sources were therapeutic level ^{90}Sr and ^{137}Cs sources that will eventually be transferred to the Nevis Lab, a 46 Ci ^{137}Cs irradiator source that will be transferred to Los Alamos National Labs, and a number of ^{137}Cs Heyman sources that will be disposed of. Radiation safety surveys were performed following the transfers to ensure that all ambient dose rates in adjacent areas were within legal limits. The source transfer was carried out so that the room in which the sources were originally housed could be renovated and made into office space.

10. The Radiation Safety Office has registered a 46 Ci ^{137}Cs source with the Off-Site Source Recovery Project of Los Alamos National Labs. Under this project, the source will be moved off of the CUMC campus and transferred to the radioactive materials license of Los Alamos National Labs. Participation in this program will save approximately $80,000 in disposal costs as well as relieve CUMC of future liability introduced by the "cradle-to-grave" legislation that governs the disposal of radioactive waste.

11. The Radiation Safety Office has received bids of $38,000 and $43,879 for the disposal of a number of unused sources whose activities are below the level of interest of the Offsite Recovery Project. Obtaining these bids involved compiling a detailed inventory and performing individual leak tests on 60 sealed sources whose activities ranged from 0.5 μCi to 8 mCi. Funding for this disposal project has been approved and the purchase order is now being finalized.

12. The radiation waste and storage and redistribution area located in the P& S Building Room B417 was closed for emergency construction between November 15 and December 1, 2005. This closure was unannounced and caused a LSV shipment to be delayed.

Personnel Dosimetry, Bioassay, and Area Monitoring

In accordance with regulatory requirements, the Radiation Safety Office operates an ALARA Program to ensure that the radiation doses resulting from operations at CUMC/NYPH/NYSPI are both within the legal limits and kept "As Low As Reasonably Achievable."

The principal methods of monitoring radiation dose include the assignment of personnel radiation dosimeters to individuals, the posting of area and environmental dosimeters, and the monitoring of all discharges of radioactive materials.

Immediate action is taken, as appropriate, in response to unusual or high dosimeter readings. Quarterly ALARA Reports are prepared and submitted to the Joint Radiation Safety Committee. These reports present the following: a) the doses of individual workers that exceeded ALARA I Limits; b) summaries of investigations of doses to individual workers that exceeded ALARA II Limits; and c) discussions of significant trends within departments that have historically experienced high individual doses. In addition, Quarterly Environmental ALARA Reports are prepared and submitted to the Joint Radiation Safety Committee. The Quarterly Environmental ALARA Report presents the quantities of radionuclides discharged to the atmosphere and the sewer system and the resulting dose to the general public.

In 2005, all doses to individual workers were less than the legal annual reportable limits as specified in RCNY Article 175, Radiation Control. All doses to the general public resulting from atmospheric discharges of radionuclides were less than the USNRC constraint limit of 10 mrem per year.

Significant activities performed in 2005 to maintain the ALARA Program were:

1. The Radiation Safety Office distributed approximately 9,000 personnel radiation dosimeters each quarter, including both monthly and quarterly badges. A total of approximately 40,000 dosimeters were distributed and collected in 2005. To maintain dosimetry records, the Radiation Safety Office uses dedicated computers with Internet and direct modem access to the database of the dosimeter supplier, Landauer Inc.

2. The Radiation Safety Office received Annual Occupational Exposure Reports (NRC Form 5) from Landauer Inc. for the year 2004 and reviewed and forwarded these reports to radiation workers as required by the New York City Department of Health regulations.

3. The Radiation Safety Office notified 112 employees with ALARA Level I readings and investigated 29 cases of ALARA Level II readings as reported by Landauer Inc. Particular attention was paid to occupational groups that typically exceed the ALARA limits, i.e., workers and researchers at the Cyclotron Facility, Angiography, the Cardiac Cath Lab, and physicians in the PET Suite.

4. The Radiation Safety Office performed 64 bioassays on radiation workers who use radioactive iodine or handle greater than 10 mCi of ^{3}H or ^{32}P.

5. The Radiation Safety Office provided all workers who had declared pregnancy with health physics counseling about risk factors. Also, additional monitoring of the fetus during the gestation period was provided, and personnel radiation exposure reports were closely followed. The work environments were evaluated and modified if necessary.

Routine Radiation Safety Compliance – Internal Inspections, Audits and Surveys

A major activity of the Radiation Safety Office is the performance of facility inspections and audits of records at approved clinical departments and research laboratories in order to ensure compliance with regulatory requirements as well as with the guidelines and policies of the Joint Radiation Safety Committee.

Significant routine internal compliance activities conducted in 2005 include:

1. Annual inspections and audits were completed of all CUMC, New York Presbyterian Hospital, and New York State Psychiatric Institute clinical facilities using radioactive materials. The facilities audited include: New York Presbyterian Hospital Nuclear Cardiology, NYPH Nuclear Medicine, Allen Pavilion Nuclear Cardiology, Allen Nuclear Medicine, and Non-Radiology Users of X-ray Machines.
2. Quarterly inventory and leak testing was performed for all radioactive sources located in the following facilities: Milstein Nuclear Medicine, Allen Pavilion Nuclear Medicine, Cyclotron, and Columbia University Health Sciences. A leaking ^{68}Ge source was identified and placed in safekeeping in the RSO storage facility. No other sources were found to be leaking. Leak Test Certificates were generated and issued.
3. 690 routine radiation safety inspections and audits were performed in Columbia University Medical Center and New York State Psychiatric Institute research laboratories. The results were communicated to the Responsible Investigators. A total of 94 deficiencies were followed up by correction of the cited deficiencies.
4. 92 equipment clearance and laboratory exit/entry surveys were performed.
5. Airflow rates were measured in 119 fume hoods in areas where volatile radioactive materials are used. In all rooms where radioactive gases or aerosols are used, ventilation rates were measured, and spill gas clearance times were calculated and posted. Adjustments were made as required to air supply and exhaust systems to obtain negative pressure conditions. Researchers whose hoods did not meet safe flow rate standards were instructed to have their hoods repaired or replaced.
6. 14 animal and carcass surveys were performed. In order to minimize contamination in animal facilities and cages, protect Animal Care staff, and ensure proper disposal of animal carcasses containing radioactivity.
7. Calibration and maintenance services were provided for 250 radiation survey instruments used throughout CUMC/NYPH/NYSPI. The Radiation Safety Office maintains a supply of portable survey instruments available for loan to Responsible Investigators and in case of emergency.
8. Radiation Safety Support was provided to 17 patients. This support is provided for temporary ^{137}Cs/^{192}Ir implants, permanent ^{103}Pd implants, and following administration of therapeutic doses of radiopharmaceuticals.

Training

In accordance with regulatory requirements the Radiation Safety Office provides initial radiation safety training to all new employees of the Columbia University Medical Center and the New York State Psychiatric Institute prior to their beginning work with radiation equipment or radioactive materials. The Radiation Safety Office then provides annual refresher training.

The Radiation Safety Office also provides training in the general area of Emergency Response Preparedness as prescribed by the Joint Radiation Safety Committee subcommittee for the Management of Radiation Incidents. This subcommittee is chaired by David Brenner, Ph.D. and has the mission of providing the University and Hospital with professional expertise in the area of possible radiological threats and advising on the appropriate responses. The Radiation Safety Office's role in this subcommittee is to provide professional and technical personnel in order to support the Joint Radiation Safety Committee's policies and recommendations.

In addition to providing training to outside departments and institutions, personnel within the Radiation Safety Office itself are continually undergoing training. Significant training activities undertaken in 2005 included:

1. Pursuant to Article 175 of the New York City Health Code, the following radiation safety courses and training sessions were presented during 2005:
   - 12 initial training sessions for individual researchers
   - 12 annual refresher sessions for researchers
   - 12 sessions for the Nursing Staff of NYPH
   - Training sessions for Dental School residents
   - Training sessions for Dental Assistant students
   - Training sessions for Radiology residents
   - Training sessions for Anesthesiology staff
   - Training sessions for the Facilities Department.
   - Training for Security Personnel at both the CUMC and Morningside campuses
   - Training for Nursing students
   - Training for Non-Radiology Users of X-ray Machines.
2. On March 19, and October 1, 2005, the officers of the Radiation Safety Office attended a semi-annual FDNY unit drill. The drill started at 9:00 AM and lasted for about two hours. FDNY units visited radioactive storage facilities and raised questions about potential hazard of radioactive materials, especially during disasters. The drill was followed by a workshop in which Radiation Safety Office staff discussed radiation protection and emergency issues that were of concern to the FDNY units.
3. The Radiation Safety Office and the Emergency Room Department continue to attend meetings to discuss emergency response to a simulated terrorist attack. Since April 1, 2003, the Radiation Safety Office has been attending the Emergency Department Subcommittee meetings with regard to preparing for terrorist activities. The Radiation Safety Office ordered portable survey meters dedicated for use at the Emergency Room at New York Presbyterian Hospital. The Radiation Safety Office also has joined the ER for routine drills as well as tabletop drills.
4. On April 12, 2005, the Radiation Safety Office held a joint training session with the Environmental Health and Safety Office. The training session discussed the CUMC/NYPH/NYSPI mixed waste policy and the "Three

R's" (Reduce, Reuse, Recycle). A follow up session, conducted on April 19, 2005 was conducted in order to discuss the various methods used to determine the level of radioactivity present in mixed waste. In particular, Geiger meters were compared with scintillation counting and the concepts of minimal detectable activity and lower limit of detection were defined.

5. On February 25, 2005, the Radiation Safety Office issued a memorandum entitled "Laboratory Security" to all principle investigators. The memorandum reminded staff that CUMC/NYPH/NYSPI policy dictates that the following tasks be implemented on an ongoing basis:

- All sealed sources and radioisotopes shall be placed in locked storage at the end of the day.
- The laboratory door shall be locked when the last person leaves.
- An accurate and up-to-date inventory of all sources shall be maintained.
- Any missing or lost sources should be immediately reported to the Radiation Safety Office.
- Only Radiation Safety Office personal are allowed to remove radioactive material from the laboratory.

6. On July 21, 2005, four Radiation Safety Office staff members attended RCRA refresher training presented by the Environmental Resource Center.

7. On September 26, 2005, three Radiation Safety Office staff members attended DOT training. Triennial attendance at this training is mandatory for all parties involved with waste shipments.

Professional Radiation Safety and Health Physics Support

The Radiation Safety Office provides professional radiation safety and health physics consultation to clinical departments, research laboratories, Authorized Users, and Responsible Investigators throughout CUMC/NYPH/NYSPI in order to ensure compliance with regulatory requirements and the ALARA program.

Specific examples of professional support provided by the Radiation Safety Office in 2005 include:

1. The Radiation Safety Office investigates spills, misadministrations, and other incidents involving radioactive materials. The Radiation Safety Office ensures that, when required, timely notice of reportable incidents is made to the New York City Department of Health, Office of Radiological Health. The Radiation Safety Office responded to the following 15 spill incidents in 2005. Further details are on file in the Radiation Safety Office and may also be found in the Radiation Safety Office's Quarterly reports to the JRSC.

- On January 19, 2005 a ^{32}P spill occurred in Room 613 of the Russ Berrie Building. The spill involved a pipette tip containing radioactive material being dropped onto the floor. Decontamination resulted in near total clean-up, with a small residual surface contamination remaining in the cracks between floor tiles. Following decontamination, removable wipe tests and surface dose measurements were well below the limits specified in Article 175. Nevertheless, in the ALARA spirit, the contaminated area was shielded with plastic for 10 half-lives.
- On April 4, 2005, a ^{99m}Tc spill occurred in the Department of Nuclear Cardiology. Contamination was identified on and around a treadmill used for stress testing. Access to the contaminated area was restricted for two days, after which time contamination levels had decayed to below the limits specified in Article 175. In order to prevent recurrence, Radiation Safety staff recommended that more attention be paid to the state of the injection site during stress tests.
- On April 19, 2005, a ^{99m}Tc spill occurred in the Department of Nuclear Cardiology. Contamination was identified on and around a treadmill used for stress testing. Access to the contaminated area was restricted for one day, after which time contamination levels had decayed to below the limits specified in Article 175. In order to prevent recurrence, Radiation Safety staff recommended that floor covers be used during stress testing.
- On May 17, 2005, a worker reported that radioactive waste had disappeared from Dr. Gingrich's lab in Room 4919-A of 1051 Riverside Drive. A lengthy investigation followed, and it was determined that the waste was mistakenly thrown away into a regular trash bin by an improperly trained housekeeper. The waste was eventually located within the building's trash compactor. In response to this incident, the Radiation Safety Office provided training to NYSPI housekeeping staff and reminded laboratory staff that access controls should be in place for all radiation areas.
- On June 24, 2005, a ^{99m}Tc spill occurred in Room 256 of 8 Hudson South (Milstein Hospital, Epilepsy Unit). The spill occurred after a patient underwent a seizure with an IV and syringe containing a full dose of an imaging radiopharmaceutical attached to his body. Personnel surveys and decontamination efforts were carried out. Contamination was identified on the patient and on two members of the nursing staff. Access to the contaminated area was restricted for 10 half-lives of the radioactive material involved. Personal doses were calculated and determined to be well within the occupational dose limits specified in Article 175.
- On April 29, 2005, a ^{201}Tl spill occurred in the Department of Nuclear Cardiology. The spill occurred when a small amount of radiopharmaceutical leaked out of a loose IV connection. Contamination was identified on a treadmill and on a lab coat. These items were stored for decay for 10 half-lives.
- On June 28, 2005, a ^{201}Tl spill occurred in the Department of Nuclear Cardiology at Allen Pavilion. The spill occurred when a small amount of radiopharmaceutical leaked out of a loose IV connection. The area of the spill was sequestered until ambient dose rates and wipe test results were below the limits specified in Article 175.
- On June 29, 2005, ^{18}F spills were reported simultaneously by the PET Suite and Radioligand Laboratory. Contaminated areas were identified and covered with plastic to prevent the further spread of contamination. The plastic was removed the following day, after 10

half-lives, at which time wipe test results were below the limits specified in Article 175.

- On July 19, 2005, a ^{99m}Tc spill occurred in the Department of Nuclear Cardiology. The spill occurred when a small amount of radiopharmaceutical leaked out of a loose IV connection. Contamination was identified on a treadmill and a pair of shoes. These items were stored for decay until wipe test results were below the limits specified in Article 175.
- On July 26, 2005, a "recordable" misadministration occurred in the Department of Nuclear Medicine. The misadministration happened after an error occurred in the preparation of a dose kit and resulted in an effective dose of approximately 239 mrem. In order to prevent recurrence, the Radiation Safety Office recommended 1.) That technologists not prepare doses unless they have been specifically assigned to do so by a manager; and 2.) That only the person who prepares the dose make entries into the pharmacy's log book.
- On August 1, 2005, a "recordable" misadministration occurred in the Department of Nuclear Cardiology. This incident involved the administration of the wrong isotope during a dual isotope rest/stress study. As a result of this incident, Nuclear Cardiology Staff indicated that a color coded labeling system will be developed to identify dual isotope patients.
- On September 16, 2005, a ^{201}Tl spill occurred in the Department of Nuclear Cardiology. The spill occurred when a small amount of radiopharmaceutical leaked out of a loose IV connection. Contamination was identified on a treadmill and on a lab coat. These items were stored for decay for 10 half-lives.
- On October 21, 2005, the Radiation Safety Office was notified of the presence of a water leak in the radioactive waste room of Dr. Deckelbaum's laboratory (Black Building 4-463). Radiation Safety Office staff determined that no radioactivity was present in the water and supervised the cleanup effort.
- On November 18, 2005, a ^{99m}Tc spill occurred in Room 640 of the Children's Tower Building (Epilepsy Unit). The spill occurred during the disposal of a syringe that had been used in an injection of a radiopharmaceutical. The contaminated area was cleaned and contaminated items were identified and stored for decay.
- On December 4, 2005, a ^{3}H spill was reported by the nursing staff on the 10th floor of the Harkness Pavillion. The spill involved an empty bottle of a radiopharmaceutical being dropped onto the floor and broken. Wipe test results were indistinguishable from background after the area was decontaminated.

2. Ahmad Hatami, Assistant Director of the Radiation Safety Office, participates as a member of the IACUC Animal Care Protocol Review Committee by reviewing all procedures that utilize radionuclides in animal research and reviewing other animal protocols.

3. The Radiation Safety Office participates as a member of the JRSC executive committee in reviewing all Human Use protocols using radiation.

4. The Radiation Safety Office provides continuing radiation safety support for the Columbia University Cyclotron Facility and the Columbia University Radioligand Laboratory for the production and synthesis of PET imaging radiopharmaceuticals. This support includes: maintenance of licenses and permits, basic radiation safety services; personnel dosimetry; area radiation monitoring and quantitative measurement and ALARA analysis of radioisotope releases to the atmosphere; review of Authorized User credentials; and review of system modifications.

5. Since the Columbia University Cyclotron Facility has been placed into operation, both the cyclotron and the radiopharmacy have been operated under contract by a qualified outside vendor—first by CTI Services Inc. and later CTI's successor corporation, PET NET Inc. In 2005, major changes occurred in the operational structure of the Columbia University Cyclotron Facility, with the result that Columbia University is in the process of completely taking over direct management of cyclotron and radiopharmacy operations. This process is expected to be completed in early 2006.

- Over the course of the first two quarters of 2005, the majority of the PETNET cyclotron and radiopharmacy staff were relocated to a new PET NET owned cyclotron facility located in Hackensack, New Jersey. The Hackensack facility continues to supply Columbia University and New York Presbyterian Hospital with PET radiopharmaceuticals.
- On July 5, 2005, the Radiation Safety Office was officially informed that PETNET would no longer be operating the Columbia University Cyclotron, though a PET NET employed NYS Licensed pharmacist would continue to manage the Facility as the Supervising Pharmacist under the NYS Pharmacy License.
- On August 8, 2005, the Radiation Safety Office was informed that David Wilson, R.Ph., former North-East Regional Manager for PETNET, would be joining Columbia University Medical Center in order to become the Pharmacist for the Cyclotron Facility. Mr. Wilson received his New York State licensure in December 2005 and was approved by the NYC DOH as a Pharmacist on the Radioactive Materials License in February 2006. Mr. Wilson is expected to be fully in charge of the Facility early in early 2006.

6. The Radiation Safety Office continues the processes of scanning paper documents using the PaperPort software application and of maintaining the RSO filing index. In 2005, several boxes of old documents, some dating as far back at the 1950s, were catalogued and scanned. Because maintenance of certain documents is an explicit regulatory requirement, these efforts are recognized as being primarily compliance motivated.

7. In 2004, the Radiation Safety Office provided consultation in the preparation of a grant application for the development of a "Center for Medical Countermeasures against Radiation" (CMCR). In the summer of 2005 CUMC was notified that the grant application had been accepted. Since that time, the Radiation Safety Office has provided support for ongoing design and construction projects related to the receipt of this grant.

Professional Radiation Safety and Medical Physics Support for Non-Radiology X-ray Activities

The dental quality assurance program is designed to optimize the radiological safety and clinical quality of dental radiography. This program is based on recommendations for quality assurance that have been promulgated by a number of professional organizations, including the National Council on Radiation Protection and Measurements (NCRP), the Bureau of Radiological Health of the Food and Drug Administration, the American College of Radiology (ACR), and the American Academy of Dental Radiology Quality Assurance Committee. In this program, the Radiation Safety Office has primary responsibility for preliminary radiation safety shielding evaluation, acceptance testing, diagnostic quality assurance, and radiation safety surveys on all dental x-ray units installed at the following locations:

- Morningside Dental Associates (2 locations): 9 intraoral units, and 1 panoramic/cephalographic
- Ambulatory Care Networked Corporation (ACNC): 2 intraoral units and 1 panoramic/cephalographic unit
- Babies Hospital OR: 1 portable intraoral unit
- Vanderbilt Clinic Teaching & Research Areas: 1 panoramic unit, 1 panoramic/cephalographic unit, 23 intraoral units, and 1 intraoral–cephalographic unit
- Dentcare Clinic (Intermed. School 183): 1 intraoral unit
- NYSPI: 1 intraoral unit and 1 panoramic unit
- Columbia Eastside: 6 intraoral units and 1 panoramic/cephalographic unit
- Columbia North: 5 intraoral units and 1 panoramic unit
- Mobile Dental Facility: 2 intraoral units
- Mannie L. Wilson Health Care Center: 5 intraoral units and 1 panoramic unit.

In agreement with the New York Presbyterian Hospital, the Joint Radiation Safety Committee has assigned the Radiation Safety Office responsibility for Radiation Safety and Medical Physics support for those clinical facilities outside the Department of Radiology that use x-ray equipment. The Radiation Safety Office and Radiology Medical Physics jointly run the audit program for these facilities. This program is conducted in accordance with the conditions of the CUMC/NYPH/NYSPI New York City X-ray Permits, as specified in Article 175 of the New York City Health Code. In this audit program, the Radiation Safety Office is primarily responsible for ensuring that each site follows the proper safety practices and keeps the proper records, while Radiology Medical Physics is responsible for performing all technical tests. The following locations are audited under this program:

- Urology Dept., Atchley 11th Floor: 1 fluoroscopy unit
- Endoscopy Department, Atchley 13th Floor: 3 C-arm fluoroscopy units
- The Spine Center, Neurological Institute, 5th Floor: 1 C-arm unit
- Sports Medicine, Dodge Fitness Center/Bakers Field: 1 mini C-arm unit
- Cystoscopy Suite, Milstein 4th Floor: 3 radiographic/fluoroscopic units
- Cardiac Care, Milstein 5th Floor: 1 C-arm unit
- Pain Management, Presbyterian Hospital 5th Floor: 1 C-arm unit
- Harkness Pavilion 9th Floor: bone densitometery units.

In 2005, the Radiation Safety Office provided the following support of the above programs:

1. The Radiation Safety Office provided support for Dr. Adi Cohen, Assistant Professor, Endocrinology, regarding the importation of a Non-FDA approved bone-density x-ray device called the XtremeCT (Manufactured by Scanco Inc., Switzerland). To expedite importation of this device, the Radiation Safety Office drafted a letter supporting the classification of the XtremeCT as a "Non-Significant-Risk Investigation Device". In addition, the Radiation Safety Office provided consultation regarding quality assurance testing. The unit was installed on December 9, 2005.
2. Radiation Safety surveys and machine performance evaluations, in addition to the standard annual q/a tests described above, were performed at the following locations:
   - ACNC Dental Facility at 99 Ft. Washington Ave. (newly installed units: 4 intraoral and 1 panoramic)
   - Large Animal Facility on the 18th Floor of the Black Building (2 fluoroscopy units)
   - Columbia Eastside Dental Associates (newly installed panoramic unit)
   - Morning Side Dental Associates, 116th Street (newly installed units: 3 intraoral)
3. Shielding design evaluations were performed during the planning phases of the following new facilities:
   - ACNC Dental Facility at 99 Fort Washington Avenue
   - Odyssey House Dental Clinic at 219 East 121st Street
   - Harlem Children's Health Initiative Dental Facility at 215 West 125th Street
   - Columbia North Facility at the Tower II residence hall.

Radiation Safety Office Personnel and Facilities

Significant personnel related activities in 2005 included:

1. In February 2005, Mutian Zhang resigned from his post as Junior Physicist.
2. In January, 2006, Michelle Kang resigned from her post as Chief Technician.
3. In November, 2005, Stephen Benson resigned from his post as Administrative Assistant.
4. In the calendar year 2004, Gerald Fischbach, M.D., Dean of Columbia University Medical Center, directed the JRSC to create a position for a "Radiological Quality Assurance Officer" to be responsible for assuring that investigations involving human subjects comply with all relevant radiation related regulatory requirements, regulatory and professional guidelines, and institutional policies and procedures. This position has yet to be filled.

Because of the combined effects of the 2004–2005 hiring freeze and the high turnover rate of Radiation Safety Office staff, the Radiation Safety Office has recently experienced difficulty maintaining an adequate staffing level. Multiple vacancies currently exist within the Radiation Safety Office. In 2006, the Radiation Safety Office is looking forward to filling all positions in order to provide the best possible safety and support services to the Columbia University Medical Center, New York Presbyterian Hospital, and the New York State Psychiatric Institute.

Professional Affiliations & Activities

AMUNDSON, SALLY A., Sc.D.
Adjunct Faculty
NCI Radiation Epidemiology Branch, National Institutes of Health, *Adjunct Investigator*
Member
Radiation Research Society, *Program Committee, Finance Committee*
International Congress of Radiation Research, Program Committee
National Council on Radiation Protection and Measurements (NCRP)
Reviewer
Cancer
Cancer Gene Therapy
Cancer Research
Carcinogenesis
Cell and Molecular Life Science
Genomics
International Journal of Radiation Oncology, Biology and Physics
Molecular Cancer Research
Radiation and Environmental Biophysics
Radiation Research
***Ad Hoc* Grant Reviews:**
Modeling and Analysis of Biological Systems (MABS) study section, NIH
Genomics Research and Development Fund, Health Canada

BALAJEE, ADAYABALAM S., Ph.D.
Member
American Association for Advancement of Science
Radiation Research Society
Indian Association of Radiation Biology
Reviewer
Nucleic Acids Research
Advances in Space Research
Medical Science Monitor
Honors
Edited a book on "DNA repair and human diseases" for Landes Biosciences, Texas, USA

BIGELOW, ALAN, Ph.D.
Member
American Physical Society
Radiation Research Society
Student Mentoring
New York City Stuyvesant High School summer student apprenticeship

BRENNER, DAVID J., Ph.D., D.Sc.
Member
Columbia University Radiation Safety Committee, *Chairperson*
National Council on Radiation Protection and Measurements (NCRP)
International Congress on Radiation Research, *Program Committee*
TV and radio appearances on the topic of CT examinations
Editorial Work
Radiation and Environmental Biophysics, Assoc. Editor

CALAF, GLORIA M., Ph.D.
Adjunct Faculty
University of Tarapaca; Faculty of Sciences; Dept. of Biology and Health, Arica, Chile, *Full Professor*
Member
Biology Society of Chile
Mastology Society of Chile
Chilean Society of Citology
Chilean Society of Cancer
New York Academy of Sciences
Tissue Culture Association
International Association of Breast Cancer Research
American Association of Cancer Research
Society of Experimental Biology and Medicine
Radiation Research Society
Teaching
University of Tarapaca, Contaminants in the Environment, May, 2005
Reviewer
Grant:
Fondo de Desarrollo Científico y Tecnológico (Fondecyt)
Manuscripts:
Cancer Detection and Prevention
British Journal of Cancer
Mutation Research
Radiation Research
International Journal of Radiation Oncology Biology Physics
International Journal of Radiation Biology
Grants
Fondecyt 1040300, *scholar grant*
UTA 4714-04, *scholar grant*
Conferences
Breast Cancer Session at X World Congress in Advances in Oncology and VIII International Symposium of Molecular Medicine (October 13–15, 2005) in Creta, Greece, *Invited Speaker and Co-Chair*
X World Congress in Advances in Oncology and VIII International Symposium of Molecular Medicine (October 13–15, 2005) in Creta, Greece, *Award of Recognition*

GEARD, CHARLES R., Ph.D.
Member
American Society of Therapeutic Radiology and Oncology (ASTRO)
Environmental Mutagen Society
Advisory Committee on Radiobiology, Brookhaven Na-

tional Laboratory
Scientific Review Panels, Research Council, Ontario, Canada

Editorial Work

International Journal of Radiation Biology, Editorial Board

Reviewer

British Journal of Cancer
Mutation Research
Radiation Research
Mutagenesis

Student Mentoring

Columbia University, resident in Radiation Oncology

HALL, ERIC J., D.Phil., D.Sc., FACR, FRCR

Member

Royal College of Radiology
British Institute of Radiology
American Board of Radiology, *Radiotherapeutic Written-Test Committee*
American Society of Therapeutic Radiology and Oncology (ASTRO)
Radiation Research Society
American Radium Society
International Association of Radiation Research, *Past President*
Columbia University, Herbert Irving Comprehensive Cancer Center, *Director, Radiation Physics and Biology Program*
Columbia-Presbyterian Medical Center, Joint Radiation Safety Committee, *Chairman*; Radioactive Drug Research Committee, *Chairman*
National Council on Radiation Protection and Measurements, Committee 1, *Emeritus Member*

Editorial Work

Intl Journal of Radiation Oncology Biology Physics, Editorial Board
International Journal of Brachytherapy
International Journal of Radiation Biology
Radiation Research
Radiology

HEI, TOM K., Ph.D.

Adjunct Faculty

Department of Radiological and Environmental Health Science, Colorado State University, Fort Collins, Co., *Adjunct Professor*
Department of Ion Beam Bioengineering, Chinese Academy of Sciences, Hefei, China, *Adjunct Professor and Doctorate Student Mentor*

Member

NIH Special Emphasis Group, *Chairman, Ad Hoc Review Panel*
Radiation Research Society, *Vice-Chairman, Commission F of Committee on Space Research*
American Association for Cancer Research
Environmental Mutagen Society
Oxygen Society

Students Mentoring

Doctoral Student of Environmental Heath Sciences, Columbia University, School of Public Health
New York City High School Science Students for Intel Science Project
Faculty Advisor for Chinese Medical Student Exchange Program

Reviewer

American Journal of Pathology
Cancer Research
Chemical Research in Toxicology
Clinical Cancer Research
Environmental Health Perspective
Free Radical Biology and Medicine
International Journal of Cancer
International Journal of Radiation Biology
Journal of Radiation Research
Mutation Research
Proceedings of the National Academy of Sciences
Radiation Research

Editorial Work

Advances in Space Sciences, Section Editor
Journal of Radiation Research

LIEBERMAN, HOWARD B., Ph.D.

Member

Summer Research Program for NYC Secondary School Science Teachers, Columbia University, *Advisory Board*
Israel Cancer Research Foundation, *Scientific Advisory Board*
Columbia University College of Physicians and Surgeons, *Faculty Council*
American Association for the Advancement of Science
American Society for Microbiology
Environmental Mutagen Society
Genetics Society of America
Radiation Research Society
Sigma Xi
Theobald Smith Society

Reviewer

Grants:
Basic and Preclinical Subcommittee C of the NCI Initial Review Group, *Member*
Joint Center for Radiation Therapy Foundation, Harvard Medical School, *Ad Hoc*
Post-Doctoral Fellowship Panel, Israel Cancer Research Foundation.
Pennsylvania Department of Health
Manuscripts:
Radiation Research

MARINO, STEPHEN A., M.S.

Member

Columbia University Radiation Safety Committee
Radiation Research Society

PONNAIYA, BRIAN, Ph.D.

Member

Radiation Research Society

Reviewer
International Journal of Radiation Biology
Radiation Research
Oncogene

YIN, YUXIN, M.D., Ph.D.
Adjunct Faculty
Assistant Professor, Department of Environmental Health Sciences, Mailman School of Public Health, Columbia University
Member
American Association for Cancer Research
Students Mentoring
Advisor for a Ph.D. student in the Department of Environmental Health Sciences, Mailman School of Public Health, Columbia University
Reviewer
Cancer Research

ZHAO, YONGLIANG, Ph.D.
Member
Radiation Research Society
American Association for Cancer Research
Grants
RSNA Research Seed Grant
NIEHS Center Pilot Grant
NASA Project Grant ■

Publications

1. **Amundson SA**, Do KT, Vinikoor L, Koch-Paiz CA, Bittner ML, Trent JM, Meltzer P and Fornace AJ Jr. Stress-specific signatures: Expression profiling of p53 wild-type and null human cells. *Oncogene* **24**:4572–9, 2005.
2. Belyakov OV, **Mitchell SA**, Parikh D, **Randers-Pehrson G**, **Marino SA**, **Amundson SA**, **Geard CR** and **Brenner DJ**. Biological effects in unirradiated human tissue induced by radiation damage up to 1 mm away. *PNAS (USA)* **102**:14203–8, 2005.
3. **Bigelow AW**, **Randers-Pehrson G**, Kelly RP and **Brenner DJ**. Laser Ion Source for Columbia University's Microbeam. *Nucl Inst Meth B* **241**:874–9, 2005.
4. **Bigelow AW**, **Ross GJ**, **Randers-Pehrson G** and **Brenner DJ**. The Columbia University Microbeam II endstation for cell imaging and irradiation. *Nucl Instrum Meth B* **231**:202–6, 2005.
5. **Brenner DJ**. Letter to the Editor: Is it time to retire the CTDI for CT quality assurance and dose optimization? *Med. Phys.* **32**:3225–6, 2005.
6. **Brenner DJ** and **Elliston CD**. In response to Radiation risk of body CT: What to tell our patients and other questions. (R.E. Levatter) *Radiology* **234**:968–70, 2005.
7. **Brenner DJ** and Georgsson MA. Mass Screening With CT Colonography: Should the radiation exposure be of concern? *Gastroenterology* **129**:328–37, 2005.
8. **Calaf GM**. Susceptibility of human breast epithelial cells in vitro to hormones and drugs. *Int J of Oncol* **28**: 285–295, 2006.
9. **Calaf G**, Alvarado M and **Hei TK**. Beta catenin is associated with breast cancer progression *in vitro. Int J Oncol* **26**:913–21, 2005.
10. **Calaf GM**, Alvarado ME and **Hei TK**. Oncoprotein expression and morphological phenotypes of human breast epithelial cells transformed by the c-Ha-ras oncogene. *Oncol Rep* **14**:885–93, 2005.
11. **Calaf GM**, Emenaker NJ and **Hei TK**. Effect of retinol on radiation- and estrogen-induced neoplastic transformation of human breast epithelial cells. *Oncol Rep* **13**: 1017–27, 2005.
12. **Calaf GM**, Roy D and **Hei TK**. Growth factor biomarkers associated with estrogen-and radiation-induced breast cancer progression. *Int J of Oncol* **28**:87–93, 2006.
13. **Calaf GM**, Roy D and **TK Hei**. Gene and protein expression altered by organophosphorous pesticides and estrogen in human breast epithelial. *Oncology* (in press).
14. **Calaf GM**, Roy D and **Hei TK**. Immunochemical analysis of protein expression in breast epithelial cells transformed by estrogens and high linear energy transfer (LET) radiation. *Histochem Cell Biol* **124**:261–74, 2005.
15. **Garty G**, **Randers-Pehrson G** and **Brenner DJ**. Development of a secondary-electron ion-microscope for microbeam diagnostics. *Nucl Instrum Meth B* **231**:60–64, 2005.
16. **Garty G**, **Ross GJ**, **Bigelow A**, **Randers-Pehrson G** and **Brenner DJ**. A microbeam irradiator without an accelerator. *Nucl Instrum Meth B* **241**:392–6, 2005.
17. **Garty G**, **Ross GJ**, **Bigelow A**, **Randers-Pehrson G** and **Brenner DJ**. Testing the stand-alone microbeam at Columbia University. *Rad Prot Dosimetry* (in press.)
18. **Garty G**, Schulte R, Shchemelinin S, Grosswendt B, **Leloup C**, Assaf G, Breskin A, Chechik R and Bashkirov V. First attempts at prediction of DNA strand-break yields using nanodosimetric data. *Rad Prot Dosimetry* (in press.)
19. **Hall EJ**. Dose-painting by numbers: a feasible approach? *Lancet Oncol* **6**:66, 2005.
20. **Hall EJ**. IMRT, Protons and the Risk of Second Cancers. *Int J Radiat Oncol Biol Physics* (in press).
21. **Hall EJ**. Multiple gene effects in radiation oncogenesis. *Radiat Res* **163**:697–8, 2005.
22. **Hall EJ**. Suffer little children-IMRT, second cancers and the special case of children. *Pediatric Blood and Cancer* **45**:366, 2005.
23. **Hall EJ**. The Inaugural Frank Ellis Lecture Iatrogenic Cancer: The impact of IMRT. *Clinical Oncol* (in press).
24. **Hall EJ**, **Brenner DJ**, Worgul B and **Smilenov L**. Genetic susceptibility to radiation. *Adv Space Research* **35**:249–53, 2005.
25. Hande MP, Azizova TV, Burak LE, Khokhryakov VF, **Geard CR** and **Brenner DJ**. Complex chromosome ab-

errations persist in individuals many years after occupational exposure to densely ionizing radiation: An mFISH study. *Genes Chromo Cancer* **44**:1–9, 2005.

26. Hu B, Han W, Wu L, Feng H, Liu X, Zhang L, **Xu A**, **Hei TK** and Yu Z. In situ visualization of DSBs to assess the extranuclear/extracellular effects induced by low-dose alpha-particle irradiation. *Radiat Res* **164**: 286–91, 2005.
27. Hu B, Wu L, Han W, Zhang L, Chen S, **Xu A**, **Hei TK** and Yu Z. The time and spatial effects of bystander response in mammalian cells induced by low dose radiation. *Carcinogenesis* **27**:245–51, 2006.
28. Inostroza J, Saenz L, **Calaf G**, Cabello G and Parra E. Role of the phosphatase PP4 in the activation of JNK-1 in prostate carcinoma cell lines PC-3 and LNCaP resulting in increased AP-1 and EGR-1 activity. *Biol Res* **38**: 163–78, 2005.
29. **Ivanov VN** and **Hei TK**. Combined treatment with EGFR inhibitors and arsenite upregulated apoptosis in human EGFR-positive melanomas: a role of suppression of the PI3K-AKT pathway. *Oncogene* **24**:616–26, 2005.
30. **Ivanov VN**, Ronai Z and **Hei TK**. Opposite roles of FAP-1 and dynamin in the regulation of Fas (CD95) translocation to the cell surface and susceptibility to Fas ligand-mediated apoptosis. *J Biol Chem* **281**:1840–52, 2006.
31. Karnitz LM, Flatten KS, Wagner JM, Loegering D, Hackbarth JS, Arlander SJH, Vroman BT, Thomas MB, Baek YU, **Hopkins KM**, **Lieberman HB**, Chen J, Cliby WA and Kaufmann SH. Gemcitabine-induced activation of checkpoint signaling pathways that affect tumor cell survival. *Molec Pharmacol* **68**:1636–44, 2005.
32. **Leloup C**, **Garty G**, Assaf G, Cristovão A, Breskin A, Chechik R, Shchemelinin S, Paz-Elizur T, Livneh Z, Schulte RW, Bashkirov V, Milligan JR and Grosswendt B. Evaluation of lesion clustering in irradiated plasmid DNA. *Intl J of Radiation Biology* **81**:41–54, 2005.
33. **Lieberman HB**. Rad9, an evolutionarily conserved gene with multiple functions for preserving genomic Integrity. *J Cell Biochem* **97**:690–7, 2006.
34. Liu SX, Davidson MM, Tang XW, Walker WF, Athar M, **Ivanov V** and **Hei TK.** Mitochondrial damage mediates genotoxicity of arsenic in mammalian cells. *Cancer Res* **65**:3236–42, 2005.
35. **Persaud R**, **Zhou H, Baker SE**, **Hei TK**, **Hall EJ**. Assessment of low linear energy transfer radiation-induced bystander mutagenesis in a three-dimensional culture model. *Cancer Res* **65**:9876–82, 2005.
36. **Piao CQ**, **Liu L**, **Zhao YL**, **Balajee AS**, Suzuki M and **Hei TK**. Immortalization of human small airway epithelial cells by ectopic expression of telomerase. *Carcinogenesis* **26**:725–31, 2005.
37. Poonepalli A, Balakrishnan L, Khaw AK, Low GK, Jayapal M, Bhattacharjee RN, Akira S, **Balajee AS**, Hande MP. Lack of poly(ADP-ribose) polymerase-1 gene product enhances cellular sensitivity to arsenite. *Cancer Res* **65**:10977–83, 2005.
38. **Ross GJ**, **Bigelow AW**, **Randers-Pehrson G**, Peng CC, **Brenner DJ**. Phase-based cell imaging techniques for microbeam irradiations. *Nucl Instrum Meth B* **241**: 387–91, 2005.
39. **Ross GJ**, **Garty G**, **Randers-Pehrson G** and **Brenner DJ**. A single-particle/single-cell microbeam based on an isotopic alpha source. *Nucl Instrum Meth B* **231**:207–11, 2005.
40. Roy D, **Calaf GM** and **Hei TK**. Allelic imbalance at 11q23-q24 chromosome associated with estrogen and radiation-induced breast cancer progression. *Int J of Oncol* (in press).
41. Roy D, Panda A, **Calaf GM** and Mitra A. Differential gene expression of sulindac-treated human breast epithelial cells. *Int J Oncol* **27**:1727–36, 2005.
42. Sachs RK and **Brenner DJ**. Solid tumor risks after high doses of ionizing radiation. *PNAS* **102**:13040–5, 2005.
43. **Smilenov LB**. Tumor development: Haploinsufficiency and local network assembly. *Cancer Lett* 2005.
44. **Smilenov LB**, **Lieberman HB**, **Mitchell SA**, **Baker R**, **Hopkins KM** and **Hall EJ**. Combined haploinsufficiency for ATM and RAD9 as a factor in cell transformation, apoptosis and DNA lesion repair dynamics. *Cancer Res* **65**:933–8, 2005.
45. Sokolov MV, **Smilenov LB**, **Hall EJ**, Panyutin IG, Bonner WM, Sedelnikova OA. Ionizing radiation induces DNA double-strand breaks in bystander primary human fibroblasts. *Oncogene* **24**:7257–65, 2005.
46. Vives S, Loucas B, Vazquez M, **Brenner DJ**, Sachs RK, Hlatky L, Cornforth M, Arsuaga J. SCHIP: statistics for chromosome interphase positioning based on interchange data. *Bioinformatics* **21**:31812, 2005.
47. **Shen WH**, Wang J, Wu J, Zhurkin VB and **Yin Y**. MKP2: A novel transcription target of p53 in apoptosis. *Cancer Res* (in press).
48. Worgul BV, **Smilenov L**, **Brenner DJ**, Vazquez M and **Hall EJ**. Mice heterozygous for the ATM gene are more sensitive to both X-ray and heavy ion exposure than are wildtypes. *Adv Space Res* **35**:254–9, 2005.
49. **Zhao Y**, El-Gabry M and **Hei TK**. Loss of Betaig-h3 protein is frequent in primary lung carcinoma and related to tumorigenic phenotype in lung cancer cells. *Mol Carcinog* **45**:84–92, 2006.
50. **Zhou HN**, **Ivanov V**, **Gillespie J**, **Geard CR**, **Amundson SA**, **Brenner DJ**, Yu Z, **Lieberman HB** and **Hei TK**. Mechanism of radiation induced bystander effect: role of COX-2 signaling pathway. *PNAS (USA)* **102**:14641–6, 2005.
51. **Zhou H**, Suzuki M, **Persaud R**, **Gillispie J**, **Randers-Pehrson G** and **Hei TK**. Contribution of bystander effects in radiation induced genotoxicity. *Acta Med Nagasaki* **50**:73–7, 2005.
52. **Zhou H**, **Xu A**, **Gillispie JA**, **Waldren CA** and **Hei TK**. Quantification of CD59(-) mutants in human-hamster hybrid ($A_{(L)}$) cells by flow cytometry. *Mutat Res* **594**:113–9, 2006.
53. **Zhu A**, **Zhou H**, **Marino SA**, **Leloup C**, **Geard CR**, **Hei TK** and **Lieberman HB**. Differential impact of mouse rad9 deletion on ionizing radiation-induced bystander effects. *Rad Res* **164**:655–61, 2005. ■